Studies in the Chemistry of Fungal Natural Products

A Thesis

submitted in partial fulfilment

of the requirements for the degree

of

Doctor of Philosophy in Chemistry

at the

University of Canterbury

by

Sonia van der Sar

University of Canterbury

Christchurch, New Zealand

September 2006

Acknowledgements

First and foremost I would like to thank my supervisors, Professors Murray Munro and John Blunt for giving me the opportunity to carry out this research. Despite being on half time for most of my time here, you never seemed to stray far from your offices. Your support and encouragement has been an asset.

Secondly, A big thanks goes to Gill Ellis for all the assays you have run over the years, and recently for your extended role as the general marine group technician. Trying to keep up with everyone's often disorganised and/or chaotic work habits I know has been a challenge.

Of course thanks goes out to the entire technical support staff of the Department of Chemistry. We are very lucky as a department to have such great in-house technical expertise. Especially to Rob McGregor, what would the department do without you? Thanks heaps for the personalised glass stoppers!! Thanks also to Wayne MacKay you have always been a smiley, cheery face round the department. Not to mention the many mechanical "emergencies" that you always responded to immediately (and with a smile). And of course Bruce Clark, thanks for the countless numbers of EIMS you ran without complaint.

To everyone past and present in X-ray crystallography who have either taken part in the data acquisiton or processing, thank you. Special thanks must go to Ward Robinson for having to put up with "poor quality natural product crystals"; Ramin for always being there with a smile to process all the data for those "poor quality crystals".

A huge thank you must also go to Blair Stuart for his expertise in molecular modelling; taking time out from his own work to provide the seemingly endless amounts of data for the appendix.

For financial assistance during my time here, I would like to thank the Chemistry Department for your assistance in the form of a Teaching Assistant scholarship. Also to the Canterbury Branch of the New Zealand Federation of Graduate Woman, the Royal Society, Canterbury Branch of the Royal Society and Rotary for your much needed travel grants for conference attendance.

A huge thank you to the marine group (past and present), I don't think you could find a friendlier group of people anywhere. I am absolutely indebted to you guys; I have to name you all because you have all played such an important part in my life; André Pinkert, Annabel Murphy, Cherry Chen (+Tony), Christian Narkowicz, David Overy (+Berta), Gerhard Lang, Jenni Gadd, Maya Mitova, Petur Dalsgaard, Philipp Kügler, Sarah Hickford, Sean Devenish, Stephan Busche, and Warren MacLean what a supportive and fantastic group to work in! Without you all, I may have finished sooner…but certainly not with the same happy memories. A special thanks must go to Gerhard, for honestly, being the best postdoc in the world, your knowledge of pretty much everything has been invaluable! And Philipp, what would I have done without you these last few months?! Thanks so much for your friendship and the distractions you (and your many aliases!!) have provided through some very difficult times.

Thanks to my Dad, you always did have a passion for chemistry, thanks for passing it on… Well here it is…the PhD, I know you would have been proud…
To Mum and Davinia, even though you never entirely understood exactly what my work was all about, I know you understood and appreciated why I was doing it.

Finally, to Aaron, thanks for your continued love and support through some frustrating and trying times; knowing I would get there in the end, even if I wasn't able to see "the light at the end of the tunnel".

Abstract

Natural products as sources of novel therapeutic agents experienced a steady increase from around the turn of the twentieth century until it peaked in the 1970s and 1980s. However since this time pharmaceutical research in natural products has experienced a decline. Despite this trend the natural products industry now seems to be experiencing a revival of sorts.

This thesis represents a continuation of the work on the isolation and structure elucidation of potential drug leads from terrestrial fungal sources that the natural products group at the University of Canterbury is engaged in.

The known compound, pseurotin A (**2.7**) and two novel diastereomers, pseurotin A_2 (**2.8**) and pseurotin A_3 (**2.9**) were isolated from the extract of a *Penicillium* sp. of fungus collected from the foreshore of a beach in Vancouver, Canada. The absolute stereochemistry of pseurotin A_2 and proposed absolute stereochemistry for A_3 were elucidated using a combination of X-ray crystallography (A_2 only), circular dichrosim, oxidative cleavage reactions, and *J*2-resoved 2D NMR experiments.

The extract of an as yet unidentified endophytic fungus has yielded eight novel compounds related to the spirobisnaphthalene class of compounds. These eight compounds fall into to distinct groupings. The spiro-mamakones, distinguished by a structurally unprecedented oxygenated spiro-nonene skeleton, comprise five compounds, spiro-mamakones A-E (**3.11**, **3.15**-**3.18**). In addition to these naturally occurring compounds, the semi-synthetic compounds, 4-oxo-spiro-mamakone A (**3.12**) and *O*-acetyl-spiro-mamakone A (**3.21**), were also synthesised. spiro-Mamakone A was found

to be racemic, while X-ray crystallography and optical rotation revealed spiro-mamakone C (**3.15**) to be present as an enantiomeric mixture (4*S**, 5*S**, 9*R**). Unfortunately the enantiomeric excess was unable to be elucidated. NOE experiments revealed spiro-mamakone B (**3.16**) to have the relative stereochemistry 4*S**, 5*S**, 9*S**. The relative stereochemistry of spiro-mamakones D (**3.17**) (4*S**, 5*S**, 8*S**, 9*S**) and E (**3.18**) (4*S**, 5*S**, 8*S**, 9*R**) was proposed from comparison of coupling constant calculations from energy-minimised models with those of the experimentally determined values. The second group, comprising three novel compounds named the mamakunoic acids, mamakunoic acid A–C (**3.8**, **3.7**, **3.10**), are characterised by their acid substituted dihydro benzofuran system. The low yield obtained of these compounds, unfortunately prevented their stereochemical elucidation.

In addition to structure elucidation, biosynthetic studies on spiro-mamakone A and mamakunoic acid B were also carried out. Analysis of the NMR spectra derived from spiro-mamakone A, labelled with isotopic acetate, revealed a situation complicated by the presence of isotopomers and racemisation, resulting in NMR spectra that were somewhat anomalous in appearance. These irregularities however, were resolved leading to the proposal that spiro-mamakone A was derived from a dihydroxynaphthalene (DHN) intermediate, which proceeds through to spiro-mamakone via an epoxide intermediate. Despite problems with purity and low yields of isotopically labelled mamakunoic acid B, it was proposed that like spiro-mamakone A, it proceeded via a DHN intermediate.

The extract derived from a Malaysian *Scleroderma* sp. was found to contain a new dichlorinated pulvinic acid derivative, methyl-3',5'-dichloro-4,4'-di-*O*-methylatromentate (**4.14**), the structure of which was confirmed by X-ray crystallography. In addition three previously reported compounds, 4,4'-dimethoxyvulpinic acid (**4.11**), methyl-3'-chloro-4,4'-di-*O*-methylatromentate (**4.12**) and methyl-4,4'-dimethoxyvulpinate (**4.13**), were also isolated.

The extract of another, as yet unidentified endophytic fungus was found to contain the new acetogenin, 1,5-dihydroxy-6-(2-hydroxyethyl)-3-methoxyacetophenone (**5.7**),

differing from the known compound, 2,4-dihydroxy-6-(2-hydroxyethyl)-3-methoxyacetophenone (**5.8**) only by virtue of the substitution pattern. The structure of **5.7** was confirmed by X-ray crystallography.

The implementation of efficient dereplication procedures is paramount for those working in the field of natural products. The recent advances that have been made in the dereplication process in the natural products group at the University of Canterbury are given using examples from this research and where necessary from other group members.

Table of Contents

Chapter 6: Dereplication Methods

Chapter 7: Experimental

Abbreviations

1D	one dimensional
2D	two dimensional
Å	angstrom(s) (bond length)
ACN	acetonitrile
AIDS	Acquired Immunodeficiency Syndrome
at	acquisition time (in NMR)
br s	broad singlet (in NMR)
BSC-1	African Green Monkey kidney cell line
c	concentration (optical rotation)
^{o}C	degrees celcius
C18	octadecyl phase (chromatography column packing)
calc	calculated
CAN	cerium ammonium nitrate
capNMR	capilliary probe nuclear magnetic resonance
capLC	capilliary HPLC
CCK	cholecystokinin
CD	circular dichroism
CD_3OD	deuterated methanol
$CDCl_3$	deuterated chloroform
CE	capilliary elcetrophoresis
CH_3CN	acetonitrile
CIGAR	constant time inverse-detection gradient accordion rescaled (heteronuclear multiple bond correlation spectroscopy) (in NMR)
CoA	coenzyme A
COSY	correlation spectroscopy

d	doublet (in NMR)
δ	chemical shift in parts per million
d1	delay (in NMR)
DBE	double bond equivalents
DCM	dichloromethane
DEA	diethylamine
DEPT	distortionless enhancement by polarisation transfer (in NMR)
DHN	dihydroxynaphthalene
dm	decoupler mode (in NMR)
DMAP	dimethylaminopyridine
DMSO	dimethylsulfoxide
DNA	deoxyribose nucleic acid
EIMS	electron impact mass spectrometry
ELSD	evaporative light scattering detector
ESIMS	electrospray ionisation mass spectroscopy
EtOAc	ethyl acetate
ϕ	dihedral angle
g	gram
GB/SA	generalised Born/surface area
hCMV	human cytomegalovirus
HIV	Human Immunodeficiency Virus
HMBC	heteronuclear multiple bond correlation spectroscopy (in NMR)
HMG-CoA	3-hydroxy-3-methylglutaryl-CoA
HPLC	high performance/pressure liquid chromatography
HREIMS	high resolution electron impact mass spectrometry
HRESIMS	high resolution electrospray ionisation mass spectrometry
HSQC	heteronuclear single quantum coherence (in NMR)
HSV	*Herpes simplex* virus
HTS	high throughput screening
Hz	hertz

IC_{50}	concentration of sample required to inhibit the P388 cell growth by 50%
INADEQUATE	incredible natural abundance double quantum transfer experiment (in NMR)
IR	infra-red
J	coupling constant (in NMR)
KBr	potassium bromide
L	litre(s)
LC	liquid chromatography
LCMS	liquid chromatography mass spectrometry
LCMS-MS	liquid chromatography tandem mass spectrometry
LC-NMR	liquid chromatography nuclear magnetic resonance
LDL	low density lipoprotein
λ_{max}	maximum wavelength
m	multiplet (in NMR)
MCMM	monte carlo multiple minimum
Me	methyl
mg	milligram
MHz	megahertz
min	minute(s)
mL	millilitre(s)
MLR Assay	mixed lymphocyte reaction
MM2	energy minimisation calculations using force field program, *MM2*
MTPA	*α*-methoxy-*α*-(trifluoromethyl) phenyl acetic acid
MTPACl	*α*-methoxy-*α*-(trifluoromethyl) phenyl acetic acid chloride
MYE	malt yeast extract
m/z	mass-to-charge ratio (mass spectrometry)
μ	micro
NCE	new chemical entity
NCI	National Cancer Institute
ng	nanogram(s)

nm	nanometres (wavelength)
NMR	nuclear magnetic resonance
NOE	nuclear Overhauser effect (in NMR)
NOESY	nuclear Overhauser enhancement spectroscopy (in NMR)
ol	overlapping (in NMR)
oxid.	oxidation
P388 Assay	murine leukaemia cells
PC12	rat adrenal pheochromocytoma cell line
PDA	photo diode array (in chromatography)
pet. ether	petroleum ether
ppm	parts per million (in NMR and errors in MS)
q	quartet (in NMR)
ROESY	rotating frame nuclear Overhauser enhancement spectroscopy (in NMR)
RP	reverse phase (in chromatography)
rt	room temperature
RT	retention time
s	singlet (in NMR)
sec	second(s)
SDS	spring dead spot
S/N	signal-to-noise ratio
sp.	species
t	triplet (in NMR)
TIC	total ion current
TP assay	thymocyte proliferation
TFA	trifluoroacetic acid
UV	ultraviolet
vs2d	vertical scale in 2D NMR

Chapter 1

Introduction

1.1 Evolution of Natural Products

A natural product is generally referred to as a secondary metabolite, in other words a metabolite that is not essential for the normal growth, development or reproducibility of an organism. Secondary metabolites usually have no effect on the producing organism, though in an indirect way a number of examples have proven to be essential for the survival of some organisms in that they have deterrent effects on predators, or competitors.[1] In the biosynthesis of secondary metabolites there exist four principle building blocks: acetate, mevalonate, shikimate and amino acids. However, most of these intermediates are also used for the production of primary metabolites such as the fatty acids, nucleosides, and polypeptides. A theory therefore has been put forward that suggests that the secondary metabolism arose as a way of using the acetate, shikimate and amino acids that were excess to requirements ('shunt metabolites'). It was proposed that

changes in genetic make up of an organism (mutations), whether they be natural chemical mistakes or exposure to chemicals, viruses or radiation, have lead to the increased production of the key intermediates. When these compounds are able to provide useful biological activities that increase the chances of survival for an organism, they are more likely to be passed on through the generations, hence, Darwin's famous theory on evolution through 'survival of the fittest' comes into play. This is particularly evident when comparing higher organisms such as humans and lower organisms that live in extreme ecological niches. Humans produce few secondary metabolites since our survival is determined by physical means. In contrast, the lower organisms such as fungi and bacteria, which generally live in highly competitive environments, are considered as major producers of secondary metabolites.

1.2 Natural Products Through History

"The Indians killed another companion of ours… and in truth the arrow did not penetrate half a finger, but as it had poison on it, he gave up his soul to our Lord." Written by Spaniard Francisco de Orellano, who accompanied the conquistadors on their murderous campaign to South America in the sixteenth century.[1] The poison referred to, was most probably that of curare, a name that was given to the extracts of the plant *Chondodendron tomentosum* and some *Strychnos* sp.[2] This muscle relaxant poison exerts its effect by antagonising the effect of acetylcholine at the neuromuscular junction. Investigations into the South American arrow poison has lead to the development and use of muscle relaxants, such as atracurium (**1.1**) to allow a reduction in anaesthesia during surgery.[3]

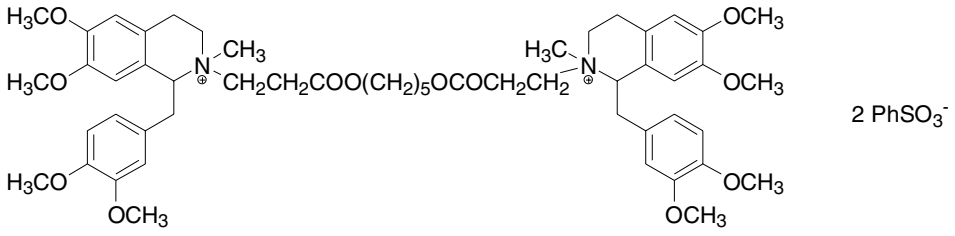

1.1

For thousands of years medicine and natural products have been linked through the use of traditional medicines and natural poisons. The first records were written on clay tablets from Mesopotamia and date from about 2600 BC. The best-known Egyptian pharmaceutical record, is the Ebers papyrus dating from 1500 BC, a document that describes around 700 drugs (mostly from plants). It includes formulas for gargles, snuffs, poultices, infusions, pills and ointments.[4] The Chinese Materia Medica and Indian Ayurvedic systems have records dating back to 1100 BC and 1000 BC respectively.[4]

These traditional medicines, which derive mostly from plants, after clinical, pharmacological, and chemical studies, formed the basis of most of the early medicines.[5] Famous examples include the antimalarial drug quinine (**1.2**) from the bark of the *Cinchona* species, asprin or acetylsalicylic (**1.3**), derived from salicylic acid, which comes from the bark of the willow tree (*Salix alba*), and morphine (**1.4**), named after Morpheus, the Greek god of sleep and dreams.[6] Morphine comes from the opium poppy, *Papaver somniferum*.

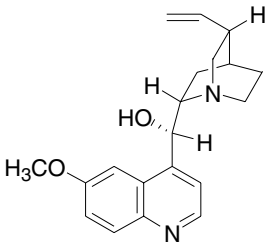

1.2

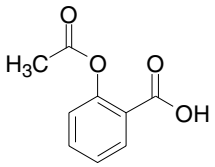

1.3

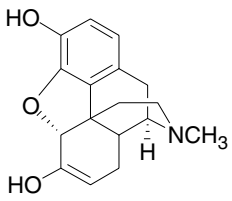

1.4

1.3 The Rise and Fall of the Natural Product Era

The discovery by Fleming in 1928 of penicillin (see Section 3.1.3.1), re-isolation and clinical studies by Chain, Florey, and co-workers in the early 1940s, and commercialisation of synthetic penicillins revolutionised drug discovery research.[7] The huge success of penicillin prompted a worldwide effort by drug companies and research groups to assemble large collections of microorganisms in order to try and discover new antibiotics.[5] The effort paid off, and in fact the early years were extremely prolific, and

included the discovery of streptomycin (**1.5**), chloramphenicol (**1.6**), chlortetracycline (**1.7**), cephalosporin C (**1.8**), erythromycin (**1.9**), and vancomycin (**1.10**). All of these compounds, or derivatives thereof are still in use as drugs to this day.[7,8]

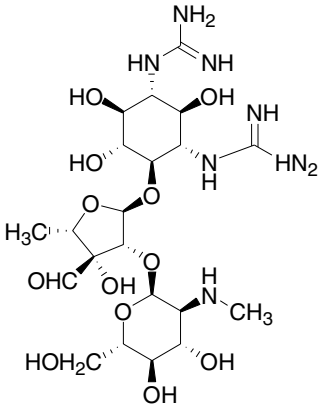

1.5

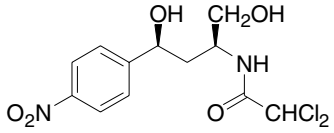

1.6

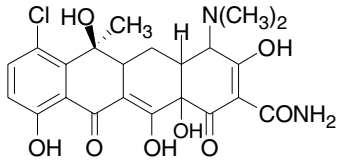

1.7

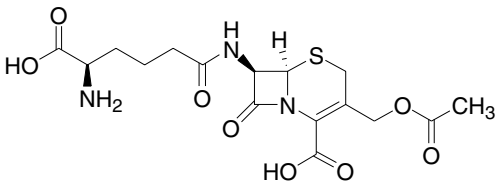

1.8

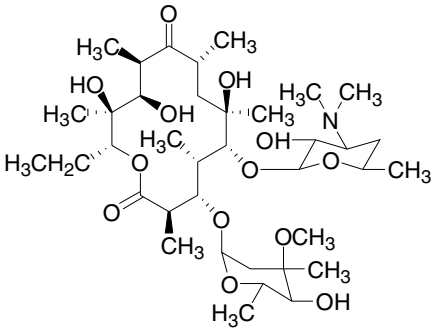

1.9

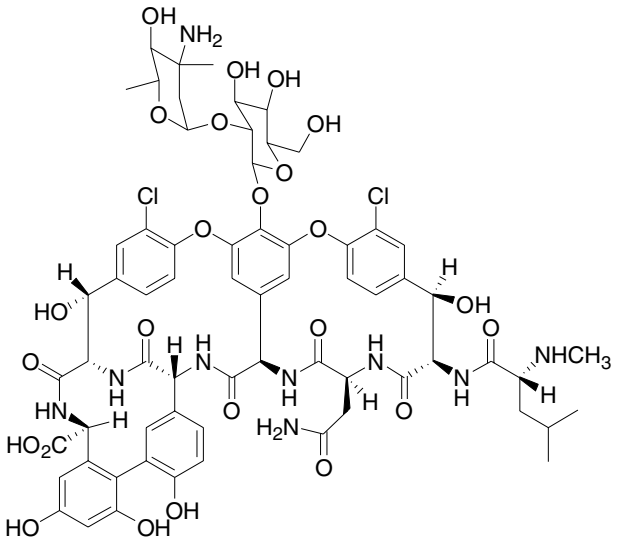

1.10

Natural products as sources of novel therapeutics peaked in the Western pharmaceutical industry in the 1970s and 1980s.[9] This was likely due to the breakthrough in the 1970's of mechanism-based screening for bioassay-guided fractionation. Some of the first compounds identified in the early 1970s using this method included the β-lactamase inhibitor, clavulanic acid (**1.11**), from *Streptomyces clavuligerus* and the HMG-CoA reductase inhibitor mevastatin (see Section 3.1.3.2) from *Penicillium citrinum*. A mixture of clavulanic acid and amoxicillin (**1.12**), known as Augmentin is still in use today as a front-line antibiotic.

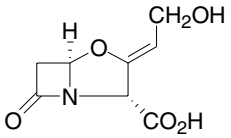

1.11

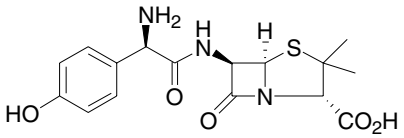

1.12

Of the 877 small-molecule new chemical entities (NCEs) introduced between 1981-2002, about half were natural products, semi-synthetic natural product analogues or synthetic compounds based on natural product pharmacophores*.[10] Despite this success, pharmaceutical research into natural products has experienced a slow decline during the past two decades. Several reasons have been blamed for the decline:[9]

1. The introduction of High-Throughput Screening (HTS) against defined molecular targets has prompted many companies to move away from natural product extract libraries towards 'screen friendly' synthetic chemical libraries.
2. Combinatorial chemistry, which offered the promise of simpler, more drug-like screening libraries with wide chemical diversity.
3. Advances in molecular biology, cellular biology and genomics increased the number of molecular targets and prompted shorter drug discovery timelines.
4. A decline in the focus of major pharmaceutical companies on therapy for infectious diseases, which has been a traditional area of strength for natural products.

* An ensemble of steric and electronic features that is necessary to ensure optimal interactions with a specific biological target structure and to trigger (or block) its biological response.

5. Possible uncertainties regarding the collection of biological materials as a result of the 1992 Rio Convention on biological diversity.
6. Most promising lead compounds have traditionally been available in very small quantities, especially those from marine organisms such as sponges. Due to the perceived supply problem, many drug companies are reluctant to pursue these sources. This leaves organic synthesis as the only option for sourcing the drug candidates for pre-clinical and clinical trials. However, due to the often lengthy synthetic routes that result from the often highly complicated architecture, long development times, low yields and impracticality of scale-up, these compounds are even more disfavoured.[11]

Drug discovery today requires rapid screening, hit identification, and hit-lead development. Unfortunately, the traditional resource intensive natural product programmes based on extract-library screening, bioassay guided isolation, structure elucidation followed by product scale-up face a huge disadvantage when compared to the defined synthetic chemical libraries.[9]

1.4 A Natural Products Revival?

Despite the trend in the pharmaceutical industry to downscale its natural product research in recent years, there could be change on the wind…….

The problems with natural products (vide infra) that resulted in these initial decisions are being addressed with technological advances, such as increasing the throughput of methods for compound purification and identification.[12] A problem also lies with the unrealised expectations from combinatorial chemistry. For a molecular screening library it is imperative that it covers a significant portion of chemical diversity, but at the same time be biased toward 'biological friendliness' and 'drug-likeness'.[13] Some of the first large combinatorial libraries, in some cases contained in excess of one million compounds that were synthesised, only to find very few, or no hits. This was the first mistake of some synthetic chemists, to design the libraries based on chemical

accessibility and maximum achievable size rather than on biologically-relevant chemical diversity or properties. This was nicely summed up by Danishefsky " a small collection of smart compounds may be more valuable than a much larger hodgepodge collection mindlessly assembled"[14] The potential for undesired side effects due to the often less specific binding characteristics of many of the simple combinatorial generated molecules was also soon realised.[11] This has prompted a renewed interest in natural products as a source of chemical diversity and lead compound generation.

So why is it that natural products win the specificity and potency race compared to artificially designed molecules? A recent article in *Science*[11] answered this question nicely "…evolutionary selection – natures own high throughput screening process for the optimisation of biologically active compounds." Natural products tend to have well-defined three-dimensional structures carrying a plethora of functional groups, which provide H-bond acceptor/donors etc. These have been fine tuned into a precise spatial orientation. The structures of the biological targets of natural products (e.g protein binding sites) are often well conserved among proteins even having different genetic sequences. This is such that the secondary metabolites that have evolved for a certain purpose and mode of action may display different, yet just as potent effects in other situations.

"There are more things between heaven and earth…."[15] Shakespeare's words still, after so many years, continue to ring true. The 'catalogue' of natural products is still far from complete. Discoveries of new structures and functions are likely to continue as unexplored sources of natural products are evaluated. The functional group diversity and design introduced into natural products during biosynthesis continues to provide lessons for chemists in how to construct biologically active mimics and provide selective ligands for cellular targets.[12]

1.4.1 New Frontiers in the Discovery of Novel Bioactives

Currently, the most interesting natural products have come from recently discovered biota. One such example was the realisation that there was a large and largely

unexplored group of fungi (Endophytes) living inside higher plants (For more on this group of fungi see Section 1.6). This has led to foccussed discovery efforts by both industrial and academic labs.

The marine environment has also received somewhat of a revival in interest, through the discovery of sponge-bacterial symbiosis, and the realisation that many metabolites once thought to be sponge metabolites, are most probably produced by symbiotic bacteria. A ground breaking study on an uncultivated bacterial symbiont of the sponge *Theonella swinhoei* has confirmed that the antitumor compounds, the theopederins and onnamides (Figure 1.1) are most likely produced by a bacterial symbiont.[16]

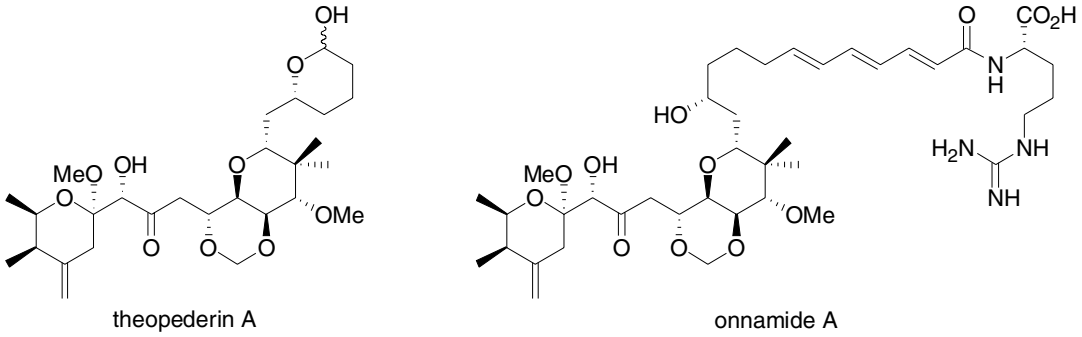

Figure 1.1: *Structures of theopederin A and onnamide A, two representative compounds from the pederin family.*

Uncultivated bacterial symbionts offer a goldmine of novel structural possibilities. Heterologous gene expression* of natural product biosynthetic pathways provides a technique whereby these potentially novel structures can be accessed. It enables the (over)-production of structurally complex substances, can provide a basis to generate novel analogues through biosynthetic engineering, and also provide a way of transferring 'silent' (not expressed under standard laboratory conditions) secondary metabolite pathways into surrogate host strains.[17] This account barely scratches the surface of this interesting new field; a full account however, is unfortunately beyond the scope of this chapter.

* The transfer of genes of a secondary metabolite biosynthetic pathway from the original microbial producer into a heterologous host (a host of a different species, in this case one that is easily cultivated).

1.5 *Fungal Secondary Metabolites*

There has been a recent and growing understanding of microbial abundance and diversity, in particular that of fungi. It has shown that the fungal world has until now, just been superficially scratched. There is in existence, a huge, still unknown and untapped microbial pool, which promises the discovery of novel, useful and economically profitable compounds.

As alluded to, fungi have historically been a gold mine of lead compounds for the pharmaceutical industry. Post 1960s, after the excitement that the discovery of penicillin had made, the attention of pharmaceutical companies and academic labs drifted away from fungi as a source of lead compounds. Efforts were instead focussed on Actinomycetes. Despite this, it was again a fungus that was responsible for the next big break through in medicine. In the 1980s, from the filamentous fungus, *Tolypocladium inflatum*, the immunosuppressive agent cyclosporin A (**1.13**) was discovered. The 1980s turned out to be the decade natural products research saw a resurgence in the discovery of useful compounds from fungal sources, not only for antibiotics but also other therapeutic areas. Success stories include, the cholesterol-lowering agent, mevinolin (**1.14**)[18], one of the so-called statins, isolated from *Aspergillus terreus*, and asperlicin (**1.15**)[19], a cholecystokinin (CCK)* antagonist from *Aspergillus alliaceus*. Structure manipulation of this compound has led to the discovery of the benzodiazepines (Figure 1.2)[20] used for the treatment of severe anxiety or insomnia.

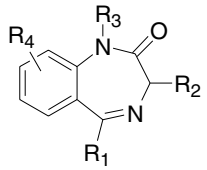

Figure 1.2: *The benzodiazepine core, the R-groups can be varied widely.*

*CCK is a regulatory peptide hormone found mainly in the gastrointestinal tract, but is also a neurotransmitter present throughout the nervous system.

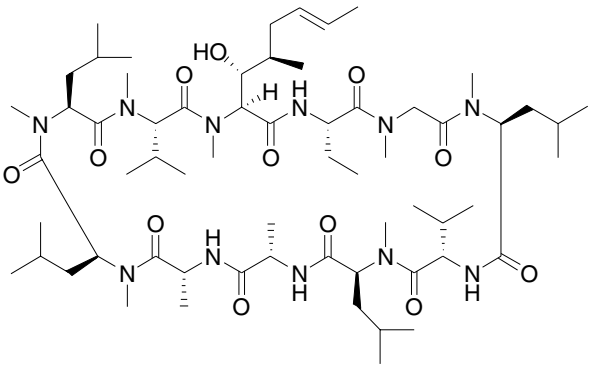

1.13

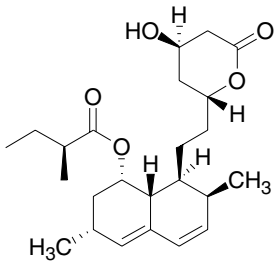

1.14

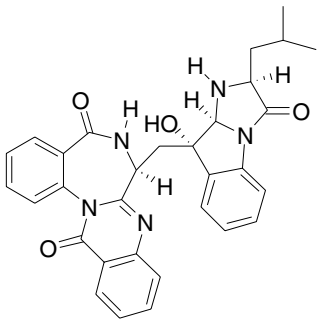

1.15

1.6 Endophytic Fungi

Endophytic fungi had previously been overlooked as potential sources of bioactive metabolites. This was most likely due to the absence of any sign of fungal colonisation in the host plant.[21] In the past few decades however, it has been realised that plants may contain countless, previously undetected, unrealised numbers of these microorganisms known as endophytes. This has prompted a worldwide scientific effort to isolate endophytes and to study their natural products. Scientists have since discovered that endophytes may represent an important area for discovery of new secondary metabolites. Of the approximately 300,000 higher plant species that exist on earth, each individual plant is thought to play host to one or more endophytes.[22]

The most widely accepted definition of an endophyte is given by that of Bacon *et al*; "microbes that colonise living, internal tissues of plants without causing any immediate, overt negative effects."[23]

The majority of endophytic species have been identified as belonging to the ascomycete and deuteromycete classes of fungi.[24]

1.6.1 The Endophyte-Host Interaction

It is thought that endophytism may have evolved from the time that higher plants first appeared on the earth millions of years ago.[25] This is supported by the fact that plant-associated microbes have been discovered in the fossilised tissues of stems and leaves.[26] It is plausible therefore, that due to these long-held associations, that some endophytes may have developed genetic systems allowing for transfer of information between themselves and the higher plants and vice versa.

In an endophyte-host interaction, the minimum contribution that the plant provides is one of nutrition.[25] There are other possibilities for these interactions. These could include, the possibility that the plant provides compounds necessary for the completion of the life cycle of the microorganism.[27] It is also possible that in some cases the endophyte could be responsible for the degradation of the dead or dying host plant, beginning the process of nutrient re-cycling. An even more important mechanism could exist. If it is likely that mechanisms exist for the exchange of nucleic acids, then it could also be possible that some of the rare molecules made by higher plants could also be produced by endophytes, for example taxol.

1.6.1.1 Taxol-a Case Study

Taxol (**1.16**) is a highly functionalised diterpenoid which is found in all the worlds species of Yew (*Taxus*) tree, although it was first isolated from the Pacific yew, *Taxus brevifolia*.[28]

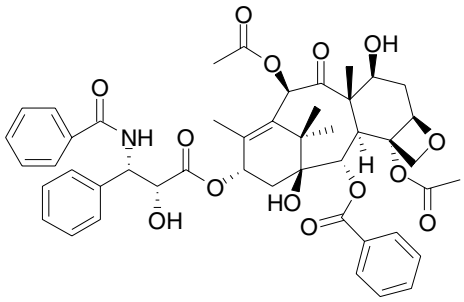

1.16

It was the world's first billion dollar anti-cancer drug, and is particularly effective against refractory breast and ovarian cancers.[21] The yew is a slow growing tree, and the inner bark of the tree yields only 0.01% to 0.03% of its dried weight of taxol. However, a full regimen of anti-tumour treatment requires 2g of purified taxol.[29] For this reason the cost of the drug is phenomenal, making it out of reach for many people.

A search for an endophyte, that was able to produce taxol was conducted on the basis that plant-associated microbes had been found to produce "plant" compounds such as gibberellins. Testing of hundreds of microbes by Stierle and co-workers, resulted in the discovery that one, a fungal endophyte, *Taxomyces andreanae* was capable of producing taxol.[29] Although the yields of taxol produced by *T. andreanae* were low (24-50 ng/L) this represented a break through in solving the supply problem, which could only lead to a decrease in the cost of this important drug to patients. Since this initial study, taxol has been found from other endophytic fungi isolated from a number of different sources other than Yew trees. These include *Pestalotiopsis microspora* from the bald cypress,[30] *P. guepini* from the Wollemi Pine (*Wollemia nobilis*),[31] and a novel fungus, *Seimatoantlerium tepuiense*, isolated from the plant, *Maguireothamnus speciosus*,[32] which belongs to the same family as blackberry and raspberry.

1.6.2 Metabolites from Endophytic Fungi

The diverse chemistry and bioactivity displayed by natural products isolated from endophytic fungi most likely stems from the fact that there are so many endophytes that

occupy literally millions of unique biological niches (higher plants) growing in so many unusual environments.[22] A selection of some of the more interesting metabolites produced by endophytic fungi are presented below. These are grouped according to their biological activity.

1.6.2.1 Antiviral Compounds

The endophytic fungus, *Cytonaema sp*. has yielded two human cytomegalovirus (hCMV) protease inhibitors, cytonic acids A (**1.17**) and B (**1.18**).[33] hCMV is a ubiquitous opportunistic pathogen that causes disease in those that are congenitally immune-deficient.

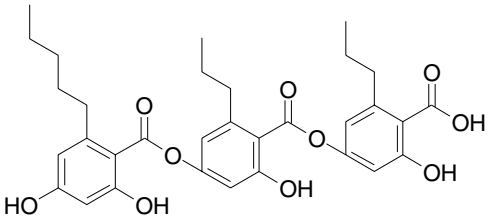

1.17

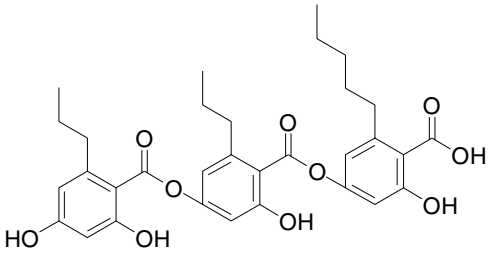

1.18

1.6.2.2 Antimicrobial Compounds

Cryptosporiopsis quercina isolated from *Tripterigeum wilfordii*, a medicinal plant native to Eurasia,[34] was found to show antifungal activity against some important human fungal pathogens, including *Candida albicans*, and *Trycophyton mentagrophytes*. The bioactive principle was found to be a novel peptide termed cryptocandin (**1.19**).[34] Cryptocandin is currently being considered for use against fungal diseases of the skin and nails.[24]

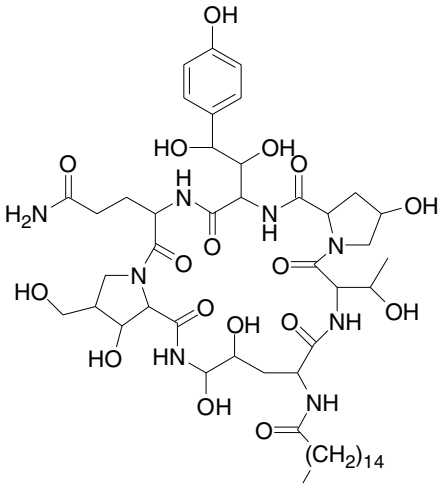

1.19

An investigation of an unidentified endophytic fungus from Costa Rica for antibiotic activity yielded Guanacastepene A (**1.20**).[35] It was shown to display antibiotic activity against methicillin-sensitive and -resistant *Staphylococcus aureus* and vancomycin-resistant *Enterococcus faecalis*. Studies have suggested that the primary mode of bactericidal action is membrane damage. It was also found that **1.20** lysed human red blood cells and caused leakage of intracellular potassium.[36]

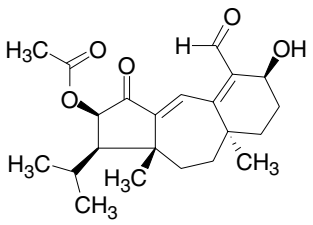

1.20

1.6.2.3 Antitumoural Compounds

Aspergillus parasiticus, an endophyte of the coastal redwood (*Sequoia sempervirens*), was found to produce the sequoiatones A (**1.21**) and B (**1.22**). These compounds showed moderate and selective inhibition of human tumour cells, with the greatest activity against breast cancer cell lines.[37]

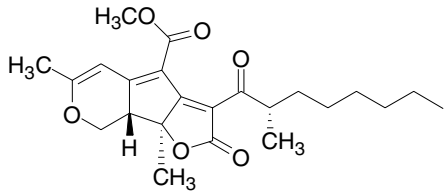

1.21

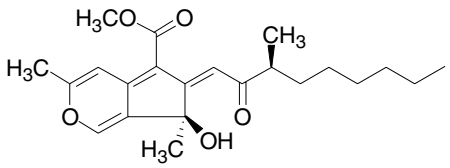

1.22

1.6.2.4 Immunosuppressive Metabolites

The study of *Fusarium subglutinans*, an endophyte of the twining vine, *Tripterygium wilfordii*, yielded two non-cytotoxic, but immunosuppressive compounds. The diterpene pyrones, subglutinol A (**1.23**) and B (**1.24**) displayed identical immunosuppressive activities in the mixed lymphocyte reaction (MLR) assay and thymocyte proliferation (TP) assay.[38]

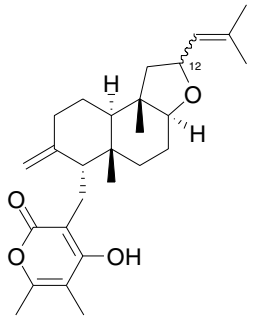

1.23, 12 = *S*

1.24, 12 = *R*

The currently approved immunosuppressive agent, cyclosporin A (**1.13**), displayed equal potency in the MLR assay but was 10^4 more potent in the TP assay.[38] The fact however, that **1.23** and **1.24** display no cytotoxicity suggests that further exploration into these compounds is required.

1.7 Work Carried Out at UoC

As part of the continuing effort to identify new bioactive natural products with pharmaceutical potential, the Marine group at the University of Canterbury has explored

various habitats. Mostly around New Zealand, but also Antarctica and other locations. Since 1998, more than 10,000 marine invertebrate and fungal specimens have been screened for cytotoxic, antifungal, antimicrobial and antiviral activity, where it has been established that ~10% of all isolates show activity in the assays.

Although much of the research carried out by the group has traditionally been marine orientated, first with marine invertebrates, and then with marine fungi, the focus has changed in recent years, in that the group is now almost entirely concentrated on the isolation of biologically active natural products from terrestrial fungi. These include such diverse groups as endophytes (fungi living inside of higher plants), entomopathogenic (insect pathogens) fungi, and biological niches such as Malaysian tropical rainforests. Coupled with the development of an HPLC UV library database used in the dereplication (see Chapter 2) of crude extracts, this "path" has quickly proven to be a rewarding one.

1.8 Aim of this Research

The primary aim of this study was to characterise the compounds responsible for the biological activity of a wide range of terrestrial fungi, collected from a variety of habitats around the world, including Canada, Malaysia and New Zealand.

Fungal extracts were selected based on the biological activity displayed in the anti-cancer, antimicrobial, and antiviral in-house assays. Extracts chosen for the structural elucidation of the active components were based on a "no hit"* criterion that had to be met following dereplication. The structure elucidation of purified compounds would be carried out using various NMR spectroscopy, and mass spectrometry techniques. Where necessary confirmation of correct structural/stereochemical assignment would be confirmed by X-ray crystallography, and/or semi-synthetic modifications.

* Not found to match any known compounds in the UV and AntiMarin databases.

Chapter 2

A Canadian *Penicillium* sp. (F2028)

2.1 General Introduction

The genus *Penicillium* is probably the most well known of the filamentous fungi, thanks to its frequent colonisation of bread and other foodstuffs and the antibiotic properties of some species. Although spoiled food is the most common instance in which they are observed, penicillia have a wide variety of habitats, including plants, animals, and in some cases other fungi.

2.1.1 Interaction with Plants

Penicillium sp. are primarily known as saprophytes growing on organic substrates including dead plant material, however a few species have evolved for growth on living

tissue.[39] One such species is *P. expansum*, which causes the soft brown rot on apples, and also cherries and grapes. Important in its infection is the degradation of hemicelluloses resulting in plant cell wall breakdown, causing cell wall loosening and increased porosity of the wall, as well as allowing the colonisation of the plant tissue.[40] It is also this species of fungus that is responsible for the production of patulin (**2.1**) in unfermented apple juice produced from poor quality fruit.[39,41]

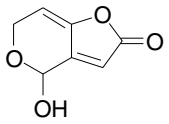

2.1

Another two species, *P. digitatum* and *P. italicum*, are responsible for the green and blue moulds of citrus fruits, where they produce a soft rot. The soft rot has been shown to be marked by a decrease in pectic substances in the fruit, which has been found to result from production of pectin methylesterase, polygalacturonase and macerating enzyme in the fungus when cultured.[42]

2.1.2 Interaction with Animals

Most species of *Penicillium* are considered quite benign with respect to causing human disease. However, one species of dimorphic fungus, *P. marneffei* can cause disease (penicilliosis) both in immunocompetent and immunocompromised people. It is especially a problem among those persons living in Southeast Asia, where it is endemic.[43-45] Over the years infection due to this pathogen has increased markedly, which is exclusively due to the increasing number of patients infected with the human immunodeficiency virus (HIV).[43] Symptoms of penicilliosis are non-specific and are similar, whether the patient has AIDS, or not. The main signs of infection include chills, fever, cough, anaemia, skin lesions, leukocytosis, and acne-like pustules and nodules on the face, trunk and extremities.[45] Without treatment, infection from *P. marneffei* is fatal.

2.1.3 Important Drugs Derived from Penicillium sp.

Despite the degradative processes that *Penicillium* sp. are involved in, they are also a highly useful source of medicinal drugs. Some of the most important drugs of the twentieth century have originated from *Penicillium* sp. of fungi. These include the antibiotic penicillin G, the cholesterol-lowering statins, and the antifungal agent, griseofulvin.

2.1.3.1 The 20th Century Wonder Drug: Penicillin.

The penicillins were the first natural product antibiotics discovered and came from a *Penicillium* sp. The initial discovery was made by Sir Alexander Fleming in 1928, when he noticed zones of inhibition on *Staphylococcus aureus* cultures contaminated with *P. notatum*.[46]

Despite this important discovery the clinical potential of the active agents produced by *Penicillium* sp. were not exploited fully. It was not until WWII that an international research effort was conducted. The object was to produce penicillin (Penicillin G) on a large scale. The effort resulted in enough penicillin to supply all the allied forces by the end of the war. The joint industrial and academic collaboration was second only in manpower and cost to the Manhattan Project. The research found that all the penicillins have a common nucleus based on a fused β-lactam-thiazolidine system.[39]

Penicillin G (**2.2**) was found to have many flaws including being active against gram-positive bacteria only. The other shortcomings included being broken down in the stomach by gastric acid and poor absorption in the blood stream. It was also found that many species of *Staphylococcus* were able to enzymatically inactivate Penicillin G.[47] For this reason several semi-synthetic derivatives were produced. These include ampicillin (**2.3**) and methicillin (**2.4**). In the case of ampicillin (**2.3**), the increased polarity gave greater activity against gram positive bacteria. In the case of methicillin (**2.4**), the bulky group attached to the amino acid side chain provides steric hindrance, which interferes with the attachment of the *Staphylococcus* enzyme.[47]

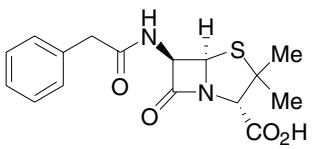

2.2

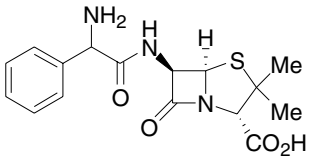

2.3

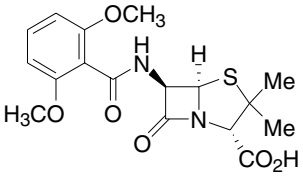

2.4

All penicillins have the same mode of action, inhibition of bacterial cell wall synthesis. More specifically, penicillins prevent the cross-linking of peptides on the mucosaccharide chains.[47]

2.1.3.2 The Statins

Discovery of the first statin resulted from the research of Akira Endo. For the answer to lowering cholesterol, he looked toward microbes, as he believed that some microbes would produce metabolites that inhibited HMG-CoA reductase (the first committed step in cholesterol biosynthesis), most likely as a defence mechanism against other microbes that needed sterols or other mevalonate-derived isoprenoids for growth.[48] Focussing on fungi and mushrooms as sources of suitable compounds, a search of over 6000 fungi was conducted over a 2 year period. The result was the discovery that a metabolite produced by the fungus *P. citrinum* inhibited lipid synthesis. The inhibiting compound became known as mevastatin (**2.5**).

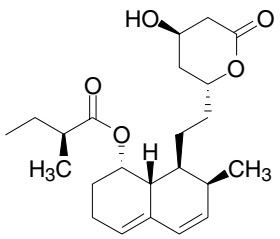

2.5

Clinical trials in 1978 went ahead, and by the mid 1980s it was found that mevastatin (**2.5**) lowered total plasma cholesterol and LDL-cholesterol by 20-40% with no serious

side effects.[48] This important discovery sparked intensive development of other cholesterol-lowering drugs, and since then a number of statins have been established as effective and safe cholesterol-lowering agents, and have been used by tens of millions of patients.[48]

2.1.3.3 Griseofulvin

The antifungal drug, griseofulvin (**2.6**) was first isolated in 1939 from *P. griseofulvum*.[49] The drug is used to treat skin infections such as jock itch, athlete's foot, ringworm and fungal infections of the scalp, fingernails and toenails.[50]

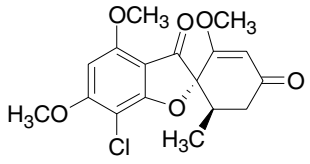

2.6

The mode of action is inhibition of fungal mitosis, where the mitotic spindle is disrupted through interaction with polymerised microtubules.[51]

2.2 Introduction

The species of *Penicillium* fungus in this study was isolated from driftwood on the foreshore of a beach in Vancouver, B.C, Canada. Mr Matthew Walters from the School of Biological Sciences purified, cultured on a small scale, and extracted this fungus a number of years ago. Since this time the extract remained frozen at -80°C.

2.3 Preliminary Investigations

The crude extract was submitted for biological testing using the in-house assay system. The extract showed no P388 activity, nor did it show antimicrobial activity. Remarkably, however it showed an antiviral activity of 4+, specific only to *Herpes simplex* virus

(HSV) (Section 7.1.6). For this reason alone the extract was pursued further. An aliquot of the crude extract was chromatographed on reverse phase C18 HPLC, using the standard gradient (Section 7.1.4). This showed the extract to have a fairly simple composition, whereby a group of three, clearly related compounds, eluting between 12-13 minutes were shown to represent the majority of the mass of the extract (Figure 2.1).

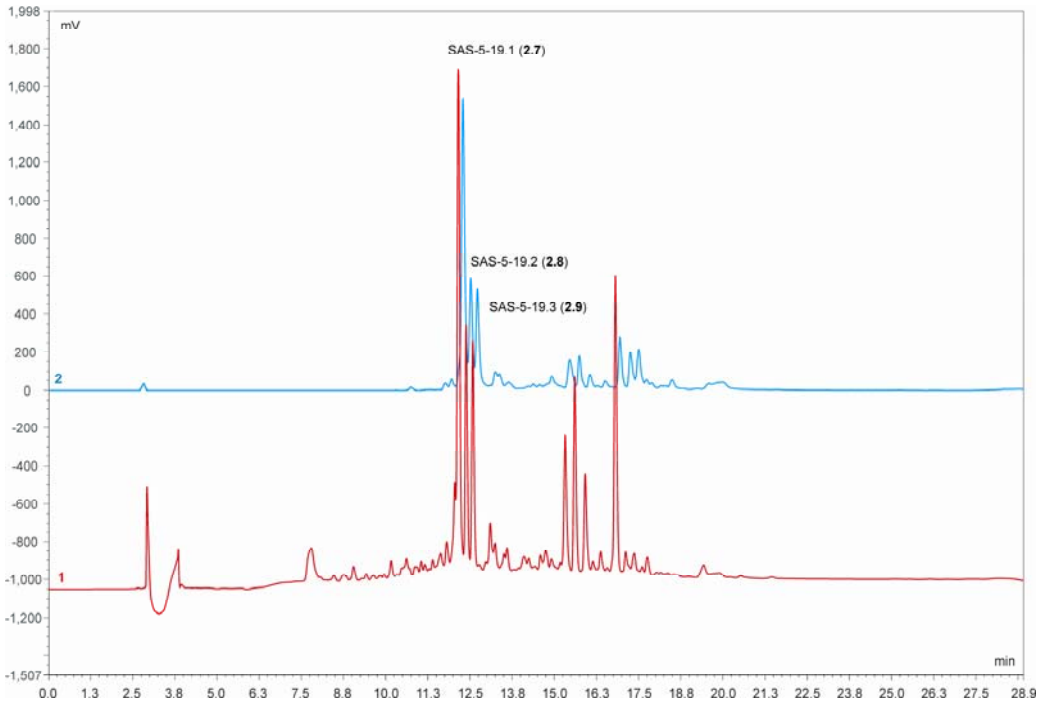

Figure 2.1: *HPLC chromatogram of F2028 showing overlay of ELSD detection (Blue).*

These three compounds were shown to have virtually identical UV chromophores, suggesting that they were very closely related in structure (Figure 2.2).

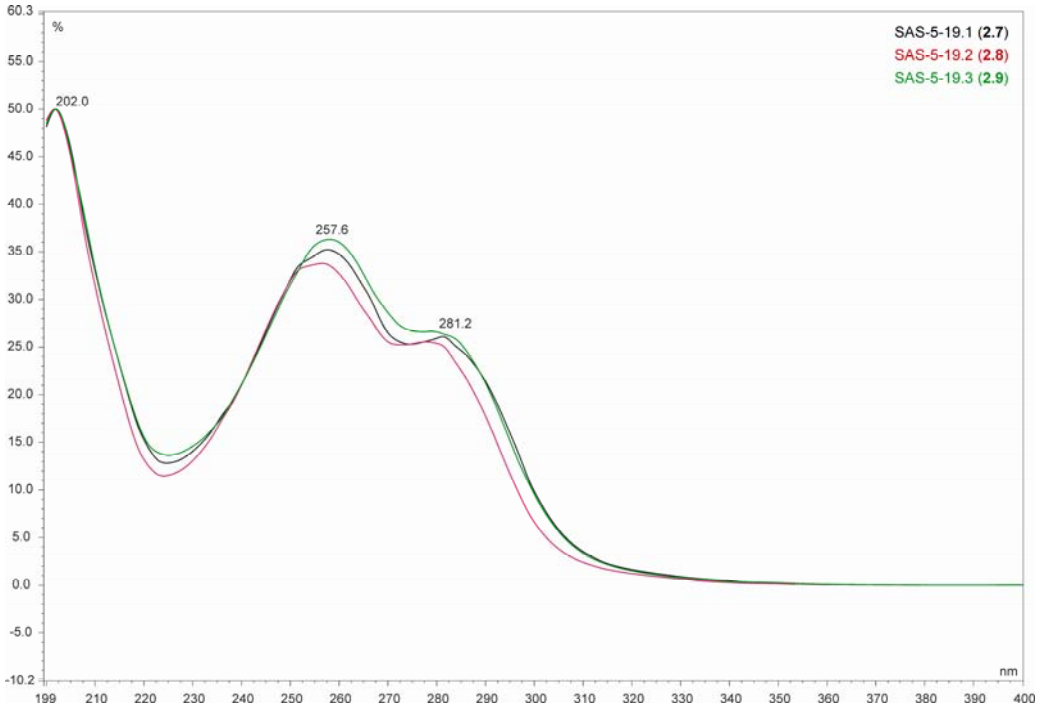

Figure 2.2: *UV profile overlay for SAS-5-19.13(**2.72.9**).*

The antiviral activity shown by the crude extract was proposed to be due to at least one of the compounds eluting between 12-13 minutes in the HPLC. The reason for this is that another extract (F2029) was also shown to contain only the compound eluting at 12.2 minutes, and it displayed identical HSV specific activity (Figure 2.3).

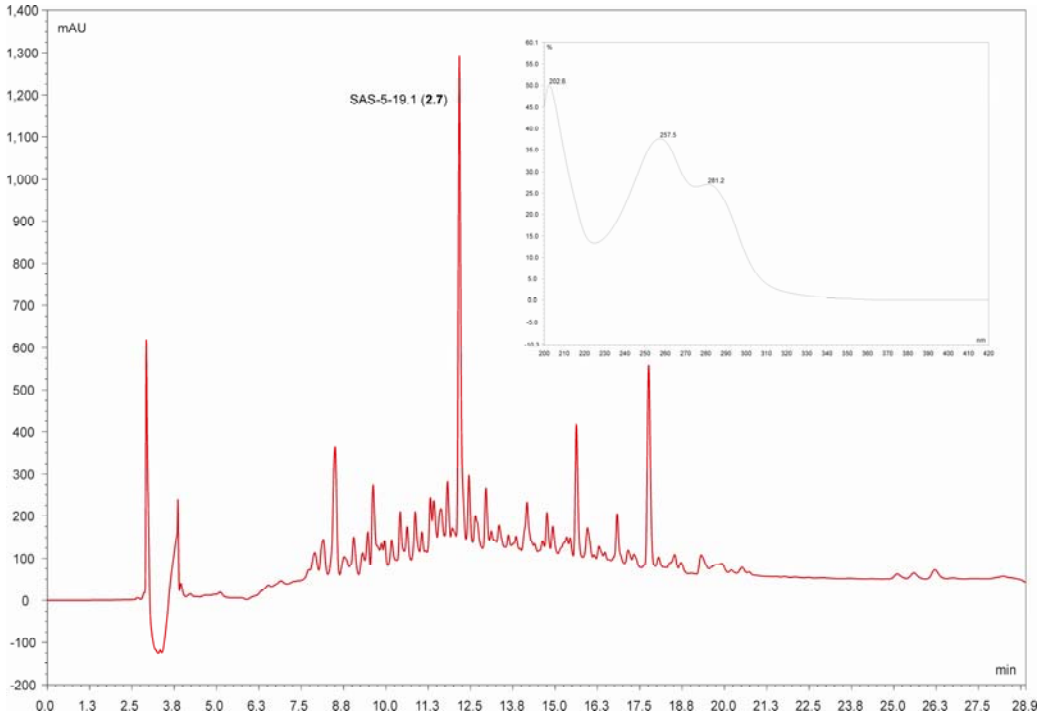

Figure 2.3: *HPLC chromatogram of F2029, with inset of the UV profile for the peak at 12.2 minutes*

2.4 Chromatography of F2028

Method development using analytical HPLC, was followed by semi-preparative HPLC (see Experimental, Section 7.3.1) and resulted in the three compounds, SAS-5-19.1–3 being isolated.

2.5 Structural Elucidation

*2.5.1 Structural Elucidation of SAS-5-19.1 (**2.7**)*

SAS-5-19.1 (**2.7**) was the major compound isolated from the extract of the *Penicillium* sp. ESIMS of an aliquot of SAS-5-19.1, collected from the HPLC gave the mass of the compound as 432 $[M+H]^+$. The ^1H NMR spectrum (Figure 2.4) showed three methyl

signals, at δ_H 0.90, 1.65, and 3.26, the latter as a methoxyl. Also present were three signals showing oxymethine-like chemical shifts at δ_H 4.38, 4.42, and 4.47.

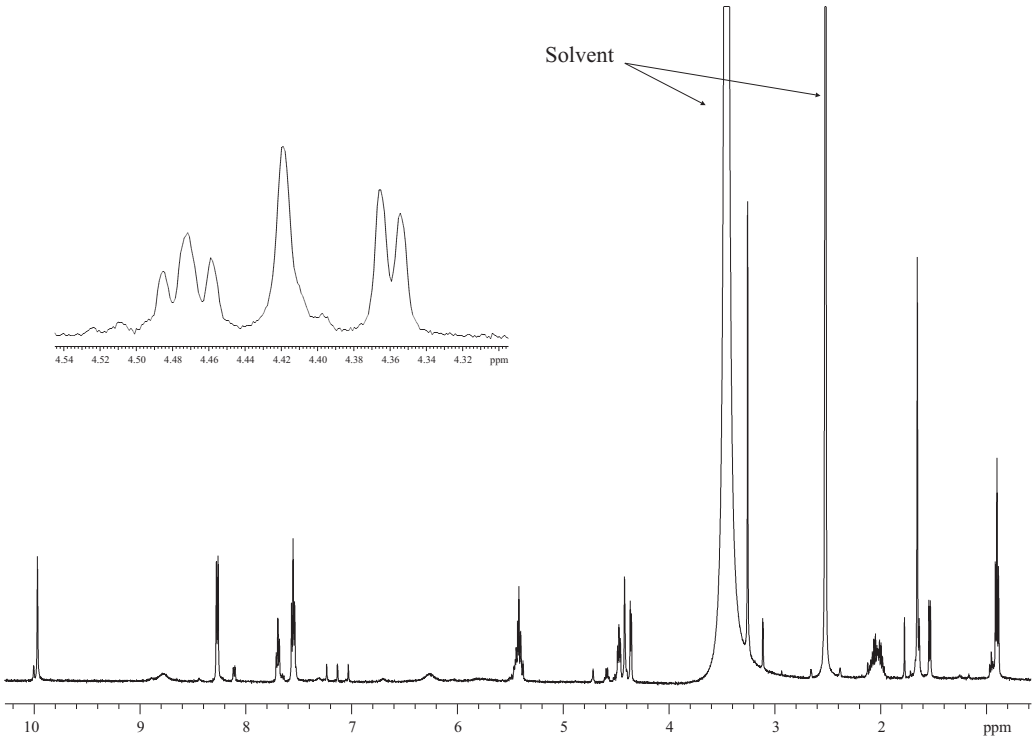

Figure 2.4: *^{1}H NMR spectrum of pseurotin A (**2.7**)in d_6-DMSO.*

Characteristic aromatic signals were shown between δ_H 7.50–8.30, the multiplicity and integrals indicating the aromatic system as a monosubstituted benzene ring. This was indicated by the 2:1:2 integral ratio of the doublet, triplet, triplet arrangement of the aromatic protons respectively (Figure 2.5). The three remaining signals were two multiplets at δ_H 5.40 and 2.05, and a singlet at 9.94. The integral and chemical shift of the signal at δ_H 5.40, indicated that it represented two protons. These were probably part of a double bond moiety. Given the chemical shift and the complex multiplicity the signal at δ_H 2.05 was proposed to be a methylene adjacent to at least a methyl group. The chemical shift of the singlet at δ_H 9.94 indicated it as an exchangeable proton on either an oxygen or nitrogen. Because **2.7** was of odd mass, it was proposed that this was a proton attached to nitrogen.

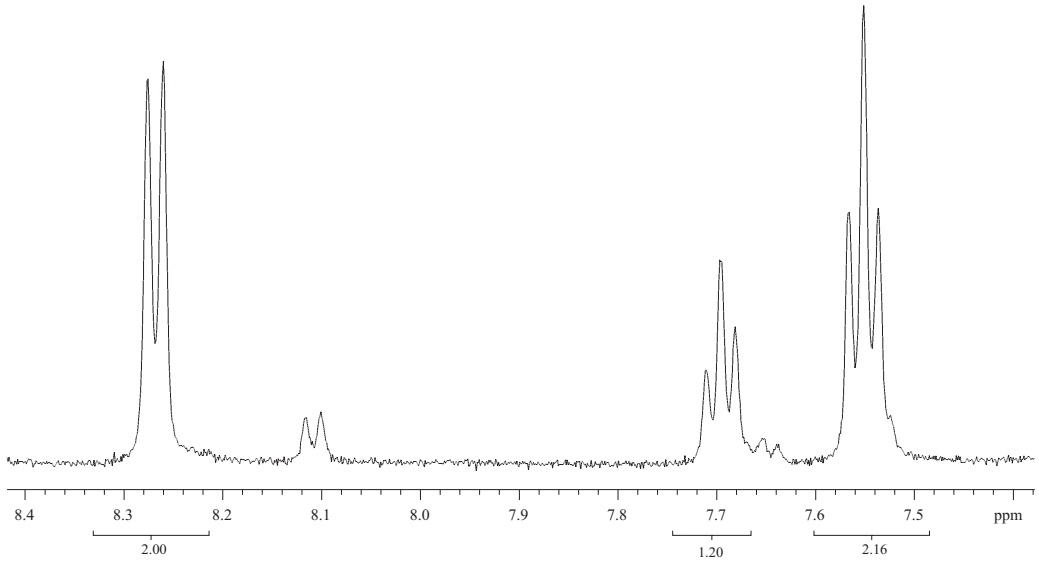

Figure 2.5: *Aromatic region of the ^{1}H NMR spectrum of* ***2.7*** *showing multiplicity and integrals.*

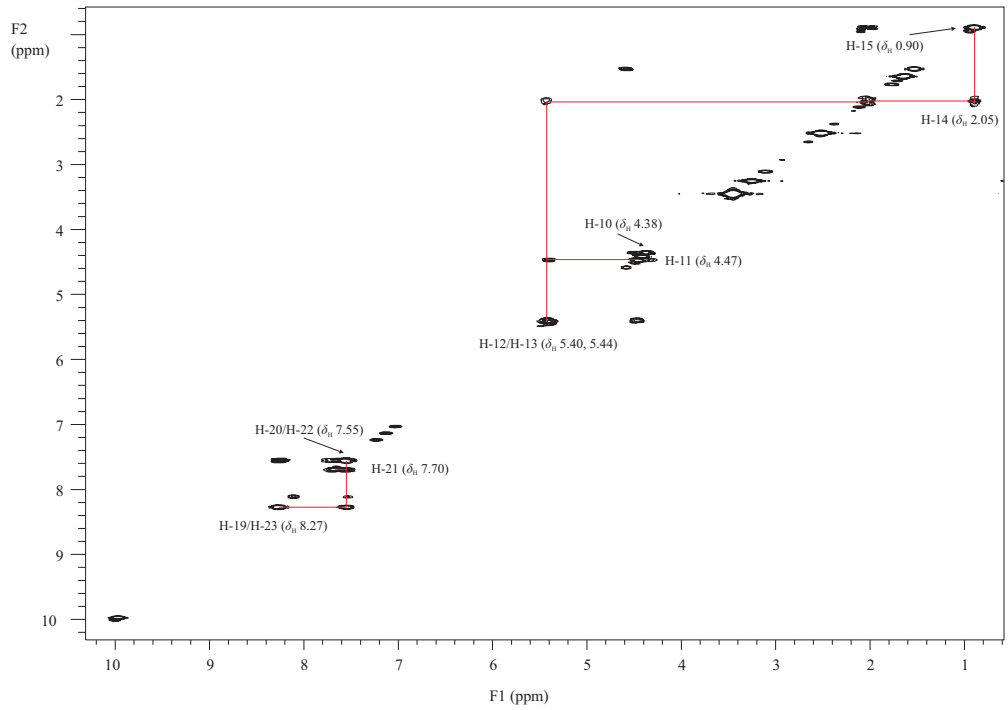

Figure 2.6: *COSY NMR spectrum of* ***2.7*** *in d_6-DMSO showing the aromatic and aliphatic spin systems.*

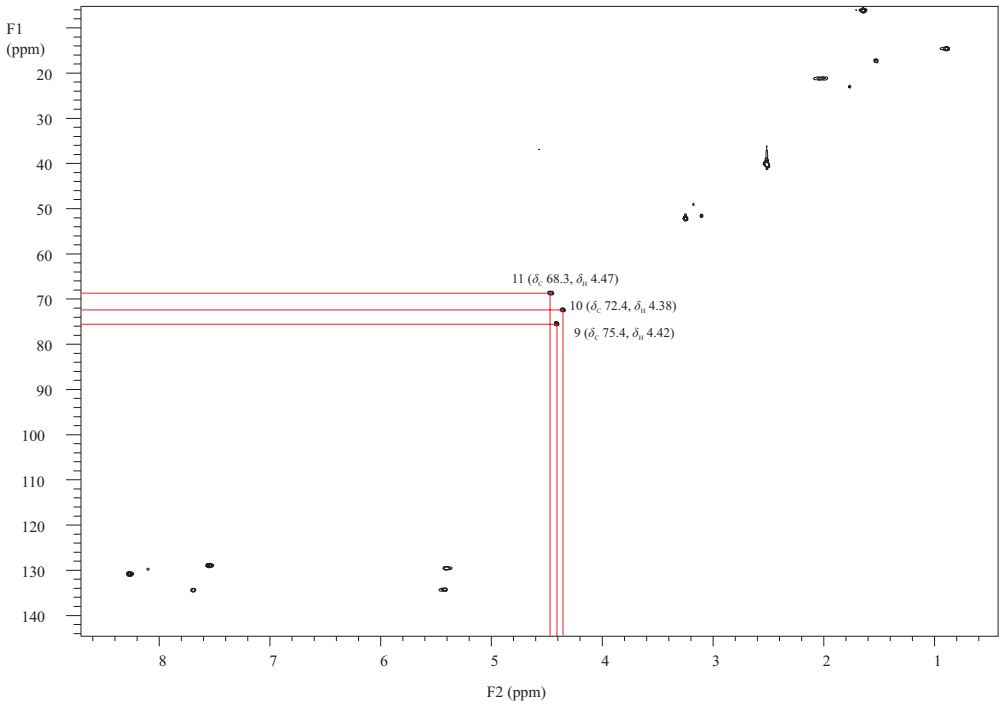

Figure 2.7: *HSQC-DEPT NMR spectrum in d_6-DMSO of* ***2.7****, highlighting the oxymethine signals.*

The COSY and HSQC NMR spectra (Figure 2.6 and Figure 2.7 respectively) confirmed the existence of two spin systems, a monosubstituted benzene (Figure 2.8a), and an aliphatic chain containing diol and double bond functionalities (Figure 2.8b).

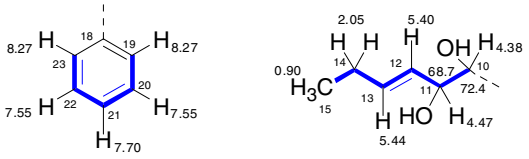

Figure 2.8: *Spin systems* ***a*** *and* ***b*** *for* ***2.7***

The benzene unit showed coupling of the triplet protons at δ_H 7.55 (H-20, H-22) to a triplet proton at δ_H 7.70 (H-21) and doublet protons at δ_H 8.27 (H-19, H-23). These protons showed $^1J_{CH}$ correlations to carbons at δ_C 129.0 (C-20, C-22), 134.5 (C-21), and 130.8 (C-19, C-23) respectively. The second system was characterised by a terminal methyl group at δ_H 0.90 (H-15) coupled to the methylene protons at δ_H 2.05 (H-14). Both

these groups of protons each showed $^1J_{CH}$ correlations to carbons at δ_C 14.6 and 21.1 respectively. The methylene protons also showed coupling to the overlapping proton at δ_H 5.44 (H-13), which in turn was coupled to the other double bond proton at δ_H 5.40 (H-12). These olefinic protons had $^1J_{CH}$ correlations to carbons at δ_C 129.5 and 134.3 respectively, thus confirming the olefinic nature of these protons and carbons. H-12 was also coupled to one of the oxymethine protons at δ_H 4.47 (H-11), which in turn showed coupling to another oxymethine proton at δ_H 4.38 (H-10). The oxymethine protons were confirmed, as such by $^1J_{CH}$ correlations to carbons at δ_C 68.7 (C-11) and 72.4 (C-10) respectively. Although no OH proton resonances were identifiable in the ^{1}H NMR spectrum, the chemical shifts of the oxymethine protons and carbons were consistent with a diol functionality. A vicinal diol, rather than epoxide was proposed based on chemical shift arguments. The protons and their respective carbons in an epoxide, would have had substantially higher field chemical shifts.

Apart from the proton signals of the methyl at δ_H 1.65 (δ_C 6.1), the methoxyl at δ_H 3.26 (δ_C 52.2), the remaining oxymethine at δ_H 4.42 (δ_C 75.4), there were no further HSQC correlations. This indicated that the balance of the carbons seen in the CIGAR spectrum (δ_C 91.6, 93.0, 112.0, 133.7, 167.1, 187.4, 196.9, and 197.3), were all quaternary. From the chemical shifts of the latter four carbons, it was presumed they were all carbonyl groups. It was unclear however, the identity of the former three carbons, as their chemical shifts were suggestive of olefinic, acetal or some other oxygen-shifted non-aromatic functionality. The carbon at δ_C 133.7, because of its chemical shift, was presumed to be the aromatic carbon at the point of substitution.

At this point a search of the AntiMarin database was conducted. A partial structure search was carried out using the mass and the two spin systems presented in Figure 2.8a and b as parameters. This revealed a match with a compound known as pseurotin A (**2.7**).[52] The ^{1}H NMR spectrum of **2.7** was compared to that of pseurotin A in the literature and was found to be identical.

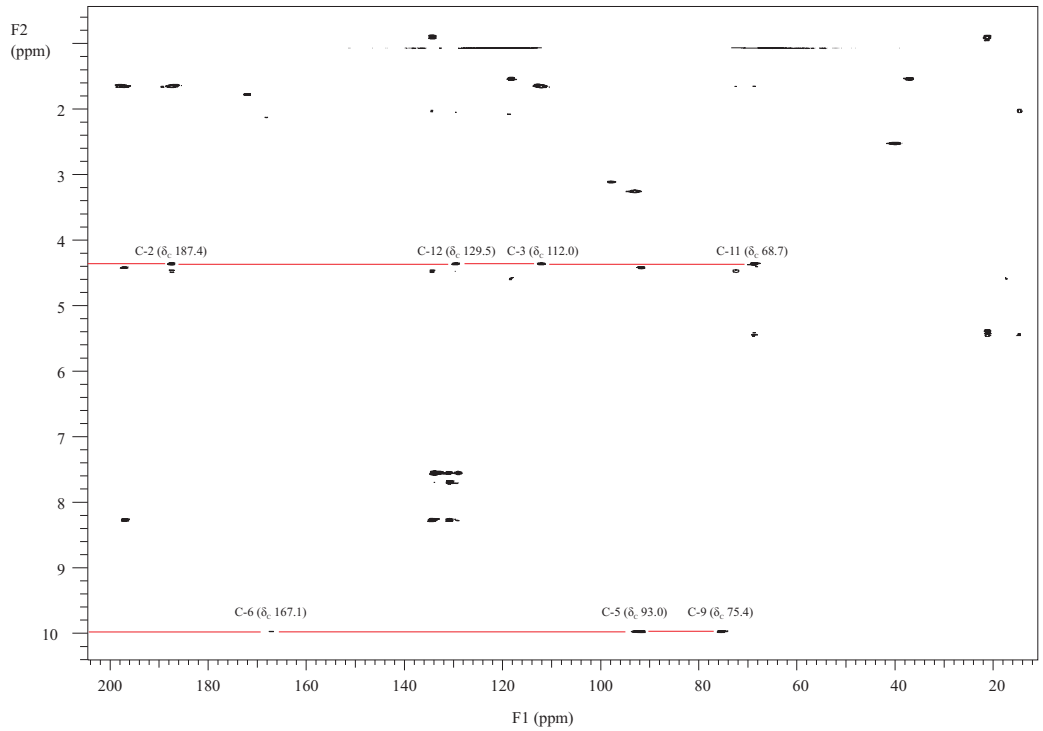

Figure 2.9: *CIGAR NMR spectrum of* ***2.7*** *in d_6-DMSO, showing the couplings that confirm the assignments for carbons at C-6 and C-2.*

The data from the CIGAR NMR spectrum was used as a final confirmation, that **2.7** was pseurotin A (Figures 2.9 and 2.10). The $^{2,3}J_{CH}$ correlations displayed by the methyl at δ_H 1.65 (H-16) to carbons at 112.0 (C-3), 187.4 (C-2), and 197.3 (C-4), confirmed the furanone portion of the molecule, while CIGAR correlations from H-10 to the carbons at C-2 and C-3 confirmed the attachment of the aliphatic side chain to the furanone. There was however one discrepancy, the chemical shift of C-2 was ~20 ppm higher than the equivalent carbon in the literature.

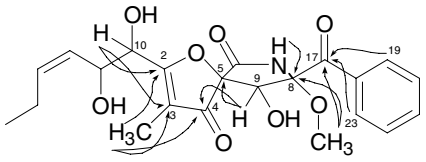

Figure 2.10: *CIGAR NMR correlations confirming* ***2.7*** *as pseurotin A.*

The pyrrolidinone was confirmed through the CIGAR correlations from both the oxymethine proton at δ_H 4.42 (H-9) and the NH proton at δ_H 9.94 (H-7). In the case of H-9 this was to a carbon at δ_C 91.6 (C-5), and for H-7 to carbons at δ_C 93.0 (C-8), and 167.1 (C-6). A correlation from H-9 to the carbonyl at C-4 confirmed the proximity of the furanone to the pyrrolidinone. Once again, however, there was a discrepancy in chemical shifts of **2.7** compared to those recorded in the literature. This time it involved the chemical shift of C-6, which according to our data was ~20 ppm less than that for the equivalent carbon in the literature. It was then realised that the literature chemical shifts were wrong, in that the carbons at C-2 and C-6 had been missassigned by inadvertently swapping the chemical shifts. Given that the structures were first reported in the late seventies, this was not surprising as 2D NMR techniques were not available. In the more recent literature this mistake had been acknowledged and corrected.[53] CIGAR correlations from the aromatic protons at H-19 and H-23 to the carbonyl carbon at δ_C 196.9 (C-17), showed the attachment of the benzene ring to a ketone, of which was shown to be connected to the rest of the molecule by a $^3J_{CH}$ CIGAR correlation from the methoxyl protons at δ_H 3.26. The methoxyl itself, was shown to be connected to C-8 through a $^3J_{CH}$ correlation. Comparison of literature and experimental NMR data is presented in Table 2.1.

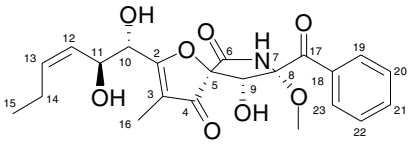

2.7

Table 2.1: *Literature and Experimental NMR data for* ***2.7****.*

position	Literature δ_C, ppm[a]	Literature δ^1H, multiplicity (J_{HH} Hz) [b]	δ_C[c], ppm[d]	δ^1H, multiplicity (J_{HH} Hz)	COSY	CIGAR
2	166.6		187.4(C)			
3	111.6		112.0(C)			
4	196.7		197.3(C)			
5	92.4		93.0 (C)			
6	186.8		167.1(C)			
7-NH		9.90, s		9.97, s		C-9, C-5, C-6
8	91.1		91.6 (C)			
9	75.3	4.41, s	75.4 (CH)	4.42, s		C-8, C-4
10	72.8	4.2-4.6, m	72.4 (CH)	4.38, d (5.5)	H-11	C-2, C-12, C-3, C-11
11	68.3	4.2-4.6, m	68.7 (CH)	4.47, t (6.7, 6.7)	H-12, H-10	C-10, C-13, C-2
12	128.4	5.1-5.7, m	129.5(CH)	5.40, m	H-11	C-14
13	134.0	5.1-5.7, m	134.3(CH)	5.44, m	H-14	C-14, C-11
14	20.6	2.10, m	21.1 (CH_2)	2.05, m	H-15, H-13	C-15, C-13
15	14.1	0.90, t (7.0, 7.0)	14.6 (CH_3)	0.90, t (7.6, 7.6)	H-14	C-13, C-14
16	5.6	1.65, s	6.1 (CH_3)	1.65, s		C-4, C-3, C-2
17	196.4		196.9(C)			
18	133.6		133.7(C)			
19	130.2	8.2-8.4, m	130.8(CH)	8.27, d (7.3)	H-20	C-17, C-21, C-23
20	128.4	7.4-7.8, m	129.0(CH)	7.55, t (7.3, 7.3)	H-19, H-21	C-21, C-19, C-22
21	133.6	7.4-7.8, m	134.5(CH)	7.70, t (7.3)	H-20, H-22	C-19, C-23
22	128.4	7.4-7.8, m	129.0(CH)	7.55, t (7.3)	H-21, H-23	C-21, C-23, C-20
23	130.2	8.2-8.4, m	130.8(CH)	8.27, d (7.3)	H-22	C-17, C-21, C-19
OCH_3	51.7	3.26, s	52.2 (CH_3)	3.26, s		C-8

[a] ^{13}C NMR data obtained at 22.63 MHz in d_6-DMSO[54,55]
[b] Data obtained at 100 MHz in d_6-DMSO[55]
[c] ^{13}C multiplicity determined from HSQC-DEPT experiments
[d] Chemical shifts determined from HSQC and CIGAR experiments.
^{1}H and 2D NMR data obtained at 500 MHz in d_6-DMSO.

The stereochemistry of **2.7**, was also confirmed as identical to pseurotin A, as an optical rotation (-10 °), revealed a similar value, within experimental error, as that given in the literature, $[\alpha]^{20}_D$ -5±1° (*c* 0.5, MeOH).[55] The compound, **2.7**, was therefore confirmed as the known compound, pseurotin A.

*2.5.2 Structural Elucidation of SAS-5-19.2 (**2.8**)*

ESIMS on compound SAS-5-19.2 (**2.8**) gave an identical mass to that of **2.7**, 432 ($[M+H]^+$). Because of this, and the identical UV chromophore displayed by both **2.7** and **2.8**, it was proposed that **2.8** was a stereoisomer of **2.7**. Initially, the ^{1}H NMR spectrum (Figure 2.11) was taken to indicate that these compounds were in fact not isomeric. This

was due to the presence of three extra signals that were not seen in the ^{1}H NMR spectrum of pseurotin A (**2.7**).

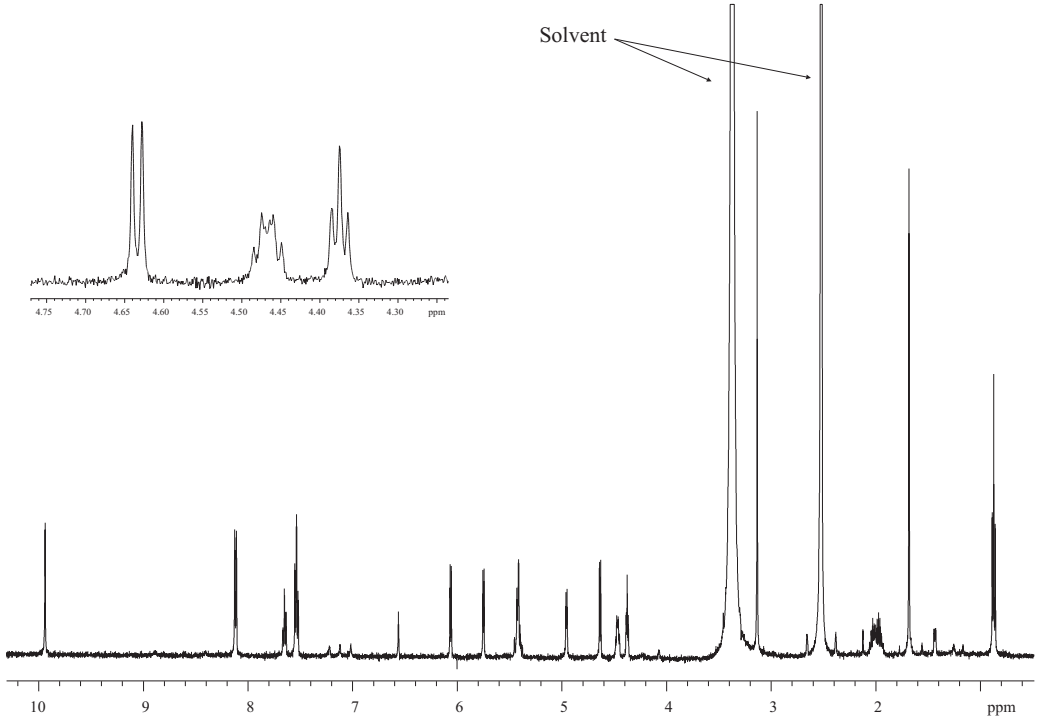

Figure 2.11: *^{1}H NMR spectrum of pseurotin A_2 (**2.8**) in d_6-DMSO.*

The HSQC NMR experiment established that the three extra protons were the exchangeable protons of hydroxyl groups, as no $^1J_{CH}$ correlations to any carbons were seen. Excluding these hydroxyl proton signals, the ^{1}H NMR spectrum was more or less identical to that of **2.7**, with the exception of slight variations in chemical shifts. Additional 2D NMR experiments, including COSY and CIGAR, determined that structurally **2.8**, was identical to **2.7**. The difference therefore, as noted must lie with the stereochemistry. As there have been no stereoisomers of pseurotin A reported in the literature, **2.8**, qualifies as a new diastereomer of pseurotin A. On this basis the compound was named pseurotin A_2. Full NMR assignments for **2.8** are presented in Table 2.2.

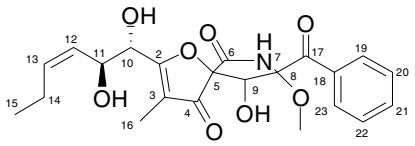

2.8

Table 2.2: *NMR data for* ***2.8***

position	δ_C[a], ppm[b]	δ^1H, multiplicity (J_{HH} Hz)	COSY	CIGAR
2	188.0 (C)			
3	111.7 (C)			
4	200.5 (C)			
5	88.6 (C)			
6	167.7 (C)			
7-NH		9.94, s		C-8, C-5, C-9
8	97.4 (C)			
9	76.1 (CH)	4.64, d (5.9)	OH-9	C-8, C-4, C-6
10	73.0 (CH)	4.38, t (5.3, 5.3)	OH-10, H-11	C-2, C-12, C-3, C-11
11	68.8 (CH)	4.47, m	H-13, OH-11, H-10	NA
12	129.5 (CH)	5.40, m	H-11	C-10, C-14
13	134.2 (CH)	5.41, m	H-14	C-14,
14	21.0 (CH_2)	2.01, m	H-15, H-13	NA
15	14.0 (CH_3)	0.88, t (7.4, 7.4)	H-14	C-13, C-14
16	5.5 (CH_3)	1.68, s		C-4, C-3, C-2
17	194.0 (C)			
18	135.1 (C)			
19	130.0 (CH)	8.12, d (7.7)	H-20	C-17, C-21, C-23
20	128.8 (CH)	7.54, t (7.7, 7.)	H-19, H-21	C-18, C-19, C-22
21	133.7 (CH)	7.65, t (7.7)	H-20, H-22	C-19, C-23
22	128.8 (CH)	7.54, t (7.7)	H-21, H-23	C-18, C-23, C-20
23	130.0 (CH)	8.12, d (7.7)	H-22	C-17, C-21, C-19
OCH_3	51.3 (CH_3)	3.14, s		C-8
9-OH		6.07, d (6.4)	H-9	C-8, C-9
10-OH		5.75, d (5.4)	H-10	C-2, C-11, C-10
11-OH		4.96, d (5.5)	H-11	C-12

[a] ^{13}C multiplicity determined from HSQC-DEPT experiment
[b] Chemical shifts determined from HSQC and CIGAR experiments
^{1}H and 2D NMR carried out at 500 MHz in d_6-DMSO.
NA-signals not observed

*2.5.3 Structural Elucidation of SAS-5-19.3 (**2.9**)*

Like the previous two compounds, **2.7**, and **2.8**, SAS-5-19.3 (**2.9**) was shown by ESIMS to have a mass of 432 $[M+H]^+$. Once again it was proposed that **2.9** was a stereoisomer of the known compound pseurotin A (**2.7**).

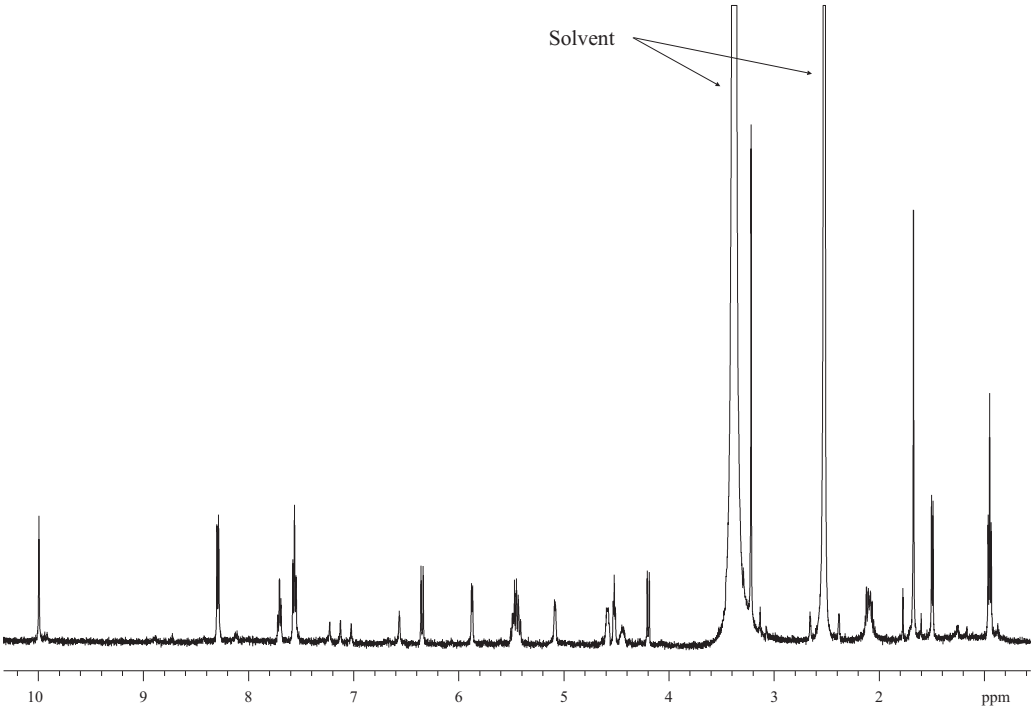

Figure 2.12: *^{1}H NMR spectrum of pseurotin A_3 (**2.9**) in d_6-DMSO.*

The ^{1}H NMR spectrum (Figure 2.12) and HSQC spectrum showed that as in the case of pseurotin A_2 (**2.8**), the hydroxyl protons were visible. Once again exclusion of the hydroxyl protons, resulted in a ^{1}H NMR spectrum that was almost identical to that for **2.7**. The remaining 2D NMR data were very similar and hence consistent with the structural aspects of the pseurotin A skeleton. This confirmed that **2.9** was yet another stereoisomer of **2.7**. The new diastereomer was assigned the name pseurotin A_3 (**2.9**). 1D and 2D NMR assignments are presented in Table 2.3.

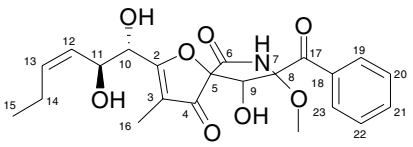

2.9

Table 2.3: *NMR data for* ***2.9***

position	δ_C[a], ppm[b]		δ^1H, multiplicity (J_{HH} Hz)	COSY	CIGAR
2	188.6	(C)			
3	112.8	(C)			
4	201.8	(C)			
5	87.6	(C)			
6	167.8	(C)			
7-NH			9.99, s		C-6, C-8, C-5, C-9
8	95.2	(C)			
9	74.8	(CH)	4.20, d (9.8)	OH-9	C-4, C-17
10	72.3	(CH)	4.52, t (5.1, 5.1)	OH-10, H-11	NA
11	68.4	(CH)	4.59, m	H-12, OH-11, H-10	NA
12	129.1	(CH)	5.43, m	H-11	NA
13	134.5	(CH)	5.47, m	H-14	C-14, C-15
14	21.1	(CH_2)	2.10, m	H-15, H-13	C-6
15	14.6	(CH_3)	0.95, t (7.4, 7.4)	H-14	C-13, C-14
16	6.0	(CH_3)	1.67, s		C-4, C-2, C-3
17	196.4	(C)			
18	134.2	(C)			
19	130.7	(CH)	8.28, d (7.7)	H-20	C-17, C-21, C-23
20	128.9	(CH)	7.56, t (7.7, 7.)	H-19, H-21	C-18
21	134.5	(CH)	7.71, t (7.7)	H-20, H-22	C-20, C-22
22	128.9	(CH)	7.56, t (7.7)	H-21, H-23	C-18
23	130.7	(CH)	8.28, d (7.7)	H-22	C-17, C-21, C-19
OCH_3	52.0	(CH_3)	3.23, s		C-8
9-OH			6.35, d (9.8)	H-9	C-8, C-9
10-OH			5.88, d (5.3)	H-10	NA
11-OH			5.09, d (4.7)	H-11	NA

[a] multiplicity determined by HSQC-DEPT experiments
[b] ^{13}C shifts determined from HSQC and CIGAR experiments
^{1}H and 2D NMR carried out at 500 MHz in DMSO-d_6
NA-signals not observed

2.5.4 Stereochemical Elucidation of Pseurotins A_2 and A_3

As the pseurotins contain five chiral centres, a systematic approach was taken to define the chirality at each centre.

*2.5.4.1 Stereochemical Elucidation of Pseurotin A_2 (**2.8**)*

An attempt at crystallisation in MeOH was successful, and produced very small crystals of low quality. Despite this, the crystals were found to diffract reasonably well and for this reason, were able to be used for X-ray crystallography. The solution of the X-ray data showed two molecules were present in an asymmetric unit, resulting in eight molecules per cell. Although the R-factor was high (15.8%), the assignment of the

relative stereochemistry of **2.8** was possible and given as 5*S**, 8*S**, 9*S**, 10*S**, 11*S** (Figure 2.13). For X-ray crystal data tables see appendix 1.

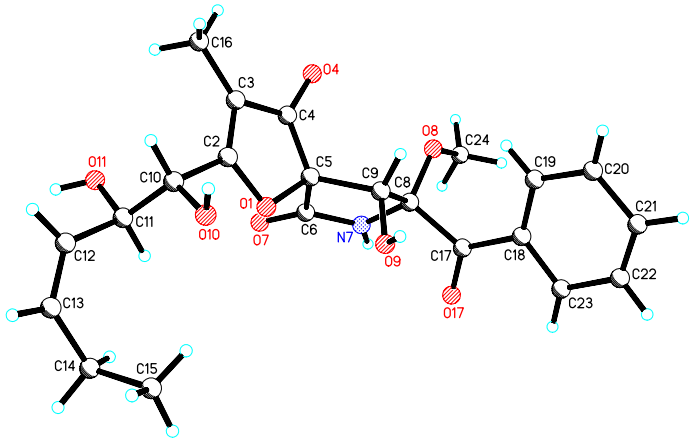

Figure 2.13: *Crystal structure drawing of* ***2.8****.*

More tentative conclusions were made as to the absolute stereochemistry of **2.8**. This involved the use of circular dichroism (CD) spectroscopy. This technique measures the difference in absorption of left-handed versus right-handed circularly polarised light, which arises due to the structural asymmetry of a molecule.

It was determined that the stereocentre at C8 could definitely be identified by this method due to the presence of the adjacent strong phenyl ketone chromophore. Although there is also a strong chromophore adjacent to C5, it is of a shorter wavelength, which was unable to be measured on the elderly spectropolarimeter available in the Department of Chemistry.

The identical nature of the traces shown by all three of the stereoisomers, A, A_2 and A_3, indicated that the stereocentre at C8 in pseurotin A_2 was the same as that in pseurotin A and A_3 (see Figure 2.14).

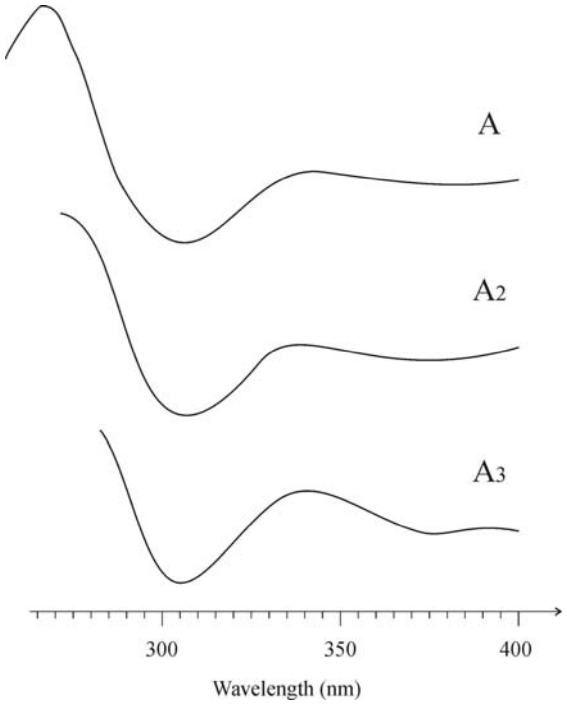

Figure 2.14: *CD spectra of pseurotins A-A3 (**2.7-2.9**).*

The chirality of all stereocentres for the known isomer, pseurotin A had previously been established as 5*S*, 8*S*, 9*R*, 10*S*, 11*S* by X-ray crystallography of a brominated derivative.[56] This meant that the relative stereochemistry provided by X-ray crystallography could be converted to an overall absolute stereochemistry, which was 5*S*, 8*S*, 9*S*, 10*S*, 11*S* (Figure 2.15).

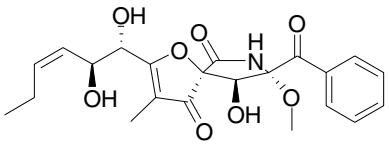

Figure 2.15: *Proposed absolute stereochemistry of pseurotin A2 (**2.8**)*

*2.5.4.2 Stereochemical Elucidation of Pseurotin A3 (**2.9**)*

The stereochemical elucidation of **2.9** was not as straight forward as that for **2.8**, primarily because it could not be successfully crystallised. Through X-ray crystallography it had been established that the isomers **2.7** and **2.8** had the same chirality

at the C-10 and C-11 stereocentres. The ^{1}H and ^{13}C NMR data for the area around C10/C-11 for **2.7** and **2.8** were identical, as was expected, and the data for **2.9** was very similar.

In order for the stereochemical differences between **2.9** and **2.7**/**2.8** to be explored, the *vicinal*-diol was cleaved with sodium periodate under acidic conditions (Scheme 2.1). The idea was to remove the C-10 and C-11 stereocentres and so eliminate the possibility that the differences in the stereochemistry of **2.9** compared to **2.7**/**2.8** lay at the *vicinal*-diol.

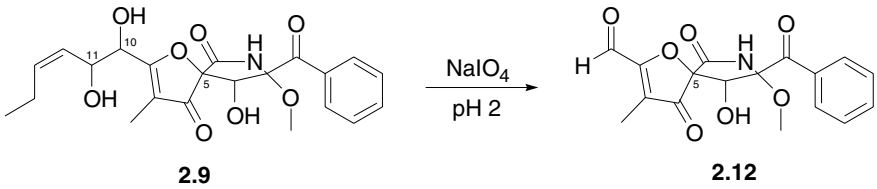

2.9 **2.12**

Scheme 2.1: *Oxidative cleavage using sodium periodate.*

HPLC (Figure 2.16) and ESIMS were used to analyse the resulting products of the reaction. The cleavage product of **2.9** showed a different retention time from both those of **2.7** and **2.8**.

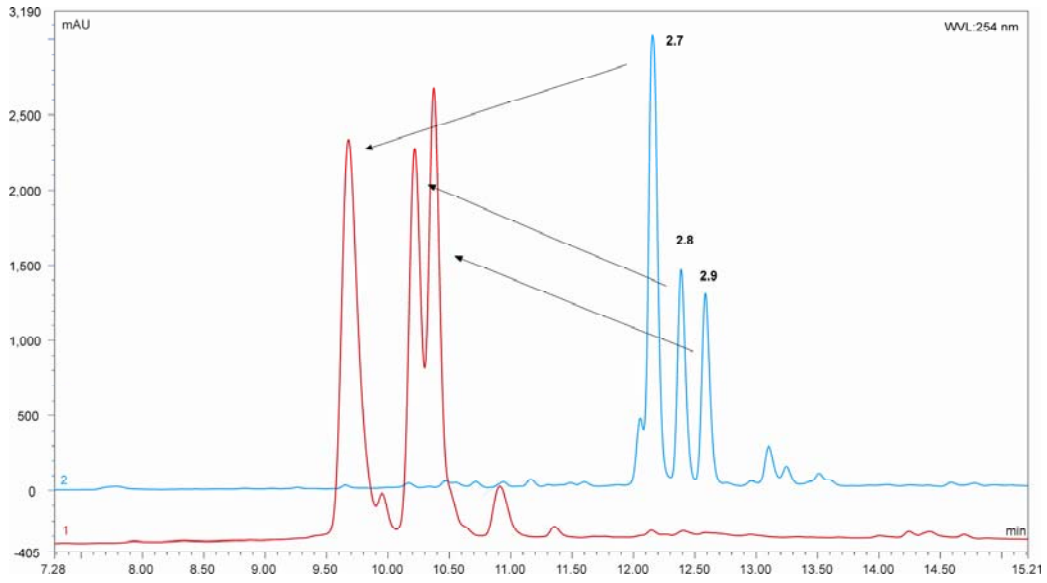

Figure 2.16: *HPLC chromatogram showing reaction products (red) of $NaIO_4$ cleavage.*

The difference in retention time for the cleavage products from **2.7** and **2.8** (9.75 and 10.25 minutes respectively) was expected as they have a diastereomeric relationship (Figure 2.17).

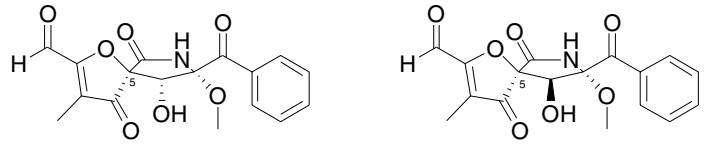

2.10 **2.11**

Figure 2.17: *Diasteromeric cleavage products of pseurotin A (**2.10**) and A_2 (**2.11**).*

This indicated that if there was a difference in stereochemistry at the diol of **2.9**, this was not the only difference when compared to **2.7**/**2.8**. If the *vicinal*-diol had been the only centre in the molecule with a different stereochemistry, the cleavage product of **2.9** would have shown the same retention time as either **2.7** or **2.8**, but it did not. As the cleavage products remained diastereomeric it was deduced that the C-5 chirality of pseurotin A_3 must be *R*- as an *S*-configuration would have led to the HPLC retention time of **2.12** being identical to either **2.10** or **2.11**, depending on the chirality at C-9.

An NMR approach was used to probe the stereochemistry of the remaining chiral centre, C-9. As there was a paucity of protons in the ring system in the vicinity of C-9, ^{1}H-^{1}H coupling constants, or NOE measurements were not suitable in this situation. The method used was measurement of long-range ^{1}H-^{13}C coupling constants. To measure this coupling constant, a more sensitive NMR technique was employed. This was a narrow-window CIGAR experiment with a higher resolution in *J*2 (carbon axis), and $^{3}J_{CH}$ couplings between H-9 and C-4 were measured for the three diastereomers.

The $^{3}J_{CH}$ for **2.7** and **2.9** were found to be <2 Hz each, whereas the measured value for **2.8** was found to be 2.8 Hz. The magnitude of $^{3}J_{CH}$ has a strong angular dependence on the dihedral angle ϕ (Figure 2.18).

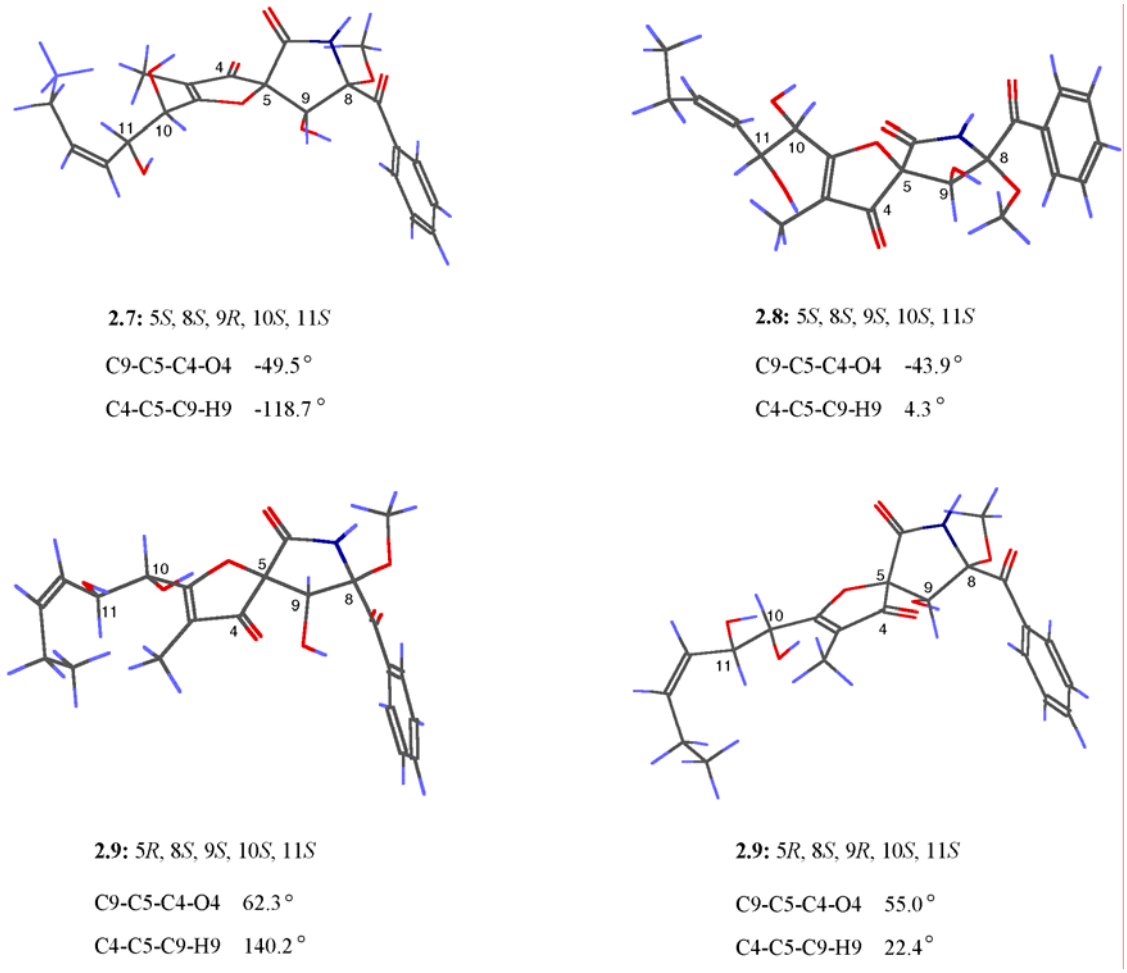

Figure 2.18: *Energy minimised (MM2) conformations for* ***2.7*** *and* ***2.8*** *as well as the two alternative MM2 conformations for* ***2.9****; each showing the H-9–H-4 dihedral angles (ϕ).*

For this reason it was concluded that the relative orientation of H-9 and C-4 were the same in **2.7** and **2.9**. Because the C-5 chirality of **2.9** had been assigned as *R*, the opposite configuration of C-5 in **2.7**, the angular dependence could only be met by assigning the C-9 chirality of **2.9** as *S*. The proposed stereochemistry for **2.9** therefore is 5*R*, 8*S*, 9*S*, 10*S*, 11*S* (Figure 2.19). The assignment of chirality at C-10 and C-11 is tentative and cannot be stated unambiguously and followed from the highly correlated ^{1}H and ^{13}C shifts for these diasteromers (see Table 2.4). That of **2.7** and **2.8** had been established by X-ray crystallography.

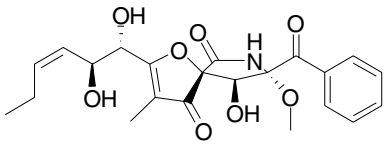

Figure 2.19: *Proposed stereochemistry for pseurotin A$_3$ (**2.9**).*

Table 2.4: *^{1}H- and ^{13}C NMR chemical shifts for the three pseurotins (**2.7**-**2.9**).*

	δ_C			δ_H		
position	**2.7**	**2.8**	**2.9**	**2.7**	**2.8**	**2.9**
2	187.4	188.0	188.6			
10	72.4	73.0	72.3	4.38, d (5.5)	4.38, t (5.3, 5.3)	4.52, t (5.1, 5.1)
11	68.7	68.8	68.4	4.47, t (6.7, 6.7)	4.47, m	4.59, m
12	129.5	129.5	129.1	5.40, m	5.40, m	5.43, m
13	134.3	134.2	134.5	5.44, m	5.41, m	5.47, m
14	21.1	21.0	21.1	2.05, m	2.01, m	2.10, m
15	14.6	14.0	14.6	0.90, t (7.6, 7.6)	0.88, t (7.4, 7.4)	0.95, t (7.4, 7.4)

All three purified compounds were subjected to the in-house antiviral assay. **2.7** was found to display antiviral activity against HSV of 4+, the diastereomers, **2.8** and **2.9** were found to be inactive against the virus. It was concluded therefore that the original antiviral activity displayed by the crude extract was the result of pseurotin A (**2.7**) only.

2.6 Discussion

Purification of the extract from a *Penicillium* sp. of fungus lead to the isolation of three pseurotins. These compounds, elucidated with 1D and 2D NMR techniques, included the known compound pseurotin A (**2.7**), and two previously unreported diastereomers of pseurotin A, pseurotin A$_2$ (**2.8**) and pseurotin A$_3$ (**2.9**).

The relative stereochemistry of **2.8** was provided by X-ray Crystallography as 5*S**, 8*S**, 9*S**, 10*S**, 11*S**. By comparison with that of the known compound **2.7**, CD spectroscopy was used to assign the absolute stereochemistry at C-8 as the *S*-configuration, leading to the proposal that the absolute stereochemistry of **2.8** was 5*S*, 8*S*, 9*S*, 10*S*, 11*S*. On the basis of CD spectroscopy, sodium periodate cleavage and *J*-resolved 2D NMR, **2.9** was assigned the absolute stereochemistry, 5*R*, 8*S*, 9*S*, 10*S*, 11*S*.

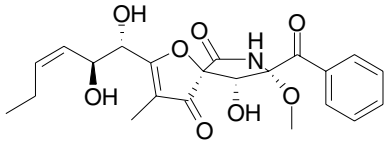

2.7

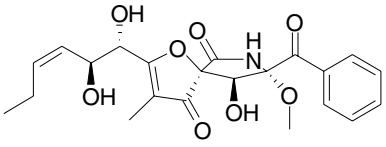

2.8

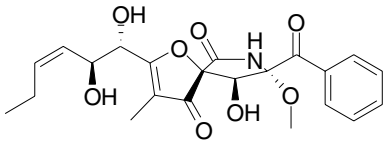

2.9

The specific HSV antiviral activity shown by the original extract did not translate to the new diastereomers, which were found to be inactive in the assay. It was concluded that the activity shown came from pseurotin A only. Upon purification pseurotin A was found to display potent antiviral activity of 4+. This would seem to indicate that in the case of these compounds, stereochemistry plays an important role in the *in vitro* activity.

The pseurotin class of compounds, of which there are now nine members, were originally isolated from *Pseudeurotium ovalis* (pseurotin's A-E), however more recently **2.7** has also been isolated from many other fungi, including *Aspergillus fumigatus*,[57] *Pochonia chlamydosporia*,[58] *Diheterospora chalmydosporia*,[59] *Pseudallescheria boydii*,[60] and a *Ulocladium* sp.[61] The observed biological activity ranged from inhibition of chitin synthase[57] to induction of differentiation of PC12 cells.[59] The isolation reported here, however, is the first instance in which pseurotins have been isolated from a *Penicillium* sp.

Chapter 3

Unique Compounds Related to the Spirobisnaphthalenes, from a New Zealand Fungal Endophyte (F5062 and F5584)

3.1 General Introduction

3.1.1 Spirobisnapthalenes

In the last fifteen years, this new class of natural product has been isolated from fungi. Metabolites of this class possess two naphthalene units that are fused together via oxidative coupling. In these structures, the naphthalene units are linked together by two or three oxygen atoms, and in most cases the naphthalene core is partially saturated or oxidised. Because the oxygen atoms linking the two halves of the molecule are usually

involved in a spiroketal bridge system, these compounds are generally referred to as the "spirobisnaphthalenes". This class of molecule can generally be divided into three sub classes, those with two oxygen bridges, such as palmarumycin CP_1 (**3.1**),[62] the spirobisnaphthalenes with three oxygen bridges, like that of preussomerin A (**3.2**),[63] and spiroxin A (**3.3**),[64] which is representative of those with two oxygen bridges and one C-C bridge.

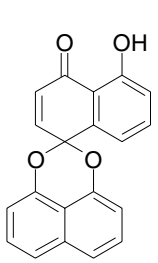

3.1

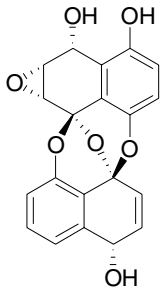

3.2

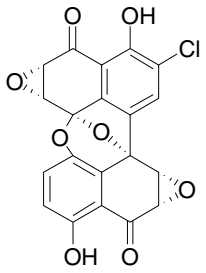

3.3

The biosynthesis of this class of compounds has been studied by several groups. Zeeck *et al.*[65] studied the biosynthesis of cladospirone bisepoxide (**3.4**), and from his studies, proposed that 1,8-dihydroxynaphthalene (DHN) (**3.5**) is a probable precursor of the spirobisnaphthalenes. This can also be concluded from the production of brown/black, DHN-derived melanin compounds that is seen to accompany the production of the spirobisnaphthalenes.

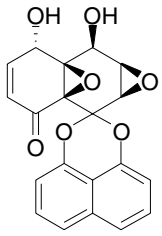

3.4

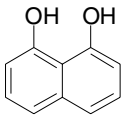

3.5

The spirobisnaphthalenes have been isolated exclusively from fungi, with the exception of work from two research groups, Kouam *et al.*,[66] and more recently Ravindranath *et al.*,[67] who have reportedly isolated the compounds from plants. However, as all other

spirobisnaphthalenes have been isolated from fungi it is most likely that these compounds were in fact produced by endophytic fungi, living within the plant host. This is supported by Prajoubklang *et al*.,[68] who have recently reported spirobisnaphthalenes from the fruits of *Diospyros ehretioides*, but found later that the compounds were only isolated from the dried fruits and weren't able to be isolated from the fresh fruit at all. This led them to propose that the spirobisnaphthalenes were produced by fungal epiphytes or endophytes.

The biological activity of this class of compounds is diverse and has been widely reported as antifungal, antibacterial and antitumoral. One such compound, Sch 49209 (**3.6**) progressed to *in vivo* testing in mice.[69]

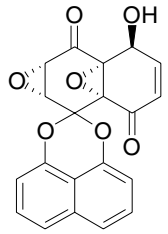

3.6

The authors found growth inhibition of lung epidermoid carcinoma and also, that the compound decreased the formation of spontaneous lung metastasis in the same model. It was also found to inhibit the growth of human tumor xenografts in athymic nude mice. However, at accumulated doses of 40 mg/kg it was found to be toxic to the animals. At the cessation of drug administration, the tumors started to regrow, which led the authors to propose that **3.6** may act in inhibiting tumor expansion by preventing cell invasion. Several enzymes have also been reported to be inhibited by this class of compounds, including phospholipase D,[70-72] DNA gyrase,[73] *Ras* farnesyl-protein transferase,[74] and thioredoxin reductase.[75]

Part 1 New Spirobisnaphthalenes from F5062

3.2 Introduction

The sterile endophytic fungus, E484, was isolated from the surface-sterilised leaves of rewarewa (*Knightia excelsa*), which had been collected in a mixed broadleaf-podocarp forest in the Kaimai-Mamaku Forest Park, Bay of Plenty, New Zealand. The fungus was grown on a MYE agar slope for small-scale biological and chemical screening.

3.3 Preliminary Investigations

The extract of the small-scale agar culture (F5062) showed excellent cytotoxicity in the P388 assay (116 ng/mL). An aliquot of this crude extract was chromatographed on reverse phase C18 HPLC (Figure 3.1), using the standard elution gradient (Section 7.1.4). The chromatogram showed a number of compounds with similar UV spectra eluting between 10 and 15 minutes. A compound eluting at 14.2 minutes was shown by ELSD to be associated with a large proportion of the mass of the extract (Figure 3.1). A search of the UV database[76] revealed that none of the peaks shown in the HPLC trace matched any common, highly cytotoxic known compounds. For this reason, as well as the toxicity displayed, the fungus was re-grown on a large scale (see Section 7.4.1 of Experimental) to enable a full chemical investigation.

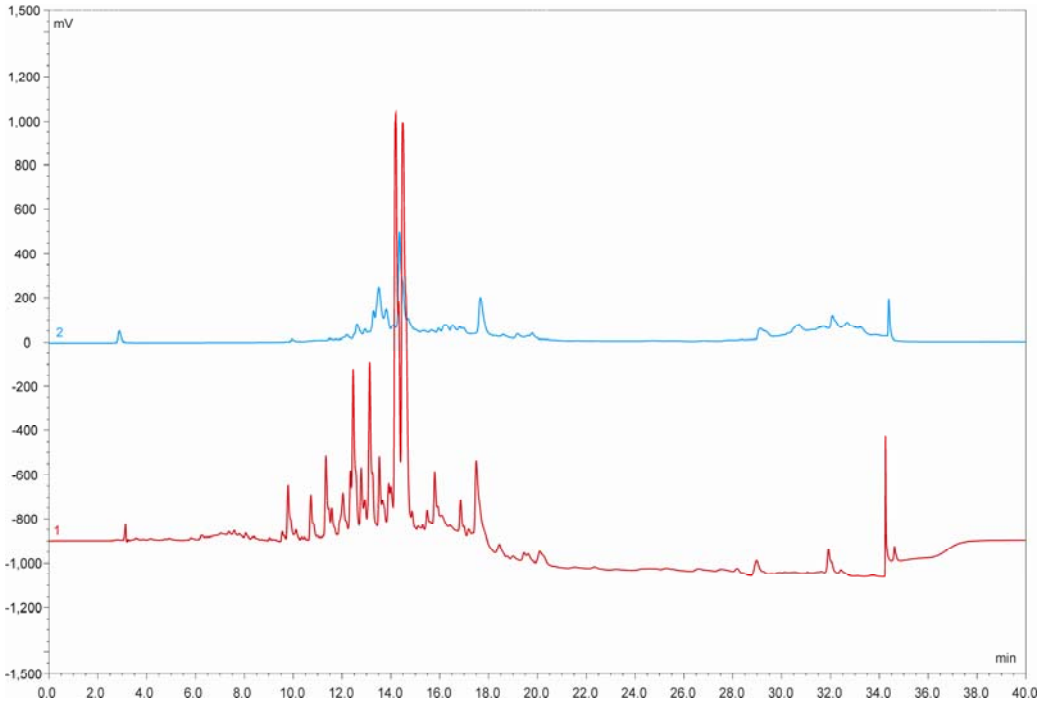

Figure 3.1: *HPLC chromatogram of the crude extract of F5062 with ELSD comparison (blue).*

3.4 Chromatography of Extract from F5062 Culture

The EtOAc extract of the large-scale culture (Section 7.4.1) was loaded on to a C18 bench column for fractionation (Section 7.4.2). The two fractions that eluted with 100% MeOH (SAS-5-64.10–11) showed the highest cytotoxicities (231 and 166 ng/mL respectively). Injection of a small amount of each of the two fractions on the analytical C18 HPLC column showed that both fractions, SAS-5-64.10 and SAS-5-64.11 contained the major compound that had eluted at 14.2 minutes. Fraction SAS-5-64.10, however, also contained three other, more polar compounds that, according to the ELSD trace, also contributed significant mass to the extract (Figure 3.2). These showed almost identical UV chromophores to the major component (Figure 3.3). Semi-preparative HPLC was carried out on SAS-5-64.10 (18.0 mg) using the method given in Section 7.3.2 of the Experimental section, to obtain the four compounds, SAS-5-64.10.1–4, with yields of 4.8, 1.9, 1.1, and 5.7 mg respectively.

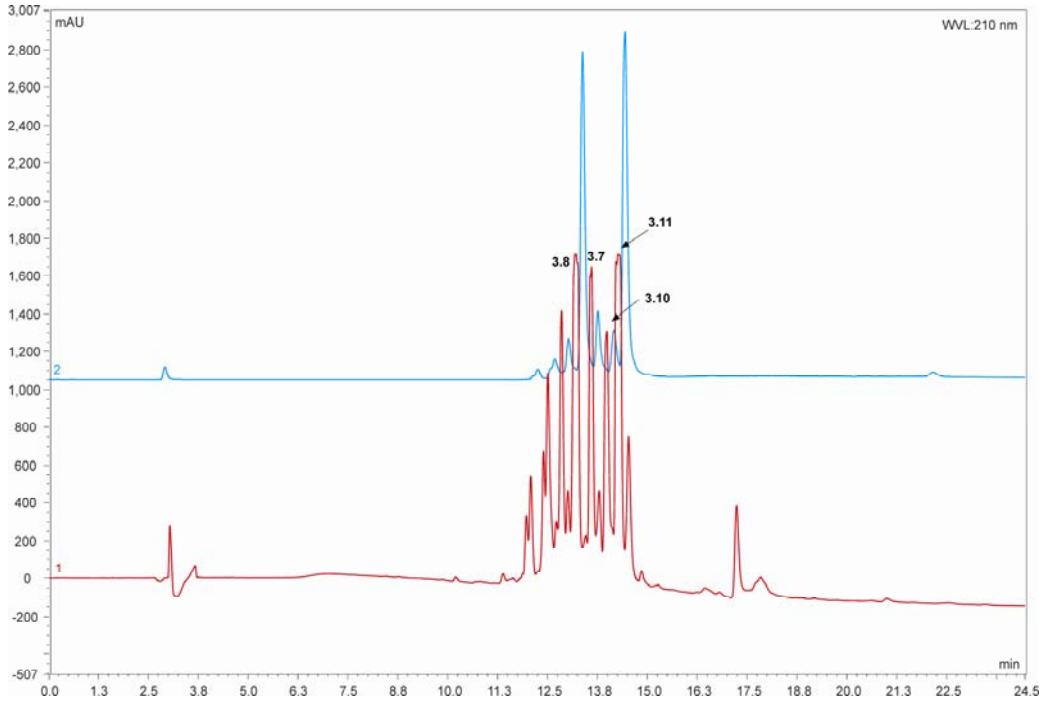

Figure 3.2: *HPLC chromatogram of fraction 10.*

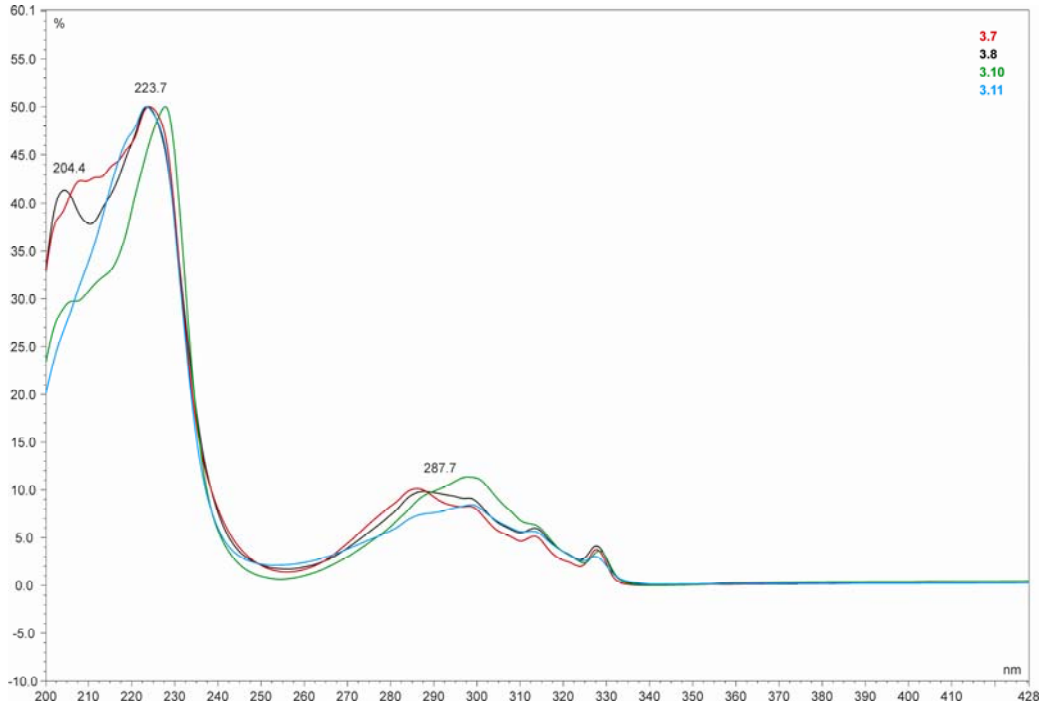

Figure 3.3: *UV profiles of important compounds from fraction 10.*

3.5 Structural Elucidation of SAS-5-64.10.1–4

*3.5.1 Structural Elucidation of SAS-5-64.10.2 (**3.7**)*

ESIMS determined the mass of SAS-5-64.10.2 (**3.7**) to be 351 ($[M+H]^+$), while HREIMS gave a molecular formula of $C_{20}H_{14}O_6$, (14 double bond equivalents). The large number of double bond equivalents indicated a high degree of unsaturation in the molecule, probably in the form of aromatic rings, but due to the absorbance only just falling in the yellow region of the UV-visible spectrum, it was likely that the rest of the double bond equivalents arose from non-aromatic ring systems, double bonds or carbonyl functionalities with little or no conjugation.

The ^{1}H NMR spectrum (Figure 3.4) showed one methylene, one oxymethine and five olefinic/aromatic signals. The ^{13}C NMR spectrum (Figure 3.5) showed a total of 20 signals, indicating no elements of symmetry were present in the molecule. Examination of the HSQC-DEPT spectrum revealed that these carbon signals were comprised of one CH_2, ten CH and nine non-protonated carbon signals. Additional 2D NMR experiments allowed the rest of the structure to be defined. The COSY spectrum showed the presence of two separated aromatic systems in the molecule. The first consisted of a 1,2,3-trisubstituted benzene ring (ring B). The protons at δ_H 6.80 (H-3), 6.92 (H-4), and 6.801 (H-5) were assigned as three adjacent protons.

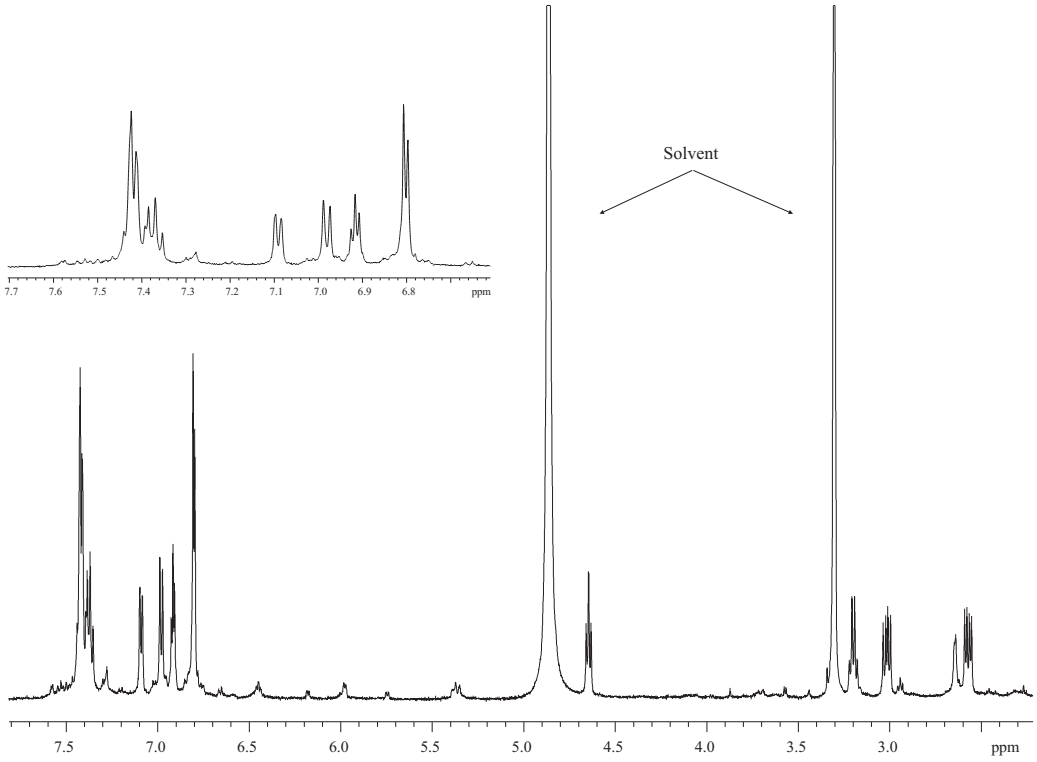

Figure 3.4: *^{1}H NMR spectrum of SAS-5-64.10.2 (**3.7**) in CD_3OD.*

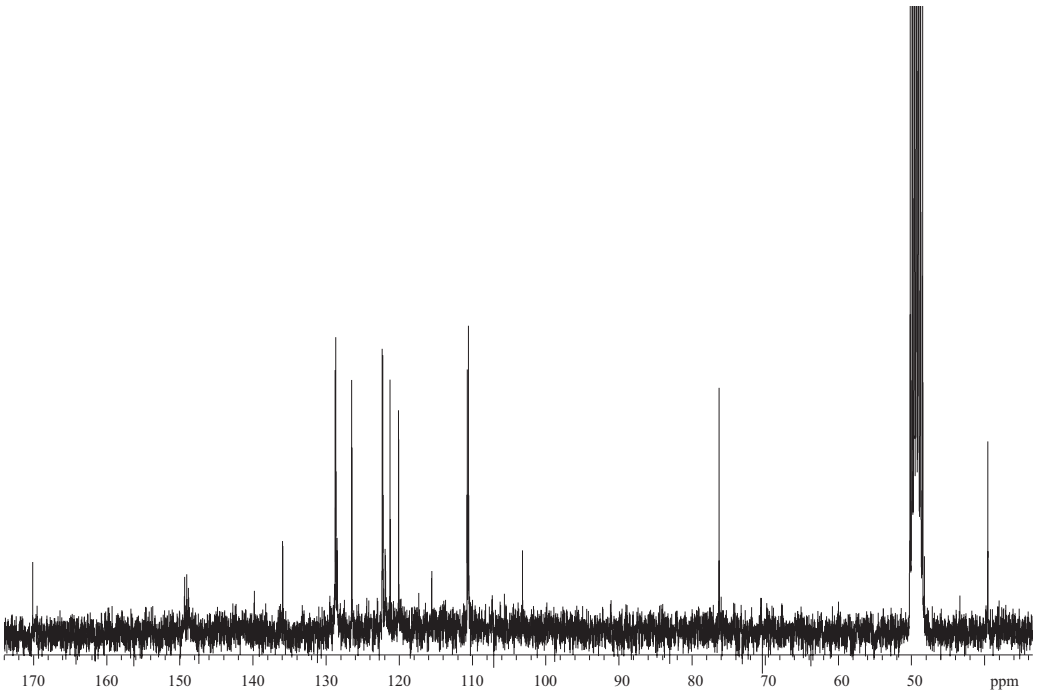

Figure 3.5: *^{13}C NMR spectrum of SAS-5-64.10.2 (**3.7**) in CD_3OD*

The proposed order of the protons on the ring is given in Figure 3.6. The proton at δ_H 6.92 is placed at H-3, while the two overlapping protons at δ_H 6.80 are in positions H-4 and H-5. In support of this arrangement are the $^{2,3}J_{CH}$ CIGAR correlations from δ_H 6.92 to carbons at δ_C 138.2 (C-7), 126.8 (C-2), 118.4 (C-5). In addition, H-4 showed a CIGAR correlation to a non-protonated carbon at δ_C 147.7 (C-6). The chemical shift of C-6 and possibly C-7, suggested oxygenation.

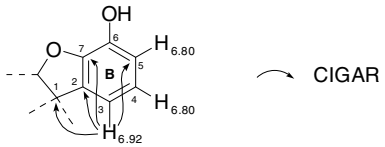

Figure 3.6: *Proposed order of protons on ring B indicated by CIGAR correlations.*

However, the proton at δ_H 6.92 appears as a triplet in the ^{1}H NMR spectrum. If this proton were situated at H-3, it would be expected to give rise to a doublet, perhaps a doublet of doublets if strong *meta* coupling were present to the proton at H-5. A ^{1}H NMR spectrum simulation of the ABC system presented in Figure 3.6 was carried out. The chemical shifts were defined from the experimental values, while the coupling constants were assumed initially as 7.0, 2.0, and 7.0 Hz for J_{34}, J_{35}, and J_{45} respectively. The results, which are shown in Figure 3.7, reveal that the proposed arrangement is probably correct, as the simulated spectrum is identical to the experimental spectrum.

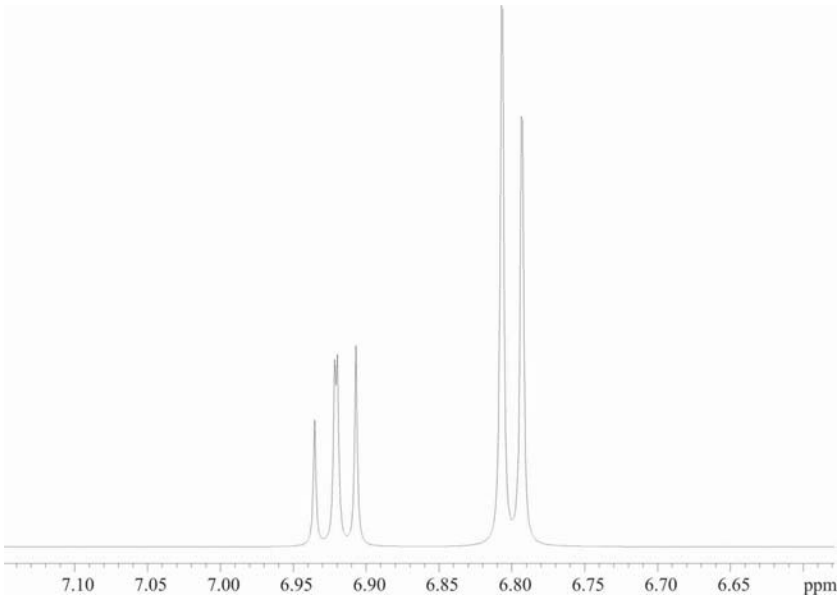

Figure 3.7: *^{1}H NMR spectrum simulation of the ABC system in* ***3.7****.*

The unusual multiplicities observed are the result of second order coupling effects. This occurs when chemical shifts of all the protons in the spin system are similar in value. This situation results in increased intensity of the peak of the signal that is closest to the peaks of its coupled neighbour, whereas for those further away, the intensity is decreased, thus leading to patterns not explained by first order coupling.

Preliminary findings from biosynthetic studies also revealed that the arrangement of protons on ring B of **3.7** was most probably the correct one (see Section 3.11.6).

A second more complex aromatic system (6-H) was indicated by the proton signals at δ_H 6.98-7.43. One component of this system was a triplet proton at δ_H 7.38 (H-17) coupled to two doublet protons at δ_H 6.98 (H-18) and δ_H 7.43 (H-16). The HSQC-DEPT spectrum showed these protons to have $^{1}J_{CH}$ correlations to carbons at δ_C 127.0 (C-17), 108.9 (C-18), and 120.7 (C-16) respectively. Within this aromatic system, a second spin system showed an identical arrangement to that of the first. This was shown by the coupling of the triplet proton at δ_H 7.41 (H-13) to the doublet protons of δ_H 7.09 (H-12) and 7.42 (H-14). $^{1}J_{CH}$ correlations from these protons were shown to carbons at δ_C 127.1 (C-13), 109.1 (C-12), and 120.6 (C-14) respectively. CIGAR correlations from the

protons at H-14 and H-16 to the non-protonated carbons at δ_C 134.3 (C-15) and 113.9 (C-20), indicated the nature of the aromatic entity as a naphthalene system. The naphthalene was shown to be a 1,8 dioxynaphthalene from the chemical shifts (δ_C 147.4 and 147.1) of the two non-protonated carbons in the 1 and 8 positions of the naphthalene, (C-11) and (C-19). CIGAR correlations from H-12 and H-13 to C-11 as well as H-17 and H-18 to C-19, confirmed C-11 and C-19 as being in the 1 and 8 positions respectively of the naphthalene (Figure 3.8). Most importantly, the CIGAR data also suggested that the naphthalene was separated from the other aromatic ring, as there were no other correlations from H-12 or H-18 to any carbon in ring B.

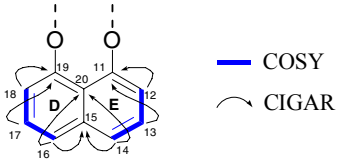

Figure 3.8: *1,8 dioxynaphthalene fragment showing COSY and CIGAR correlations*

The balance of the signals in the ^{1}H NMR spectrum consisted of a one proton doublet of doublets at δ_H 4.65 (H-8) coupled to both a one proton doublet of doublets at δ_H 2.57, and another one proton doublet of doublets at δ_H 3.02. HSQC-DEPT data revealed these two protons to be a diastereotopic methylene moiety (H-9a, H-9b).

The ^{13}C NMR spectrum also suggested the presence of an acid or ester carbonyl signal (C-10), at 168.4 ppm. The CIGAR spectrum showed correlations from the H-8, H-9a and H-9b protons to the carbonyl at C-10 as well as to the carbon at δ_C 101.5 (C-1). The former indicated the connectivity of the oxymethine and methylene containing spin system through to the carbonyl, and the latter to the oxygenated aromatic ring (Figure 3.9).

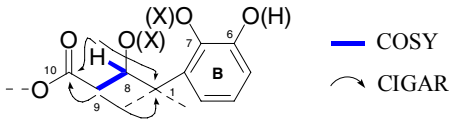

Figure 3.9: *COSY and CIGAR correlations showing connectivity of side chain and ring B.*

At this point, the substituent on C-6 was assumed to be an hydroxyl. No such assumption was made for C-7 however. The chemical shift of C-7 (138.2 ppm) was a little high-field to be substituted with a free hydroxyl, the chemical shift was more reminiscent of a junction carbon shifted by oxygen.

A search of the AntiMarin database[77] using the 1,8 dioxygenated naphthalene fragment as a search parameter, indicated a reasonably large group of spirobisnaphthalene compounds, all bearing a spiroketal linked 1,8 bisnaphthalene moiety in common. NMR data of the spiroketal-linked naphthalene of a spirobisnaphthalene from the literature[78] were compared to those for **3.7**, and was revealed to show very good correlations. The spiroketal (ring C) system also explained why the two halves of the molecule were unable to be linked by CIGAR data. A thorough search of AntiMarin and SciFinder Scholar revealed no compounds that matched all of the NMR data for **3.7**, indicating possibly a new type of spirobisnaphthalene.

From the CIGAR correlations (H-8, H-9a, and H-9b to C-1) mentioned previously, as well as a $^{4}J_{CH}$ CIGAR correlation from H-4 to C-1, it was obvious that the dioxygenated aromatic ring and the fragment bearing the oxymethine were connected to the naphthalene through the spiroketal moiety. Assuming that C-10 was a carboxylic acid, the molecular formula revealed that only one oxygen was to be accounted for in the structure. It was therefore proposed that C-8 and C-7 were substituted with a common oxygen, forming a furan ring (ring A). A further check of the literature revealed no compounds that showed any similarity to the uppermost portion of **3.7**. The compound has been assigned the trivial name, mamakunoic acid B (**3.7**). A full list of NMR data is presented in Table 3.1.

A P388 assay revealed **3.7** to be inactive (>12500 ng/mL).

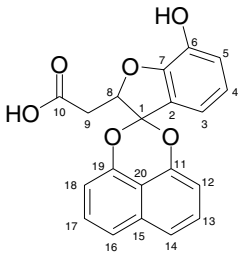

3.7

Table 3.1: *NMR data for* ***3.7***

position	δ_C, ppm	δ^1H, multiplicity (J_{HH} Hz)	COSY	CIGAR
1	101.5 (C)			
2	126.8 (C)			
3	124.8 (CH)	6.92 t (6.6, 6.6)	H-4	C-7, C-6, C-2, C-4
4	119.6 (CH)	6.80 d (4.7)	H-3, H-5	C-7, C-6, C-2, C-5, C-1
5	118.4 (CH)	6.80 d (4.7)	H-4	C-6, C-2, C-4
6	147.7 (C)			
7	138.2 (C)			
8	74.6 (CH)	4.65 dd (6.6, 7.7)	H-9a, H-9b	C-10, C-2, C-1, C-9
9	37.9 (CH_2)	a: 2.57 dd (6.6, 13.0)	H-8, H-9b	C-10, C-1, C-8
		b: 3.02 dd (13.0, 7.7)	H-8, H-9a	C-10, C-1, C-8
10	168.4 (C)			
11	147.4 (C)			
12	109.1 (CH)	7.09 d (7.1)	H-13	C-11, C-15, C-14, C-20
13	127.1 (CH)	7.41 m	H-12, H-14	C-11, C-15, C-12
14	120.6 (CH)	7.42 m	H-13	C-16, C-11, C-19, C-15, C-20, C-12
15	134.3 (C)			
16	120.7 (CH)	7.43 m	H-17	C-14, C-20, C-19, C-18, C-11, C-15
17	127.0 (CH)	7.38 m	H-16, H-18	C-19, C-15, C-18
18	108.9 (CH)	6.98 d (7.1)	H-17	C-19, C-16, C-20
19	147.1 (C)			
20	113.9 (C)			

^{1}H and 2D experiments carried out at 500 MHz in CD_3OD. ^{13}C data obtained at 75 MHz in CD_3OD.

*3.5.2 Structural Elucidation of SAS-5-64.10.1 (**3.8**)*

Compound SAS-5-64.10.1 (**3.8**) was purified as one of the minor components of fraction SAS-5-64.10. ESIMS indicated this compound had a mass of 369 ($[M+H]^+$). Also present in the +ve ion MS was a $[M-H_2O]^+$ fragment peak at 351, indicating the presence of an hydroxyl moiety in the molecule. The mass of **3.8**, 18 mass units more than that of **3.7**, suggested the addition of H_2O. The hydration of **3.7** to form **3.8** could only occur

between the oxymethine and the hydroxyl at C-7, thus opening the furan ring (see Figure 3.10).

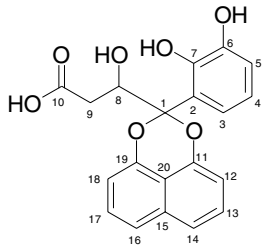

Figure 3.10: *Proposed structure for* ***3.8***

The ^{13}C NMR spectrum of **3.8** (Figure 3.11) showed a total of 16 carbons signals, four less than that given by the molecular formula, suggesting that the molecule contained either an element of symmetry, or that some of the signals are coincidentally overlapped. Comparison of the spectrum with that of **3.7** (Figure 3.5) revealed the two to be very similar. The major differences were that the some of the signals representative of the naphthalene system appeared as overlapping signals, whereas in the ^{13}C NMR spectrum of **3.7**, they had been clearly separated. Also a small downfield shift was seen for the resonance of the carbons at C-7 and C-8. In order to confirm the proposed structure of **3.8** (Figure 3.10), the 1D and 2D NMR spectra were analysed.

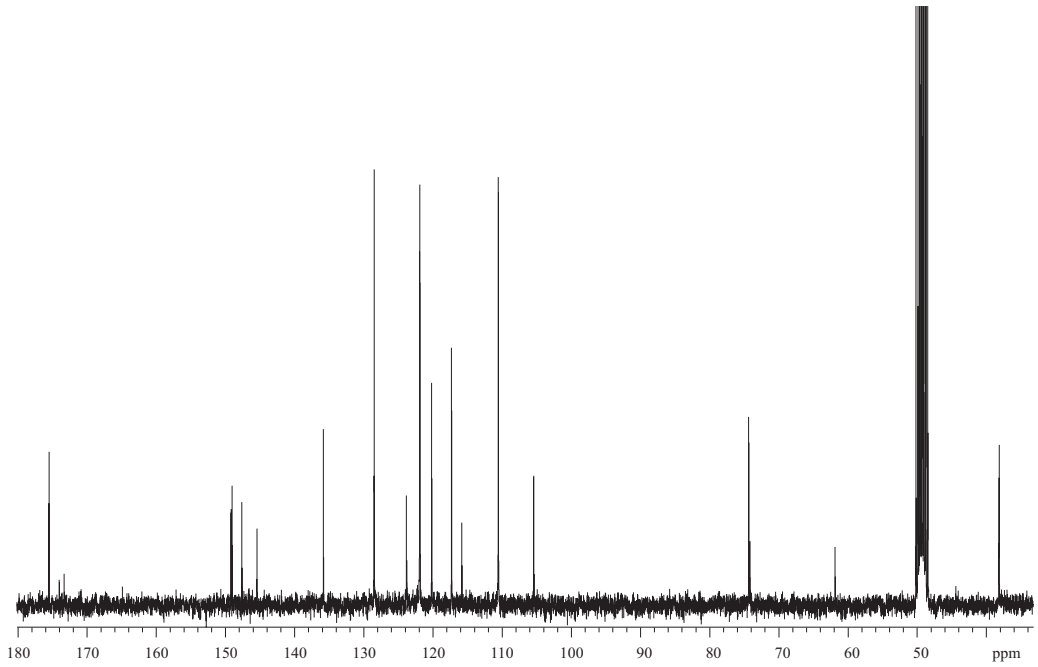

Figure 3.11: *^{13}C NMR spectrum of SAS-5-64.10.1 (**3.8**) in CD_3OD.*

The ^{1}H NMR spectrum (Figure 3.12) indicated only small differences in chemical shifts between the spectra of **3.7** and **3.8**. Despite the differences in the chemical shifts of the naphthalene signals between **3.7** and **3.8**, COSY, HSQC-DEPT and CIGAR NMR spectra confirmed that the lower portion of the molecule was also a naphthalene unit (rings D and E).

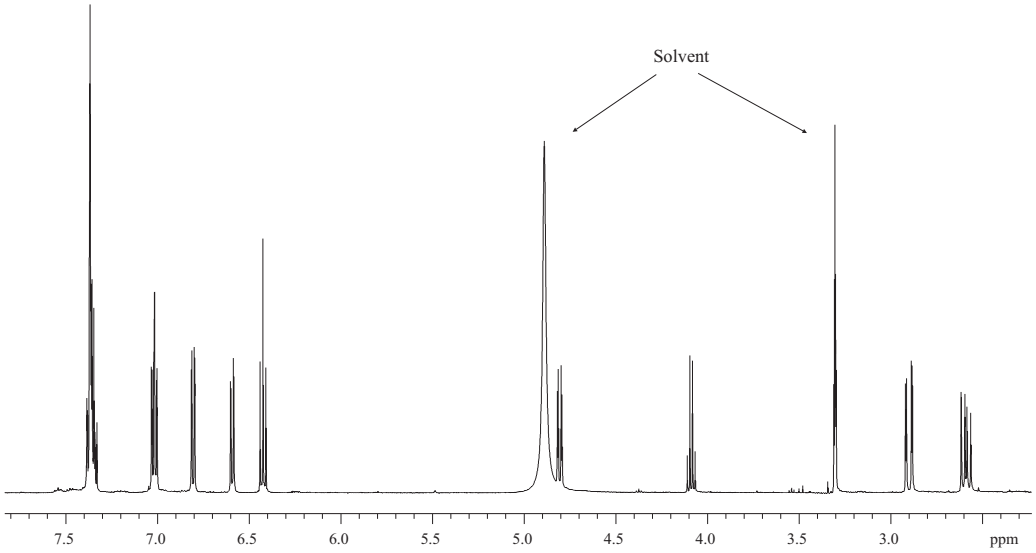

Figure 3.12: *^{1}H NMR spectrum of SAS-5-64.10.1(**3.8**) in CD_3OD.*

An overlapping triplet proton at δ_H 7.35 (H-17) was shown to be coupled to an overlapping triplet proton at δ_H 7.02 (H-18) and an overlapping doublet proton at δ_H 7.37 (H-16). Examination of the overlapping triplet at δ_H 7.02 revealed that it was in fact two overlapping doublets, integrating for two protons, one of them (H-12) part of the other spin system. This arrangement was repeated with identical proton chemical shifts for the carbons of the other spin system (H-12–H-14), together forming rings D and E of the naphthalene moiety. CIGAR correlations from the protons at H-14 and H-16 to the non-protonated carbons at δ_C 134.2 (C-15) and 114.2 (C-20), showed these carbons to be the point of fusion between rings D and E, to form the naphthalene moiety. The carbons at δ_C 126.8 (C-13 and C-17), 120.2 (C-14 and C-16), and 108.9 (C-12 and C-18) were, as noted (vide infra), seen in the ^{13}C NMR spectrum to have twice the intensity of other protonated carbons. Because the carbons at δ_C 147.3 (C-11) and 147.5 (C-19) did not show the same chemical shift, symmetry of this system was impossible, therefore the overlap of C-12–C-18 is best explained as coincidental overlap.

The spiroketal system (ring C) was also indicated by the presence of the oxygenated carbons of the naphthalene moiety at δ_C 147.5 and 147.3 (C-19 and C-11 respectively) and also the spiroketal carbon at δ_C 103.8 (C-1). The 3-hydroxy-butyric acid moiety was

confirmed through the COSY correlations from the methylene protons at δ_H 2.59 (H-9a) and 2.90 (H-9b) to the oxymethine proton at δ_H 4.81 (H-8). CIGAR correlations from these same protons to the carbonyl carbon at δ_C 173.8 (C-10), confirmed the placement of the acid moiety at C-10.

As for **3.7**, ring B of **3.8** was confirmed to be a 1,2,3-trisubstituted aromatic ring. The protons at δ_H 6.81 (H-3), 6.42 (H-4), and 6.59 (H-5) were assigned as three adjacent protons from the COSY spectrum. CIGAR correlations observed from these protons to the two carbons at δ_C 146.0 (C-6) and 143.8 (C-7) confirmed the oxygenation at these carbons. The connection of the butyric acid spin system through to that of the aromatic spin system was shown from the CIGAR correlations of the protons at H-8–H-9b to the spiroketal carbon at C-1. In turn protons H-3 and H-4 from ring B, showed CIGAR correlations also to C-1.

As with mamakunoic acid B (**3.7**), no matches were found in the literature, it was therefore considered to be a new compound and given the trivial name, mamakunoic acid A (see Figure 3.10).

Table 3.2: *1D and 2D NMR data for* ***3.8***

position	δ_C, ppm		δ^1H, multiplicity (J_{HH} Hz)	COSY	CIGAR
1	103.8	(C)			
2	122.2	(C)			
3	120.3	(CH)	6.81 dd (8.0, 1.6)	H-4	C-7, C-6, C-4, C-5, C-1
4	118.5	(CH)	6.42 t (8.0, 8.0)	H-3, H-5	C-7, C-6, C-2, C-3, C-5, C-1
5	115.7	(CH)	6.59 dd (8.0, 1.6)	H-4	C-7, C-6, C-2, C-3, C-4
6	146.0	(C)			
7	143.8	(C)			
8	72.7	(CH)	4.81 dd (10.2, 2.9)	H-9a, H-9b	C-10, C-2, C-1, C-9
9	36.5	(CH_2)	a: 2.59 dd (10.2, 15.6)	H-8, H-9b	C-10, C-1, C-8
			b: 2.90 dd (15.6, 2.9)	H-8, H-9a	C-10, C-1, C-8
10	173.8	(C)			
11	147.3	(C)			
12	108.9	(CH)	7.02 t *ol*	H-13	C-11, C-15, C-14, C-20
13	126.8	(CH)	7.35 t *ol*	H-12, H-14	C-11, C-15, C-12
14	120.2	(CH)	7.37 d *ol*	H-13	C-16, C-20, C-12, C-19, C-15
15	134.2	(C)			
16	120.2	(CH)	7.37 d *ol*	H-17	C-14, C-20, C-18, C-11, C-15
17	126.8	(CH)	7.35 t *ol*	H-16, H-18	C-19, C-15, C-18
18	108.9	(CH)	7.02 t *ol*	H-17	C-19, C-15, C-16, C-20
19	147.5	(C)			
20	114.2	(C)			

^{1}H and 2D experiments carried out at 500 MHz in CD_3OD. ^{13}C data collected at 75 MHz in CD_3OD.
ol - overlapping

Further work, including elucidation of the stereocentre at C-8, and obtaining biological activity data and HREIMS data was reluctantly abandoned due to the degradation/transformation of this compound very soon after isolation. The form of transformation of **3.8**, was found to be methylation of the carboxylic acid by CD_3OD, forming a deuterated methyl ester (**3.9**), while in the NMR sample tube. This compound was characterised by both ESIMS and NMR (see experimental), and the P388 assay revealed that **3.9** was not biologically active (>32.5 μM).

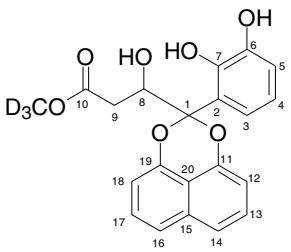

3.9

Following purification of the CD_3O ester, very little pure compound was left (0.6 mg). If a greater amount of compound had been obtained there might have been a way to elucidate the stereochemistry. This could have involved hydrolysing the CD_3O ester followed by re-esterification in order to protect the acid group, and then derivatisation with Mosher's ester at 8-OH. The problem with this approach lies is that Mosher's esterification is not selective, hence esterification of both the 6-OH and 7-OH would almost certainly result. Esterification at these positions would likely have an effect on the same protons affected by esterification at 8-OH, leading to ambiguous results.

*3.5.3 Structural Elucidation of SAS-5-64.10.3 (**3.10**)*

The compound, SAS-5-64.10.3 (**3.10**) was isolated as another minor component from the column fraction, SAS-5-64.10. ESIMS showed that the compound had a mass of 379 ($[M-H]^-$) while HREIMS fitted the molecular formula $C_{21}H_{16}O_7$, corresponding to 14 double bond equivalents.

The ^1H NMR spectrum of **3.10** (Figure 3.13) showed the presence of the naphthalene system with δ_H 6.98 (H-12, H-18), 7.48 (H-13, H-17), 7.56 (H-14, H-16). Also present were methylene protons at δ_H 2.44 (H-9) and 2.59 (H-9a) and an oxymethine proton at δ_H 4.97 (H-8), as seen in the previous compounds, **3.7** and **3.8**. The major difference observed for **3.10** was a large methoxyl singlet signal at δ_H 3.81.

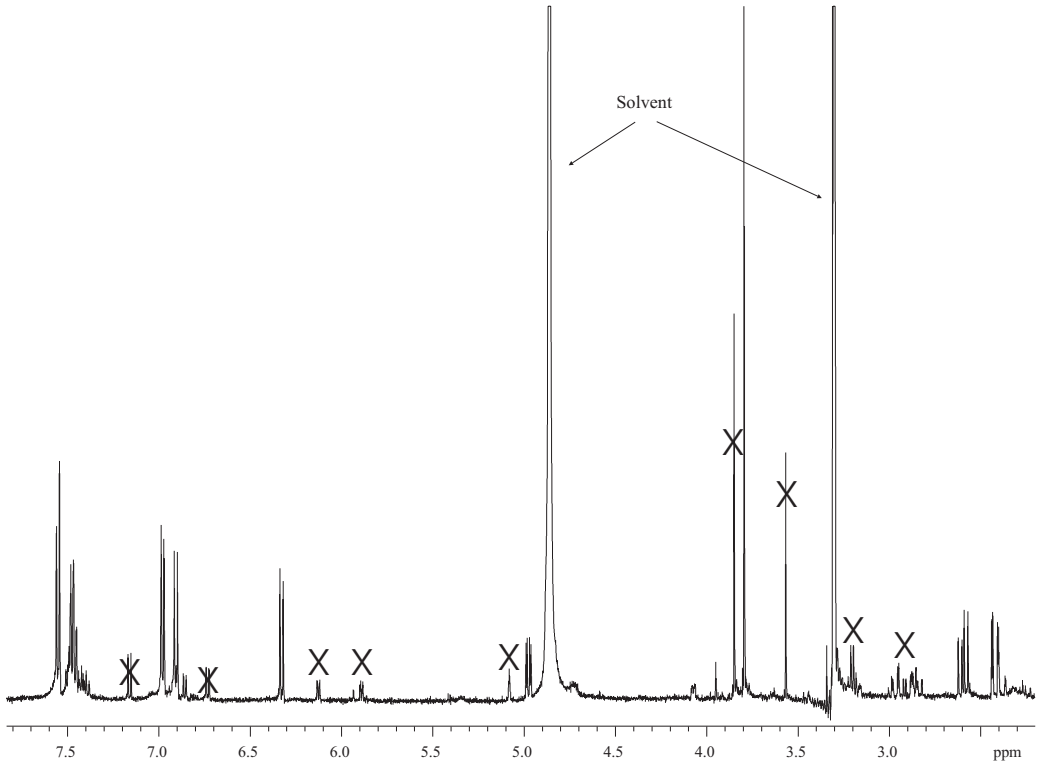

Figure 3.13: *^{1}H NMR spectrum of SAS-5-64.10.3 (**3.10**) in CD_3OD. Crosses indicate impurities.*

Comparison of the 1D and 2D NMR spectra of **3.10** with **3.7** indicated that rings A, C, D and E were identical to those in **3.7**. Ring B in **3.7** was therefore a 1,2,3,4 tetra-substituted aromatic ring with the two adjacent aromatic protons appearing as doublets at δ_H 6.91 and 6.34. The additional methoxyl group was placed on ring B. The order of the substituents around ring B was elucidated with the assistance of CIGAR correlations (Figure 3.14).

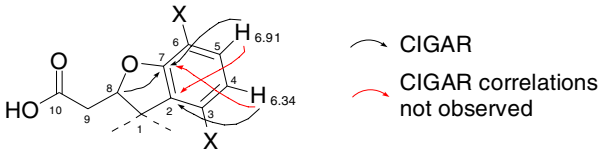

Figure 3.14: *Elucidation of the order of substituents on ring B through CIGAR correlations*

The two quaternary carbons, δ_C 149.7 (C-7) and 111.9 (C-2) were placed at the two junction points between the furan and aromatic rings. A strong $^3J_{CH}$ CIGAR correlation

was observed between the proton at δ_H 4.97 (H-8) and C-7. A lack of correlations from the proton at δ_H 6.91 to C-2 and from δ_H 6.34 to C-7 suggested the placement of these protons as H-5 and H-4 respectively. The positions of the methoxyl and hydroxyl substituents were established by 1D NOE correlations (Figure 3.15).

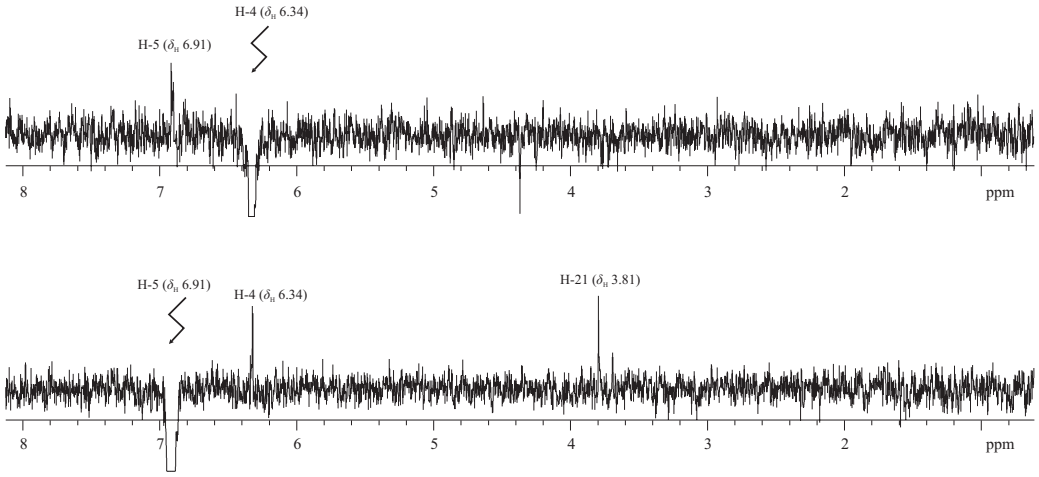

Figure 3.15: *1D NOE spectrum of* ***3.10*** *in CD_3OD showing irradiation of H-5 (bottom) and H-4 (top).*

When H-5 was irradiated, both H-4 and the methoxyl proton signals were enhanced. When H-4 was irradiated only the H-5 proton signal was enhanced. There were no enhancements of any proton signals when the methoxyl proton was irradiated. These results confirm the placement of the H-5 proton as between those of H-4 and the methoxyl substituent, which means that only the C-6 position can carry the methoxyl substituent. The hydroxyl was placed in the only remaining position, C-3.

The resulting structure (**3.10**) also gave no matches to any compounds in the literature. The compound was therefore considered new and given the name mamakunoic acid C (**3.10**). A full NMR data table is presented in Table 3.3.

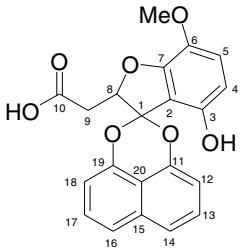

3.10

Table 3.3: *1D and 2D NMR data for* ***3.10***

position	δ_C, ppm		δ^1H, multiplicity (J_{HH} Hz)	COSY	CIGAR
1	108.4	(C)			
2	111.9	(C)			
3	149.2	(C)			
4	107.9	(CH)	6.34 d (8.8)	H-5	C-4, C-6, C-2
5	118.3	(CH)	6.91 d (8.8)	H-4	C-7, C-6
6	138.3	(C)			
7	149.7	(C)			
8	85.9	(CH)	4.97 dd (10.7, 3.6)	H-9a, H-9b	C-10, C-7, C-2, C-1, C-9
9	35.3	(CH_2)	a: 2.59 dd (10.7, 16.2)	H-8, H-9b	C-10, C-1, C-8
			b: 2.44 dd (16.2, 3.6)	H-8, H-9a	C-10, C-1, C-8
10	171.8	(C)			
11	148.1	(C)			
12	108.8	(CH)	6.98 d (7.7)	H-13	C-11, C-14, C-20
13	127.2	(CH)	7.48 dd (7.7, 1.8)	H-12, H-14	C-11, C-15
14	120.6	(CH)	7.56 d (8.5)	H-13	C-19, C-20, C-16, C-11, C-15
15	134.4	(C)			
16	120.6	(CH)	7.56 d (8.5)	H-17	C-19, C-20, C-14, C-11, C-15
17	127.2	(CH)	7.48 dd (7.7, 1.8)	H-16, H-18	C-19, C-15
18	108.8	(CH)	6.98 d (7.7)	H-17	C-19, C-16, C-20
19	148.1	(C)			
20	113.3	(C)			
21	56.6	(CH_3)	3.81 s		C-6

[1]H and 2D data obtained at 500 MHz in CD_3OD.
[13]C chemical shifts were determined from HSQC and CIGAR NMR experiments.

Although compound **3.10** was not obtained 100% pure and in sufficient quantity to readily purify, the biological activity was determined. In the P388 assay **3.10** was found to have an IC_{50} of 2335 ng/mL. However, considering that neither of the other mamakunoic acids showed any activity, this moderate activity is likely the result of an impurity. A re-culture of the E484 fungus to obtain more of these compounds (**3.7**, **3.8** and **3.10**) was carried out, but did not produce the desired metabolites (see Section 3.7).

*3.5.4 Structure Elucidation of SAS-5-64.10.4 (**3.11**)*

The remaining compound purified from the C18 column fraction, SAS-5-64.10 was the major compound of the extract, SAS-5-64.10.4 (**3.11**). ESIMS indicated a mass of 321 ($[M+H]^+$), while HREIMS provided a molecular formula of $C_{19}H_{12}O_5$, corresponding to 14 degrees of unsaturation.

Comparison of the ^1H and ^{13}C NMR spectra of **3.11** (see Table 3.4 and Figures 3.16 and 3.17 respectively) with those of the mamakunoic acids showed that **3.11** also contained the spirobisnaphthalene substructure. Other than this **3.11** was a very different molecule to the mamakunoic acids. The most notable differences were the absence of the acid carbonyl and the methylene carbon. Instead, **3.11** showed two ketone resonances at δ_C 201.1 and 198.6 and a quaternary carbon at δ_C 68.9.

Using COSY and HSQC correlations, the protons not involved in the spirobisnaphthalene were classified as belonging to two different spin systems. The first was a three proton spin system comprising of one proton at δ_H 5.93 (J = 5.8, 2.0 Hz) (H-2) correlated to a broad singlet proton at δ_H 5.30 (H-4) and a proton at δ_H 6.40, also a doublet of doublets (J = 5.8, 1.9 Hz) (H-3).

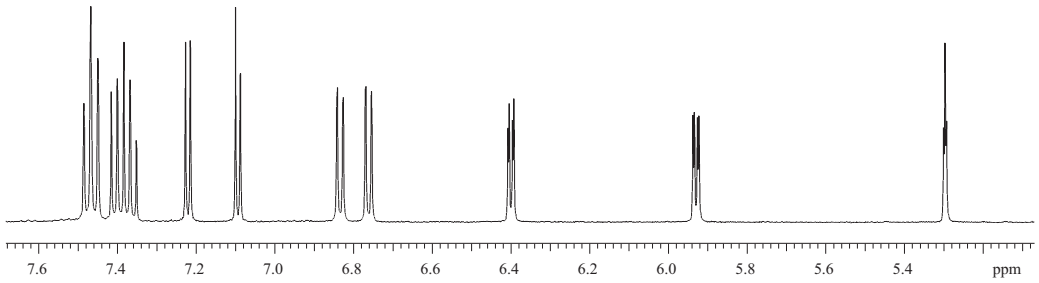

***Figure 3.16:** ^1H NMR spectrum of SAS-5-64.10.4 (**3.11**) in CD_3OD.*

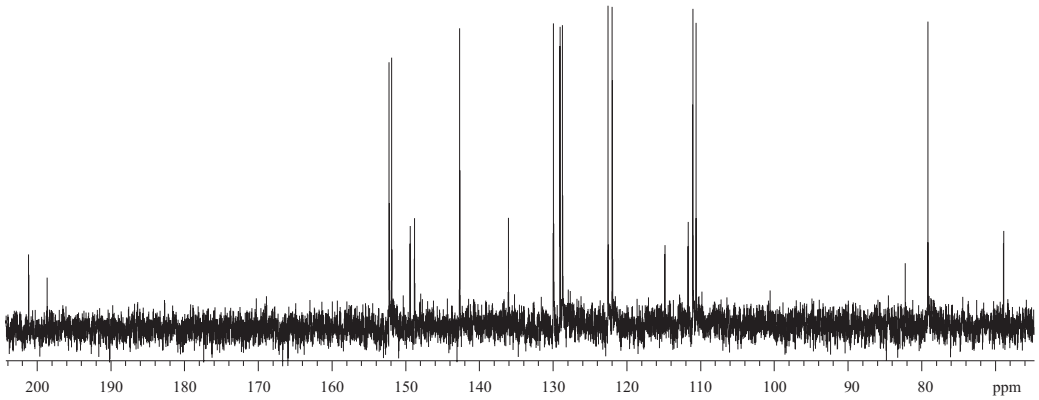

Figure 3.17: *^{13}C NMR spectrum of SAS-5-64.10.4 (**3.11**) in CD_3OD.*

The proton at H-4 had a $^{1}J_{CH}$ correlation to the carbon at δ_C 79.1 (C-4), suggesting that H-4 was an oxymethine proton. The protons H-2 and H-3 showed $^{1}J_{CH}$ correlations to carbons at δ_C 129.9 (C-2) and 142.7 (C-3) respectively. From these data the spin system was proposed to be an allylic alcohol or ether. In the CIGAR spectrum the proton at H-2 showed $^{2,3}J_{CH}$ correlations to C-3 and C-4, to the spiroketal carbon C-1, and the quaternary carbon at δ_C 68.9 (C-5). The H-3 proton also showed a $^{3}J_{CH}$ correlation to C-5, hence a five-membered ring (ring A), attached to the 1,8 bisnaphthalene via the spiroketal was constructed (Figure 3.18).

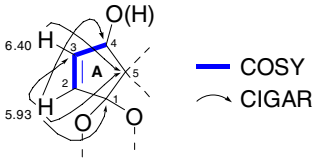

Figure 3.18: *Important COSY and CIGAR correlations observed for ring A*

The second spin system was a two-proton system and showed a doublet proton at δ_H 7.09 (J = 5.7 Hz) (H-7) coupled to another doublet proton at δ_H 7.22 (J = 5.7 Hz) (H-8). The HSQC spectrum showed that these protons had $^{1}J_{CH}$ correlations to carbons at δ_C 151.9 (C-7) and 152.2 (C-8) respectively. In the CIGAR NMR spectrum the protons at H-7 and H-8 both showed $^{2,3}J_{CH}$ correlations to the two carbonyls at δ_C 198.6 (C-6) and 201.1(C-9). CIGAR correlations from the protons at H-7 and H-8 to the quaternary carbon at C-5

enabled the closure of a cyclopentadione ring (ring B), and simultaneously revealed that the point of attachment of the two five-membered rings was a spirocentre (Figure 3.19).

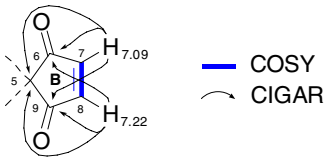

Figure 3.19: *COSY and CIGAR NMR correlations for ring B.*

The alternative isomer (Figure 3.20) in which the ketones are placed adjacent to each other would also fit the observed CIGAR correlations, but this was not considered a possibility because the chemical shifts of the two olefinic carbons would be quite different from those actually observed.

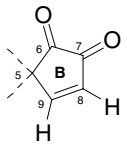

	δ_C
C-6	198.8
C-7	184.8
C-8	129.4
C-9	170.6

Figure 3.20: *Alternative substitution pattern of ring B including ACD Labs chemical shift calculations.*

Taking account of the structural components elaborated, just 1 Da was unaccounted for, suggesting that the oxygen substituent attached at C-4 was an hydroxyl and not part of an ether.

The structure of **3.11** was found to have no matches in the literature, confirming it as a new natural product. The top half of the molecule comprising rings A and B was in fact so unusual it was found to be structurally unprecedented, not just in the spirobisnaphthalene class of compounds, but also in the natural product and synthetic compound literature. In light of the new carbon skeleton, the compound was given the name spiro-mamakone A (**3.11**). A complete list of NMR data is presented in Table 3.4.

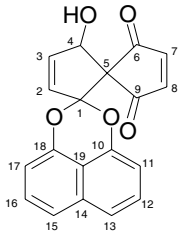

3.11

Table 3.4: *NMR data for* ***3.11***

position	$\delta^{13}C^{a}$, ppm	δ^{1}H ppm, multiplicity, (J_{HH} Hz)	COSY	CIGAR
1	111.7 (C)			
2	129.9 (CH)	5.93 dd (5.8, 2.0)	H-3, H-4	C-5, C-4, C-1, C-3
3	142.7 (CH)	6.40 dd (5.8, 1.9)	H-2, H-4	C-5, C-4, C-2
4	79.1 (CH)	5.30 brs	H-3, H-2	C-2, C-3, C-6, C-9
5	68.9 (C)			
6	198.6 (C)			
7	152.2 (CH)	7.09 d (5.7)	H-8	C-5, C-8, C-6, C-9
8	151.9 (CH)	7.22 d (5.7)	H-7	C-5, C-7, C-6, C-9
9	201.1 (C)			
10	149.4 (C)			
11	111.0 (CH)	6.83 d (7.3)	H-12	C-19, C-13, C-14, C-10
12	129.0 (CH)	7.40 t (7.8, 7.8)	H-13, H-11	C-10, C-14, C-19, C-11
13	122.0 (CH)	7.45 d (8.8)	H-12	C-18, C-14, C-15, C-19, C-11
14	136.1 (C)			
15	122.5 (CH)	7.47 d (8.8)	H-16	C-10, C-14, C-13, C-19, C-17
16	128.7 (CH)	7.36 t (7.8, 7.8)	H-15, H-17	C-18, C-14, C-19, C-17
17	110.6 (CH)	6.76 d (7.3)	H-16	C-19, C-15, C-14, C-18
18	148.8 (C)			
19	114.8 (C)			

[a] No. of attached protons determined by HSQC-DEPT experiments.
^{1}H and 2D NMR experiments carried out at 500 MHz in CD_3OD . ^{13}C data obtained at 75 MHz.
Carbon assignments for C-2 and C-3 based on the results of CIGAR NMR data for spiro-mamakone C (**3.16**).

spiro-Mamakone A (**3.11**) showed potent activity in the P388 (IC_{50} 0.33 μM) and was a strong inhibitor against *Bacillus subtilis* (12 mm), *Trichophyton mentagrophytes* (10 mm) and *Cladosporium resinae* (6 mm) in the antimicrobial assays.

*3.5.4.1 Confirmation of spiro-Mamakone A (**3.11**) – The Hemi-Synthesis of 4-oxo-spiro-Mamakone A (**3.12**)*

In an attempt to obtain confirmation of this unusual structure by X-ray crystallography, efforts were made to obtain suitable crystals of **3.11**. These attempts were unsuccessful. However, a simple modification, through oxidation of the allylic alcohol at C-4, was made to produce a more symmetrical compound. It was predicted that removal of the stereocentre at C-4, would render H-7 and H-8 magnetically equivalent.

Oxidation with freshly prepared manganese oxide (see Scheme 3.1 and Experimental) proceeded smoothly to give the expected triketone, in which the H-7 and H-8 protons were indeed found to be equivalent in the ^{1}H NMR spectrum (Figure 3.21).

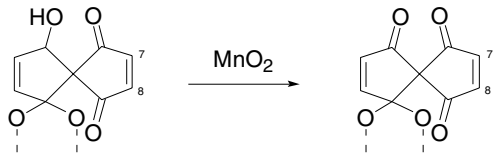

3.11 **3.12**

Scheme 3.1: *Oxidation of spiro-mamakone A (**3.11**)*

Another consequence of the oxidation is the symmetrisation of the intact naphthalene unit. This is a consequence of the newly introduced mirror plane, which passes through both centres, making rings D and E symmetrically equivalent. This change from C_1 to C_s symmetry is also reflected in the simplified ^{1}H and ^{13}C NMR spectra.

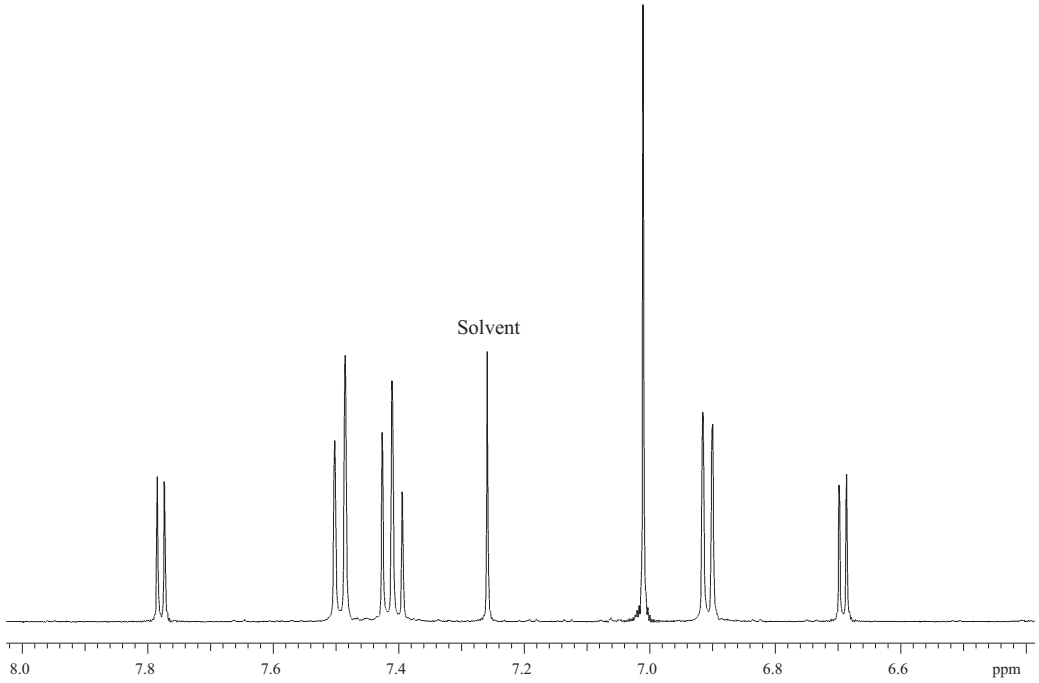

Figure 3.21: *^{1}H NMR spectrum of 4-oxo-spiro-mamakone A (**3.12**) in $CDCl_3$.*

The CIGAR spectrum confirmed that a ketone had replaced the hydroxyl at C-4. This was seen from the correlations from the two doublet protons at δ_H 7.77 (H-3) and 6.69 (H-2) to an α,β-unsaturated ketone at δ_C 196.0 (C-4). The IR spectrum also showed the conversion was successful, indicated by an additional carbonyl stretch at 1763 cm^{-1}. The remaining 2D NMR data were in agreement with the structure of **3.12** (see Experimental for ^{1}H and ^{13}C NMR data). EIMS confirmed the mass as 318 ($[M]^{+}$). The new compound was given the name 4-oxo-spiro-mamakone A (**3.12**).

As expected, **3.12**, like that of the parent compound, **3.11**, displayed similar potent biological activity. In the P388 assay the IC_{50} of **3.12** was determined to be 1.13 μM, while in the antimicrobial assay it was shown to display moderate inhibition (3 mm) of *B. subtilis*, *T. mentagrophytes,* and *C. resinae*.

3.5.4.2 Oxidative Removal of the Spiroketal

An investigation into the relationship between the structure and bioactivity of spiro-mamakone A, prompted the modification of **3.11** using a deprotection strategy. It was proposed that the spiro-nonadiene portion of the molecule probably contributed most to the observed activity. This theory was borne out from the observation that the mamakunoic acids, although bearing the 1,8-dihydroxynaphthalene and spiroketal subunits, were not bioactive in the P388 assay.

Oxidative removal of the spiroketal with cerium ammonium nitrate (CAN) (see Scheme 3.2 and Experimental for this chapter), proceded to give the expected spiro-nonadiene triketone (**3.13**).

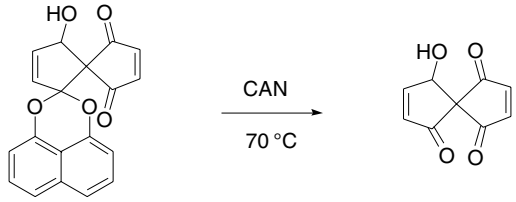

3.11 **3.13**

Scheme 3.2: *Oxidative deprotection of spiro-mamakone A (**3.11**).*

The ^{1}H NMR spectrum (Figure 3.22) showed the expected, 5 unique proton environments assumed for the deprotected molecule. Confirmation that the product was indeed that of the triketone followed from interpretation of the HSQC-DEPT and CIGAR NMR spectra. The CIGAR spectrum showed the presence of three magnetically non-equivalent ketone resonances (δ_C 201.4, 199.2 and 196.4), while the HSQC-DEPT spectrum confirmed the continued presence of the allylic alcohol at C-4. This was indicated from the $^{1}J_{CH}$ corelation observed from the proton at δ_H 5.15 (H-4) to the carbon at δ_C 75.0 (C-4)

In the P388 assay the IC_{50} of **3.13** was determined to be 22.7 μM. Due to the impure nature of the reaction product these results can not be considered particularly accurate Attempts at scaling up and purification of this reaction failed to generate greater amounts

or material of greater purity. **3.13** seemed to very unstable as shortly after generation and/or purification degradation took place.

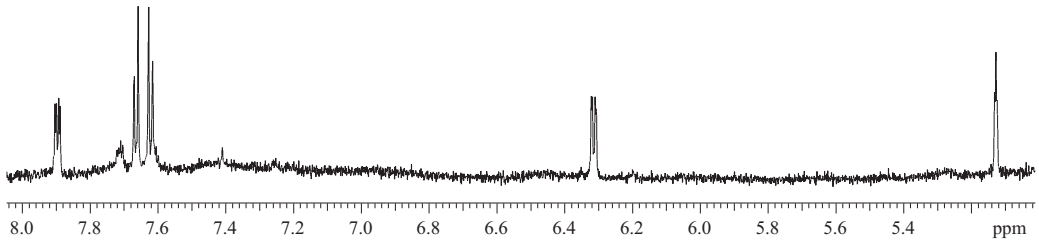

Figure 3.22: *^{1}H NMR spectrum of **3.13** in CD_3OD.*

*3.5.4.3 Stereochemistry of spiro-Mamakone A (**3.11**)*

The structure of **3.11** contains a single stereocentre at C-4, but the absence of any optical rotation suggested that **3.11** existed as a racemic mixture. This could be verified by esterification of **3.11** with both (*S*)- and (*R*)-α-methoxy-α-(trifluoromethyl)phenylacetic acid (MTPACl) (Mosher acid chlorides). If **3.11** were a racemic mixture then each of these derivatisations would produce the same pair of diastereomers. Esterification of **3.11** was carried out by addition of the (*S*)- and (*R*)-Mosher acid chlorides to a mixture of **3.11** and dimethylaminopyridine (DMAP) in pyridine (see Scheme 3.3 and Experimental) according to the method of Ward et al.[79]

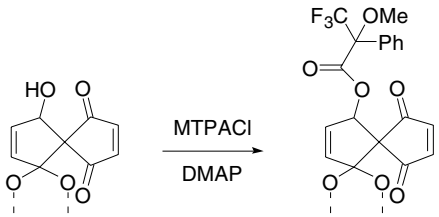

3.11

Scheme 3.3: *Esterification of **3.11** with Mosher's acid chloride (MTPACl)*

The resulting HPLC chromatogram (Figure 3.23) provided confirmation that **4.11** was a racemic mixture.

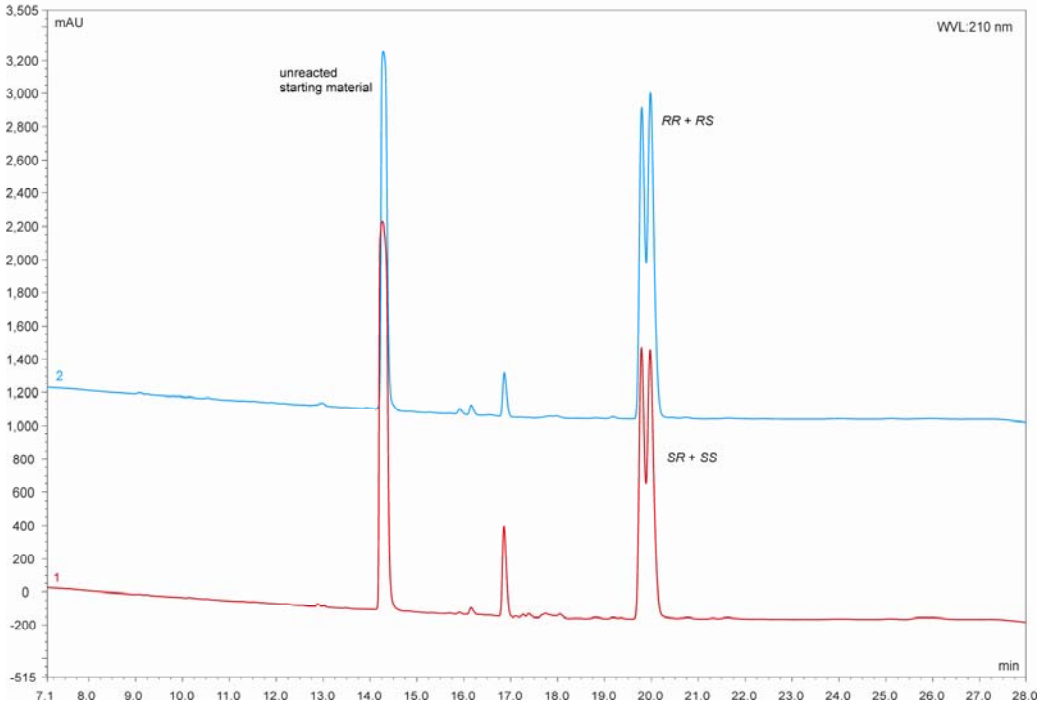

Figure 3.23: *HPLC chromatogram showing reaction products of Mosher esterification.*

For each of the derivatised products, two peaks of equal intensity were observed at identical retention times. These peaks represent the two diastereomers, which are formed when a chiral derivatisation occurs at a racemic centre. To confirm that the peaks at around 20 minutes were the desired ester products, the peaks were individually collected from the HPLC and submitted for direct inject ESIMS. All four peaks showed identical mass peaks at 559 ($[M+Na]^+$), confirming them as esterification products of **3.11** (Figure 3.24).

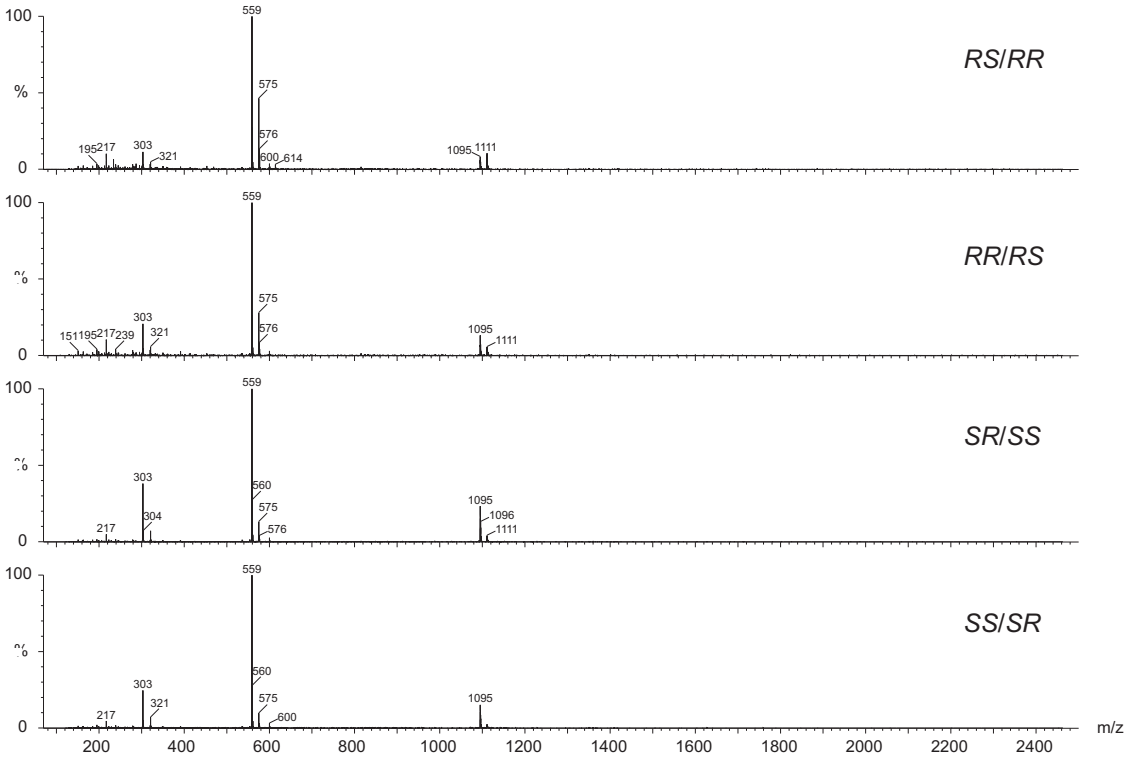

Figure 3.24: *ESIMS showing the characteristic $[M+Na]^+$ adducts (559 Da) of the esterification products of* ***3.11****.*

3.6 Discussion

Purification of an extract from an unidentified endophytic fungus (F5062) has resulted in the isolation of four new compounds of the spirobisnaphthalene class. This rather large class, which include the palmarumycins, cladospirones, diepoxins and preussomerins, all contain a common spiroketal-linked 1,8 bisnaphthalene moiety. The first three compounds have been named mamakunoic acid A, B and C.

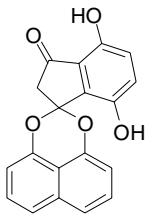

3.14

Mamakunoic acid B and C differ from the already known spirobisnaphthalenes by virtue of an acid functionality attached to a furan ring. In terms of the spirobisnaphthalene class of compounds they most resemble palmarumycin C_6 (**3.14**),[80] but only in that they both contain an indan system, connected to the 1,8-dihydroxy naphthalene via a spiroketal bridge. Mamakunoic acid B was identified as the ring-closed dehydration product from mamakunoic acid A.

The fourth compound was identified as a spirobisnaphthalene of an unprecedented structural type, featuring an oxygenated spirononadiene ring system, and was named spiro-mamakone A. The spirononadiene and spioketal of **3.11** give the molecule an unusual spatial orientation (Figure 3.25).

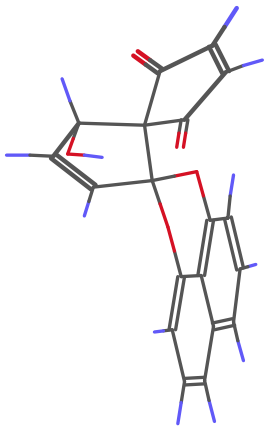

Figure 3.25: *Energy minimised model (MM2) of* ***3.11****, showing unusual spatial orientation.*

Fredericamycin A, an antitumour antibiotic produced by *Streptomyces griseus*[81] (Figure 3.26), was found to contain the closest partial carbon skeleton containing a spirocentre comparable to that of **3.11**.

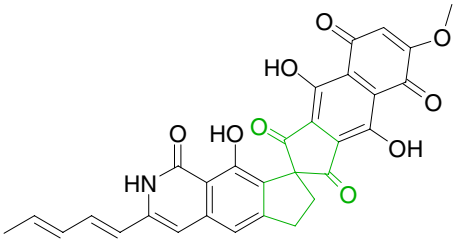

Figure 3.26: *Structure of fredericamycin A, showing the spiro ring system (green) similar to that of* ***3.11***

Due to the almost symmetrical nature and lack of CIGAR correlations linking the two halves of the molecule, the assignment of the chemical shifts (except in the ring junction positions) for the 1,8-dioxynaphthalene portion of the molecule in all four of these new molecules is arbitrary. For example the chemical shift assignments given for positions C-11 (δ_C 111.0, δ_H 6.83) can be interchanged with those on the opposite side, C-17, of the adjacent ring (δ_C 110.6, δ_H 6.76).

Part 2 New Spirobisnaphthalenes from F5584

3.7 Preliminary Investigations of F5584

The fungus E484 (renamed F5584) was re-grown in order to obtain more of the mamakunoic acids A, B, and C (**3.7**, **3.9**, and **3.10**). It was envisioned that a full characterisation, including stereochemistry, could be obtained with more material.

The solid agar culture of F5584 was grown under the same conditions as the original F5062 culture (see Experimental). A total of 24 Plates gave some 249 mg of crude extract. HPLC analysis of an aliquot of the crude extract using an RP C18 column showed that the extract was very different to that of F5062 (Figure 3.27).

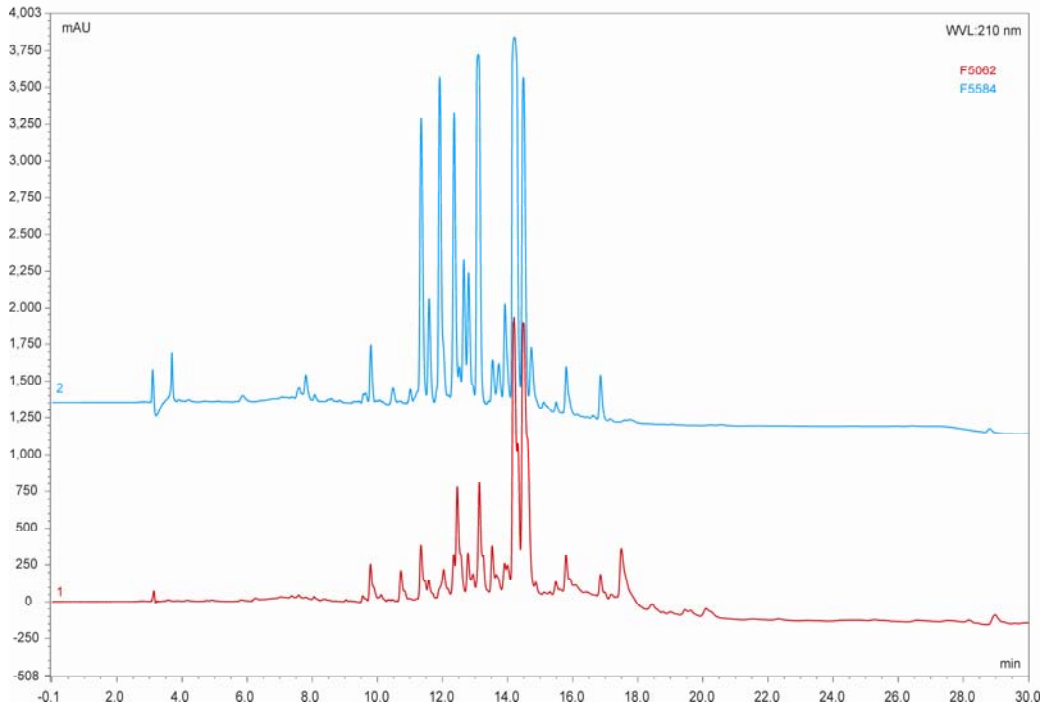

Figure 3.27: *Comparison of the HPLC chromatograms of F5062 and F5584.*

There was only one peak in common between the two extracts. This was the major peak eluting at 14.2 minutes, representing spiro-mamakone A (**3.11**). Despite the extract not containing compounds **3.7**, **3.9**, and **3.10**, the UV chromophores of the other peaks were almost identical to that of **3.11** (Figure 3.28). In the hope of finding compounds related to the structurally unprecedented spiro compound, **3.11**, the extract was pursued further.

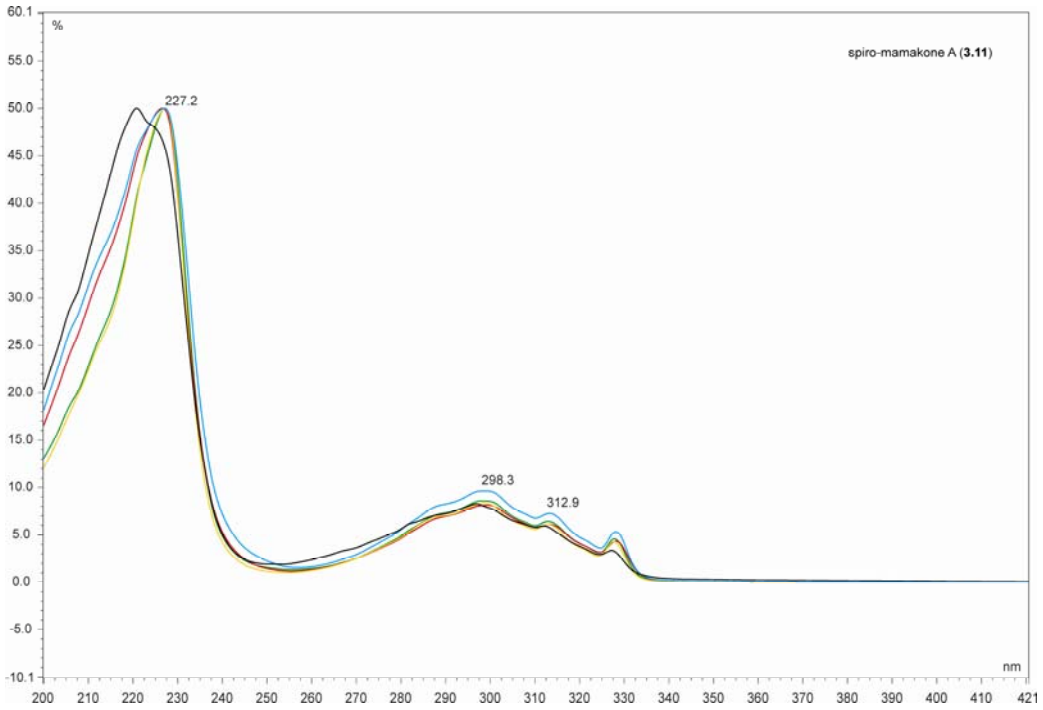

Figure 3.28: *UV spectra overlay of the major peaks in the HPLC of F5584.*

3.8 Chromatography of F5584

The crude extract of F5584 was subjected to reverse phase (C18) flash chromatography using a stepped gradient for elution (see Experimental). Two sequential fractions (SAS-5-103.9 and SAS-5-103.10) that eluted with MeOH/H_2O (9:1), contained the compounds related to **3.11** (Figure 3.29). The fraction, SAS-5-103.11 that eluted at 100% MeOH contained **3.11**. At this stage fractions SAS-5-103.9 and SAS-5-103.10 were considered sufficiently pure for purification by semi-preparative HPLC. Details of the two gradient

methods that were used to elute the compounds of interest are detailed in the Experimental section.

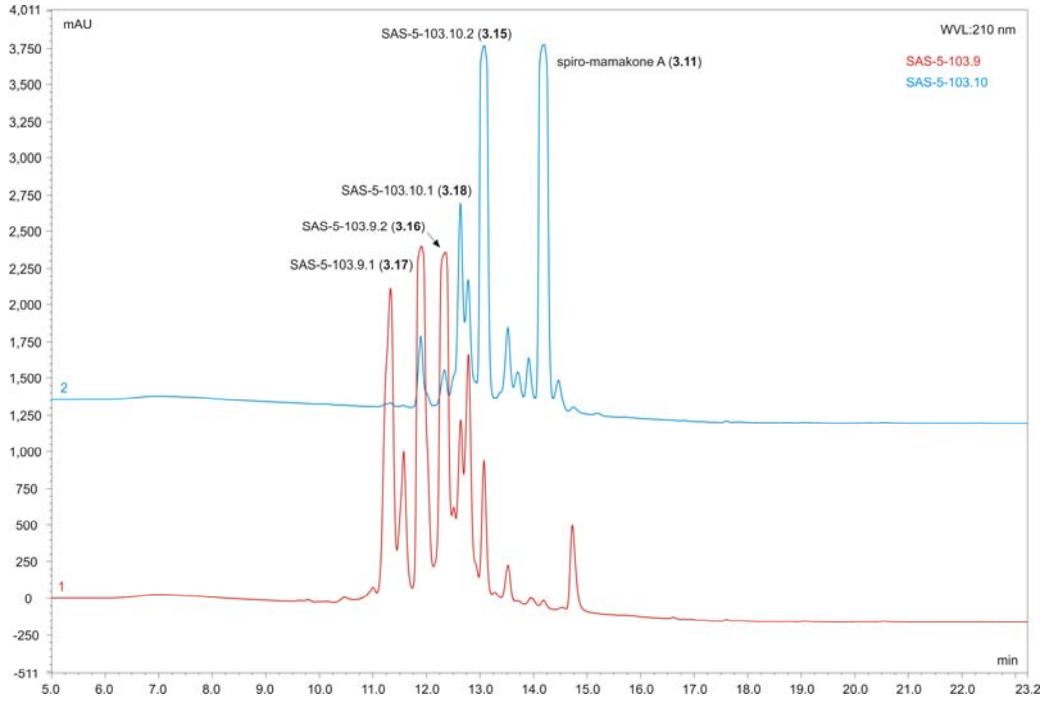

Figure 3.29: *HPLC chromatograms of fractions 9 and 10, indicating those compounds purified.*

Purification of SAS-5-103.9 yielded two compounds, SAS-5-103.9.1 (10.8 mg) and SAS-5-103.9.2 (4.9 mg). The purification of SAS-5-103.10 yielded three compounds, SAS-5-103.10.1 (2.1 mg), SAS-5-103.10.2 (11.8 mg) and spiro-mamakone A (**3.11**) (3.6 mg).

3.9 Structure Elucidation

*3.9.1 Structural Elucidation of SAS-5-103.10.2 (**3.15**)*

SAS-5-103.10.2 (**3.15**) was one of the other major components of the crude extract. ESIMS indicated the mass to be 323 ($[M+H]^+$). An $[M-H_2O]^+$ ion peak at *m/z* 305 suggested the presence of an hydroxyl entity in the molecule. The difference of two mass units between **3.11** and **3.15** could be accounted for by the reduction of one of the

carbonyls in **3.15** to an hydroxyl group. This was supported by HREIMS, which gave a molecular formula of $C_{19}H_{14}O_5$, indicating the molecule had 13 degrees of unsaturation, one less than for **3.11**. The ^{1}H NMR spectrum (Figure 3.30) was very similar to that of **3.11**.

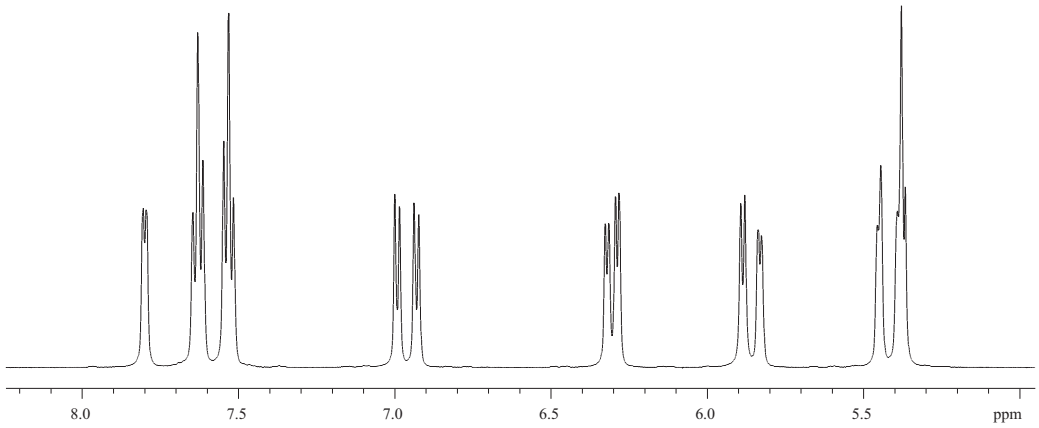

Figure 3.30: *^{1}H NMR spectrum of SAS-5-103.10.2 (**3.15**) in DMSO-d_6.*

The aromatic signals between 6.90-7.60 ppm indicated that **3.15** also contained the 1,8 bisnaphthalene system. Other than this, the notable differences in the spectrum were the presence of a down-field one proton doublet at δ_H 7.80, and rather than just one proton signal in the oxymethine region of the spectrum (as in **3.11**), there were now two, (an overlapping proton signal at δ_H 5.38 and a broad singlet at δ_H 5.44). This was further evidence in favour of the reduction of one of the ketones. The ^{13}C NMR spectrum (Figure 3.31) showed the carbon signals of the 1,8 bisnaphthalene moiety at δ_C 147.8 (C-18), 147.7 (C-10), 134.0 (C-14), 127.6 (C-16), 127.6 (C-12), 120.7 (C-13), 120.4 (C-15), 113.4 (C-19), 109.0 (C-17) and 109.1 (C-11).

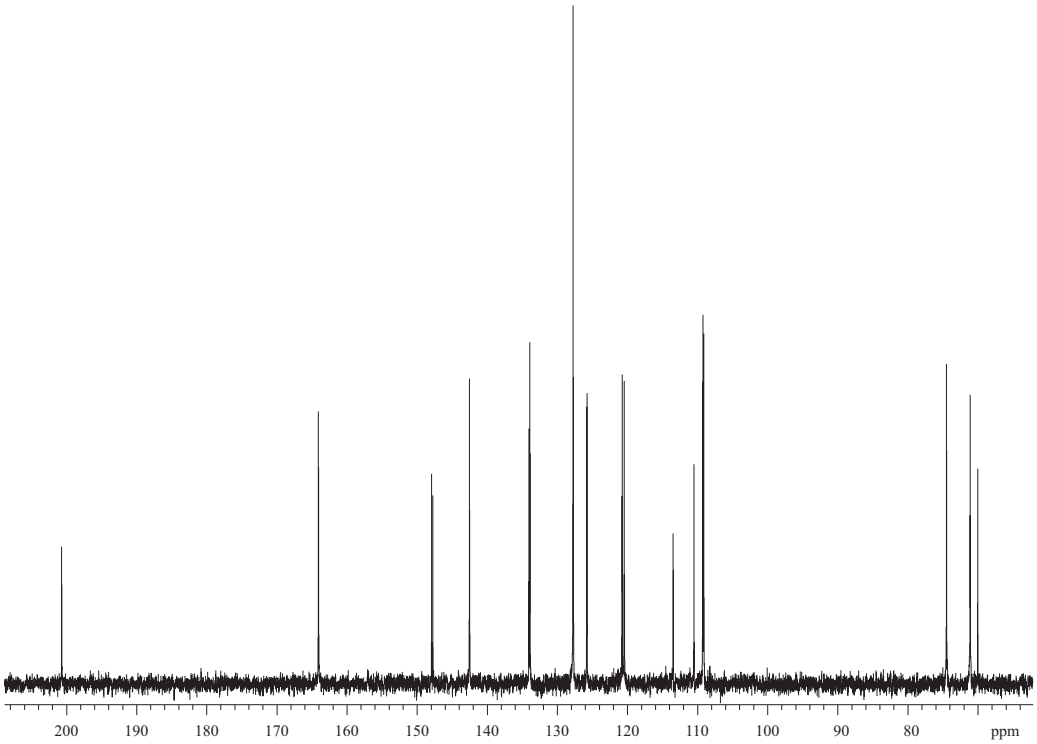

Figure 3.31: *^{13}C NMR spectrum of SAS-5-103.10.2 (**3.15**) in DMSO-d_6.*

The connectivities of the aromatic protons at 6.90-7.60 ppm to these carbons, forming the naphthalene system, were confirmed by COSY, HSQC and CIGAR experiments. Also present in the ^{13}C NMR spectrum was a quaternary carbon at δ_C 110.4 representing the spiroketal carbon. A quaternary carbon at δ_C 69.9 was assumed to be the spirocentre carbon, thus **3.15** appeared to be part of the spiro-mamakone series, rather than the mamakunoic acid series. Also present in the spectrum were two oxymethine carbons at δ_C 74.4 and 71.0 and only one α,β-unsaturated ketone carbon (at δ_C 200.6). 2D NMR correlations provided the remaining connections to form the upper portion of the molecule.

COSY correlations from a one proton doublet at δ_H 5.83 (H-2) to another proton doublet at δ_H 6.28 (H-3) and a broad singlet proton at δ_H 5.44 (H-4) suggested that the structure of ring A in **3.11** was retained in ring A of **3.15**. Interestingly, the H-4 proton showed three COSY correlations rather than two. The third correlation was to a proton at δ_H 5.37. This proton showed no correlations to any carbons in the HSQC experiment, and was

therefore assigned the C-4 hydroxyl proton. Another proton signal at δ_H 5.88 showed COSY correlations to the H-9 proton on ring B, but showed no correlations in the HSQC spectrum. Thus, this was presumed to be the C-9 hydroxyl proton. The HSQC and CIGAR correlations confirmed this (Table 3.5). This meant that the point of difference between **3.11** and **3.15** was located in ring B.

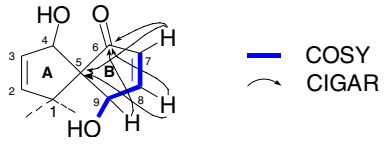

Figure 3.32: *COSY and CIGAR correlations for ring* ***B****.*

In ring B, COSY correlations were observed from the one proton doublet of doublets at δ_H 7.80 (H-8) to a one-proton doublet at δ_H 6.32 (H-7) and an overlapping proton signal at δ_H 5.38 (H-9) (Figure 3.32). The pattern was immediately suggestive of the allylic alcohol moiety seen in ring A. The HSQC spectrum confirmed that the H-9 proton was part of a second oxymethine, as was shown by the observed $^1J_{CH}$ correlation to the carbon at δ_C 71.0 (C-9). The protons at H-7 and H-8 showed $^1J_{CH}$ correlations to carbons at δ_C 133.8 and 164.0 respectively. CIGAR correlations from the protons at H-7, H-8 and H-9 to a carbonyl carbon at δ_C 200.6 confirmed that C-6 was the location of the α,β-unsaturated ketone. Correlations from H-7 and H-8 to C-5, showed that like **3.11**, the connection of the two rings, A and B, was via the spiro centre. The CIGAR correlation from the hydroxyl proton at δ_H 5.37 was to the carbon at δ_C 142.4, rather than δ_C 125.7. This confirmed that C-3 had a chemical shift of 142.4 ppm rather than C-2. This was interesting as the ACD Labs© software, as well as the literature predicted that the more downfield chemical shift (142.4 ppm) would be C-2, and the more upfield chemical shift (125.7 ppm) to be C-3. These assignments were subsequently confirmed by the biosynthetic studies (see Section 3.14.1).

The reduction of a carbonyl on ring B means that unlike **3.11**, **3.15**, contains three stereocentres, C-4, C-9 and the spirocentre, C-5. Because the spirocentre is chiral it means that the placement of the ketone or hydroxyl at either C-6 or C-9 is valid as it is

not a structural issue, but rather a stereochemical one. The stereochemistry of **3.15** is discussed below in Section 3.9.1.1.

All 1D and 2D NMR data (see Table 3.5) were in excellent agreement with the structure proposed (**3.15**). The upper portion of the molecule contains the same novel carbon backbone as compound **3.11**. The new compound was given the name spiro-mamakone C (**3.15**).

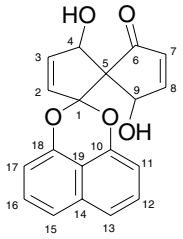

3.15

Table 3.5: *NMR data of* ***3.15***

position	$\delta^{13}C^a$, ppm	δ^1H ppm, multiplicity, (J_{HH} Hz)	COSY	CIGAR
1	110.4 (C)			
2	125.7 (CH)	5.83 d (5.9)	H-3	C-3, C-1, C-4, C-5
3	142.4 (CH)	6.28 d (5.9)	H-4, H-2	C-2, C-1, C-4, C-5
4	74.4 (CH)	5.44 brs	4-OH	C-6, C-2, C-3, C-1, C-9, C-5
5	69.9 (C)			
6	200.6 (C)			
7	133.8 (CH)	6.32 d (5.7)	H-9	C-6, C-8, C-9, C-5
8	164.0 (CH)	7.80 d (5.7)	H-7, H-9	C-6, C-7, C-9, C-5
9	71.0 (CH)	5.38 *ol*	9-OH	C-8, C-7, C-1
10	147.7 (C)			
11	109.1 (CH)	6.93 d (8.0)	H-12	C-10, C-14, C-12, C-13, C-19
12	127.6 (CH)	7.53 *ol*	H-13, H-11	C-10, C-14, C-13, C-19, C-11
13	120.7 (CH)	7.64 *ol*	H-12	C-18, C-14, C-15, C-19, C-11
14	134.0 (C)			
15	120.4 (CH)	7.62 *ol*	H-16	C-10, C-14, C13, C-19, C-17
16	127.6 (CH)	7.53 *ol*	H-15, H-17	C-18, C-14, C-15, C-19, C-17
17	109.0 (CH)	6.99 d (8.0)	H-16	C-18, C-14, C-16, C-15, C-19
18	147.8 (C)			
19	113.4 (C)			
4-OH	74.4	5.37 *ol*	H-4	C-3, C-4, C-5
9-OH	71.0	5.88 d (6.8)	H-9	C-8, C-9, C-5

[a] No. of attached protons determined by HSQC-DEPT experiments.
^1H and 2D NMR data obtained at 500 MHz in DMSO-d_6. ^{13}C NMR carried out at 75 Mhz.
ol- overlap.

3.15 was assessed for biological activity and found to be very active. The IC_{50} of 0.95 μM was of the same order as that of the parent compound **3.11** (0.33 μM). In the

antimicrobial assays, **3.15** strongly inhibited the growth of *B. subtilis* (7 mm) and *T. mentagrophytes* (5 mm), but unlike **3.11** had no activity against *C. resinae*.

*3.9.1.1 Stereochemistry of spiro-Mamakone C (**3.15**)*

Fortunately, after the slow evaporation of MeOH at 4°C, suitable crystals of **3.15** were obtained. Not only did X-ray crystallography confirm the structure of this new class of compound, but it also gave the relative stereochemistry as 4*S**, 5*S**, 9*R** (Figure 3.33).

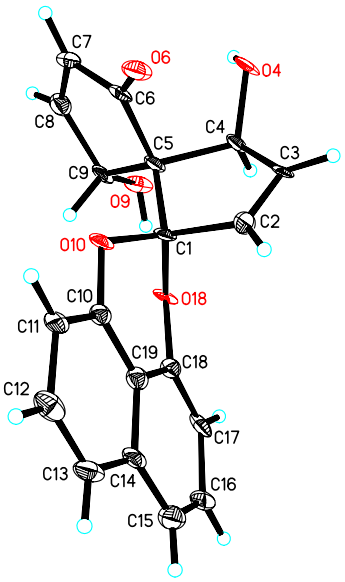

Figure 3.33: *Crystal structure drawing of **3.15**.*

It was surprising, however, to find that the enantiomer (4*R*, 5*R*, 9*S*), was also present in the crystal. This would usually be indicative of a racemic mixture. This however was not the case, as an optical rotation measurement had shown **3.15** to have optical activity. The only possible explanation for this observation was that **3.15** existed as an enantiomeric excess, and the crystal that was analysed coincidently contained both enantiomers.

This meant that appropriate derivatisation of **3.15** with a group carrying a heavy atom followed by crystallisation to obtain the absolute stereochemistry was now, no longer necessary.

In order to confirm the presence of an enantiomeric excess, derivatisation of **3.15** with Mosher acid chlorides was carried out following the methods used for the derivatisation of **3.11** (see Experimental, Section 7.3.6). Unfortunately, the esterification products were not able to be detected by HPLC or ESIMS. Due to limited material available, esterification was not attempted a second time. It is envisioned that this work will be carried out at a later date.

*3.9.2 Structure Elucidation of SAS-5-103.9.2 (**3.16**)*

Another of the major compounds from the C18 column fraction, SAS-5-103.10 was purified. This was SAS-5-103.9.2 (**3.16**). ESIMS revealed the compound to also have a mass of 323 ($[M+H]^+$), identical to that of **3.15**. As was also seen in the ESIMS of **3.15**, there were peaks at 305 ($[M-H_2O]^+$) and 355 ($[M+Na]^+$). HREIMS also gave a molecular formula identical to that of **3.15** ($C_{19}H_{14}O_5$), hence the number of double bond equivalents were also the same as for **3.15**. From these data it was obvious that **3.16**, was an isomer of **3.15**. The ^{13}C NMR spectrum (Figure 3.34) indicated that it was probably a stereoisomer, as the spectrum showed chemical shifts that were very similar to those of **3.15**. The ^{1}H NMR spectrum (Figure 3.35) of **3.16** contained two less proton signals than that of **3.15**, however apart from the extra signals, the spectrum appeared to be very similar to that of **3.15**.

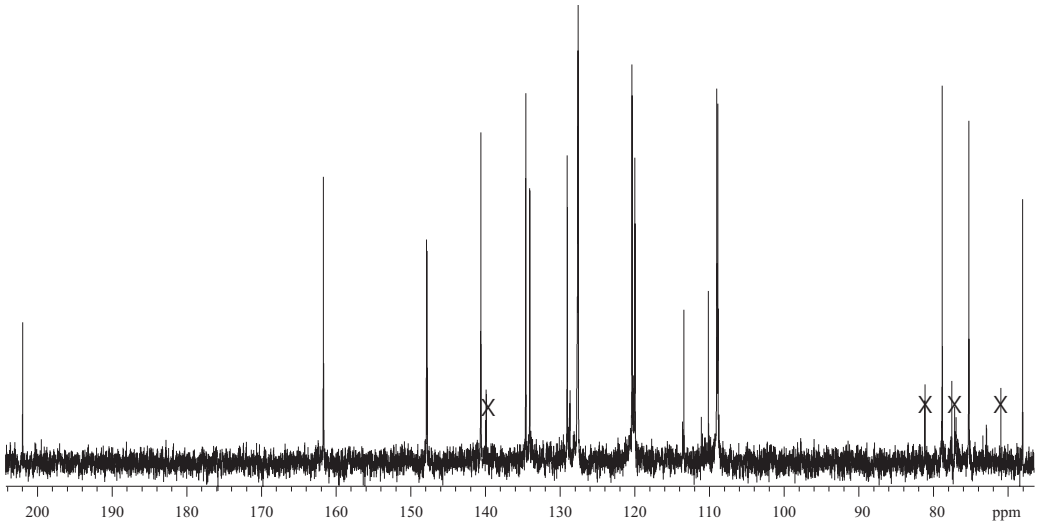

Figure 3.34: *^{13}C NMR spectrum of SAS-5-103.9.2 (**3.16**) in* DMSO-d_6. *Crosses indicate impurities.*

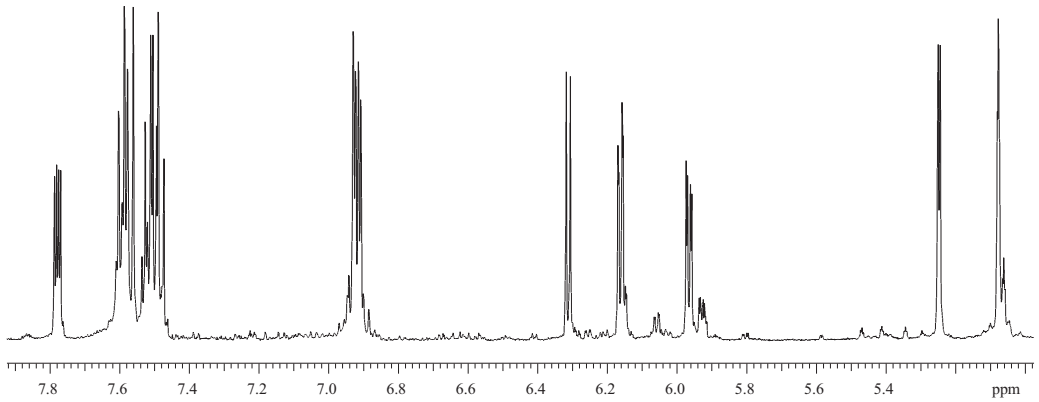

Figure 3.35: *^{1}H NMR spectrum of SAS-5-103.9.2 (**3.16**) in DMSO-d_6.*

COSY and HSQC NMR spectra revealed that the spin systems for both the 1,8-dioxynaphthalene and the upper portion of **3.16** were identical to those of **3.15**. Ring A was confirmed as identical to ring A in **3.15**. Unlike for **3.15**, no hydroxyl proton signals were observed. Appearance of signals for exchangeable protons is expected in DMSO-d_6, and it is therefore unusual that the exchangeable protons were not seen in this spectrum.

All other 1D and 2D NMR data (Table 3.6) were found to be in excellent agreement with **3.16** being a diastereomer of **3.15**.

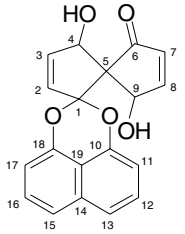

3.16

Table 3.6: *NMR data for* ***3.16***

position	$\delta^{13}C^{a}$, ppm	$\delta^{1}H$ ppm, multiplicity, (J_{HH} Hz)	COSY	CIGAR
1	110.1 (C)			
2	129.0 (CH)	5.95 dd (6.4, 2.0)	H-3, H-4	C-3, C-1, C-4, C-5
3	140.5 (CH)	6.15 dd (6.2, 1.4)	H-3, H-4	C-2, C-1, C-4, C-5
4	78.7 (CH)	5.06 brs	H-3, H-2	C-6, C-3, C-2, C-9
5	68.0 (C)			
6	201.9 (C)			
7	134.5 (CH)	6.30 d (5.9)	H-8	C-6, C-8, C-9, C-5
8	161.6 (CH)	7.77 dd (5.9, 3.0)	H-7, H-9	C-6, C-7, C-9, C-5
9	75.2 (CH)	5.25 d (3.0)	H-8	C-6, C-8, C-7, C-4
10	147.7 (C)			
11	108.8 (CH)	6.90 d (7.2)	H-12	C-10, C-13, C-19
12	127.5 (CH)	7.46 *ol*	H-13, H-11	C-10, C-14, C-19, C-11
13	119.9 (CH)	7.56 *ol*	H-12	C-18, C-14, C-15, C-19, C-11
14	134.0 (C)			
15	120.3 (CH)	7.59 *ol*	H-16	C-10, C-14, C-13, C-19, C-17
16	127.5 (CH)	7.48 *ol*	H-15, H-17	C-18, C-14, C-19, C-17
17	108.9 (CH)	6.92 d (7.2)	H-16	C-18, C-15, C-19
18	147.8 (C)			
19	113.3 (C)			

[a] No. of attached protons determined by HSQC-DEPT experiments.
^{1}H and 2D NMR experiments carried out at 500 MHz in DMSO-d_6. ^{13}C NMR data obtained at 75 MHz.
ol- overlap.

The new compound was given the name spiro-mamakone B (**3.16**). Like that of its isomer (**3.15**), **3.16**, was also found to display strong biological activity. It showed potent cytotoxicity in the P388 assay (1.39 μM) and moderate to high inhibition in the antimicrobial assay (7mm and 8 mm for *B. subtilis* and *T. mentagrophytes* respectively).

*3.9.2.1 Stereochemistry of spiro-Mamakone B (**3.16**)*

An NOE spectrum (Figure 3.36) of **3.16** was obtained. When the proton resonance for H-4 was irradiated the proton signal for H-9 was enhanced.

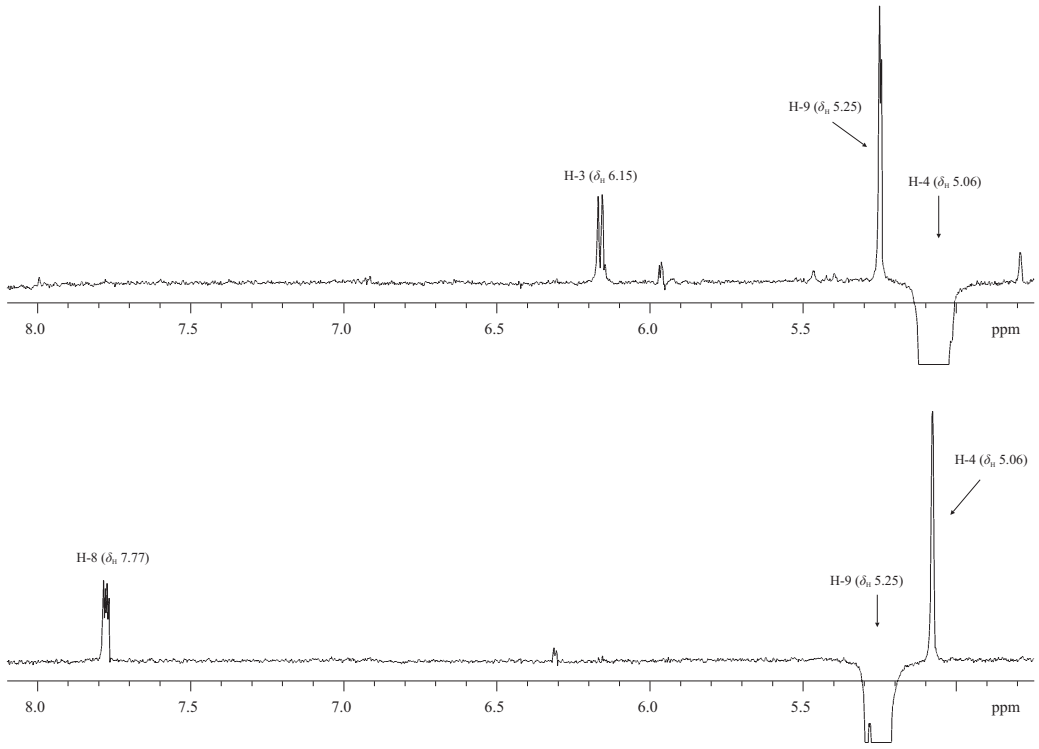

Figure 3.36: *1D NOE NMR spectrum of **3.16**, showing the results of irradiation at H-9 (bottom) and H-4 (top).*

In order to deduce the relative stereochemistry of **3.16**, energy-minimised (MM2) models of the four possible diastereomers were generated. The models, created using CHEM 3D software, gave the distance through space (Å), between H-4 and H-9 for each of the diastereoisomers. As strong NOE correlations are not normally seen beyond a spacing of 3.0 Å, it can be deduced that the relative stereochemistry of **3.16** therefore, is 4*S**, 5*S**, 9*S**, as presented in Figure 3.37b.

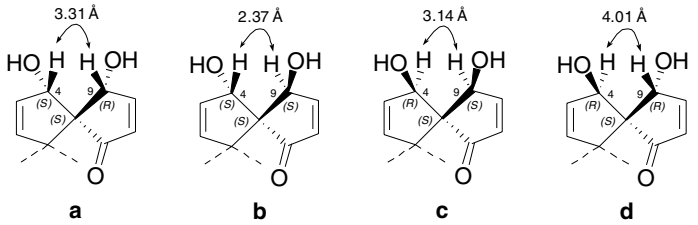

Figure 3.37: *The four possible diastereomers for* ***3.16****, showing H-4–H-9 bond distances (Å).*

The possibility that **3.16** was a purely racemic mixture was disregarded as it was found to be optically active. Like that of **3.15**, it could however exist as a partial racemate. An investigation of this possibility by Mosher derivatisation might have been a possibility had the amount of remaining material been sufficient. The difficulty with working with diols is that introduction of the chiral auxiliary will lead to bis-MTPA esters; each of the phenyl rings producing a combination of shielding/deshielding not only on the protons nearest the chiral centre, but also on the substitiuents of the other chiral centre.[82] In a recent article by Freire *et al*., they describe the use of chiral auxiliaries for determining a reliable absolute stereochemistry of diols.[83] Although this work was applied to linear diols, it will be applied to the spiro-mamakone structure at a future date to explore the level of stereochemical complexity.

*3.9.3 Structure Elucidation of SAS-5-103.9.1 (**3.17**)*

SAS-5-103.10.1 (**3.17**) was also one of the major compounds purified from the extract of F5584. ESIMS gave the mass as *m*/*z* 341 ($[M+H]^+$), however this ion peak was of very low intensity. The base peak was instead at 323 ($[M-H_2O]^+$). A small ion peak at 363 ($[M+Na]^+$) was also observed, confirming *m*/*z* 341 as the correct mass. HREIMS on this compound suggested a molecular formula of $C_{19}H_{16}O_7$, indicating 12 degrees of unsaturation in the molecule.

The ^{1}H NMR spectrum (Figure 3.38) showed aromatic signals between δ_H 6.85-7.49 representing H-11–H-17 of the 1,8-bisnaphthalene system in the lower portion of the molecule. A broad singlet at δ_H 5.51 and two protons at δ_H 5.76 and 6.17 each appearing

as a doublet of doublets, were presumed to represent an allylic alcohol moiety, analogous to ring A of **3.11**, **3.15** and **3.16**.

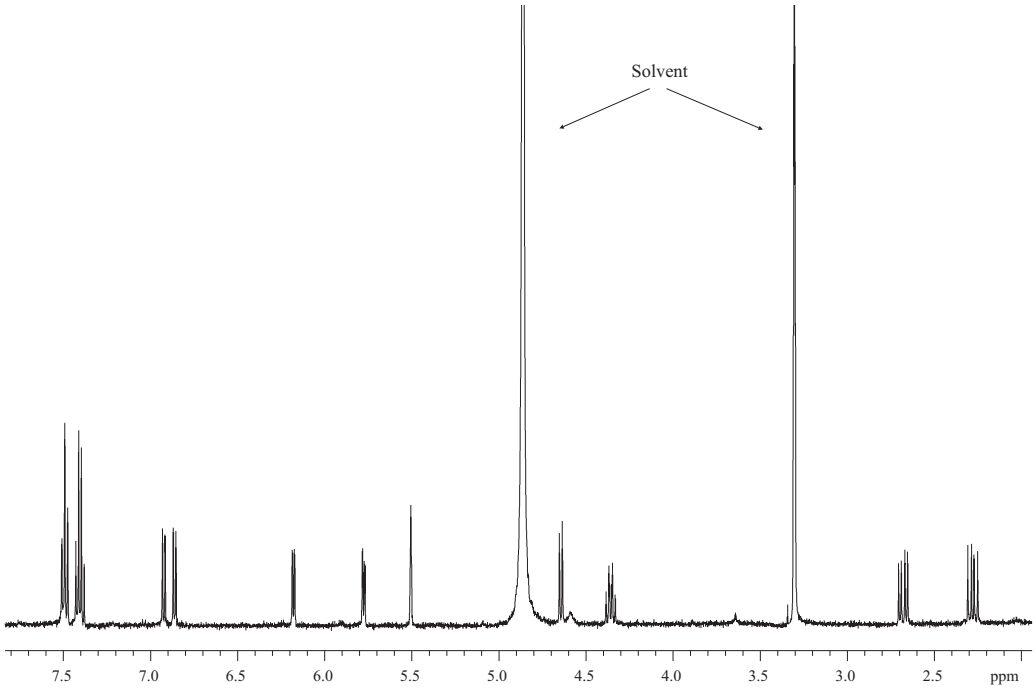

Figure 3.38: *^{1}H NMR spectrum of SAS-5-103.9.1 (**3.17**) in CD_3OD.*

The remainder of the ^{1}H NMR spectrum showed two, one proton doublet of doublets at δ_H 2.29 and 2.68, a one proton doublet of triplets at δ_H 4.37 and a one proton doublet proton at δ_H 4.65. This portion of the ^{1}H NMR spectrum did not show any similarity to any of the previously isolated spiro-mamakone molecules.

The ^{13}C NMR spectrum (Figure 3.39) showed a total of eighteen signals, one short of the molecular formula, an indication that two of the carbons signals were overlapping.

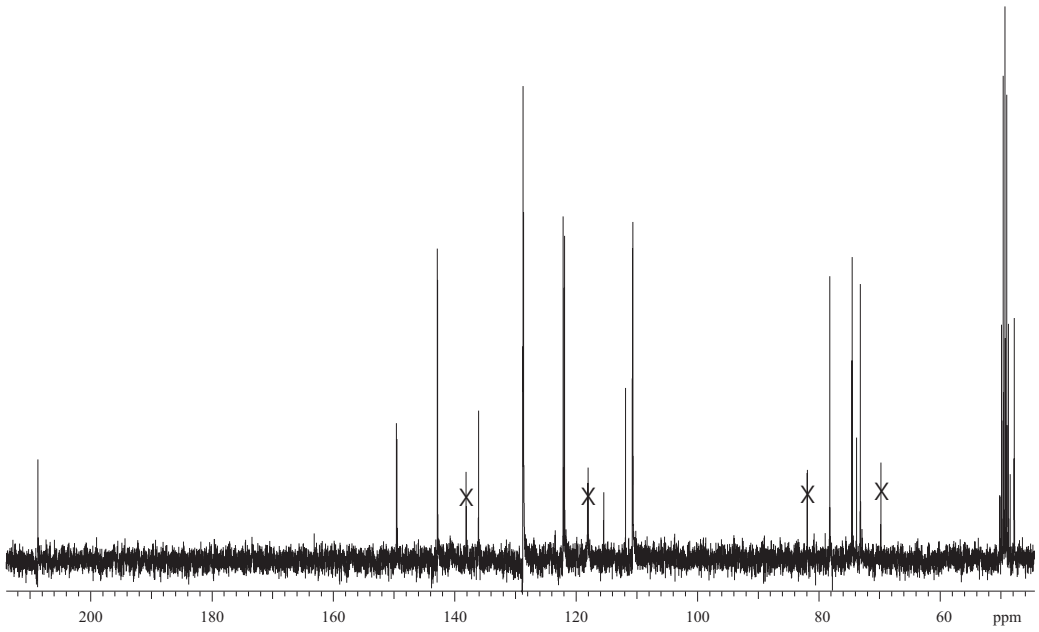

Figure 3.39: *^{13}C NMR spectrum of SAS-5-103.9.1 (**3.17**) in CD_3OD.Crosses indicate impurities.*

These carbons were most likely C-12 and C-16 (δ_C 128.71 and 128.73 respectively) of the naphthalene ring, as these carbons had shown near identical chemical shifts in the previously isolated spiro-mamakone molecules, **3.11**, **3.15** and **3.16**. The presence of the spirobisnaphthalene part of the molecule was confirmed by comparison of the carbon chemical shifts for C-10–C-19 and C-1 with those for **3.11**, **3.15**, and **3.16,** where they were found to be in good agreement. The major differences between the ^{13}C NMR spectrum for **3.17** and those of the other spiro-mamakones, were a high field carbon at δ_C 47.8 and an extra carbon in the 70 ppm region, probably indicative of the presence of an extra hydroxyl grouping. Because the A, C, D, and E rings were already proposed to be identical to those of the other spiro-mamakones, and confirmed by 2D NMR data (Table 3.7), the differences observed were the result of structural changes to ring B. The ring B spin system, shown in Figure 3.40, was shown by COSY data to contain a proton at δ_H 4.37 correlated to a proton at δ_H 4.65 and to the two protons at δ_H 2.29 and 2.68.

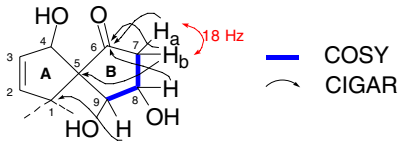

Figure 3.40: *COSY and CIGAR correlations for ring B.*

The HSQC NMR spectrum showed that these latter two protons had a $^{1}J_{CH}$ correlation to the same carbon at δ_C 47.8, thereby confirming these protons as diastereotopic methylene protons. $^{1}J_{CH}$ correlations were also observed from δ_H 4.37 and 4.65 to carbons at δ_C 73.2 and 78.2 respectively, thus confirming a diol moiety. COSY NMR also determined that the methylene protons and the proton at δ_H 4.65 were adjacent to only one proton and therefore the other adjacent position must contain a quaternary carbon. CIGAR correlations from both the methylene protons and the proton at δ_H 4.37 to a carbonyl at δ_C 208.7 indicated the presence of a ketone on ring B. A CIGAR correlation from H-4 on ring A to this same carbonyl meant that the ketone at δ_C 208.7 was placed at C-6 of ring B. As mentioned previously it was proposed that both the methylene protons and the proton at δ_H 4.65 were adjacent to quaternary carbons. The methylene protons were found to have the very large geminal coupling constant of J = 18.0 Hz. This large coupling constant is very characteristic of a geminal coupling of a methylene adjacent to a carbonyl. For this reason the methylene protons at δ_H 2.29 and 2.68 were arbitrarily assigned to H-7a and H-7b respectively. Based on the COSY correlations previously mentioned the protons at δ_H 4.37 and 4.65 were assigned to the adjacent positions, H-8 and H-9 respectively. A CIGAR correlation from H-7b to the carbon at C-5 (δ_C 73.8) confirmed the attachment of ring B to that of ring A through the spirocentre at C-5. A $^{3}J_{CH}$ CIGAR correlation was also seen from H-9 to C-1, not only confirming the position of this proton, but also the proximity of ring B to that of A. All 1D and 2D data (Table 3.7) were in excellent agreement to that of the proposed structure, **3.17**. The new compound was given the name spiro-mamakone D (**3.17**).

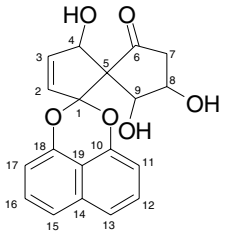

3.17

Table 3.7: *NMR data for* ***3.17***

position	$^{13}C^{a}$, ppm		Experimental ^{1}H, multiplicity, (J_{HH} Hz)	COSY	CIGAR
1	111.8	(C)			
2	128.73	(CH)	5.76 dd (5.9, 2.0)	H-4, H-3	C-3, C-1, C-4, C-5
3	142.8	(CH)	6.17 dd (5.9, 1.4)	H-2, H-4	C-2, C-1, C-4
4	74.5	(CH)	5.51 brs	H-2, H-3	C-6, C-2, C-3, C-1, C-9, C-5
5	73.8	(C)			
6	208.7	(C)			
7	47.8	(CH_2)	a: 2.29 dd (18.0, 10.5)	H-8, H-7b	C-6, C-1, C-9, C-8
			b: 2.68 dd (18.0, 7.5)	H-8, H-7a	C-6, C-5, C-9, C-8
8	73.2	(CH)	4.37 dt (10.3, 8.2, 8.2)	H-9, H-7a, H-7b	C-6, C-9, C-7
9	78.2	(CH)	4.65 d (8.1)	H-8	C-1, C-8, C-7
10	149.6	(C)			
11	110.6	(CH)	6.85 d (7.7)	H-12	C-10, C-14, C-13, C-19
12	128.71	(CH)	7.40 t (7.7)	H-13, H-11	C-10, C-14, C-13, C-19, C-11
13	121.9	(CH)	7.47 d (8.3)	H-12	C-18, C-14, C-15, C-19, C-11
14	136.1	(C)			
15	122.1	(CH)	7.49 d (8.3)	H-16	C-10, C-14, C-13, C-19, C-17
16	128.73	(CH)	7.39 t (7.7)	H-15, H-17	C-18, C-14, C-15, C-19, C-17
17	110.7	(CH)	6.92 d (7.7)	H-16	C-18, C-14, C-15, C-19
18	149.5	(C)			
19	115.4	(C)			

[a] No. of attached protons determined by HSQC-DEPT experiments.
^{1}H and 2D NMR experiments carried out at 500 MHz in CD_3OD.

The introduction of an extra hydroxyl into ring B increased the number of stereocentres to four, equating to eight possible diastereomers. Approaches taken to elucidating the stereochemistry are discussed in Section 3.10.5.

The P388 activity of **3.17** was assessed, and found to have an IC_{50} of 3.76 μM. Unlike the parent compound (**3.11**) and the diasteromeric partially reduced derivatives, **3.15** and **3.16**, spiro-mamakone D (**3.17**) did not show any antimicrobial activity.

*3.9.4 Structural Elucidation of SAS-5-103.10.1 (**3.18**)*

SAS-5-103.10.1 (**3.18**) was purified from the F5584 extract as a minor component. ESIMS gave the mass as 341 ($[M+H]^+$), identical to that of **3.17**. As seen in the ESIMS of **3.17**, it was the $[M-H_2O]^+$ ion (*m*/*z* 323) that was most abundant. As expected, HREIMS suggested the molecular formula $C_{19}H_{16}O_6$, indicating the molecule also had 12 double bond equivalents. Because **3.15** and **3.16** had already been elucidated as diastereomers, it was proposed that **3.17** and **3.18** were also diastereomers.

Interpreting the ^{1}H NMR spectrum (Figure 3.41) was unfortunately not as simple as it could have been, as the sample of **3.18** was not entirely pure. Despite this, the desired signals were clearly distinguishable from those for the impurity.

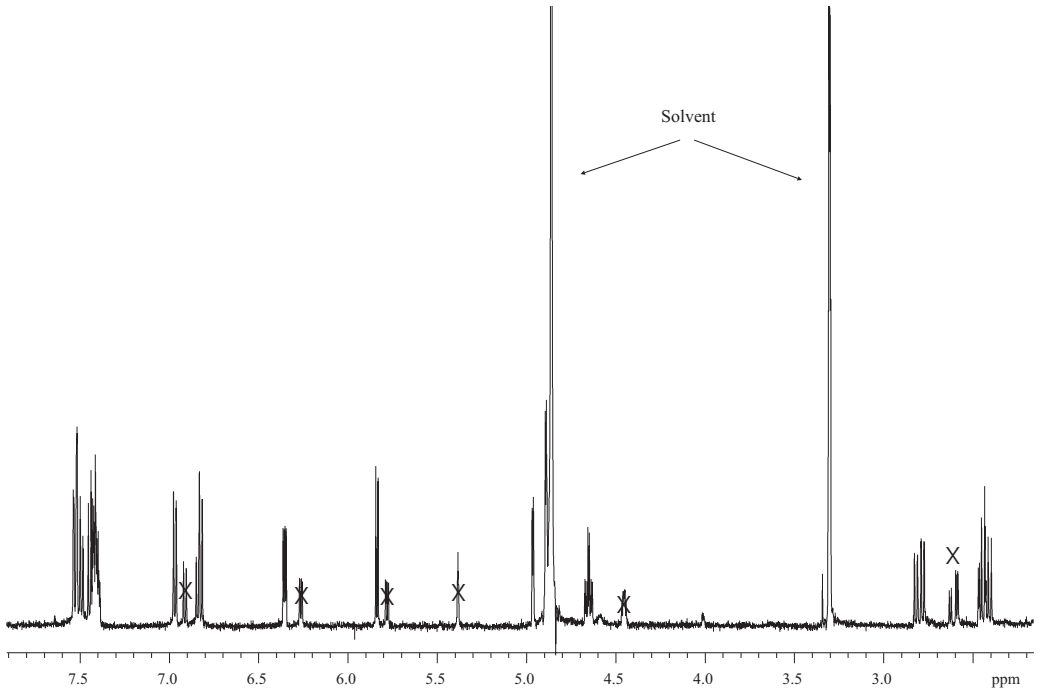

***Figure 3.41:** ^{1}H NMR spectrum of SAS-5-103.10.1 (**3.18**) in CD_3OD. Crosses indicate impurities.*

It was apparent from the ^{1}H NMR (Figure 3.41) and COSY spectra that **3.18** was an isomer of **3.17**. This was shown by the 1,8-bisnaphthalene proton signals between δ_H 6.82 and 7.53. Also present were methylene signals appearing as doublets of doublets at δ_H 2.43 and 2.80. The large geminal coupling constant of J_{HH} = 18.5 Hz, indicated that

the methylene protons were again adjacent to a carbonyl, as was shown for **3.17**. Proton signals at δ_H 6.35, 5.84 and 4.89 were observed for the allylic alcohol moiety on ring **A**. Also present was a proton at δ_H 4.65, with a doublet of triplets multiplicity, indicating coupling to both methylene protons and a neighbouring oxymethine proton.

The remaining 2D NMR data (Table 3.8) were in excellent agreement with the structure proposed (**3.18**). This new compound, a diastereomer of the previously isolated spiro-mamakone D (**3.17**), was given the name spiro-mamakone E (**3.18**). Discussions on stereochemistry are given in Section 3.9.5.

Biological data was not obtained due the impure nature of the sample, and its subsequent degradation.

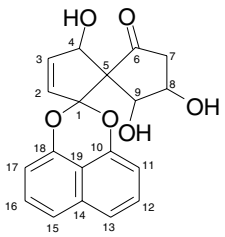

3.18

Table 3.8: *NMR data of* ***3.18***

position	$^{13}C^{a}$, ppm^{b}	Experimental ^{1}H, multiplicity, (J_{HH} Hz)	COSY	CIGAR
1	110.5 (C)			
2	129.5 (CH)	5.84 d (6.4, 2.0)	H-3	C-3, C-1, C-4, C-5
3	139.7 (CH)	6.35 dd (5.9, 2.9)	H-2, H-4	C-4
4	76.1 (CH)	4.89 d (3.0)	H-3	C-6, C-2, C-3, C-1
5	72.2 (C)			
6	211.1 (C)			
7	42.7 (CH_2)	a: 2.43 dd (18.5, 9.0)	H-8, H-7a	C-6, C-8
		b: 2.80 dd (18.5, 8.5)	H-8, H-7b	C-6, C-8
8	68.2 (CH)	4.65 dt (8.9, 8.5, 3.5)	H-9, H-7a, H-7b	C-9
9	74.1 (CH)	4.97 d (3.5)	H-8	C-6, C-7
10	147.3 (C)			
11	108.9 (CH)	6.82 d (7.6)	H-12	C-10, C-13, C-19
12	127.1 (CH)	7.42 *ol*	H-13, H-11	C-10, C-14
13	120.6 (CH)	7.53 *ol*	H-12	C-18, C-14, C-13, C-19, C-11
14	134.4 (C)			
15	120.7 (CH)	7.52 *ol*	H-16	C-10, C-14, C-15, C-19, C-17
16	127.1 (CH)	7.44 *ol*	H-15, H-17	C-18, C-14
17	109.1 (CH)	6.97 d (7.6)	H-16	C-18, C-15, C-18
18	147.6 (C)			
19	113.8 (C)			

[a] No. of attached protons determined by HSQC-DEPT experiments.
[b] Carbon chemical shifts determined from HSQC and CIGAR experiments.
^{1}H and 2D NMR experiments carried out at 500 MHz in CD_3OD.
ol- overlap.

*3.9.5 Stereochemical Assignment of spiro-Mamakones D (**3.17**) and E (**3.18**)*

A different approach to the stereochemical elucidation was taken with **3.17** and **3.18**. The approach taken was to calculate all coupling constants for all possible stereoisomers and to then compare these values against the experimentally determined coupling constants. This required the input of dihedral angles and spatial orientation (stereochemistry) of the adjacent carbons into the computer program, MestReJ. The programme calculates coupling constants based on the modified Karplus equation, known as the Haasnoot-de Leeuw-Altona equation. The calculated coupling constants are then compared to the experimentally obtained coupling constants. A match of experimental with calculated coupling constants can thus provide a tentative relative stereochemistry.

Minimum energy conformations for each of the eight possible diastereomers for **3.17**, and **3.18** were modelled using CHEM-3D computer software. The dihedral angles (ϕ) between each of the proton pairs, H-8, H-9; H-8, H7a and H-8, H-7b, were measured from the modelled structures. These dihedral angles, together with the stereochemistry of the carbon centres of the adjacent proton pairs, were entered into the Mestre-J program to generate the coupling constants (Figure 3.42).

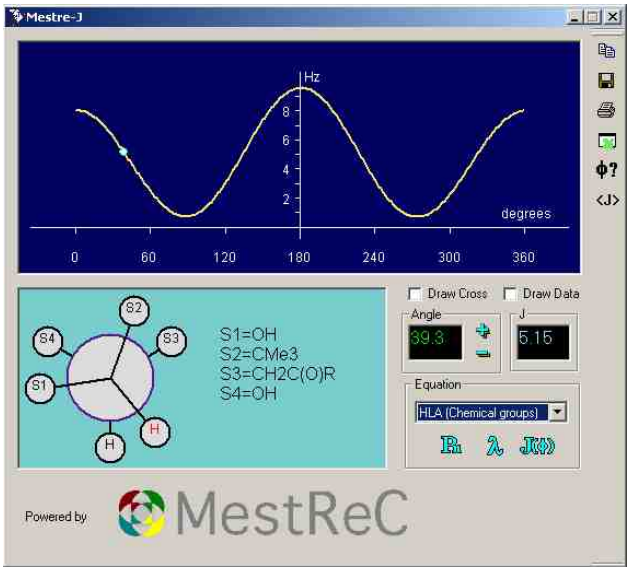

Figure 3.42: *Screen capture of the Mestre-J program, showing the calculated coupling constant of the H-8, H-9 proton pair, resulting from specification of the dihedral angle and carbon substituents.*

The results of the Mestre-J calculations, as well as the actual experimental coupling constants, for the proton pairs of **3.17** and **3.18** are presented in Table 3.9. Initially the results seemed very promising, in that the data allowed a relative stereochemistry for both molecules to be proposed. This can be seen in Table 3.9, where the closest matches to the experimental data of **3.17** and **3.18** are 4*S*, 5*S*, 8*S*, 9*S* and 4*S*, 5*S*, 8*S*, 9*R* respectively. The initial proposal that **3.17** and **3.18** were *trans* and *cis* isomers respectively, across the diol was confirmed by these calculations, as the coupling constants for the two orientations are very distinctive.

Table 3.9: *Coupling constants calculated by Mestre-J for the possible diastereomers, as well as experimental coupling constants for* ***3.17*** *and* ***3.18****.*

calculated	H-8-H-9		H-8-H-7a		H-8-H-7b	
	ϕ (°)	J_{HH} (Hz)	ϕ (°)	J_{HH} (Hz)	ϕ (°)	J_{HH} (Hz)
4*S*, 5*S*, 8*S*, 9*S*	156.0	**9.48**	13.5	**10.17**	137.0	**6.13**
4*S*, 5*S*, 8*R*, 9*R*	75.0	1.95	96.4	1.17	26.6	7.41
4*R*, 5*S*, 8*S*, 9*S*	162.4	9.81	28.3	8.91	152.1	8.88
4*R*, 5*S*, 8*R*, 9*R*	94.4	0.56	122.3	4.76	1.4	10.17
4*R*, 5*S*, 8*S*, 9*R*	39.3	5.15	18.7	9.86	142.3	7.13
4*S*, 5*S*, 8*S*, 9*R*	45.0	**4.41**	27.5	**9.01**	151.1	**8.71**
4*S*, 5*S*, 8*R*, 9*S*	39.3	4.75	91.0	0.84	30.5	6.78
4*R*, 5*S*, 8*R*, 9*S*	36.4	5.15	91.6	0.87	31.2	6.66
experimental						
3.17		**8.1**		**10.5**		**7.5**
3.18		**3.5**		**9.0**		**8.5**

To help confirm these proposed stereochemical assignments, NOE experiments were carried out on both **3.17** and **3.18**. The *cis* isomer (**3.18**) showed only one NOE relationship, that between H-8 and H-9 (Figure 3.43).

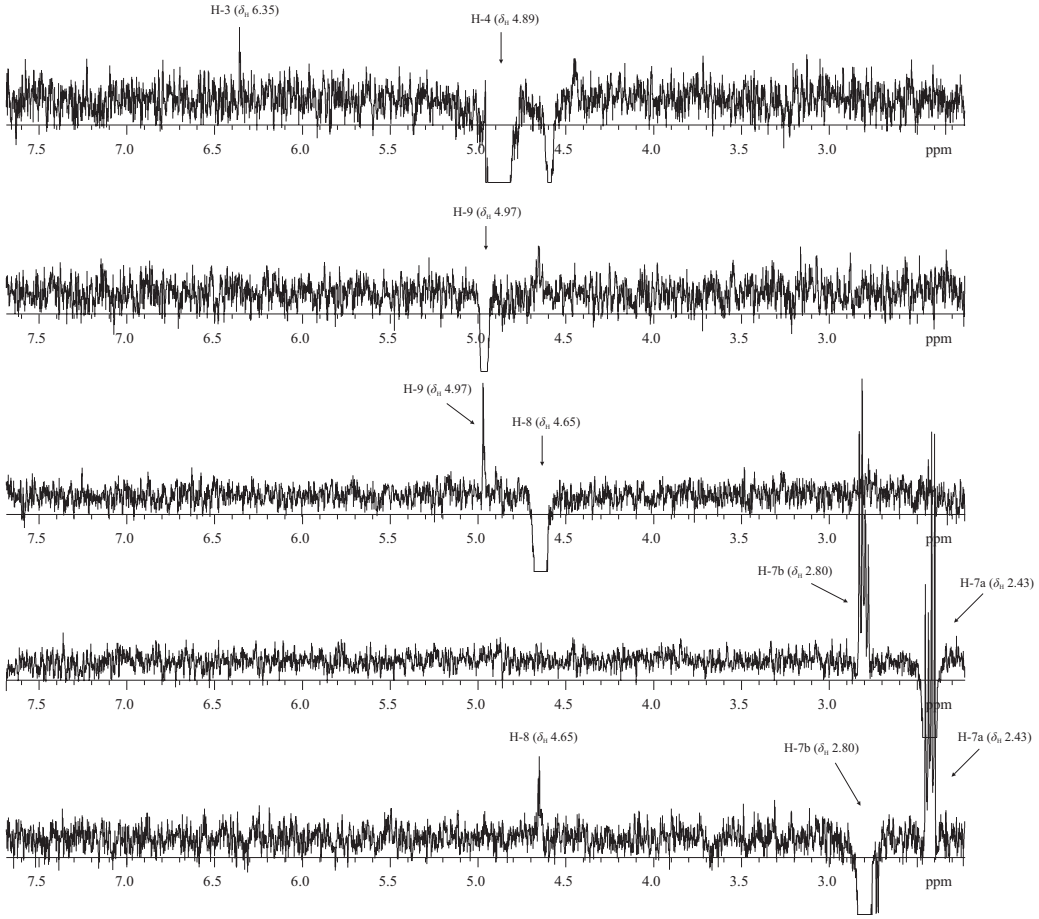

Figure 3.43: *1D NOE NMR spectra for* ***3.18*** *showing irradiation of (from bottom to top) H-7b, H-7a, H-8, H-9, and H-4.*

This relationship was not able to confirm the stereochemical assignment as this was not the only diastereomer predicted by Mestre-J to show an NOE relationship for the H-8 to H-9 proton pair. According to the calculated bond distances for the 4*S*, 5*S*, 8*S*, 9*R* diastereomer an NOE would be expected between one of the methylene protons at H-7 and H-8, however this was not seen. In the NOE spectrum of the *trans* diastereomer (**3.17**) (Figure 3.44), the opposite problem was encountered.

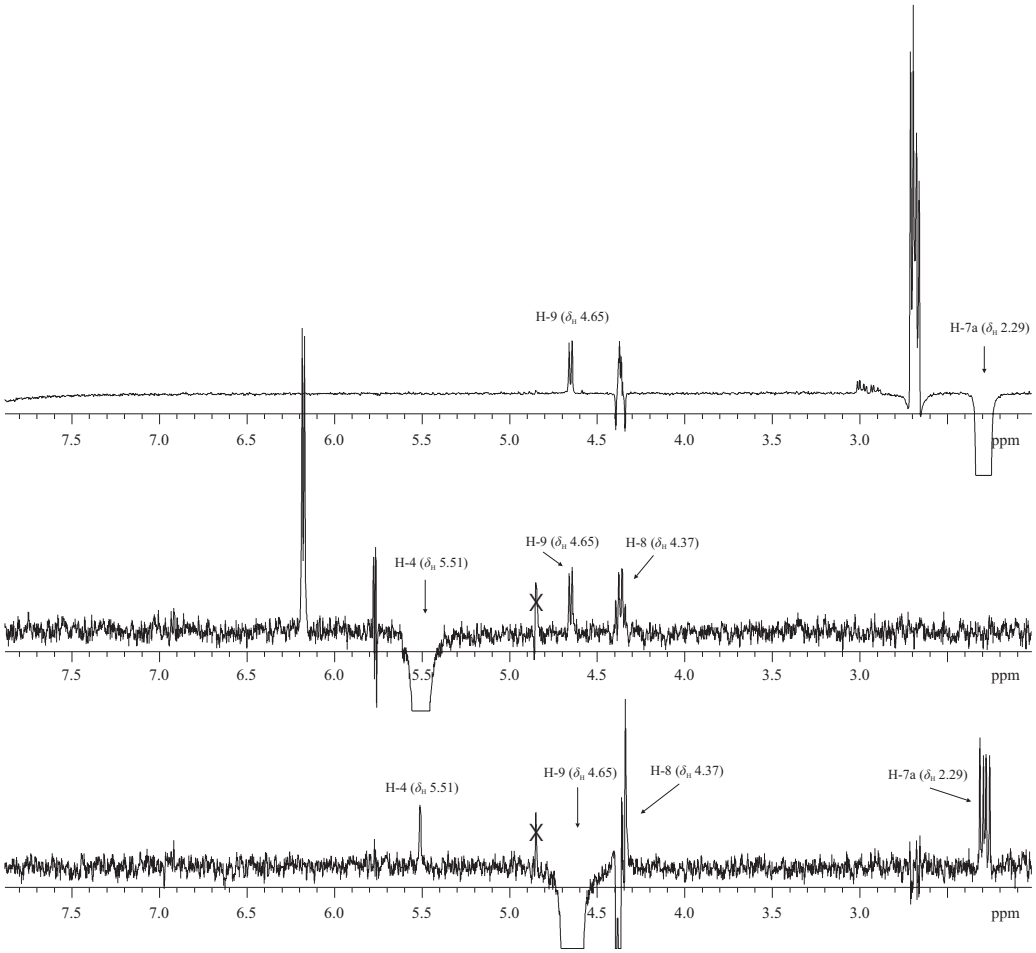

Figure 3.44: *1D NOE NMR spectra for* ***3.17*** *showing enhancements upon irradiation of H-9 (bottom), H-4 (centre), and H-7a (top).*

In Table 3.10, the bond distances for all relevant pairs in the *trans* diastereomers are presented, these reveal that very few NOE's would be expected for any of them; even the 4*S*, 5*S*, 8*S*, 9*S* isomer that Mestre-J calculated as being the closest match to the experimental data. The experimental data, however shows NOE relationships between all of the proton pairs (Figure 3.44). The most interesting/puzzling NOE correlation exists between H-4 on ring A and H-8 on ring B. The long bond distances (>4.0 Å) calculated for the H-4, H-8 proton pair makes an NOE correlation very unlikely. A strong NOE correlation is also seen from H-4 to H-9. According to the calculated bond distances (Table 3.10), the only isomer that would display this NOE correlation would be

4*R*, 5*S*, 8*S*, 9*S*, unfortunately the data for this isomer did not match that calculated for **3.17** by MestRe-J.

Table 3.10: *Bond distances of diastereomeric possibilities for* ***3.17*** *and* ***3.18****.*

	Bond distance (Å)						
	9-8	**9-7a**	**9-7b**	**8-7a**	**8-7b**	**4-9**	**4-8**
4*S*, 5*S*, 8*S*, 9*S*	3.056	3.851	3.036	2.372	3.042	3.632	5.169
4*S*, 5*S*, 8*R*, 9*R*	2.685	4.202	4.017	2.832	2.395	3.824	4.943
4*R*, 5*S*, 8*S*, 9*S*	3.085	3.843	2.825	2.404	3.081	2.262	4.728
4*R*, 5*S*, 8*R*, 9*R*	2.809	3.936	4.222	2.967	2.344	3.274	4.492
NOE observed?	*yes*	*yes*	*yes*	*yes*	*yes*	*yes*	*yes*
4*R*, 5*S*, 8*S*, 9*R*	2.470	4.177	4.046	2.379	3.06	3.201	4.821
4*S*, 5*S*, 8*S*, 9*R*	2.476	4.226	3.965	2.406	3.087	3.829	4.899
4*S*, 5*S*, 8*R*, 9*S*	2.351	3.829	2.840	2.814	2.414	3.596	5.401
4*R*, 5*S*, 8*R*, 9*S*	2.386	3.919	2.975	2.81	2.421	2.236	4.459
NOE observed?	*yes*	*no*	*no*	*no*	*no*	*no*	*no*

Because the structure of the closely related compound, spiro-mamakone C (**3.16**) was confirmed by X-ray crystallography, the chances that the structure elucidation of both **3.17** and **3.18** had been misinterpreted were very slim. Instead it was considered that the molecules of **3.17** and **3.18** might possibly be undergoing conformational changes in solution. CHEM 3D, which is able to model only energy minimised (MM2) models, may not take into account such occurrences during the modelling process. For this reason, both low- and high-energy conformations of the molecule were then modelled using the 2005 Schrodinger molecular modeling suite (See Experimental, Section 7.3.9). Unfortunately, even then the data obtained from this approach (see Appendix 2) was unable to clarify the problem. Even using the highest energy conformations the bond distances between H-4 and H-8 were all too large to generate an NOE effect. Surprisingly however, the modelled data was in very good agreement with the dihedral angles and bond distances obtained from the CHEM 3D modelled compounds.

3.10 Discussion

Purification of the extract from the re-culture of the unidentified endophytic fungus, E484, resulted in the isolation of four new compounds, and one that had previously been

isolated. Like the compounds from the first culture (F5062) these were of the spirobisnaphthalene class. The new compounds were named spiro-mamakones B, C, D, and E. The known compound was the novel spirononadiene, spiro-mamakone A (**3.11**). Spiro-mamakones B-E were named as such because they contained the two cyclopentane rings connected at a spirocentre, like that of spiro-mamakone A. Like that of the previouly isolated mamakunoic acids and spiro-mamakone A, the ^{1}H and ^{13}C chemical shifts of the 1,8-dioxynaphthalene portion of spiro-mamkones B-E are interchangeable with those in the opposite position of the ring. This of course excludes the two junction positions between the rings.

spiro-Mamakones C and B were elucidated as diastereomers that are partially reduced derivatives of spiro-mamakone A. X-ray crystallography found that spiro-mamakone C had the relative stereochemistry of 4*S*, 5*S*, 9*S,* but also that it was present as an enantiomeric excess. Spiro-mamakone B was found to have a relative stereochemistry of 4*S*, 5*S*, 9*R*. It stands to reason that if spiro-mamakone C was found to contain an enantiomeric excess, then quite possibly spiro-mamakone B could also exist like this.

Spiro-mamakones D and E were found to show not only reduction of the ketone at C-9, but also hydroxylation of the ring B alkene, to give an hydroxyl/methylene moiety. The relative stereochemistry of the two diastereoisomers, D and E was tentatively proposed on the basis of the calculation of coupling constants by the computer programme, Mestre-J as 4*S*, 5*S*, 8*S*, 9*S*, and 4*S*, 5*S*, 8*S*, 9*R* respectively.

Spiro-mamakones B-D were potently cytotoxic in the P388 assay, in the same range as that of the parent compound, spiro-mamakone A. The antimicrobial activity, however, was somewhat reduced compared to that of spiro-mamakone A. No meaningful biological activity was obtained for spiro-mamakone E, but based on the similarity to spiro-mamakone D it is expected to be comparable.

The relationship between the biological activity and the stereochemistry of these compounds is also worth speculating on. Could this be a case like that of thalidomide,[84] where one enantiomer displays significantly different activity to that of the opposite enantiomer? Given that none of the spiro-mamakones were isolated as enantiomerically

pure compounds this is a distinct possibility, and hence is worth investigating in future work.

Part 3 Biosynthetic studies

3.11 Introduction

The isolation of the structurally unprecedented spiro-mamakones (**3.11**, **3.15**–**3.18**) led to the formulation of a biogenetic hypothesis for their formation. Spiro-mamakones are clearly related to the general group of 1,8-dihydroxynaphthalene-derived compounds, the spirobisnaphthalenes. The biosynthesis of this general group has been well studied in recent years[65,85] and had established that both halves (top and bottom) are polyketide-derived via the intermediacy of 1,8-dihydroxynaphthalene (DHN) (**3.5**). The biosynthetic pathway leading to DHN (**3.5**) is shown in Scheme 3.4.

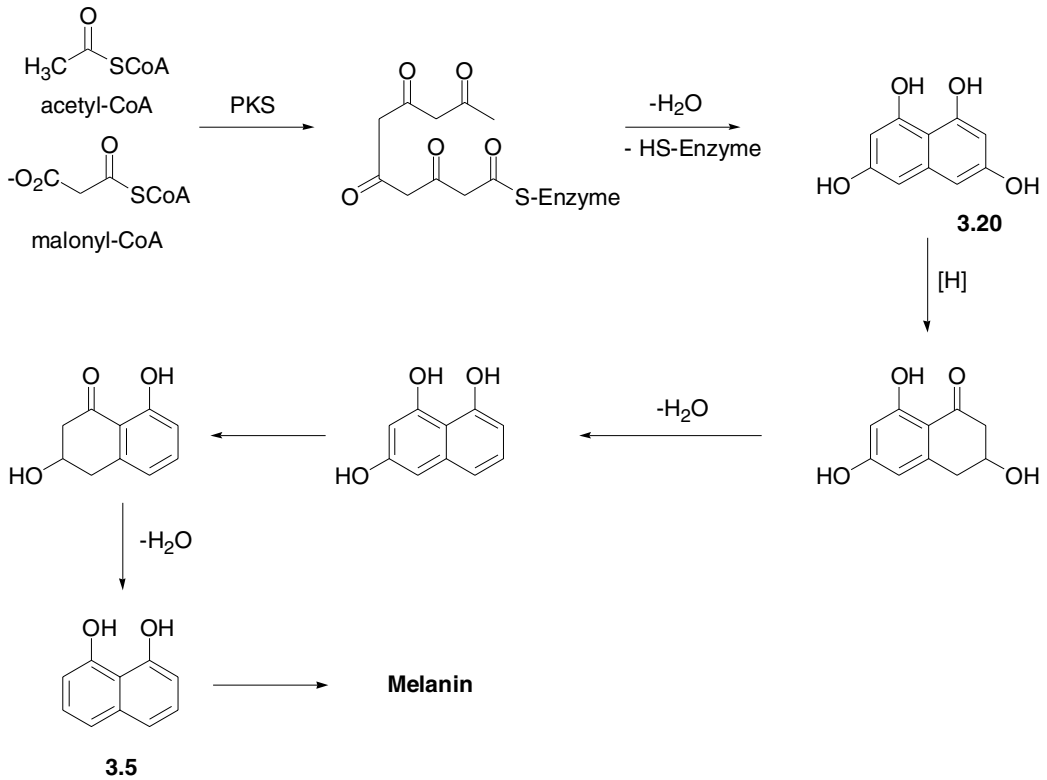

Scheme 3.4: *DHN (**3.5**) Biosynthesis*

It is also worth commenting that the interpretation of the labelling experiments was rendered more complex by the presence of isotopomers.* This is a consequence of the C_2 symmetry of the 1,3,6,8-tetrahydroxynaphthalene (**3.20**) intermediate, also present in the biosynthesis of DHN, as shown in Scheme 3.4. The "bottom"-half of the spiro-mamakones is proposed to arise from DHN. The origin of the "top"-half however, was less certain. Again it was considered most likely that it too arose from DHN. Two mechanisms were proposed (Scheme 3.5a and 3.5b). The mechanisms were formulated on the consideration of some of the known spirobisnaphthalenes, specifically those of the diepoxide, cladospirone bisepoxide (**3.4**) and palmarumycin C_6 (**3.13**), which bear a cyclopentane ring attached to a dihydroxybenzene in the "upper" half of the molecule. The ring junction epoxide seen in **3.4** was proposed as an intermediate in the biosynthesis of **3.11** as this could undergo the rearrangement and subsequent carbon cleavage required to form the nonadiene portion of the molecule. The first biogenetic proposal (Scheme 3.5a) was loosely based on the mechanism proposed for the formation of the spirocentre in fredericamycin A.[86,87] This involved an oxidative rearrangement of DHN (**3.5**) followed by two 1,2-shifts. The second proposal, (Scheme 3.5b), involves the same rearrangement of a DHN (**3.5**) molecule to the same dihydroxynaphthyl epoxide. In this alternative, the oxidation/rearrangement product is oxidatively cleaved leading to a ring opened structure containing carboxylic acid and aldehyde functionalities. Following this are decarboxylation and deprotonation steps, forming a symmetric carbanion intermediate, which would readily cyclise generating the other cyclopentene ring upon attack on the aldehyde.

* Isotopomers (isotopic isomers) are isomers that have the same number of each isotopic atom but differ in their positions. Isotopomers can be either constitutional isomers e.g $CH_2DCH{=}O$ and $CH_3CD{=}O$ or isotopic stereoisomers, e.g (R)- and (S)-CH_3CHDOH.

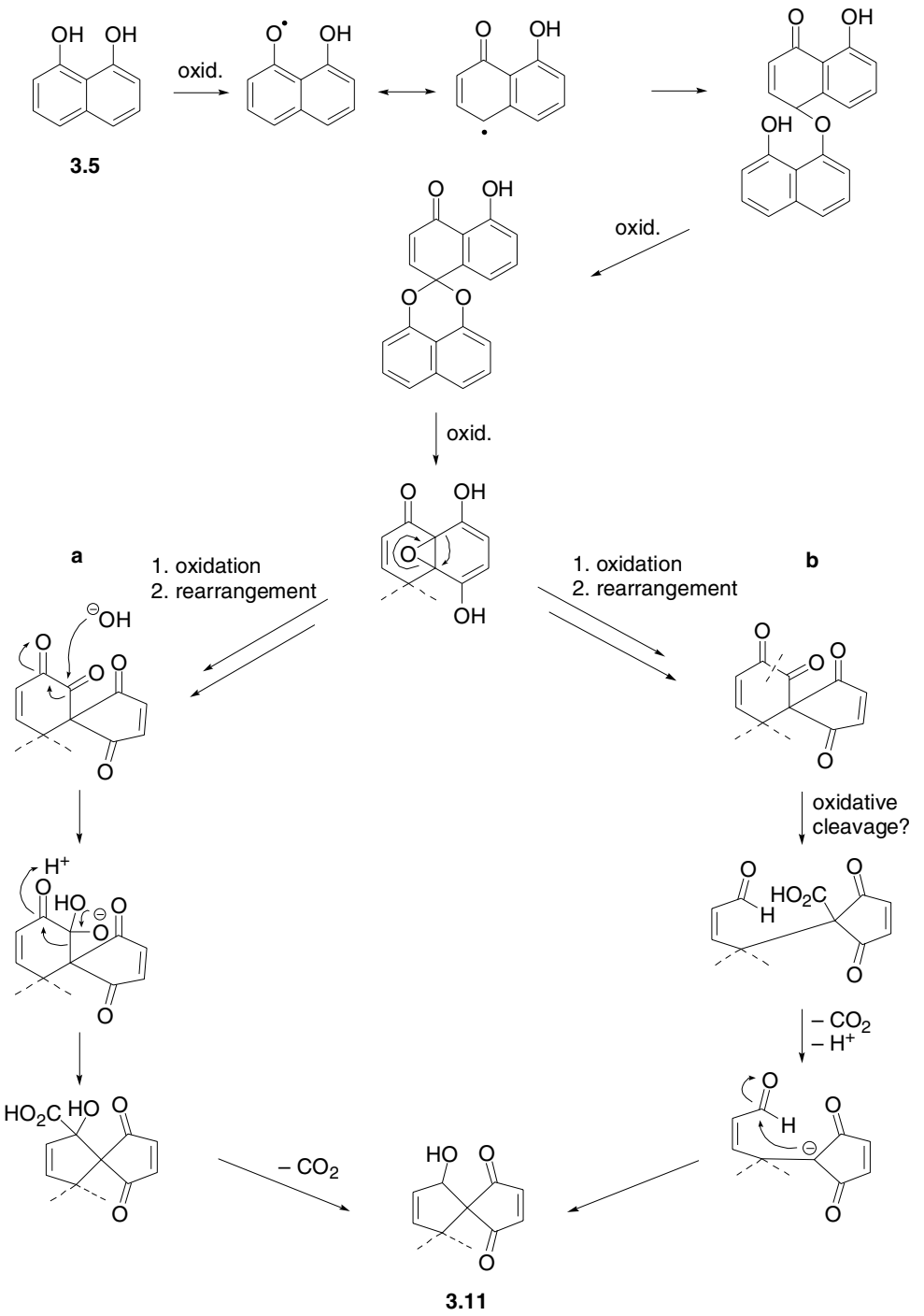

Scheme 3.5: *The two possible mechanisms (**a** and **b**) for the formation of spiro-mamakone A (**3.11**).*

To test these hypotheses, biosynthetic experiments were carried out. These involved administration of ^{13}C-isotopically labelled precursors to the growing fungal culture. The experiments concentrated on the biosynthesis of spiro-mamakone A. The reason was that **3.11** was known to be reliably produced, and in high yields, and that any data obtained could presumably be applied to the other spiro-mamakones given their structural similarity. Isotopically labelled acetate was used on the presumption that **3.11** was of polyketide origin formed via DHN from the condensation of acetyl-SCoA with malonyl-SCoA.

3.12 Preliminary Investigations

The original culture medium for the fungus E484, was solid agar plates (see Experimental), however this was not suited to feeding studies, as it raises the problem of how to get uniform application of the labelled precursor molecules to the growing fungus. For this reason biosynthetic studies with fungi are typically carried out in liquid media. A time-course experiment was carried out to ascertain not only whether **3.11** is produced in liquid culture, but also the stage of fungal growth when production of spiro-mamakone A is initiated and if the spiro-mamakones are subsequently metabolised. This information was important because if the precursors are added too early in the fermentation, it could result in a rate of incorporation that is too high. Such a situation can cause problems in the interpretation of NMR experiments using doubly labelled material. The opposite problem can also arise if the precursors are added too late. That is, that the rate of incorporation could be too low, which could also impede the interpretation of the NMR data, as it would then be difficult to distinguish labelled carbons from non-labelled.

Time-course experiments (see Experimental) were carried out using both static and shake conditions. The production of the metabolites was monitored daily by HPLC analysis, using the "standard gradient" (see Section 7.1.7.2 in Experimental) in conjunction with an ELSD detector. The shake culture displayed maximum production of spiro-mamakone A, after just 6 days (Figure 3.45).

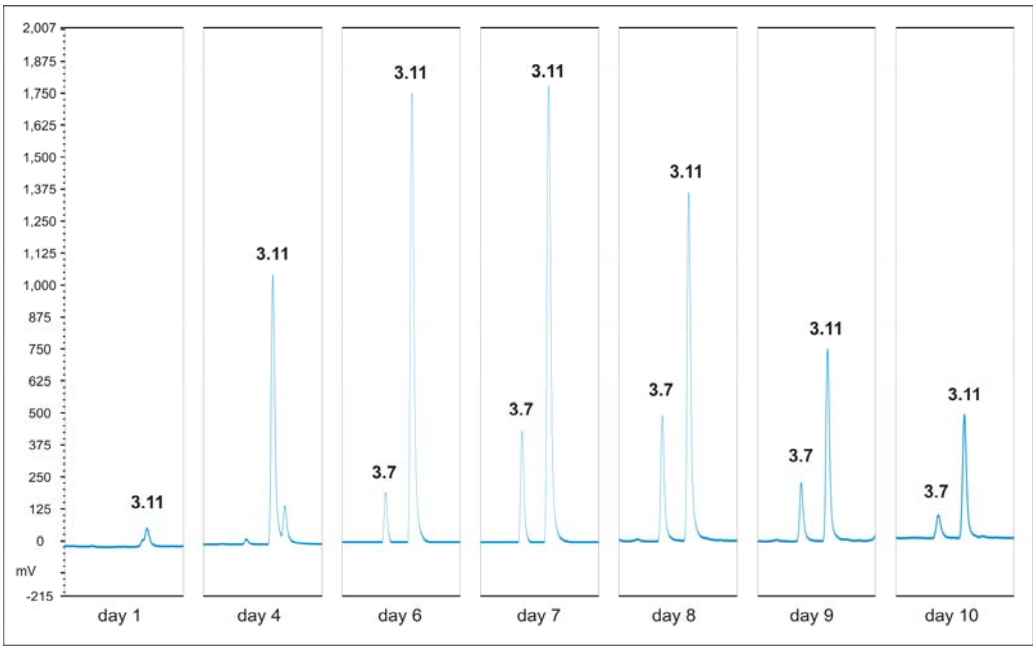

Figure 3.45: *ELSD traces (12.5-16.0 minutes) showing daily variation in metabolite formation during time-course experiments in shake conditions.*

At this time the culture consisted of almost entirely spiro-mamakone A, along with mamakunoic acid B (**3.7**), found to be present as a minor component. The static culture was much slower growing. Although production of spiro-mamakone A peaked after 8 days, the culture took 7 days to show appreciable amounts of **3.11** (Figure 3.46).

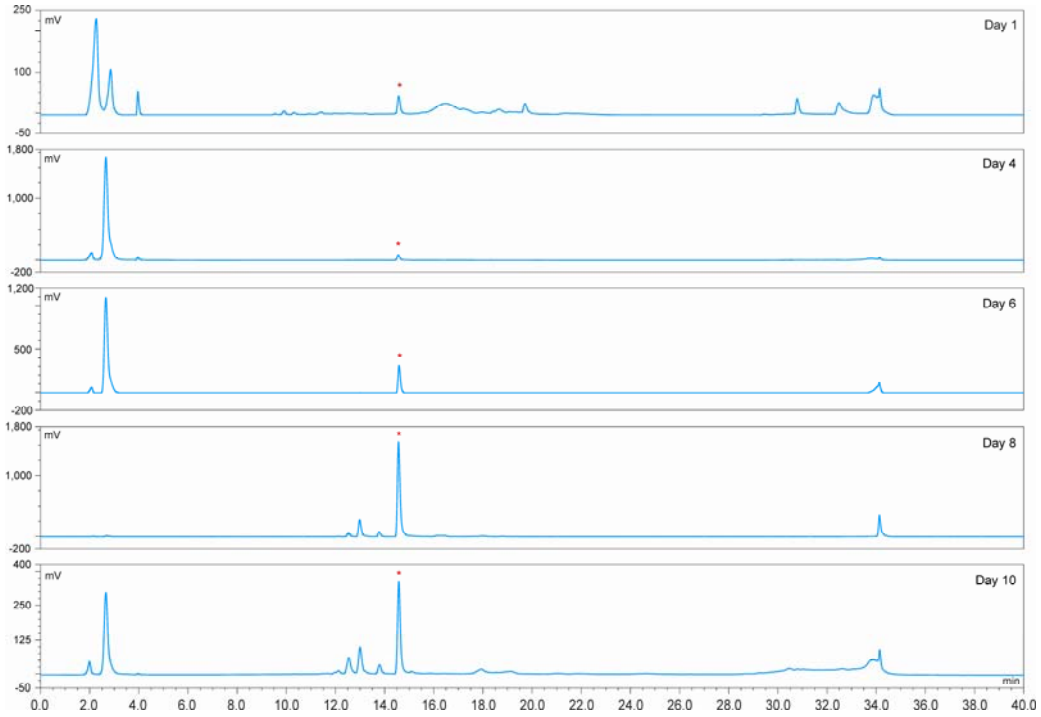

Figure 3.46: *Stacked HPLC chromatograms from the static time-course experiments, clearly showing increase in production of* ***3.11*** *(*)*

Other minor components were also produced in the static culture; more than were seen in the shake culture.

The decision was made to use shake conditions for the biosynthetic experiments. This was based on the shorter time period involved, as well as a less complicated extract that the shake culture presented compared to that of the static. It was also decided that due to the almost immediate production of large amounts of **3.11** in the liquid culture, addition of the isotopically-labelled precursors would take place just 24 hours after inoculation of the growth media with the fungus.

3.13 Fermentation and Isolation

Four separate cultures (each containing 200 mL of liquid media) of the fungus E484 were each inoculated with labelled acetate, two with singly-labelled acetate, [1-^{13}C]-, and [2-^{13}C]-, and the remaining two, with doubly-labelled acetate, one containing full strength

[1,2-^{13}C]-acetate (90%), and the other, half strength [1,2-^{13}C]-acetate (45%). The half strength was included as a precaution in case the incorporation of the full strength doubly-labelled acetate was too high. Preparation of the labelled acetate inoculums is detailed in the Experimental section for this chapter (Section 7.3.13) .

Six days after inoculation, the cultures were extracted with EtOAc using the standard protocol (Section 7.1.2, Experimental). Purification of the resultant extract by semi-preparative HPLC, yielded pure spiro-mamakone A, as well as mamakunoic acid B (present as a mixture with an unidentified contaminate) from each of the four cultures.

*3.14 Enrichment of **3.11** with [1-^{13}C]- and [2-^{13}C]-Acetate*

The ^{13}C NMR spectrum obtained after purification of natural abundance spiro-mamakone A (Figure 3.47a) was compared to spiro-mamakone A enriched from [1-^{13}C]-acetate (Figure 3.47b) and [2-^{13}C]-acetate (Figure 3.47c). A visual comparison of spectrum **a** with that of **b** and **c** was enough to show which of the carbons showed incorporation of the isotopic labels. A quantitative measurement of incorporation was not possible as the molecule contained no carbon atoms that were not acetate derived, that could be used to standardise the carbon signals of the enriched molecule relative to those of the unlabelled version.

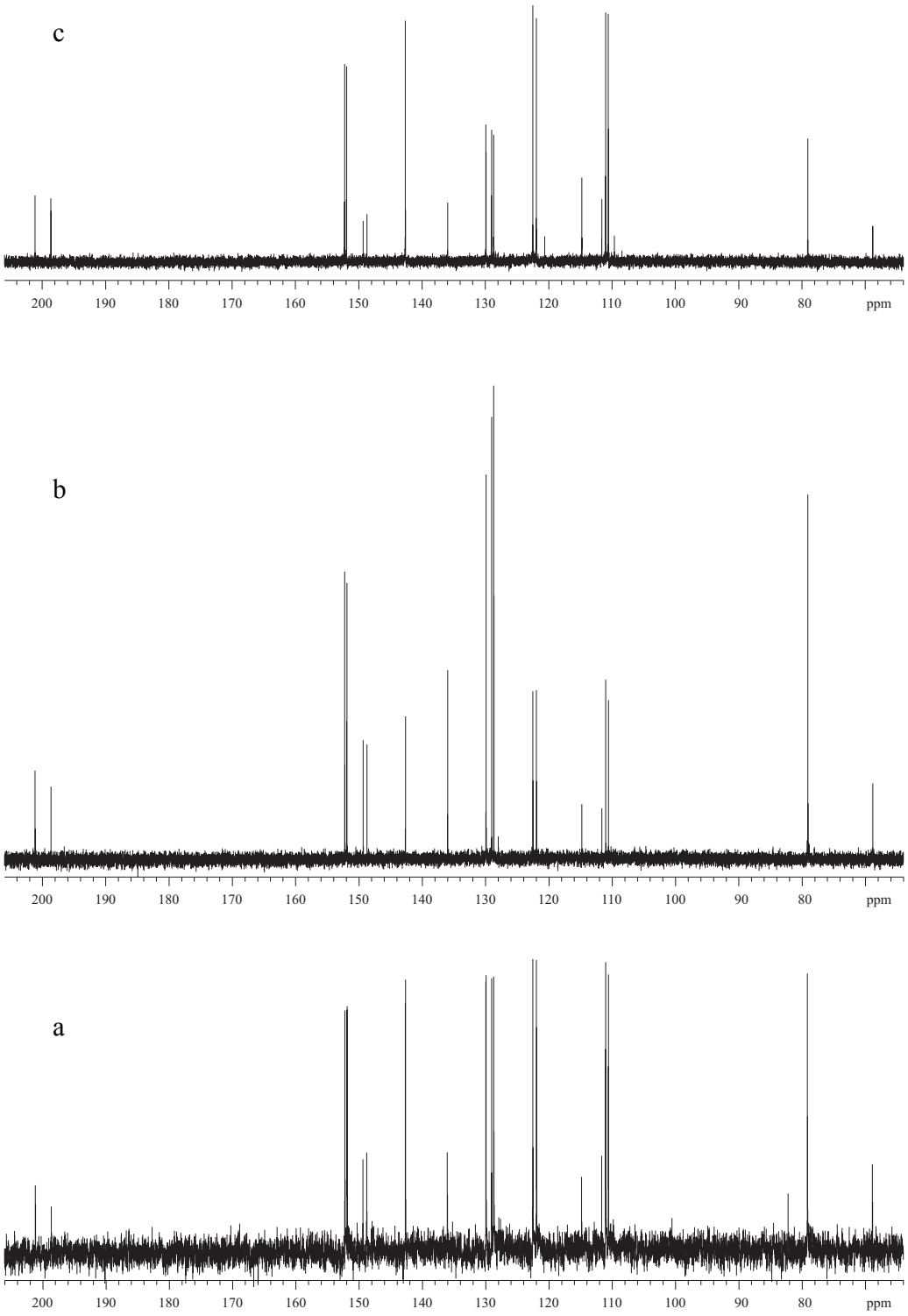

***Figure 3.47**: Comparison of ^{13}C NMR spectra derived from unlabelled (**a**), [1-^{13}C]-acetate (**b**) and [2-^{13}C]-acetate enriched (**c**) spiro-mamakone A (**3.11**). All obtained in CD_3OD.*

3.14.1 Quantitative Measurement of Enrichment

In order to obtain a reference point for determining a quantitative measurement of incorporation, acetylation was performed on the unlabelled spiro-mamakone A (**3.11**), as well as spiro-mamakone A enriched with the singly labelled acetates. The reaction was carried out using acetic anhydride and pyridine (Scheme 3.6), to produce *O*-acetyl-spiro-mamakone A (**3.21**)

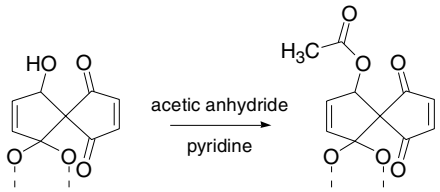

3.11 **3.21**

Scheme 3.6: *Acetylation of* ***3.11****.*

Analysis of the ^{1}H and ^{13}C NMR spectra (Figure 3.48 and 3.49 respectively) confirmed the success of the reaction. An additional methyl signal at δ_H 1.97, and the expected downfield shift of the allylic carbinol proton from δ_H 5.30 to δ_H 5.80 were observed in the ^{1}H NMR spectra. In the ^{13}C NMR spectrum, the addition of a methyl signal at δ_C 20.7 (C-21), and an ester carbonyl carbon at δ_C 172.9 (C-20) were observed (see Experimental, Section 7.3.13 for a full listing of ^{1}H and ^{13}C chemical shifts).

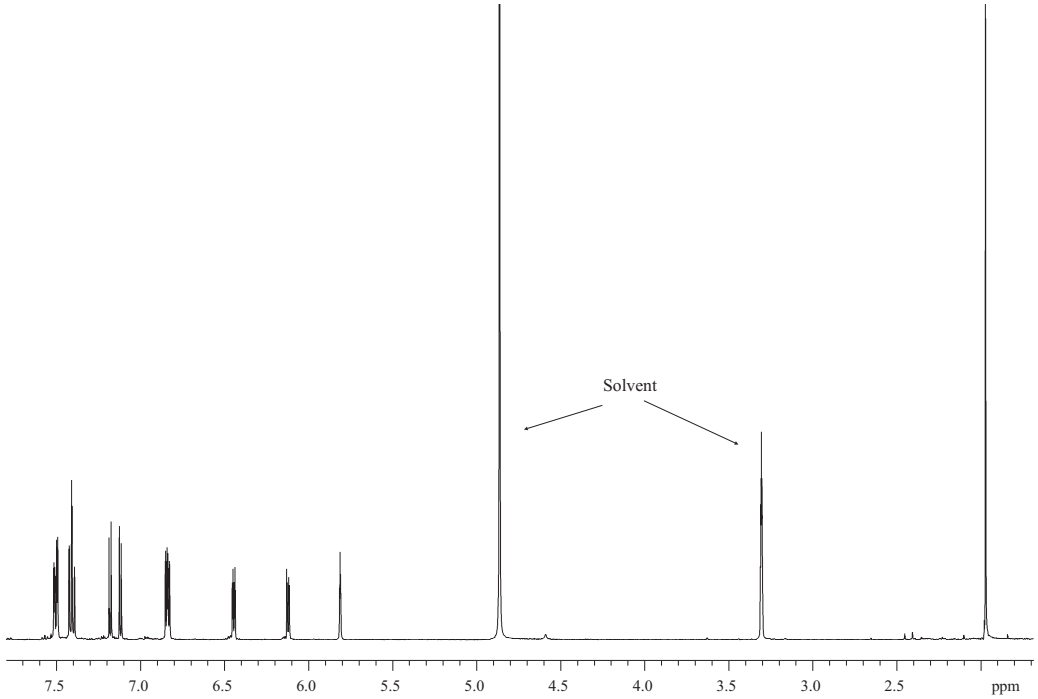

Figure 3.48: *^{1}H NMR spectrum of O-acetyl-spiro-mamakone A (**3.21**) in CD_3OD.*

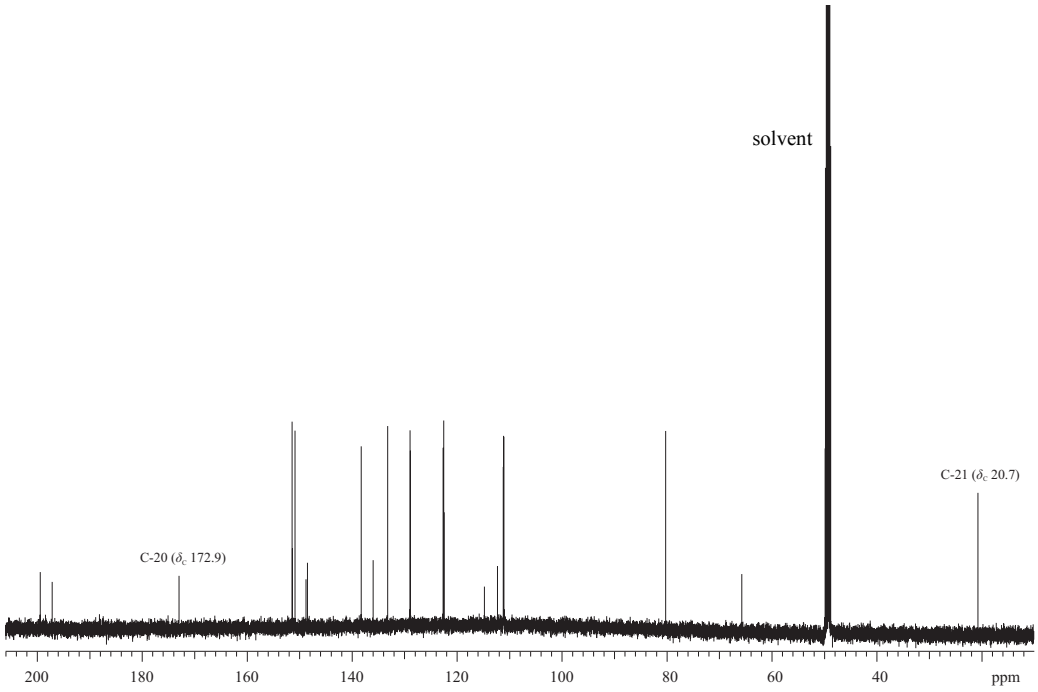

Figure 3.49: *^{13}C NMR spectrum of O-acetyl-spiro-mamakone A (**3.21**) in CD_3OD.*

Quantitation using ^{13}C NMR spectroscopy is unable to be carried out using the standard ^{13}C NMR experiment. This is because the relaxation times of the ^{13}C nuclei are variable. In a standard ^{13}C NMR experiment, many ^{13}C nuclei that have long relaxation times often are not allowed sufficient time to achieve full relaxation back to the ground state before reirradiation. In the subsequent spectrum these nuclei appear as low intensity signals, while those that have faster relaxation times (and hence have adequate time to relax) appear more intense. A further reason for differences in the measured signal intensities in ^{13}C NMR spectroscopy is a consequence of NOEs between ^{1}H and ^{13}C nuclei. For these reasons quantitative measurements based on peak area, or intensity are impossible due to the broad range of signal intensities and line widths. In this situation a modified ^{13}C NMR experiment is used, whereby the delay (d1), acquisition time (at) and decoupler mode (dm) are fine-tuned in order to attain a very long relaxation delay time, but at the same time maintain decoupling, but minimise NOE enhancement, using inverse-gated decoupling (decouples only ^{1}Hs during acquisition) (see Experimental, Section 7.1.13 for parameters). This ensures that all carbons respond in a relatively equivalent manner.

The resulting "quantitative" ^{13}C NMR spectra for unlabelled as well as [1-^{13}C]-, and [2-^{13}C]-labelled *O*-acetyl-spiro-mamakone A are displayed in Figure 3.50 a, b, and c respectively. Enrichment at each carbon (Table 3.11) was calculated by determining the peak intensities relative to the intensity of the acetate carbonyl signal at 172.9 ppm, which had originated from a natural abundance source, and then dividing these relative intensities by the relative intensities of the same peaks in the natural abundance spectrum. These calculations enabled the elucidation of the labelling pattern shown in Figure 3.51. As expected, the 1,8-dihydroxy naphthalene portion of the molecule displayed a regular polyketide folding pattern, as shown by the alternating labelling of the carbons in this ring system.

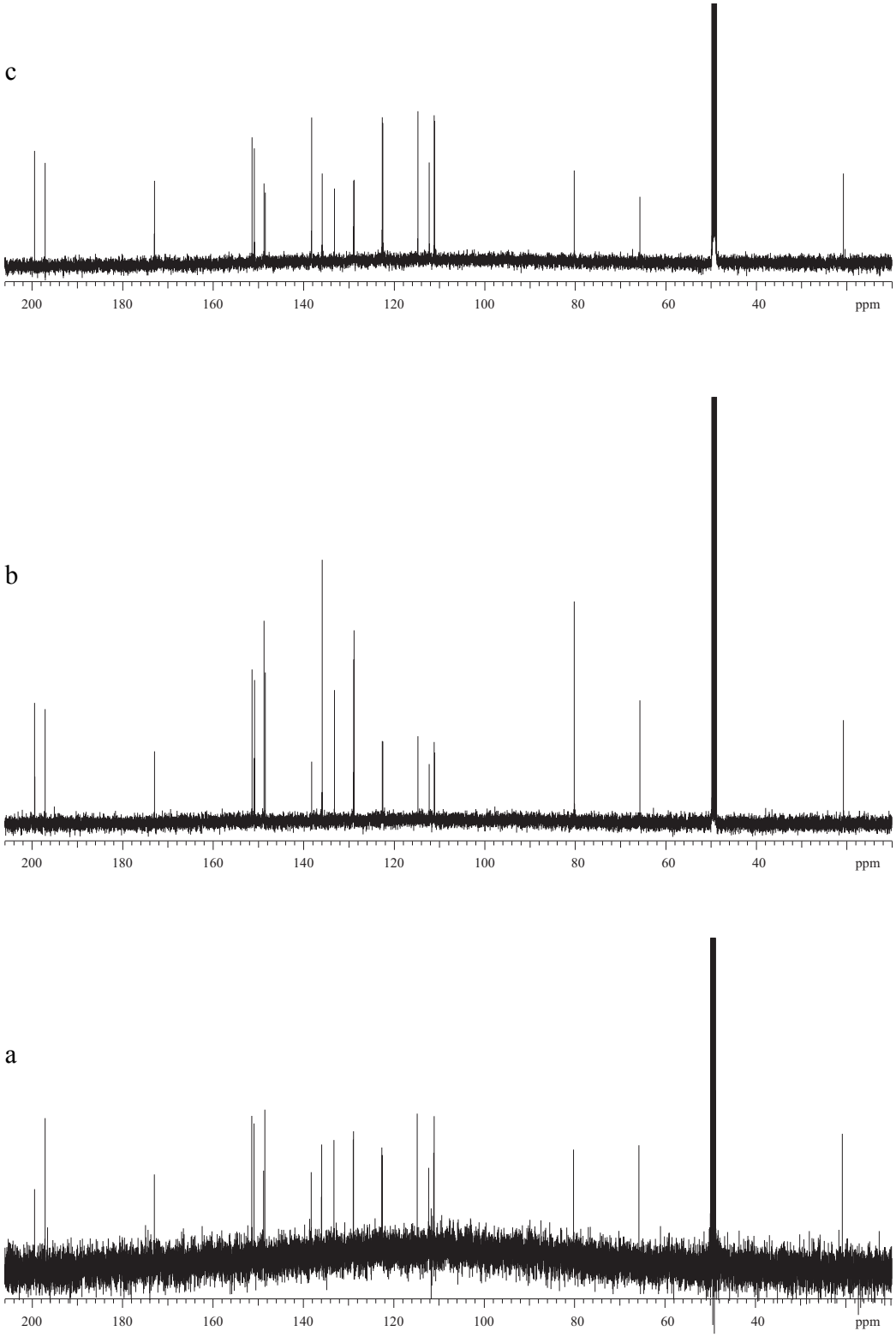

Figure 3.50: *Quantitative ^{13}C NMR comparison for O-acetyl-spiro-mamakone A (**3.21**). From a-c respectively, unlabelled, [1-^{13}C]-, and [2-^{13}C]-labelled material.*

Table 3.11: *Quantitative incorporation of labelled precursors into spiro-mamakone A (**3.11**), derivatised to O-acetyl-spiro-mamakoneA (**3.21**) after labelling experiments.*

position	[1-^{13}C]	[2-^{13}C]	position	[1-^{13}C]	[2-^{13}C]
1	0.92	1.58	**12**	3.01	1.05
2	2.09	0.81	**13**	0.89	1.63
3	0.95	1.73	**14**	2.66	1.00
4	2.27	1.01	**15**	0.94	1.73
5	1.74	0.85	**16**	2.04	0.81
6	1.34	1.10	**17**	0.90	1.54
7	1.52	1.35	**18**	2.19	0.89
8	1.58	1.32	**19**	0.93	1.65
9	1.50	1.36	**20 (C=O)**	1.00	1.00
10	2.03	0.72	**21 (Me)**	0.81	0.78
11	0.83	1.50			

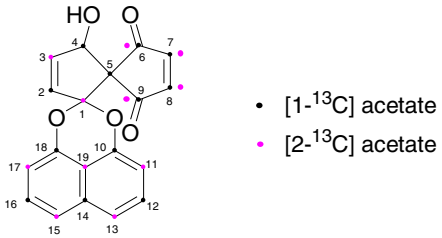

Figure 3.51*: Labelling pattern for **3.11**.*

Interpretation of the data for the nonadiene portion of the molecule, however was not as straightforward. The ^{13}C NMR spectrum derived from the [2-^{13}C]-acetate experiment clearly showed that C-1 and C-3 were labelled, whereas C-6–C-9 appeared to be of intermediate enrichment (see Table 3.11). The ^{13}C NMR spectrum derived from the [1-^{13}C]-acetate experiment showed that not only C-2, C-4, C-5 but also C-6–C-9 were labelled, again, appearing to display an intermediate level of enrichment. First, these results confirmed the NMR chemical shift assignments of C-2 and C-3 as that shown in Table 3.4. In addition, this labelling pattern showed C-1 acetate-derived carbons in positions C-4 and C-5. Two C-1 acetate-derived carbons adjacent is impossible, unless of course a C-2 acetate-derived carbon has been lost from between them. This was encouraging as this is the scenario required by both Schemes 3.5a and 3.5b. This data also confirmed that the carbon lost was derived from the C-2 of an acetate unit, a feature also required by Schemes 3.5a and 3.5b.

The other significant finding from the [1-^{13}C]- and [2-^{13}C]-acetate feeding experiments was that C-6–C-9 were labelled from each experiment, but at lower calculated incorporations than those noted for C-1–C-5 in the appropriate experiment. This was interpreted as supporting Scheme 3.5b, which proceeds via a C_2-symmetric enedione. This intermediate would lead to the apparent labelling by both [1-^{13}C]- and [2-^{13}C]-acetate at each of C-6–C-9 (Figure 3.52).

Other support for Scheme 3.5b comes from the conclusion that in the final step of Scheme 3.5b, in the Knoevenagel-type reaction, when the stabilised carbanion attacks the aldehyde group (Figure 3.52) there may well be little chiral induction and a racemate would result. Spiro-mamakone A (**3.11**) is isolated as a racemate.

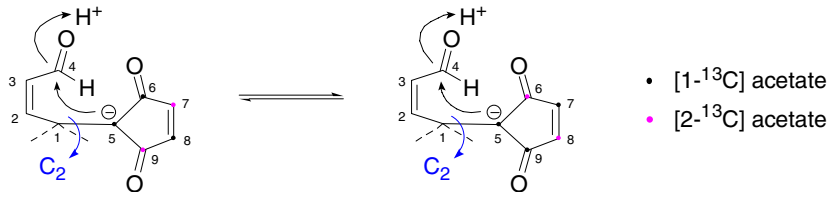

Figure 3.52: *Mechanism (Knoevenagel-type reaction) for the labelling observed for* ***3.11****.*

*3.15 Enrichment of **3.11** with [1,2-$^{13}C_2$]-Acetate*

Incorporation experiments using [1,2-$^{13}C_2$]-acetate are used to establish the direction of the folding pattern for the polyketide chain.[87] In the case of the spiro-mamakones it will also be a useful way to establish the cleavage sites of the acetate in the formation of the nonadiene ring system. Coupling constants were determined for all carbons (Table 3.12) from the derived ^{13}C NMR spectrum (Figure 3.53 and 3.54), however in some cases the low signal-to-noise ratios (most notable for the spiroketal and carbonyl carbons) and signal overlap made the *J* value calculations questionable.

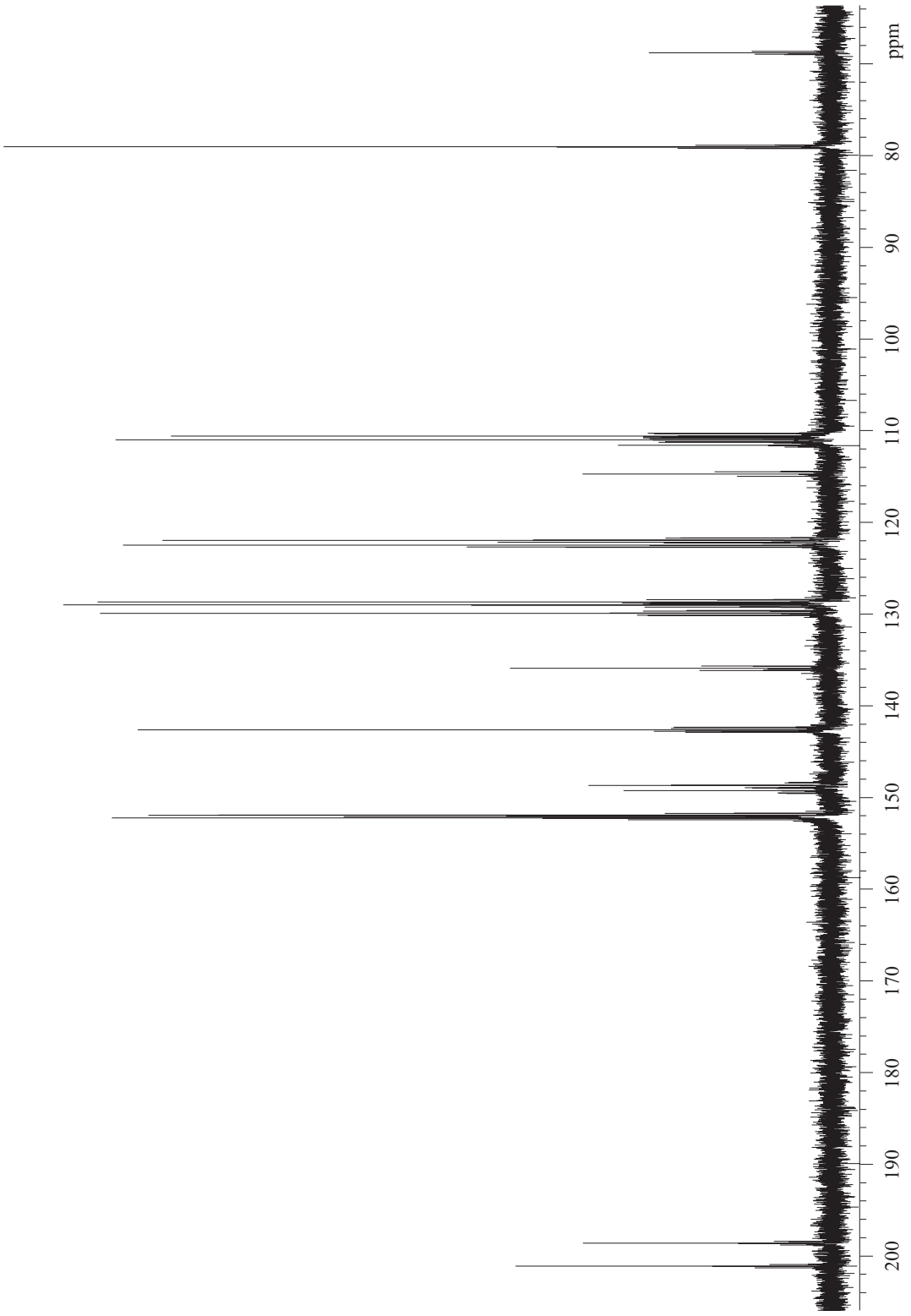

Figure 3.53: *^{13}C NMR spectrum derived from* ***3.11*** *enriched with [1,2-$^{13}C_2$]-acetate.*

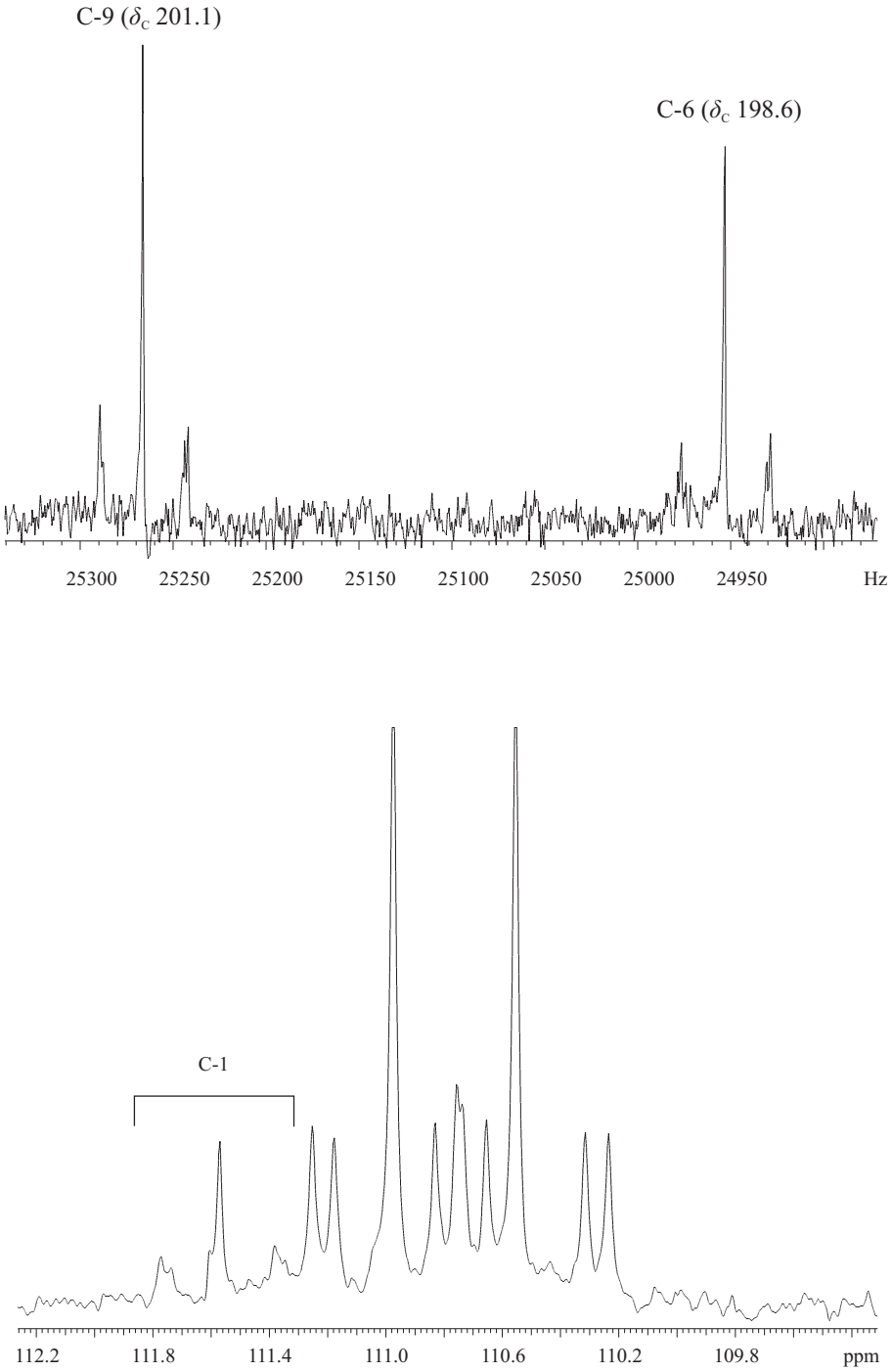

Figure 3.54: *Examination of the satellite patterns for C-9, C-6 and C-1 from the ^{13}C NMR spectrum in Figure 3.53, showing the effect of low signal-to noise.*

Table 3.12: *^{13}C –^{13}C coupling constants for spiro-mamakone A (**3.11**).*

position	δ^{13}C ppm	[1,2-^{13}C], J_{CC} Hz	position	δ^{13}C ppm	[1,2-^{13}C], J_{CC} Hz
1	111.7	53.7, 44.1	**11**	111.0	55.5, 75.1
2	129.9	69.9, 53.7	**12**	129.0	60.4, 55.5
3	142.7	69.9, 43.5	**13**	122.0	ND
4	79.1	43.5	**14**	136.1	56.5
5	68.9	44.1	**15**	122.5	56.5
6	198.6	47.9, 44.1	**16**	128.7	60.4, 55.4
7	151.9	47.9	**17**	110.6	55.4, 75.1
8	152.2	47.5	**18**	148.8	75.1, 61.1
9	201.1	47.5, 44.1	**19**	114.8	61.1
10	149.4	75.1, 61.1			

ND-not determined

The overall incorporation of the labelled acetate was calculated as 1.3%. This was achieved by integration of the natural abundance peak and the satellites. The integrals of the satellites were multiplied by the natural abundance of carbon (1.1%) and then divided by the integral of the natural abundance peak.

The next step in the analysis was to measure and analyse the data from the INADEQUATE NMR experiment.

3.15.1 [1,2-$^{13}C_2$]-Acetate INADEQUATE NMR

The INADEQUATE NMR spectrum (Figure 3.55) experiment showed carbon-carbon coupling within the same acetate unit, potentially allowing the direction of the polyketide to be elucidated. If the incorporation of the [1,2-$^{13}C_2$] acetate is very high however, coupling between adjacent acetate units can sometimes also be seen. Naturally, this can lead to ambiguous results. This was not of concern in the spiro-mamakone work as the incorporation was low. This level of analysis was necessary due to the complexity generated by the isotopomers present. This is shown in the analysis of the naphthalene portion of spiro-mamakone A (**3.11**).

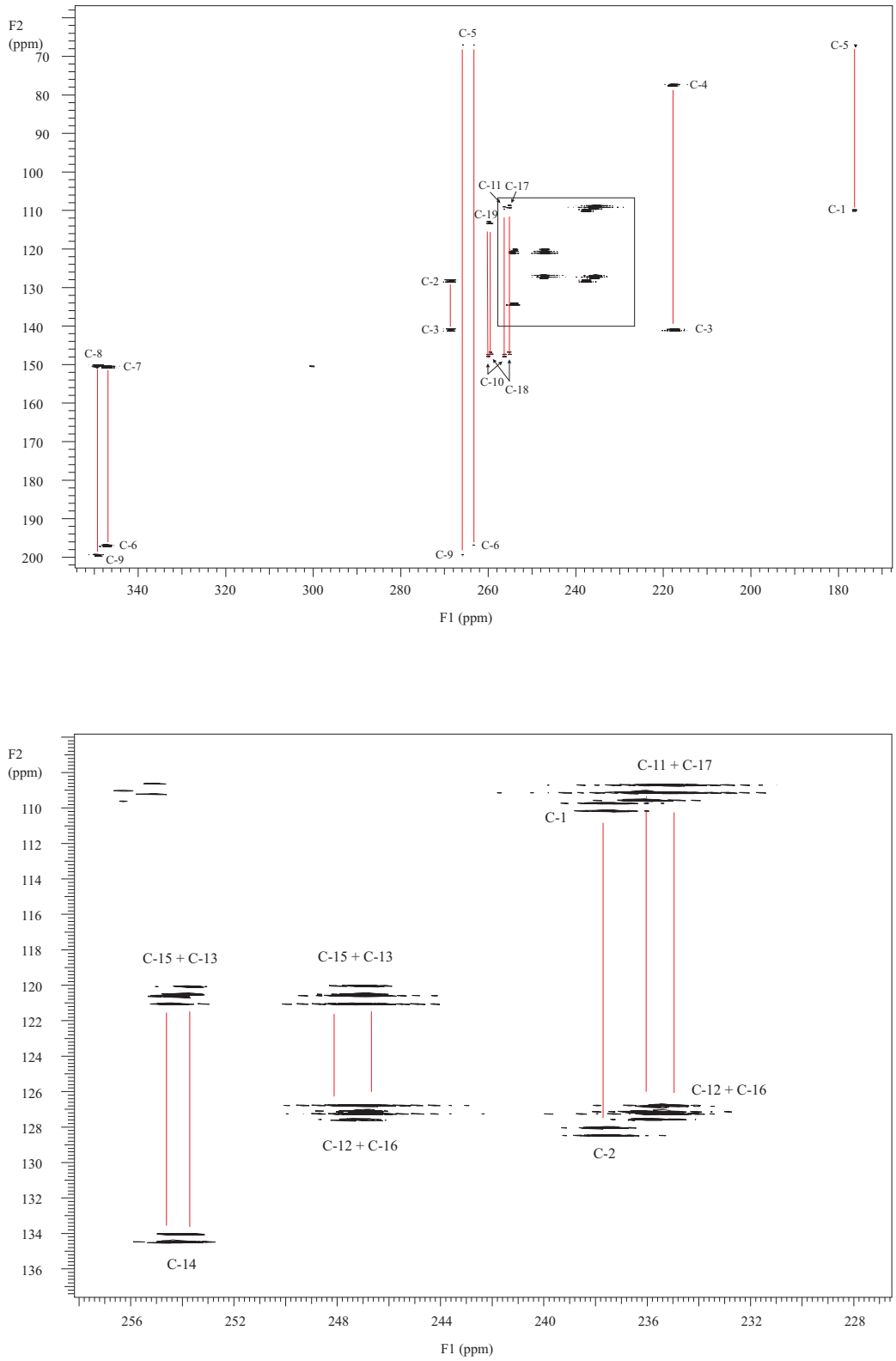

Figure 3.55: *^{13}C INADEQUATE NMR spectrum with inset of overlapping region (bottom).*

Most of the carbon resonances (Table 3.12) show TWO pairs of satellite signals. This can be interpreted as indicating TWO separately labelled sets of molecules and is supported by the INADEQUATE NMR data, which shows all the combinations necessary (e.g $^{1}J_{C}{}^{10}{}_{C}{}^{19}{}_{C}$ / $^{1}J_{C}{}^{10}{}_{C}{}^{11}{}_{C}$; $^{1}J_{C}{}^{12}{}_{C}{}^{11}{}_{C}$ / $^{1}J_{C}{}^{12}{}_{C}{}^{13}{}_{C}$ etc.) in the naphthalene ring. This can be interpreted as that shown in Figure 3.56.

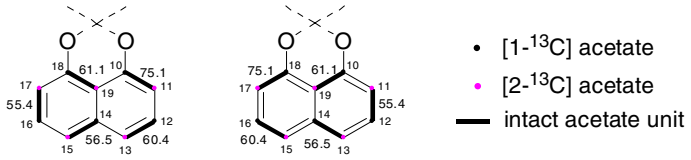

Figure 3.56: *Labelling of the naphthalene portion of spiro-mamakone A (**3.11**), indicating the effect of isotopomerism.*

Although there is some ambiguity in the region C-13–C-15 (Figure 3.57), the appropriate correlations in this region are observed in the INADEQUATE NMR experiment ($^{1}J_{C}{}^{12}{}_{C}{}^{13}{}_{C}$; $^{1}J_{C}{}^{13}{}_{C}{}^{14}{}_{C}$; $^{1}J_{C}{}^{14}{}_{C}{}^{15}{}_{C}$; $^{1}J_{C}{}^{15}{}_{C}{}^{16}{}_{C}$).

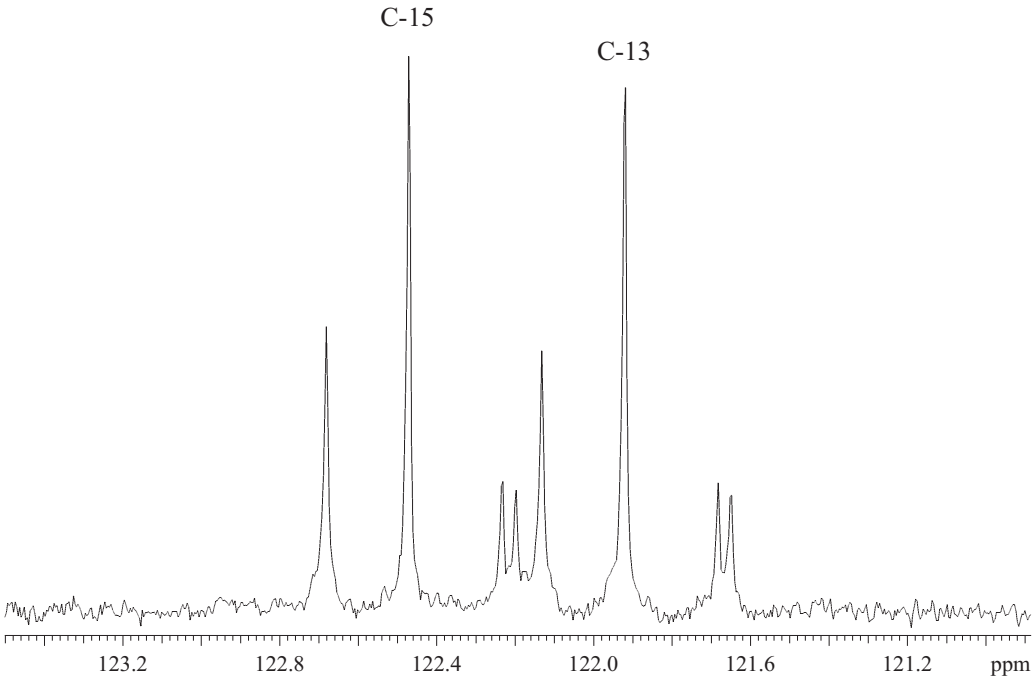

Figure 3.57: *C-13/C-15 region of the [1,2-$^{13}C_2$]-acetate ^{13}C NMR spectrum of **3.11**.*

In consideration of the reason why two coupling constants were not seen for C-19 and C-14 in the [1,2-$^{13}C_2$]-acetate NMR it was concluded that the coupling constants for each of the two adjacent carbons were so similar, so as not to be visible as two resolved satellite peaks. This is of course a consequence of the near symmetrical nature of the naphthalene subunit. The two possible incorporation patterns that these data suggest have already been reported for the related spirobisnaphthalene, cladospirone bisepoxide.[65] In this study it was reported that both the "top"- and "bottom"-halves of the molecule showed this incorporation pattern, hence resulting in four isotopomers.

For spiro-mamakone A, this however is not the case. Although **3.11** is also believed to start with a DHN intermediate in both halves of the molecule, the labelling pattern on the "top" of **3.11** is very different to that on the "bottom". For the "top" half of the spiro-mamakone molecule, the nonadiene portion, the anticipated labelling patterns from the [1,2-$^{13}C_2$]-acetate feeding experiment are summarised in Figure 3.58. Only the outcomes from Scheme 3.5b are shown, as Scheme 3.5a does not go through a symmetric intermediate that is capable of interchanging the labels in the C-6–C-9 portion of the nonadiene, an absolute requirement established from the [1-^{13}C]- and [2-^{13}C]-acetate experiments.

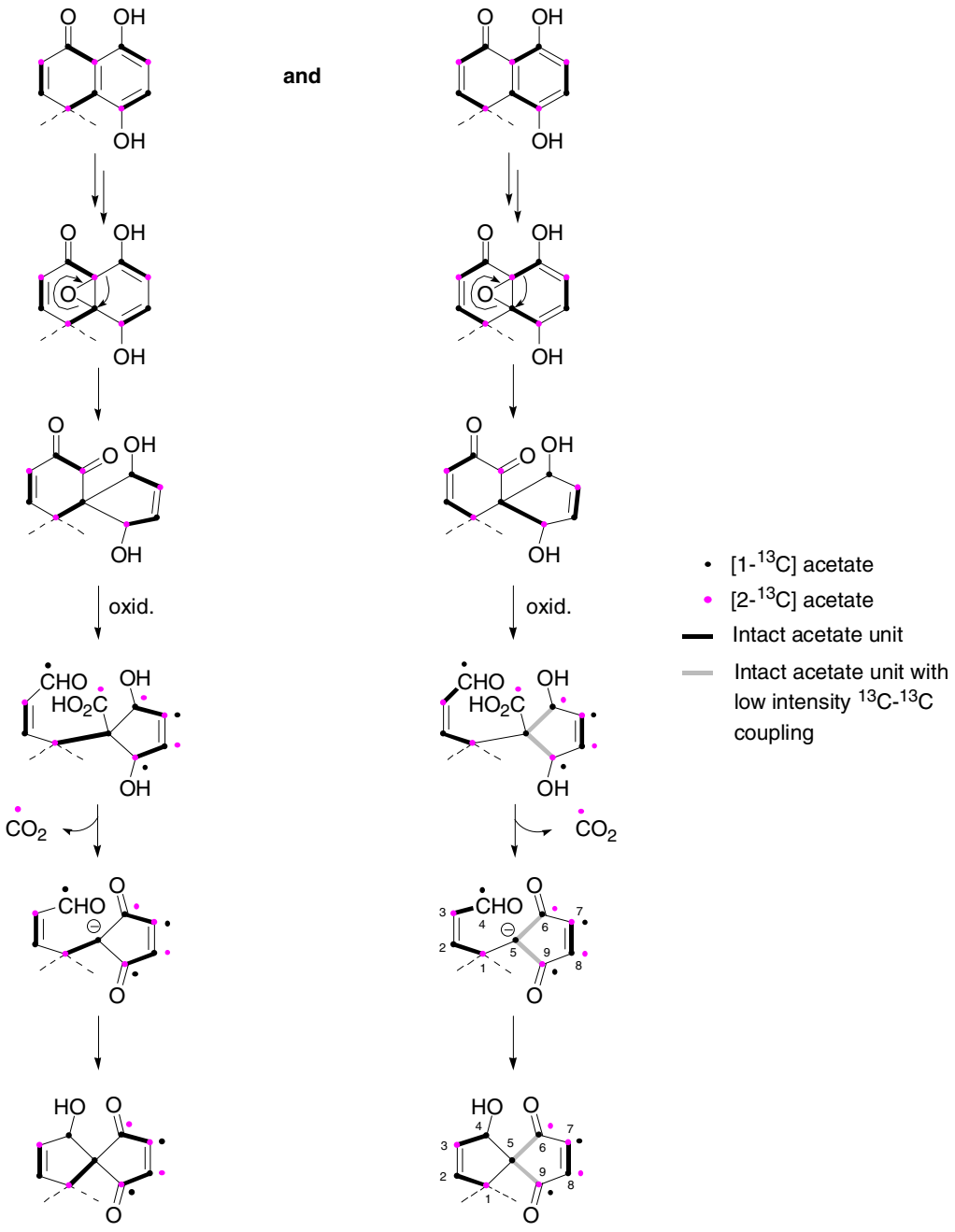

Figure 3.58: *Labelling patterns obtained from the [1,2-$^{13}C_2$]-acetate feeding experiment.*

From the analyses of the INADEQUATE NMR experiment, the derived $^{1}J_{CC}$ values (Table 3.12) and the appearance of the ^{13}C-^{13}C satellites in the ^{13}C NMR spectrum of the

enriched sample from the [1,2-$^{13}C_2$]-acetate feeding experiment (Figure 3.59), it was possible to confirm the biogenetic hypothesis outlined in Scheme 3.5b.

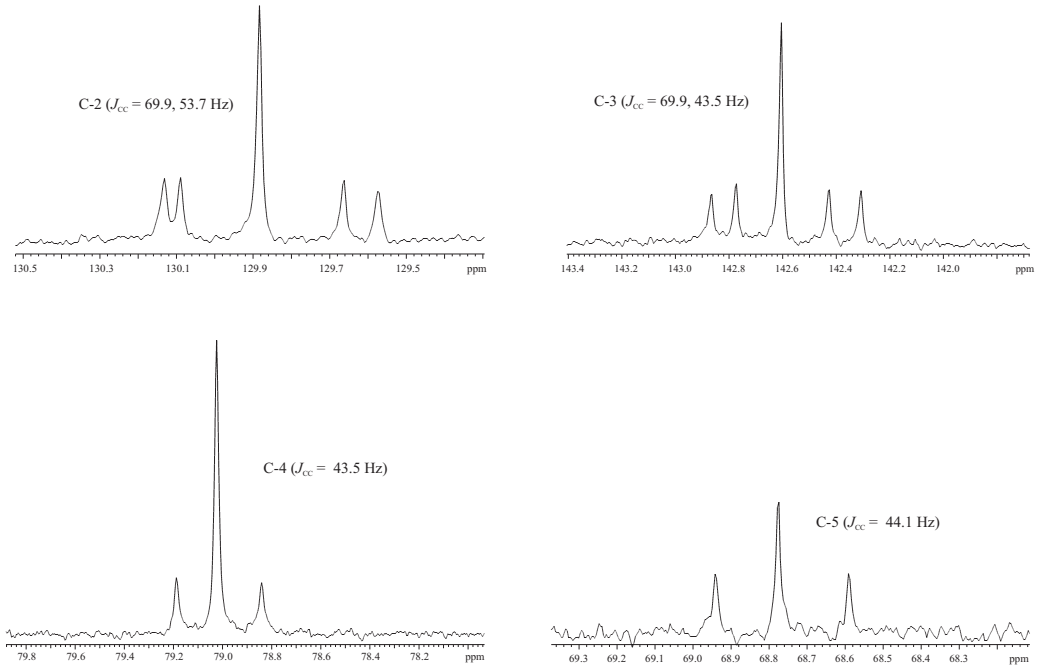

Figure 3.59: *Key satellite patterns from the ^{13}C NMR spectrum of* ***3.11*** *enriched with [1,2-$^{13}C_2$]-acetate.*

It was expected that the C-4 carbon on the spirononadiene portion of the ring would not show any coupling and therefore no satellites, as it was proposed that the C-2 acetate derived carbon from the DHN intermediate was cleaved between that of C-4 and C-5. The INADEQUATE NMR spectrum and coupling constants from the ^{13}C NMR spectrum showed that this however, was not the case, C-4 showed a *J* value of 43.7 Hz, since C-3 also showed a *J* value of 43.7 Hz, and was seen to show a strong coupling in the INADEQUATE NMR spectrum, it indicated an intact acetate unit lay at the C-3–C-4 position. Even more unusual was that carbons C-1–C-3 all showed coupling to two different carbons each. As well as coupling to C-4, C-3 also showed coupling to C-2 with a typical double bond *J* value of 70.1 Hz. In turn C-2 also showed a coupling to C-1 with a *J* value of 53.8 Hz. The carbon at C-5 was found to show an even more complex coupling pattern. Although the ^{13}C NMR spectrum showed only one pair of satellites, the

INADEQUATE NMR spectrum showed a rather different picture. Not only was a strong coupling from C-5 seen to C-1 at J = 44.1 Hz, two other couplings were observed in the INADEQUATE NMR spectrum to the carbons at C-6 and C-9. Although these couplings were certainly weaker than those of C-5–C-1, they were believed to be greater than the intensity of natural abundance, as no intensity enhancement (vs2d) was required in processing the spectrum to view these correlations (Figure 3.55).

It was proposed that only one pair of satellites were observed for C-5 because the coupling constant from C-5–C-1 was almost identical to those from C-5 to the ketone carbons at C-6 and C-9. The expected strong coupling from C-6 and C-9 to C-7 and C-8 respectively was also seen. According to the biogenetic hypothesis proposed in Scheme 3.5b and the isotopomer effect presented in Figure 3.58, coupling between C-7 and C-8 should also be observed. At first this was not obvious from either the ^{13}C NMR or INADEQUATE NMR spectra. A thorough analysis of the INADEQUATE NMR spectrum however found a correlation. The ^{13}C NMR data was found to agree with this, however due to the near identity of chemical shifts of the two carbons, the pattern of signals generated by these labelled carbons was very irregular. In the ^{13}C NMR spectrum, rather than each signal appearing with two satellites, an unexpected satellite pattern was observed (Figure 3.60). This was attributed to the "roof effect" resulting from second order coupling effects.[88]

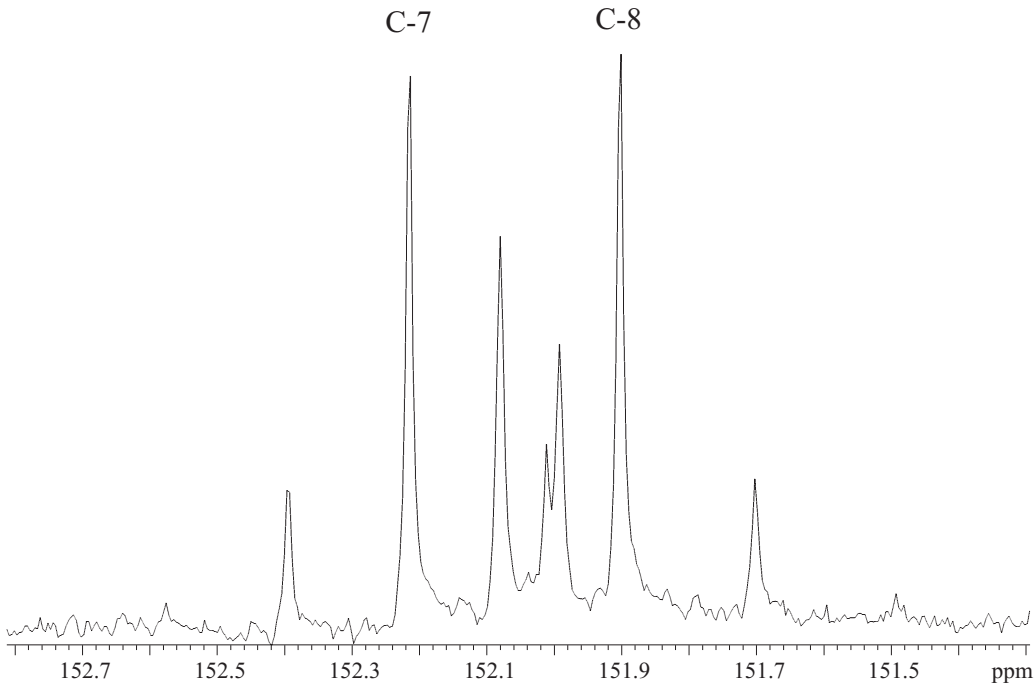

Figure 3.60: *Unexpected satellite pattern observed for C-7 and C-8.*

The most important discovery was that there was no significant coupling observed between C-4 and C-5 in the INADEQUATE NMR. However, when the vertical scale was increased, coupling could be seen. This was attributed to the coupling between C-4 and C-5 from the ^{13}C carbons of natural abundance origin. The ^{13}C INADEQUATE NMR spectra in Figure 3.61 show that the intensity of the C-4 to C-5 coupling is around five times less than that seen for the weak, but real couplings of C-5/C-6 and C-5/C-9. This is because the C-4/C-5 coupling can only be viewed at a vertical scale at least twice that of the C-5/C-6 and C-5/C-9 coupling.

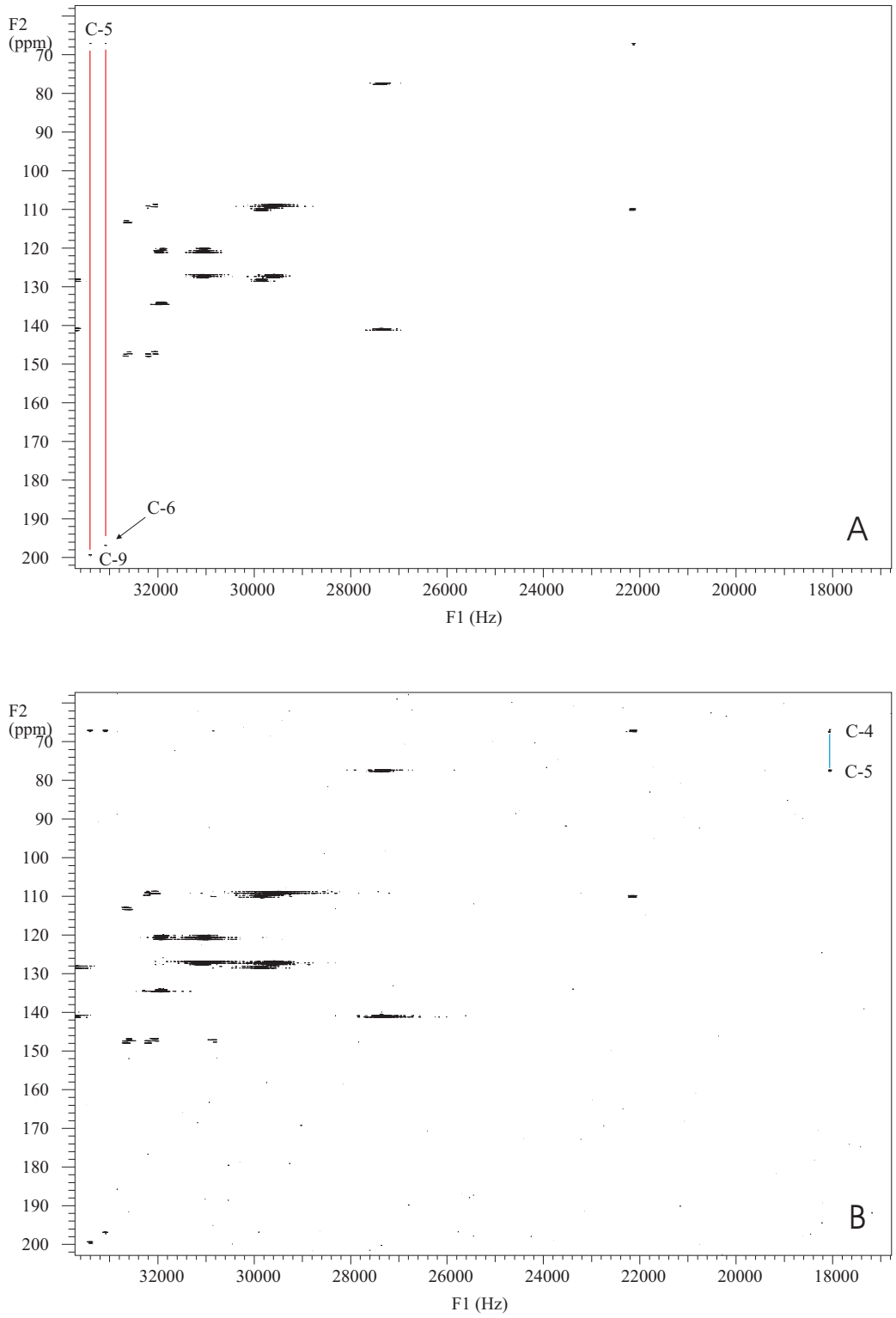

Figure 3.61: *^{13}C INADEQUATE NMR processed using vs2d=50 (**A**), and vs2d=100 (**B**).*

This lack of coupling is crucial to supporting the biogenetic hypothesis presented in Scheme 3.5b, as the proposal requires a C-2 carbon to be lost from between these two carbons, and hence no coupling would be expected.

All of the couplings observed in the INADEQUATE/^{13}C NMR spectra are consistent with the biogenetic hypothesis presented in Scheme 3.5b with the added complexity of isotopomerism. Figure 3.62 gives a summary of the labelling pattern observed from the NMR spectra. Because of the free rotation about the C_2 axis of the carbanion, half of the molecules originating from isotopomer **b**, will show an intact acetate between C-5 and C-6, while the other half will show the acetate between C-5 and C-9. Overall only one quarter of molecules will show C-5/C-6 coupling, another quarter will show C-5/C-9, the other half of molecules, which originate from isotopomer **a**, show no coupling between C-5–C-6/C-9. This is proposed to be the reason why the intensity of these couplings is less than the other couplings.

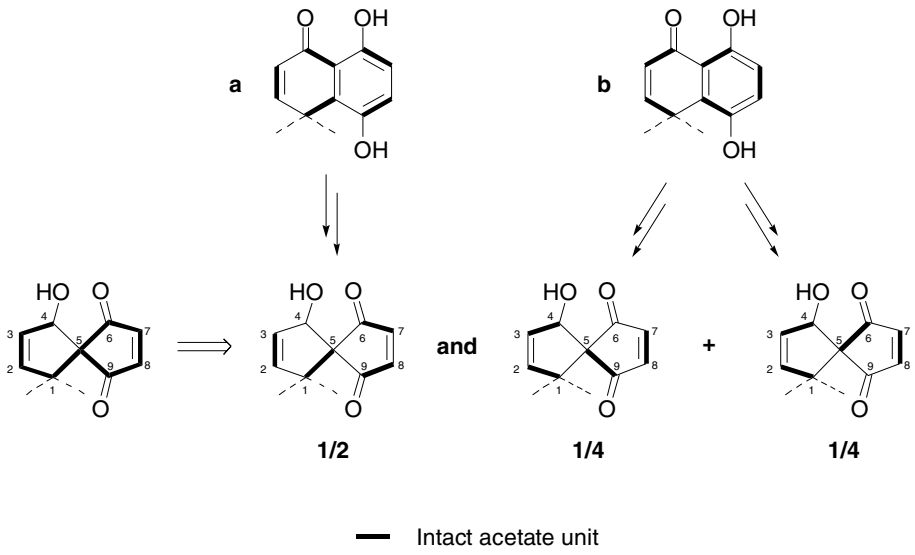

Figure 3.62: *Summary of labelling observed from INADEQUATE NMR and ^{13}C NMR spectra.*

The most probable explanation for the incorporation pattern therefore, is racemisation. Attack of the carbanion at the aldehyde carbonyl equally on both faces would also result in the bottom half of the molecule (the naphthalene) showing racemisation. This would be observed in all carbons, as they would appear to show coupling to two different

carbons; this is exactly what is seen for this unusual molecule. This also explains the observed racemate of spiro-mamakone A. It is uncommon for natural products to display this property, due to specificity of biosynthetic enzymes. A racemic molecule however, is precisely the type of molecule expected to result from the biogenetic hypothesis presented in Scheme 3.5b, where free rotation at the carbanion would statistically, lead to half of the population of molecules being a product of attack at one face while the other half, a result from attack at the opposite face.

At this stage, although the direction of the polyketide chain is clear, the starter unit has been unable to be determined. The folding pattern appears to be that of a regular fungal polyketide. This is also supported by the co-production of the natural product, mellein in the growing culture. The biosynthesis of mellein was elucidated by Abell and co-workers,[89,90] and was found to consist of a regular polyketide folding pattern as shown in Figure 3.63.

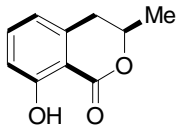

Figure 3.63: *The regular polyketide folding pattern of mellein.*

*3.16 Enrichment of Mamakunoic Acid B (**3.7**) with Labelled Acetate*

As mentioned in Section 3.13, mamakunoic acid B, isolated from the first culture of E484 (Section 3.5.2), was also found to be produced in the isotopically labelled fungal culture, used for the biosynthetic studies of spiro-mamakone A (**3.11**). Although the quantity produced was much less than that of spiro-mamakone A, and complicated by the presence of a major impurity, it was decided to proceed with the analysis of the labelled ^{13}C NMR spectrum. It was originally thought that the mamakunoic acids could be a precursor molecule to the spiro-mamakones. For this reason it was important to obtain as much biosynthetic information as possible.

Comparison of the [1-^{13}C]- and [2-^{13}C] acetate NMR with that of the natural abundance ^{13}C NMR (Figure 3.64) showed which carbons were labelled with [1-^{13}C] acetate, and which were labelled with [2-^{13}C] acetate.

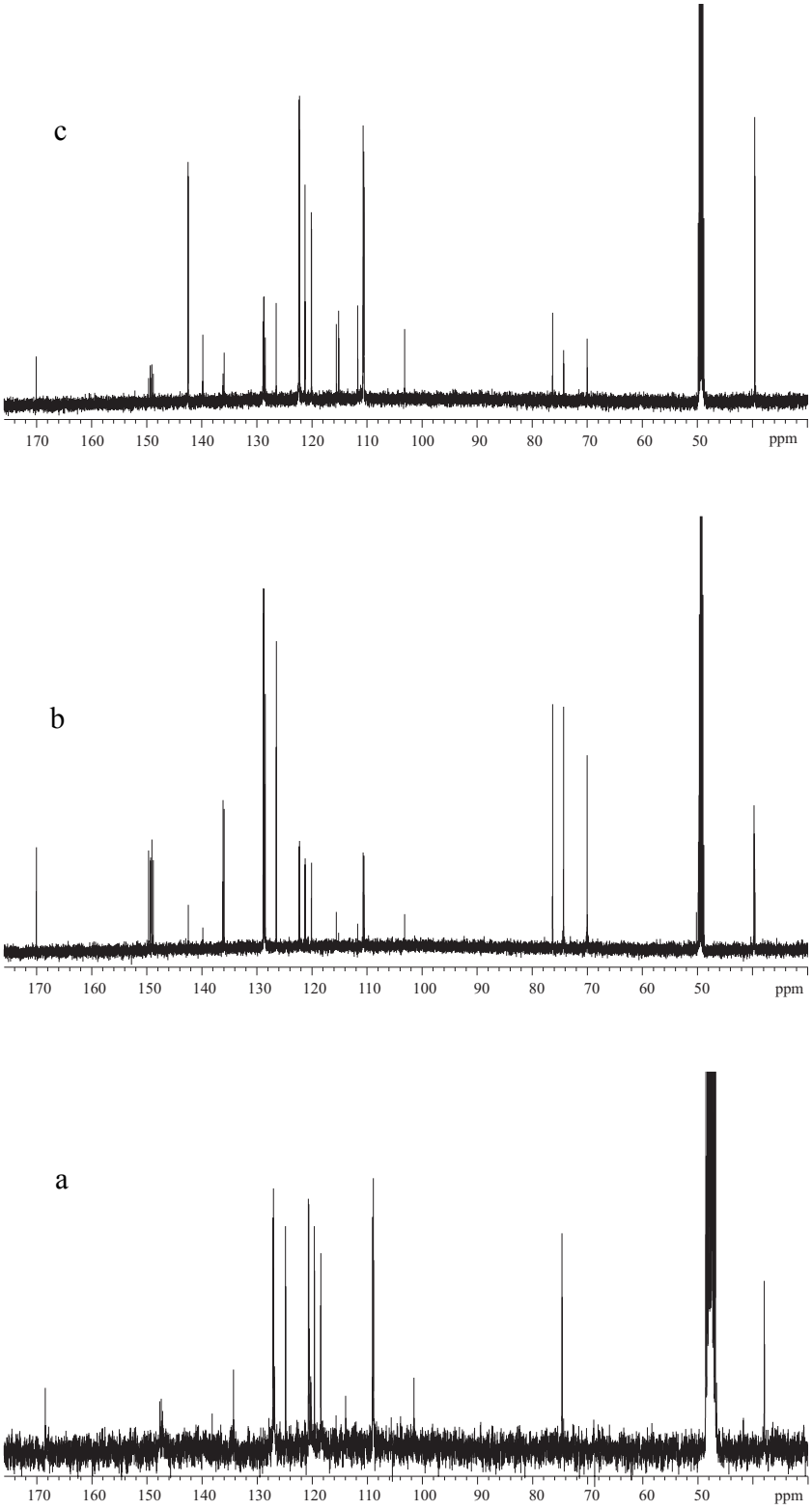

Figure 3.64: *^{13}C NMR spectra for unlabelled (**a**), [1-^{13}C]- (**b**) and [2-^{13}C]-acetate (**c**) enriched mamakunoic acid B (**3.7**).*

Although the spectrum of the labelled compounds contained a major impurity, the correct ^{13}C NMR signals for mamakunoic acid B were extracted by comparison with the natural abundance spectrum, which had contained minimal impurities. This cursory analysis resulted in the labelling pattern presented in Figure 3.65.

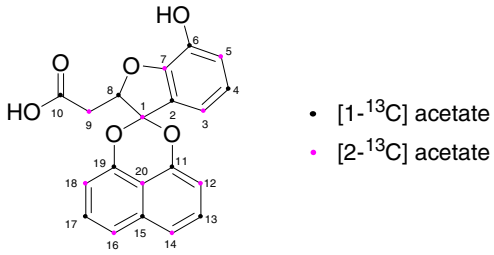

Figure 3.65: *Labelling pattern for mamakunoic acid B (**3.7**).*

The carbons of the naphthalene subunit showed a regular polyketide incorporation pattern, where every second carbon contained the same isotopic label. C-11, C-13, C-15, C-17, and C-19 were all shown to show incorporation of [1-^{13}C] acetate, whereas C-12, C-14, C-16, C-18, and C-20, all showed [2-^{13}C] acetate incorporation. The upper part of the molecule also showed a regular polyketide incorporation pattern. C-2, C-4, C-6, C-8, and C-10 all showed enrichment with [1-^{13}C] acetate, whereas all the odd numbered carbons, C-1, C-3, C-5, C-7, and C-9 showed enrichment with [2-^{13}C] acetate (Figure 3.65). The relative rate of incorporation for the singly labeled acetates were evaluated/estimated by determining the peak intensities relative to the intensity of the quaternary carbon signal at 135.9 ppm, and the quaternary carbon at 115.6 ppm for the [1-^{13}C]- and [2-^{13}C] acetate respectively, and then dividing these relative intensities by the relative intensities of the same peaks in the natural abundance spectrum (Table 3.13).

Table 3.13: *Incorporation of singly loabelled acetate in mamakunoic acid B (**3.7**).*

position	[1-^{13}C]	[2-^{13}C]	position	[1-^{13}C]	[2-^{13}C]
1	0.71	1.61	**11**	2.98	1.21
2	4.29	1.24	**12**	0.60	1.81
3	0.59	1.65	**13**	1.78	0.76
4	1.97	0.74	**14**	0.64	1.81
5	0.64	1.63	**15**	2.47	1.00
6	2.54	0.96	**16**	0.59	1.85
7	0.88	2.95	**17**	1.97	0.68
8	1.62	0.88	**18**	0.50	1.34
9	0.69	2.27	**19**	3.19	1.59
10	2.31	1.30	**20**	1.00	2.28

Unfortunately, these results were very misleading, compared to the visual analysis of the heights of the peaks compared with those of the natural abundance spectrum. The reason for this is the differing intensities of the carbons in the natural abundance spectrum (See Section 3.14.1). Unfortunately in this case, acetylation and the use of the modified ^{13}C NMR experiment, was not able to be performed. There were several reasons for this. Firstly, very little of the unlabelled mamakunoic acid B was isolated (1.9 mg). This was enough to get a normal ^{13}C NMR spectrum, but most definitely not enough to obtain the modified version, as used for spiro-mamakone A. The second factor is that after acetylation and purification of the labelled mamakunoic acid B, it was likely there would be even less compound to work with; certainly too little for running the modified ^{13}C NMR spectrum.

The ^{13}C NMR spectrum (Figure 3.66) obtained from [1,2-$^{13}C_2$]-acetate labelled mamakunoic acid B, was also of very poor quality. Like the ^{13}C NMR of the equivalently labelled spiro-mamakone A, doublet satellites were observed for some of the carbons, these included C-5 and C-8. However, some carbons were not observed as doublets. These included C-2, C-3, and C-7. The *J* values of carbons, C-9, C-4, and C-6 were unable to be determined due to overlap of impurity signals and/or signals of overlapping carbons, creating a very complex coupling pattern. The *J*-values of C-1, and C-10 were also found to be difficult to determine due to the low signal-to-noise ratio. This was especially true for C-1, where it was unclear whether it showed two satellites, or just one. The C-10 carbon was expected to show just one coupling as it is terminal, and

is adjacent to just one other carbon. This appeared to be the case, however extraction of the exact coupling constant was difficult due to the low signal-to-noise ratio of one of the satellites (Figure 3.66-inset).

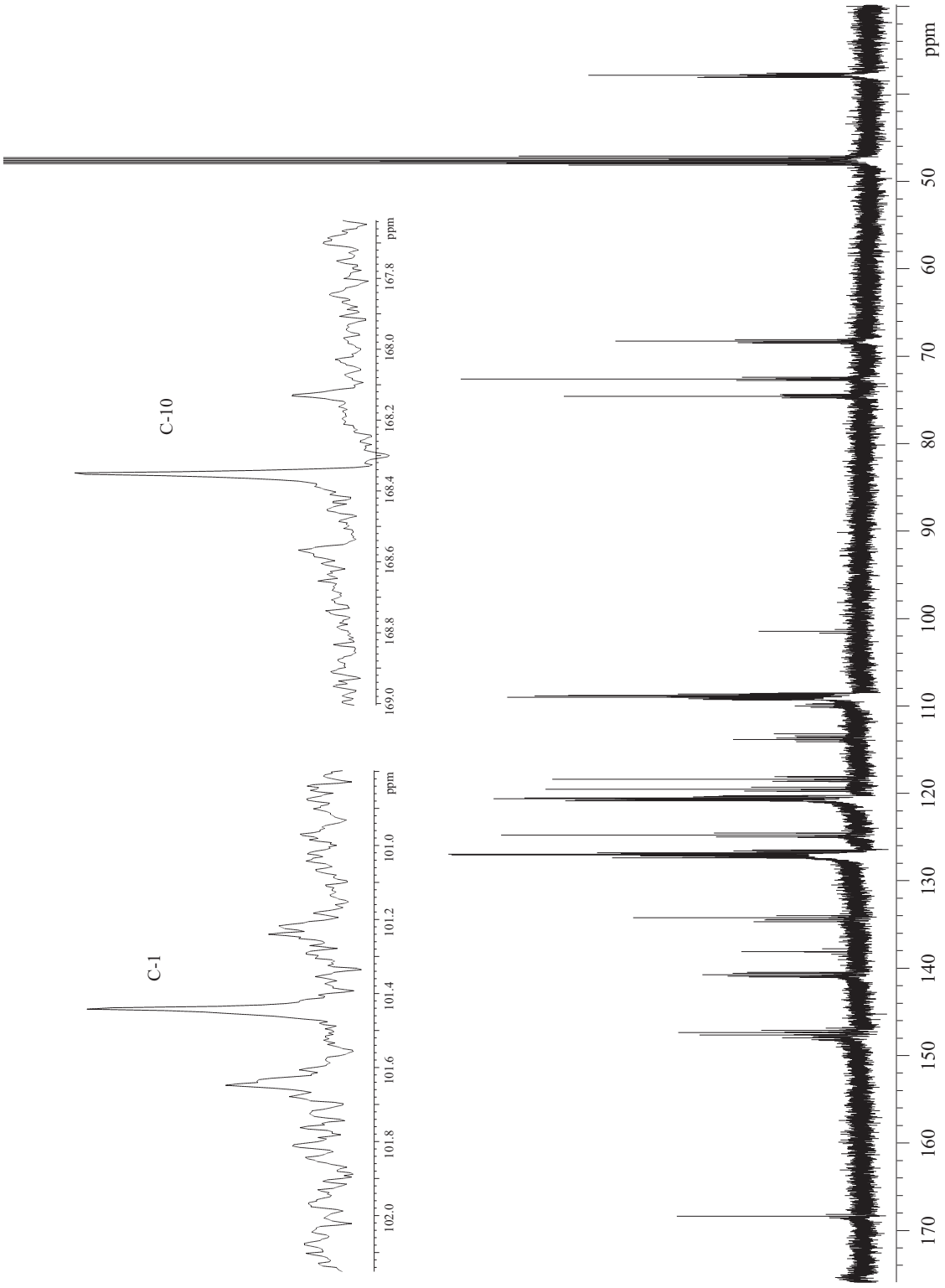

Figure 3.66: *^{13}C INADEQUATE NMR spectrum for* ***3.7****.*

The *J*-values of the naphthalene carbons were also unable to be measured due to the low signal to noise ratio and overlap of impurity signals (Figure 3.67). Unfortunately, these problems could not be resolved as the amount of material that was isolated was insufficient for running an INADEQUATE NMR experiment.

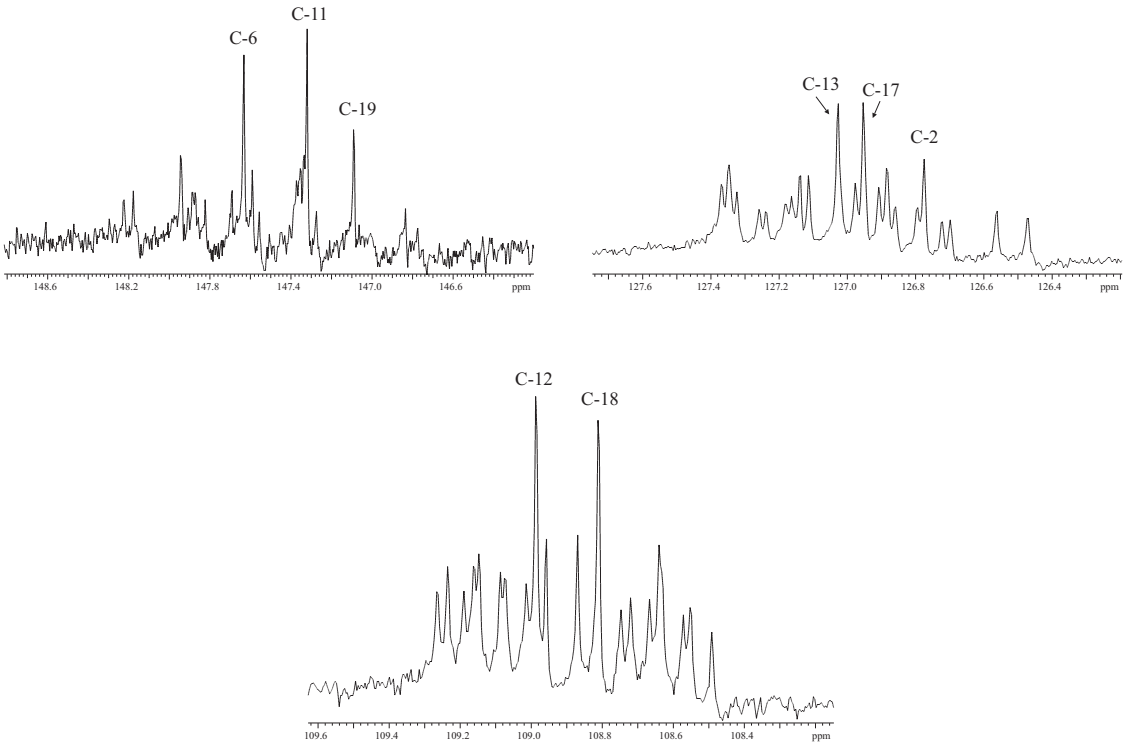

Figure 3.67: *Satellite patterns of some of the naphthalene carbons of* ***3.7*** *showing their complexity.*

From the data obtained from the [1-^{13}C]- and [2-^{13}C]-acetate feedings, it was concluded that mamakunoic acid B (**3.7**), like spiro-mamakone A (**3.11**), had originated from modification of DHN (**3.5**), rather than a C_6-C_4 precursor, such as that shown in Figure 3.68.

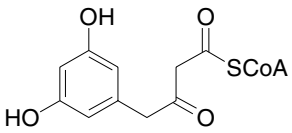

Figure 3.68: *C_6-C_4 precursor molecule.*

If DHN (**3.5**) is accepted as the biosynthetic precursor for the mamakunoic acids as well as the spiro-mamakones, it is possible to extend the biogenetic hypothesis leading to the spiro-mamakones to include the mamakunoic acids by a simple modification to the key intermediate. If the epoxy intermediate is reduced rather than rearranged it is possible to generate a plausible pathway to the mamakunoic acids (Figure 3.69). The observed labelling pattern for mamakunoic acid B (**3.7**), as far as it has been observed, fits this hypothesis.

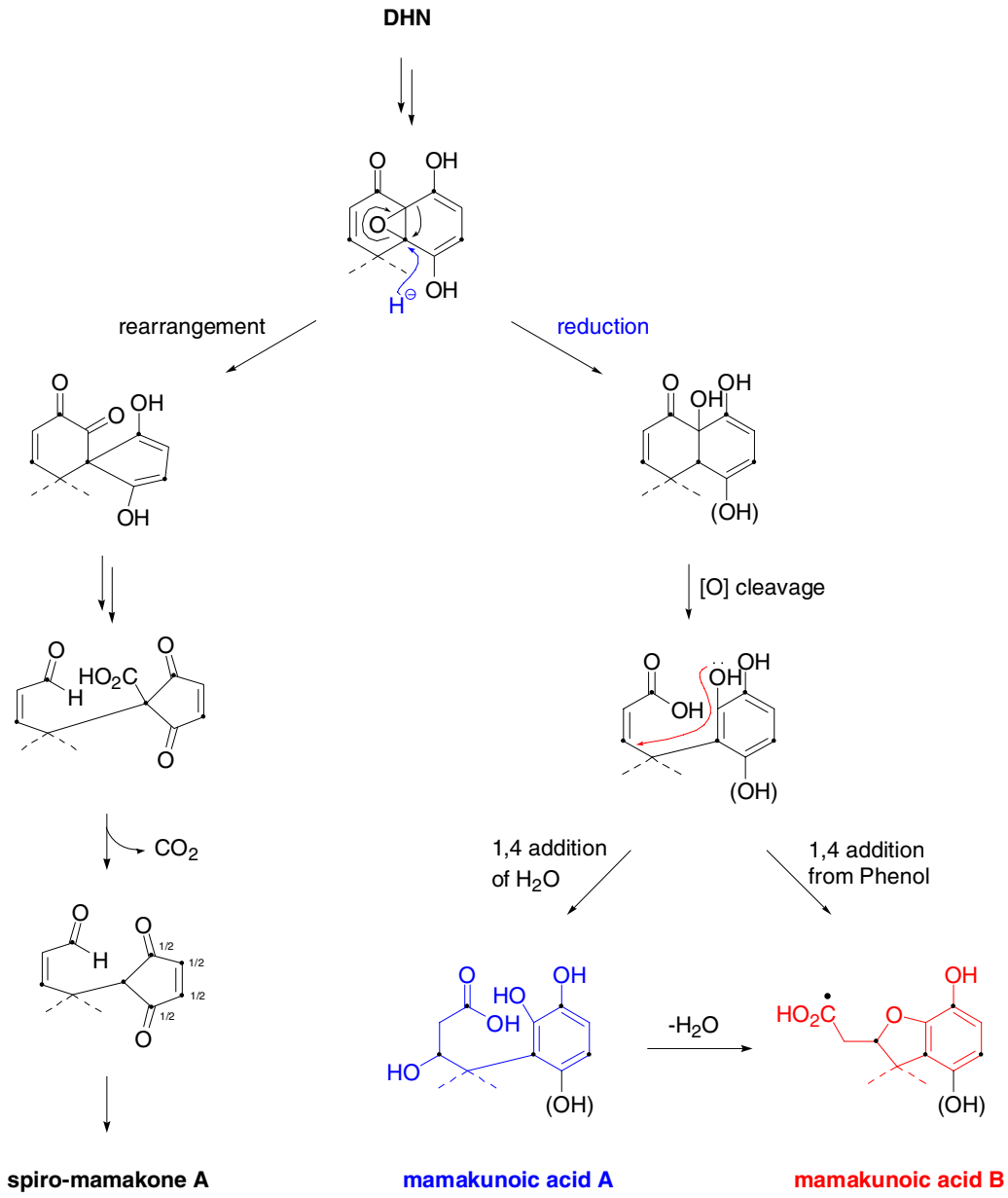

Figure 3.69: *Proposed biogenetic scheme for formation of the mamakunoic acids, compared to that for formation of the spiro-mamakones. Filled circles indicate [1-^{13}C]-acetate labelling.*

3.16.1 Future Work

Due to lack of material and time constraints the biosynthetic studies of mamakunoic acid B (**3.7**) were unable to be continued. This project should however be completed, to enable a more complete picture of this interesting group of molecules. Future work

would include the labelled cultures being grown on a significantly larger scale to ensure that adequate quantities of the labelled acid were produced. If the labelled acid was again found to co-elute with an impurity then further semi-preparative HPLC purification using a different gradient would need to be carried out. Once the singly labelled material was pure, methylation with diazomethane would be used in order to obtain an unlabelled internal standard, which would be used subsequently in the modified ^{13}C NMR experiments to quantitatively determine the rate of incorporation. Finally INADEQUATE NMR would be carried out on the doubly labelled material to confirm or disprove the biogenetic hypothesis proposed for the mamakunoic acids.

3.17 Discussion

The isolation of the structurally unprecedented spiro-mamakones prompted the study of their biosynthesis by incorporation experiments using ^{13}C-labelled precursors. Both **3.11**, and **3.7** were isolated, but only **3.11** was obtained in a sufficient quantity to obtain a full set of data, so that the labelling could be evaluated.

The ^{13}C NMR spectrum of **3.11**, produced after enrichment with [1-^{13}C]-acetate showed strong enrichment of 8 carbon signals, and intermediate enrichment of 4 carbon signals. The labelling pattern exhibited in the upper half of the molecule, placed two C-1 derived acetate carbons adjacent to each other, indicating cleavage of a C-2 derived carbon. Those labelled with [2-^{13}C]-acetate also showed strong enrichment of 8 carbon signals, and 4 carbons that carried intermediate enrichment. The four carbons of intermediate enrichment were the same as for those from the [1-^{13}C]-acetate labelled material, located on the enedione ring in the "upper" half of the molecule.

Both the ^{13}C and 2D INADEQUATE NMR spectra of **3.11**, after the incorporation of [1,2-$^{13}C_2$]-acetate (1.3% enrichment) displayed ^{13}C–^{13}C couplings between all 19 pairs of carbons, although this technique was supposed to indicate which carbons originated from the same acetate unit, this highly unusual phenomenon instead indicated that each carbon had two couplings (inter-acetate coupling was disregarded due to the very low incorporation).

The unusual results obtained from the incorporation experiments, supported the proposed biogenetic hypothesis presented in Scheme 3.5b, whereby it proceeds via a C_2-symmetric enedione intermediate, and the isotopomer effect initiated by the C_2-symmetric 1,3,6,8-tetrahydroxynaphthalene (**3.20**), an intermediate in the biosynthesis of the proposed **3.11** precursor molecule, DHN (**3.5**). These data are proposed to reveal that the two halves of the molecule are formed from two separate polyketide chains, each assembled from 5 intact C_2 units, and connected together by oxidative coupling. Rearrangement of an epoxide intermediate followed by oxidative cleavage, decarboxylation and finally cyclisation is proposed to be the basis for the formation of **3.11**. Although the starter unit was not defined in this study the polyketide chain appears to follow a regular fungal folding pattern.

For mamakunoic acid B (**3.7**), only minimal data was obtained for the incorporation of isotopic labels. The ^{13}C NMR spectra of **3.7** produced after enrichment with [1-^{13}C]- and [2-^{13}C]-acetate showed enrichment of 10 alternate carbon signals each (a regular polyketide incorporation pattern). The ^{13}C NMR spectrum from [1,2-$^{13}C_2$]-acetate incorporation was unable to give complete data on the ^{13}C–^{13}C couplings due to impurities and low signal to noise ratios. However it was apparent that some of the carbons at least, exhibited the same "double coupling" phenomena displayed by the carbons in **3.11**. From the minimal data obtained, it was proposed that like **3.11**, **3.7** also initially arose from a DHN (**3.5**) intermediate. However, rather than rearrangement of the epoxide intermediate, as was proposed for **3.11**, reduction of the epoxide intermediate is instead proposed (Figure 3.69).

Chapter 4

Malaysian Gasteromycete *Scleroderma* sp. (F5031)

4.1 General Introduction

The *Scleroderma* sp. are otherwise known as earthballs or poison puff balls. They fall in to the group of Basidiomycete fungi known as Gasteromycetes. This group of fungi is characterised by the spore bearing structures, which are totally enclosed in a basidiocarp (fruiting body) and never exposed. They occur as ecto-mycorrhizal associates of a wide range of trees, including oak and eucalytus[91] or as saprotrophs in soil or rotting wood.[92] The fruiting bodies are formed at the surface of the soil or just below and are reminiscent of a potato in appearence. About 25 species of *Scleroderma* have been described world-wide,[92] and at least four of these are known to be poisonous: *Scleroderma albidum, S. areolatum, S. cepa and S. citrinum*. Symptoms of poisoning can occur within an hour of eating and include the general signs of central nervous system disruption, including loss

of consciousness, severe abdominal pains, vomiting, perspiration, generalised tingling sensations, spasms, paralysis and anaphylactic shock.[91,93]

4.1.1 Metabolites from Scleroderma

The chemistry of the earthballs has been reported to be largely unknown.[93] In fact so far there are only two classes of natural products that have been described that are known to come from *Scleroderma* sp., lanostane type triterpenes and pulvinic acid derivatives.

4.1.1.1 Triterpenoids

Triterpenoids represent a large class of natural products. The sterols, such as lanosterol are C_{30} compounds that appear to have an essential role as constituents of cell membranes, where they help maintain structural integrity and control permeability. Other sterols however are metabolised to produce biologically active molecules such as vitamin D and the human sex hormones.[1]

So far only a handful of triterpenoids have been reported from *Scleroderma* sp. and all of these are lanosterol-type triterpenoids. Examples of this type, (20*S*, 22*S*, 23*E*)-22-*O*-acetyl-25-hydroxylanosta-8,23(*E*)-dien-3-one (**4.1**), isolated from *S. citrinum,*[94] and lanosta-8,24-diene-3β,23-diol (**4.2**) isolated from *S. aurantium*[95] are shown below. The former of these (**4.1**) was found to display strong antiviral activity against *Herpes simplex* type 1 (HSV-1).[94]

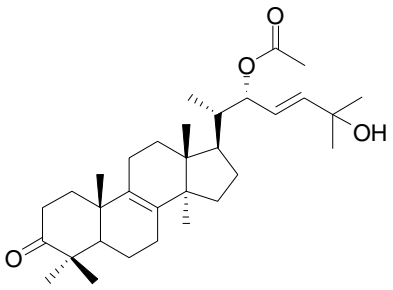

4.1

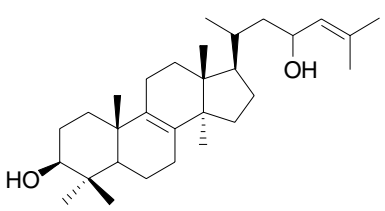

4.2

4.1.1.2 Pulvinic acid derivatives

The pulvinic acid derivatives are arylpyruvic acid derived pigments from the shikimate-chorismate pathway of secondary metabolism.[96] The parent structure, vulpinic acid (**4.3**), was first described as a metabolite of lichens (plants living in a symbiotic relationship with fungi and algae). Vulpinic acid is responsible for the yellow colour observed in some of these plant-fungi/algae symbionts.[97] These days however, it is a common metabolite, isolated from certain species of Basidiomycetes. Compound **4.3** has been found to possess antiinflammatory properties, and although the therapeutic ratio is good it was found to cause hyperventilation and in many cases was followed by convulsions and death of test animals.[98] Although these observations were first documented by Soderberg in 1952,[99] these properties were probably known to Eskimos, who used lichens containing vulpinic acid to poison wolves.[98]

The pulvinic acids are not only common to *Scleroderma* sp. but also to other fungi in the order Boletales. This has been suggested to indicate a close relationship between the Boletales and gasteroid Sclerodermatales.[100] Other than **4.3**, a range of natural pulvinic acid derivatives exist, including: xerocomic acid[101] (**4.4**), 3,4,4'-tri-*O*-methylxercomic acid methyl ester (**4.5**)[102] and atromentic acid (**4.6**).[103]

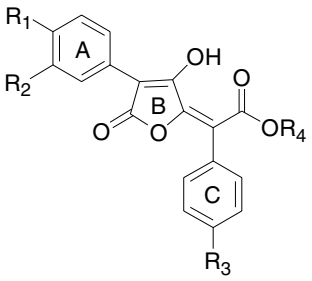

	R_1	R_2	R_3	R_4
4.3	H	H	H	CH_3
4.4	OH	OH	OH	H
4.5	OCH_3	OCH_3	OCH_3	CH_3
4.6	OH	H	OH	H

Interestingly, it has been found that the hydroxylated pulvinic acids such as **4.4** and **4.6**, are responsible for the yellow and red colours of most boletales, and cause a blue colouration to develop on the flesh of the fungus when the fruiting bodies are cut or bruised.[96] The compounds responsible for the blue colouration have been identified as xerocomic acid[101] (**4.4**), also isolated from *Scleroderma*,[104] and variegatic acid (**4.7**).[105]

The blue colour was found to form upon oxidation of these pulvinic acid derivatives by oxidases and is due to the formation of delocalised hydroxyquinone methide ions[101,105] (Figure 4.1).

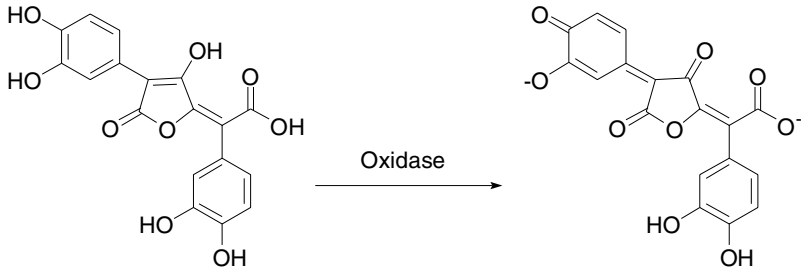

Figure 4.1: *The blueing reaction of variegatic acid.*

Pulvinic acid dimers have also recently been isolated from *Scleroderma citrinum*, including norbadione A (**4.8**), badione A (**4.9**) and sclerocitrin (**4.10**).[104] The former two of these had previously been isolated only from the Boletus, *Xerocomus badius*.[106]

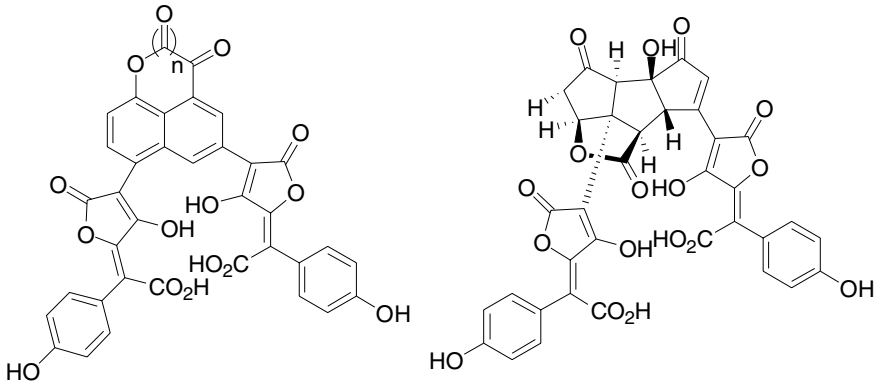

After the nuclear reactor accident at Chernobyl, high concentrations of ^{137}Cs were found in the fruit bodies of *Xerocomus badius*. It was found that this was due to the complexation of the ^{137}Cs by the naphthalenoid pulvinic acids, **4.7** and **4.8**, that are naturally present in the mushroom as their potassium salts.[107] This finding has attracted

the attention of some European research groups who are hoping to develop bioremedial methods for cleaning polluted environments.[108]

4.2 Introduction

The fruiting bodies of a *Scleroderma* sp. (F5031) were collected from a forest in Kuala Lompat, Pahang in Malaysia in June 2004. This extract was transported to the University of Canterbury, New Zealand for chemical investigation.

4.3 Preliminary Investigations

A biological activity profile of the crude extract was obtained before an in-depth investigation was carried out. The crude extract was submitted for P388 (Section 7.1.3), antimicrobial and antiviral assays (Section 7.1.5-6). At a concentration of 10 mg/mL the extract showed no activity towards the in-house viral strains, but did show weak P388 activity (IC_{50} 66640 ng/mL) and particularly strong antimicrobial activity against *B. subtilis* (Sm11). For this reason it was decided to investigate the extract further.

To obtain a visual profile of the extract, an aliquot of the extract was chromatographed on reverse phase C18 HPLC using the standard gradient (Section 7.1.7.2). HPLC (Figure 4.2) revealed the extract to be relatively simple in nature, consisting mainly of what seemed to be a four closely related compounds, as judged by the similarity of their UV profiles (Figure 4.3). Based on the HPLC profile the assumption was made that the four related compounds each contained a highly conjugated system, consistent with the intense orange colour of the extract and absorbance in the yellow region of the UV-visible spectrum (Figure 4.3).

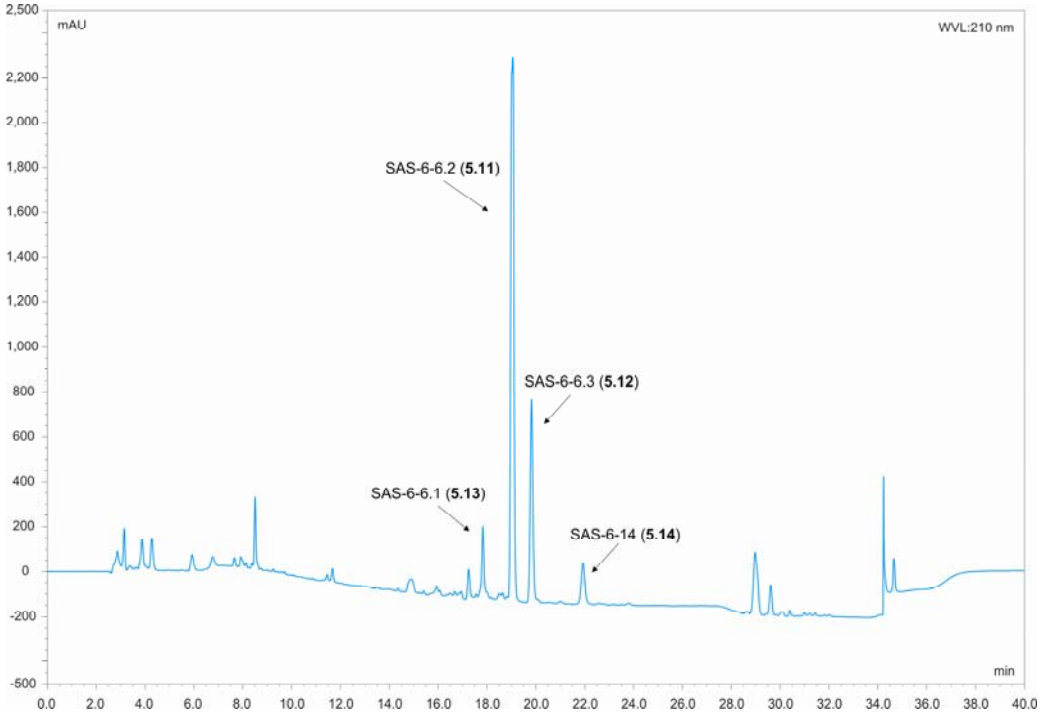

Figure 4.2: *HPLC chromatogram showing elution profile of the crude extract of F5031*

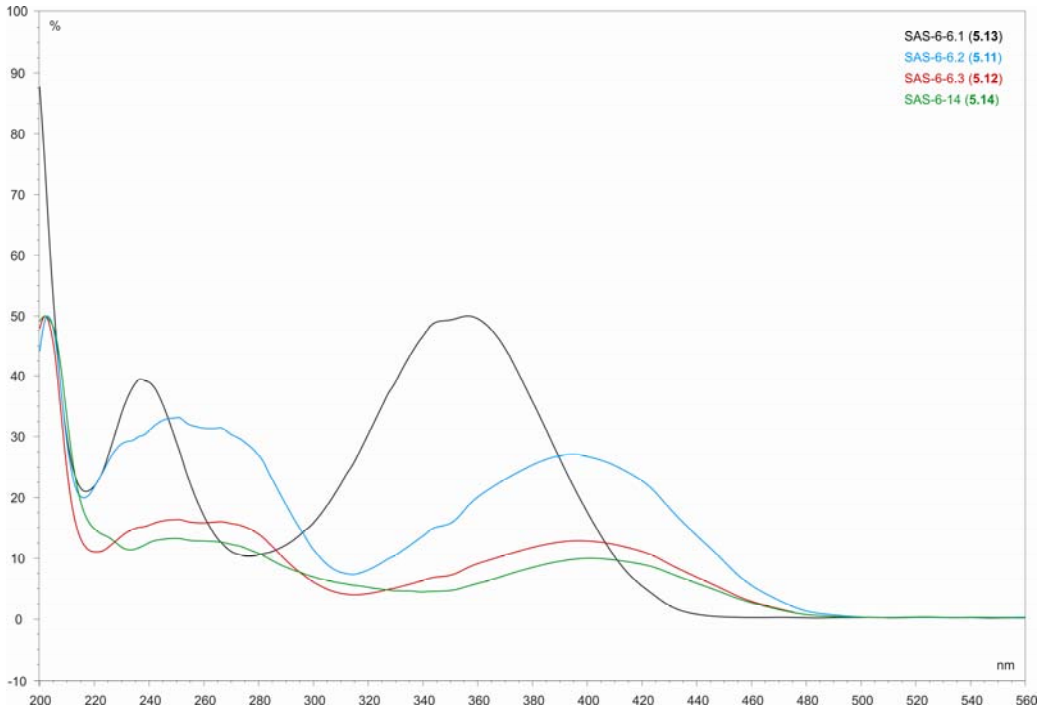

Figure 4.3: *UV profile overlay of SAS-6-6.1–3, and SAS-6-14*

4.4 Chromatography of F5031

Before attempting chromatography, the extract was partitioned with MeOH/Pet. ether. The MeOH soluble material (474 mg) was found to contain all of the four compounds in question. Due to the simple nature of the MeOH fraction, chromatography was kept to the bare minimum, with semi-preparative HPLC being the only form of chromatography carried out in order to obtain each of the four compounds in a sufficiently pure form (detail of the method used is given in the Experimental-Section 7.5.1).

4.5 Structural Elucidation

4.5.1 Structural Elucidation of SAS-6-6.2 (**4.11**)

SAS-6-6.2 (**4.11**) was the major compound isolated from the extract of the *Scleroderma* sp. ESIMS determined the mass of the compound to be 383 Da $[M+H]^+$. The ^{1}H NMR (Figure 4.4) and COSY spectra indicated the presence of two separated aromatic spin systems. The ortho coupling (J_{HH} = 8.9 Hz) displayed by the two sets of protons on each ring, A and C (A: δ_H 8.12; δ_H 6.95, C: δ_H 7.19; δ_H 6.92) suggested two *para*-disubstituted systems.

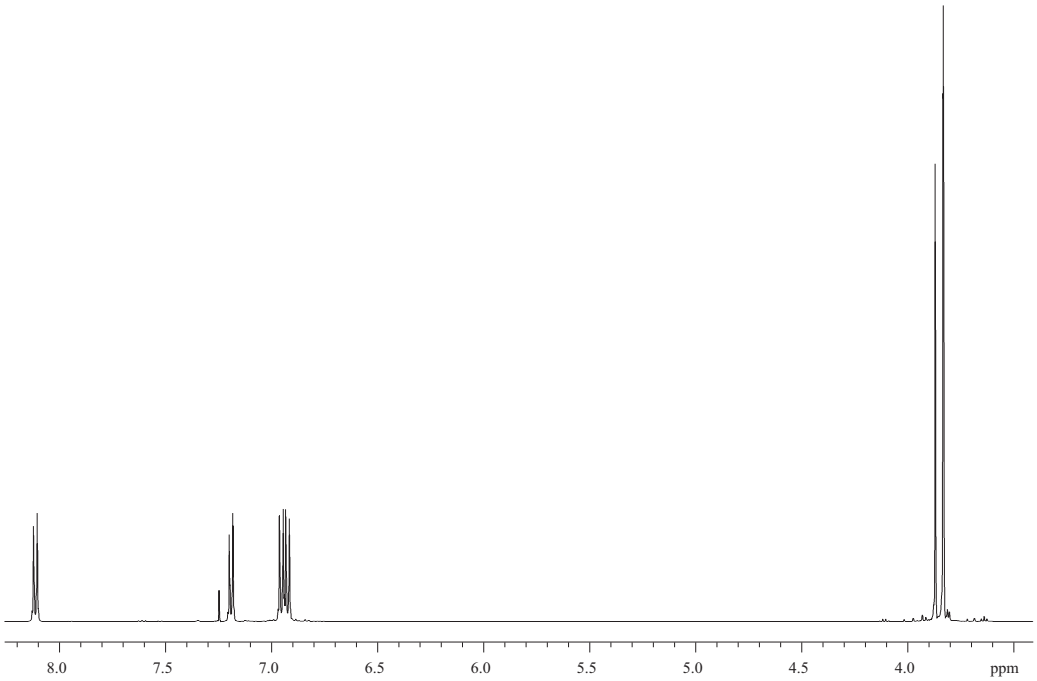

Figure 4.4: *^1H NMR spectrum of* ***4.11*** *in $CDCl_3$*

Correlations in the CIGAR NMR spectrum showed that each ring was substituted with one methoxyl group. This was confirmed with correlations from the proton signals on each ring to oxygenated carbons at δ_C 159.7 and 159.5 on rings A and C respectively. Additional CIGAR correlations from the two sets of protons on both rings *ortho* to the methoxyl moiety (A: δ_H 6.95 and C: δ_H 6.92) to carbons at δ_C 121.8 and 124.3 respectively, completed the definition of the two aromatic rings. CIGAR correlations observed from δ_H 8.12 and 7.19 to carbons at δ_C 105.2 and 115.1 respectively, suggested that the unidentified part of the molecule that lay between rings A and C was unsaturated.

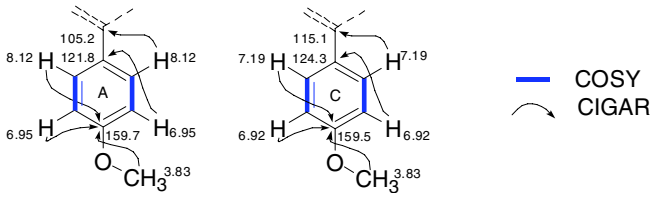

Figure 4.5: *COSY and CIGAR correlations for* ***4.11****.*

Correlations in the CIGAR and HSQC-DEPT NMR spectra allowed a further fragment of the molecule to be determined. A methyl group at δ_H 3.87 was shown to have a CIGAR correlation to a carbon at δ_C 171.9. These methyl protons were also seen to have a $^1J_{CH}$ correlation to δ_C 54.4. These correlations indicated a methyl ester moiety.

The lack of any other protons in the ^{1}H NMR indicated that the remaining piece of the molecule, which lay in between the aromatic rings, was highly functionalised, most probably by double bonds, given the highly coloured nature of the purified compound, and oxygen.

The mass of 382 Da assigned to this structure by ESIMS indicated that 85 mass units remained to be accounted for. The ^{13}C NMR (Figure 4.7) indicated that the three carbons unaccounted for included a shielded carbonyl carbon at δ_C 166.2 and two other quarternary carbons at δ_C 158.7 and 154.7. It was assumed at this point that the 33 remaining mass units could be accounted for by two oxygen atoms, one of them presumably forming a hydroxyl moiety, thus accounting for the uneven number of mass units left over.

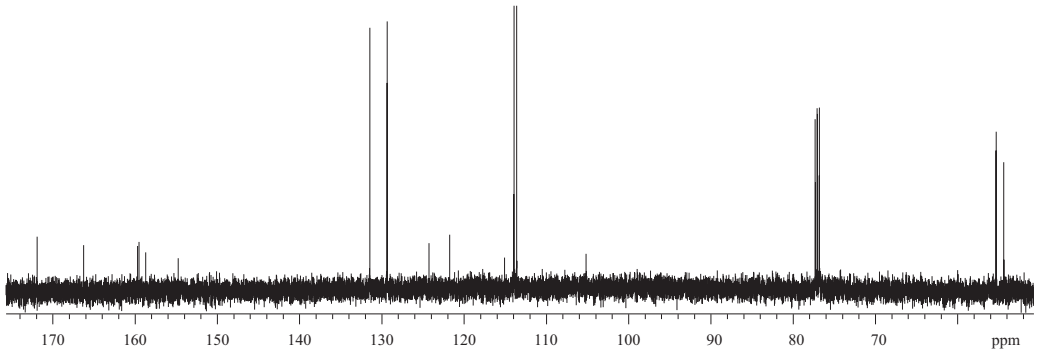

Figure 4.7. *^{13}C NMR spectrum of* ***4.11*** *in $CDCl_3$*

At this point a search of AntiMarin was conducted using the two 1,4-disubstituted benzenes and the methyl ester substructures as search parameters. A match was found to a group of compounds derived from vulpinic acid (**4.3**). These compounds contained two

six-membered aromatic ring systems separated by a hydroxy- or methoxy- substituted furanone ring. One of these compounds (**4.11**) had a mass of 382 Da.

A comparison of the experimental ^{1}H NMR data with the literature data for compound **4.11** (Table 4.1) unequivocally confirmed a match with the known compound, 4,4'-dimethoxyvulpinic acid, a vulpinic acid derivative previously isolated from several species of *Scleroderma*.[94,102]

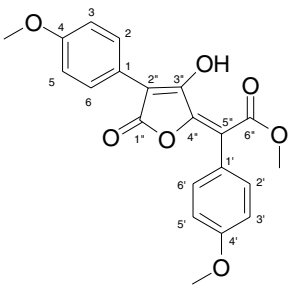

4.11

Table 4.1: *Literature and experimental (in $CDCl_3$) NMR data for* ***4.11***

[a]Literature ^{1}H ppm, multiplicity, (J_{HH} Hz)	Position	δ^{13}C ppm	δ^{1}H ppm, multiplicity, (J_{HH} Hz)	COSY	CIGAR
	1	121.8 (C)			
8.10 d (9.0)	2	129.4 (CH)	8.11 d (8.9)	H-3	C-4, C-6, C-2"
6.91 d (9.0)	3	113.9 (CH)	6.96 d (8.9)	H-2	C-4, C-1, C-5
	4	159.7 (C)			
6.91 d (9.0)	5	113.9 (CH)	6.96 d (8.9)	H-6	C-4, C-1, C-3
8.10 d (9.0)	6	129.4 (CH)	8.11 d (8.9)	H-5	C-4, C-2, C-2"
3.82 s	4-OCH_3	55.3 (CH_3)	3.83 s		C-4
	1'	124.3 (C)			
7.18 d (8.6)	2'	131.4 (CH)	7.19 d (8.9)	H-3'	C-4', C-6', C-5"
6.94 d (8.6)	3'	113.6 (CH)	6.93 d (8.9)	H-2'	C-4', C-1', C-5'
	4'	159.5 (C)			
6.94 d (8.6)	5'	113.6 (CH)	6.93 d (8.9)	H-6'	C-4', C-1', C-3'
7.18 d (8.6)	6'	131.4 (CH)	7.19 d (8.9)	H-5'	C-4', C-2', C-5"
3.82 s	4'-OCH_3	55.3 (CH_3)	3.83 s		C-4'
	1"	166.2 (C)			
	2"	105.2 (C)			
	3"	158.7 (C)			
	4"	154.7 (C)			
	5"	115.1 (C)			
	6"	171.9 (C)			
3.86 s	CO_2CH_3	54.4 (CH_3)	3.87 s		C-6"

[a] Carried out at 600 MHz in $CDCl_3$ using TMS as the internal standard.[109]
^{1}H and 2D experiments carried out at 500 MHz in $CDCl_3$. ^{13}C carried out at 75 MHz in $CDCl_3$.

*4.5.2 Structural Elucidation of SAS-6-6.3 (**4.12**)*

Compound SAS-6-6.3 (**4.12**) was the second most prevalent compound in the extract. ESIMS indicated the compound not only had a mass of 417 $[M+H]^+$ but was also contained a single chlorine substituent, indicated by the isotopic peak ratio $[MH]^+/[MH+2]^+$ of 3:1 (Figure 4.8).

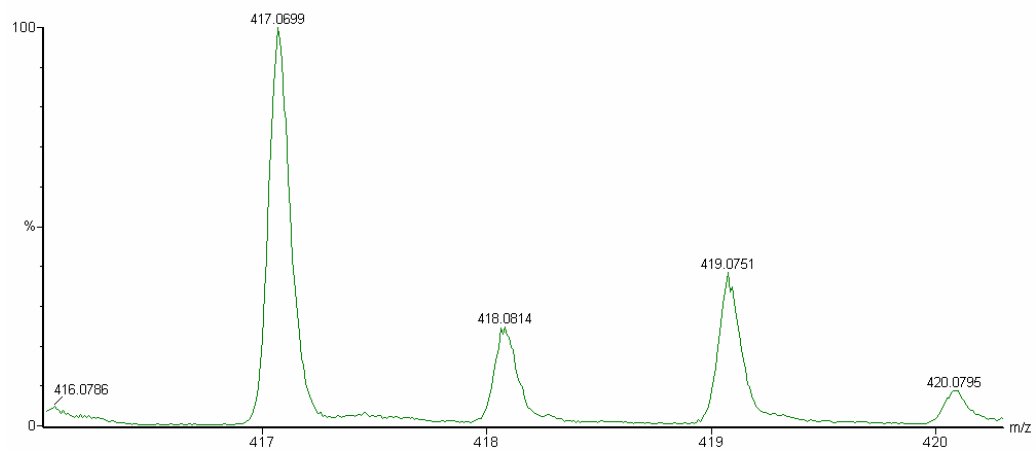

Figure 4.8. *Enlarged view of +ve ESIMS showing chlorine isotope pattern displayed by* ***4.12***

The general features of the ^{1}H NMR spectrum of **4.12** (Figure 4.10), very closely resembled that of **4.11**, except for differences in one of the aromatic rings. Rather than two identically substituted aromatic rings showing only *ortho* coupling as in **4.11**, ring C on **4.12** appeared to carry a non-hydrogen substituent *ortho* to the methoxyl. The protons in the ring appeared as a doublet of doublets at δ_H 7.13 with *meta* coupling to a doublet at δ_H 7.26 (J_{HH}= 2.0 Hz), and ortho coupling to a doublet at δ_H 6.94 (J_{HH} = 8.7 Hz) (see Figure 4.9).

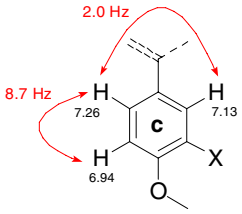

Figure 4.9: *Proposed substitution pattern for ring C.*

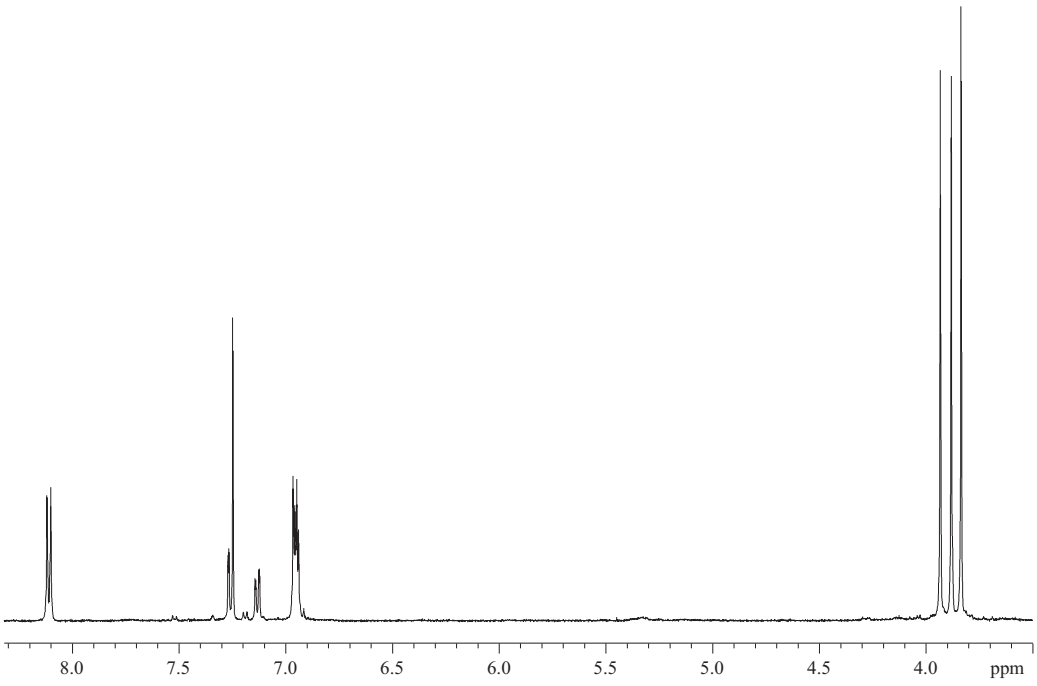

Figure 4.10. *^1H NMR spectrum of* ***4.12*** *in $CDCl_3$.*

The non-hydrogen substituent on the second ring was proposed as a chlorine atom as required by the isotopic pattern in the ESIMS, leading to the proposed structure (**4.12**). The structure was confirmed from COSY, HSQC-DEPT and CIGAR spectra. A literature search revealed that the NMR data (Table 4.2) matched those of a known compound, methyl-3'-chloro-4,4'-di-*O*-methylatromentate, a vulpinic acid derivative previously isolated from *Pulveroboletus auriflammeus*.[102]

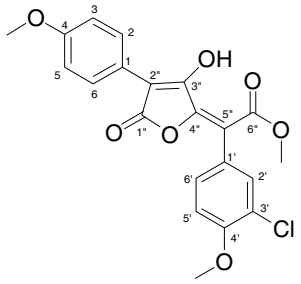

4.12

Table 4.2: *Literature and experimental (in $CDCl_3$) data for* ***4.12***

[a]Literature ^{1}H ppm, multiplicity, (J_{HH} Hz)	Position	δ^{13}C ppm[b]	δ^1H ppm, multiplicity, (J_{HH} Hz)	COSY	CIGAR
	1	121.7 (C)			
8.33	2	129.5 (CH)	8.11 d (8.7)	H-3	C-4, C-6, C-2"
6.77	3	114.0 (CH)	6.96 d (8.7)	H-2	C-4, C-1, C-5
	4	159.7 (C)			
6.77	5	114.0 (CH)	6.96 d (8.7)	H-6	C-4, C-1, C-3
8.33	6	129.5 (CH)	8.11 d (8.7)	H-5	C-4, C-2, C-2"
3.74 s	4-OCH_3	55.3 (CH_3)	3.84 s		C-4
	1'	122.3 (C)			
7.77 d (2.0)	2'	131.8 (CH)	7.26 d (2.0)	H-6'	C-4', C-6, C-1', C-5"
	3'	125.0 (C)			
	4'	155.3 (C)			
7.12 d (8.8)	5'	111.6 (CH)	6.94 d (8.7)	H-6'	C-4', C-3', C-1'
7.56 dd (8.8, 2.0)	6'	129.8 (CH)	7.13 dd (8.7, 2.0)	H-2', H-5'	C-4', C-2', C-5", C-5'
3.92 s	4'-OCH_3	56.2 (CH_3)	3.93 s		C-4', C-5'
	1"	ND (C)			
	2"	105.5 (C)			
	3"	ND (C)			
	4"	ND (C)			
	5"	113.7 (C)			
	6"	171.5 (C)			
3.83 s	CO_2CH_3	54.4 (CH_3)	3.88 s		C-6", C-5"

[a] Carried out at 400 MHz in acetone-d_6 using TMS as an internal standard.[102]
[b] Determined from HSQC-DEPT and CIGAR experiments.
ND-Not determined.

*4.5.3 Structural Elucidation of SAS-6-6.1 (**4.13**)*

Compound SAS-6-6.1 (**4.13**) was one of two minor components isolated from the extract of the *Scleroderma* sp. LCMS of the partitioned extract revealed this compound to have a mass of 397 $[M+H]^+$. As with SAS-6-6.3, the ^{1}H NMR spectrum of SAS-6-6.1 (Figure **4.11**) showed a very close resemblance to that of 4,4'-dimethoxyvulpinic acid, the only

apparent difference being an extra methoxyl group, giving a total of four rather than three.

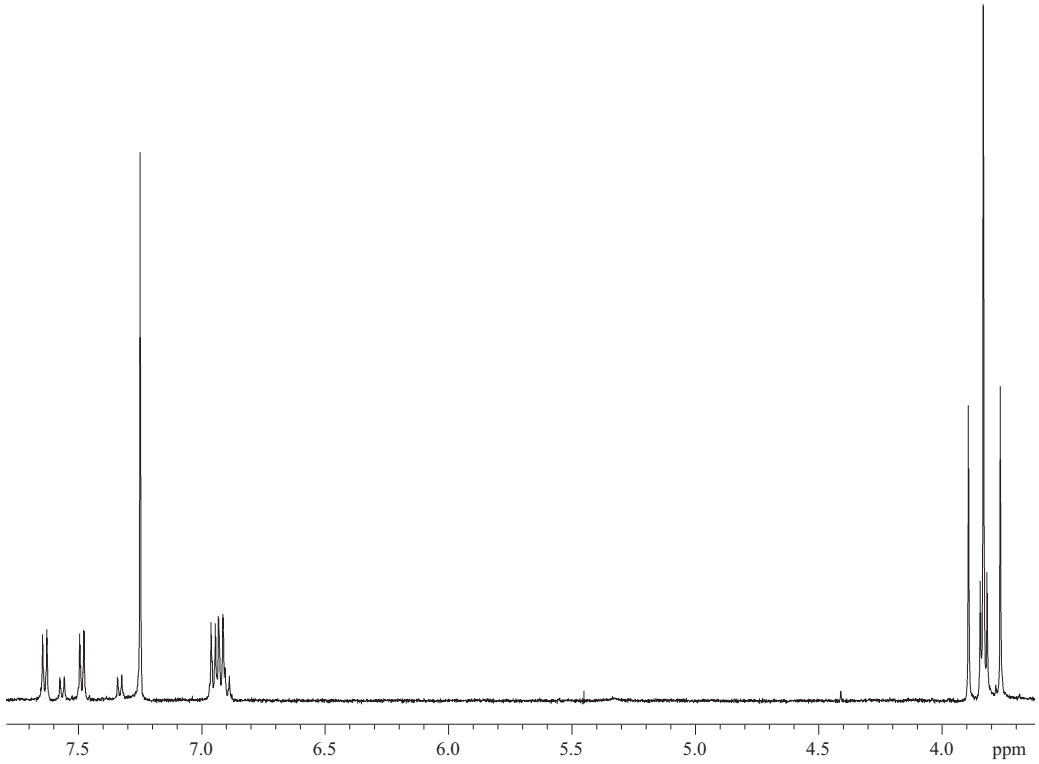

Figure 4.11. *^{1}H NMR spectrum of **4.12** in $CDCl_3$. NB small impurities at 7.32, 7.56, and ~3.8 pm.*

As observed for **4.11**, both of the aromatic rings in **4.13** were 1,4-disubstituted with methoxyl substitution at the 4 and 4' positions. This was supported by the *ortho* coupling (J_{HH} = 8.7 Hz) displayed by the two sets of protons on each of the rings, A and C (A: δ_H 7.49; δ_H 6.95, C: δ_H 7.64; δ_H 6.92), and also by the CIGAR correlations from the aromatic protons and also from the two methyl resonances at δ_H 3.83, to two oxygen bearing carbons (δ_C 160.1 and 160.5 respectively). A comparison of HSQC-DEPT and CIGAR data of **4.13** with those of **4.11** backed up the initial assumption that the two molecules were identical except for the replacement of one hydroxyl moiety with that of a methoxyl in **4.13**. Given that there was only one oxygen that could be methylated and still fit the NMR and MS data, it was proposed that a methoxyl had replaced the hydroxyl group on

C-3" (**4.13**). A literature search followed by comparison of ^{1}H and ^{13}C NMR data (Table 4.3) established that **4.13** was methyl 4,4'-dimethoxyvulpinte, a vulpinic acid derivative previously isolated from *Scleroderma* sp.[94,109]

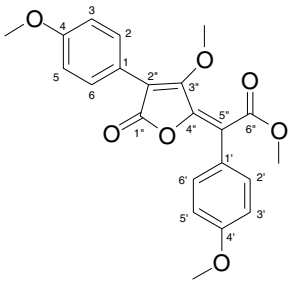

4.13

Table 4.3: *Literature and experimental (in $CDCl_3$) NMR data for* ***4.13***

[a]Literature ^{13}C	[b]Literature ^{1}H ppm, multiplicity, (J_{HH} Hz)	Position	$\delta^{13}C$ ppm[c]		$\delta^{1}H$ ppm, multiplicity, (J_{HH} Hz)	COSY	CIGAR
120.6		1	120.6	(C)			
131.0	7.59 d (8.8)	2	131.1	(CH)	7.49 d (8.7)	H-3	C-4, C-6, C-2"
114.3	6.87 d (8.8)	3	114.2	(CH)	6.95 d (8.7)	H-2	C-4, C-1, C-5
160.5		4	160.5	(C)			
114.3	6.87 d (8.8)	5	114.2	(CH)	6.95 d (8.7)	H-6	C-4, C-1, C-3
131.0	7.59 d (8.8)	6	131.1	(CH)	7.49 d (8.7)	H-5	C-4, C-2, , C-2"
55.3	3.71 s	4-OCH_3	55.4	(CH_3)	3.83 s		C-4
123.6		1'	123.7	(C)			
130.8	7.44 d (8.7)	2'	130.8	(CH)	7.64 d (8.7)	H-3'	C-4', C-5"
114.0	6.90 d (8.7)	3'	114.2	(CH)	6.92 d (8.7)	H-2'	C-4', C-1', C-5'
160.1		4'	160.1	(C)			
114.0	6.90 d (8.7)	5'	114.2	(CH)	6.92 d (8.7)	H-6'	C-4', C-1', C-3'
130.8	7.44 d (8.7)	6'	130.8	(CH)	7.64 d (8.7)	H-5'	C-4', C-5"
55.3	3.78 s	4'-OCH_3	55.4	(CH_3)	3.83 s		C-4'
168.1		1"	ND	(C)			
108.2		2"	108.3	(C)			
162.2		3"	162.2	(C)			
140.3		4"	ND	(C)			
115.6		5"	116.1	(C)			
167.4		6"	167.5	(C)			
52.7	3.84 s	CO_2CH_3	52.8	(CH_3)	3.89 s		C-6"
60.9	3.78 s	OCH_3	61.0	(CH_3)	3.76 s		C-3"

[a] Carried out at 100.62 MHz in $CDCl_3$ using solvent as the internal standard.
[b] Carried out at 600 MHz in $CDCl_3$, using the solvent as the internal standard.
[c] Determined from HSQC-DEPT and CIGAR experiments. ND-Not determined

*4.5.4 Structural Elucidation of SAS-6-14 (**4.14**)*

SAS-6-14 (**4.14**) was obtained as an intense yellow amorphous solid. ESIMS determined the molecular weight of the compound as 451/453/455 ($[M+H]^+$/$[MH+2]^+$/$[MH+4]^+$). These isotopic peak ratios in the vicinity of $[M+H]^+$ indicated the presence of two chlorine atoms in the molecule (Figure 4.12).

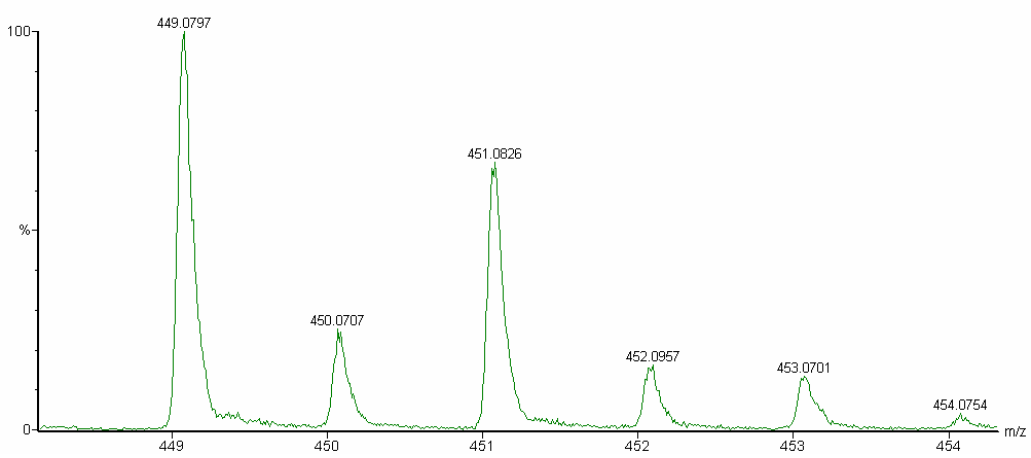

Figure 4.12: *Negative ion ESIMS showing the isotope effect of two chlorine atoms*

The ^{1}H (Figure 4.13) and ^{13}C NMR (Figure 4.14) spectra for **4.14**, as with the previous two vulpinic acid derivatives (**4.12** and **4.13**), bore a strong resemblance to those of **4.11**.

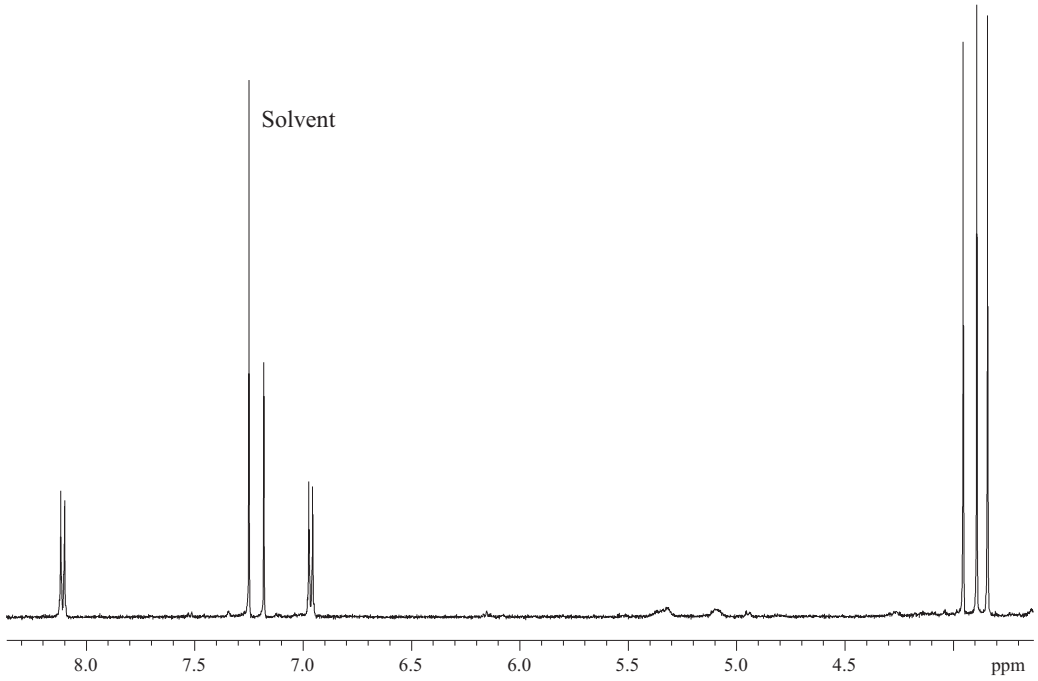

Figure 4.13: *^{1}H NMR spectrum of* ***4.14*** *in $CDCl_3$.*

As with **4.12**, the structural differences appeared to be in ring C only, with just a singlet proton resonance at δ_H 7.19 on this ring. Integrals revealing that the singlet proton represented two protons indicated a symmetrically substituted ring. It was noted that **4.14** still retained the methoxy substitution pattern on the aromatic rings that was seen for the previous three compounds (COSY, HSQC and CIGAR NMR spectra). Comparison of the CIGAR and ^{13}C data (Figure 4.15) with those for **4.11** revealed that the pair of carbons at δ_C 113.6 were replaced by a pair of quaternary carbons at δ_C 129.4 in **4.14**. The placement of the non-hydrogen substituents in the 3' and 5' positions was shown by CIGAR correlations from the proton at δ_H 7.19 to the carbons at δ_C 129.4 and 112.1.

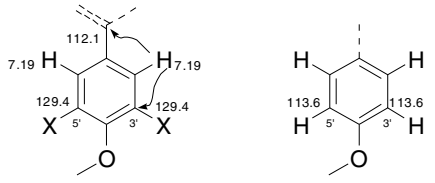

4.14 **4.11**

Figure 4.14. *CIGAR NMR correlations for ring C of* ***4.14****. Also shown is the comparison of* δ_C *at C-3' and C-5' for compounds* ***4.14*** *and* ***4.11****.*

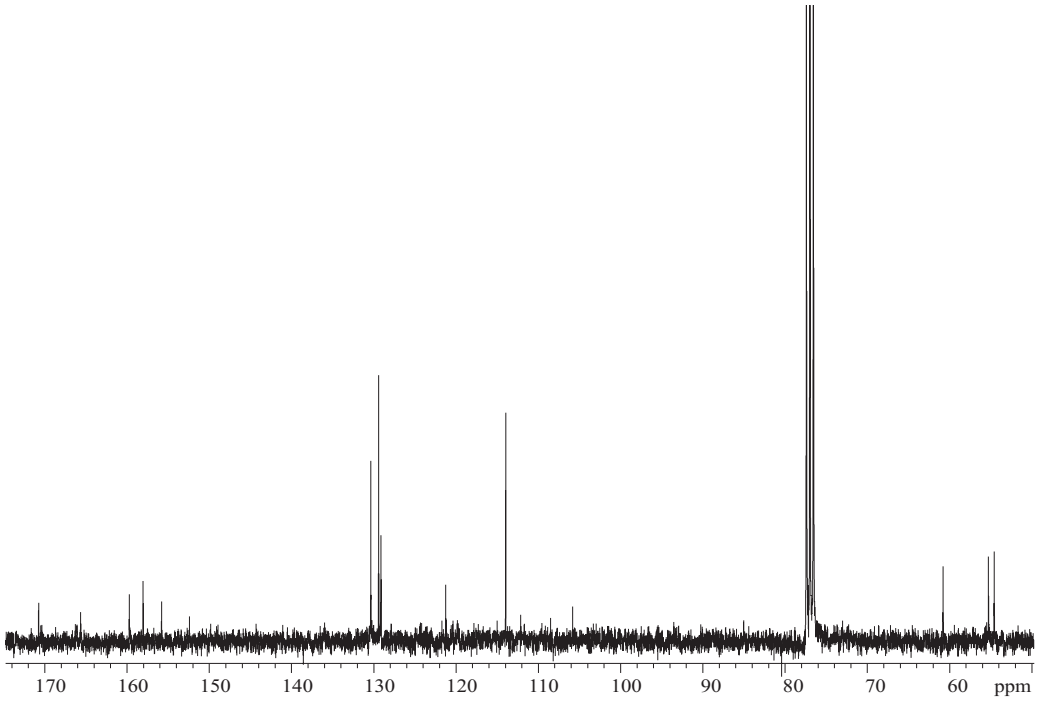

Figure 4.15*.* ^{13}C *NMR spectrum of* ***4.14*** *in* $CDCl_3$*.*

Given the isotope pattern seen in ESIMS, these carbons at δ_C 129.4 were proposed to be chloro substituted (**4.14**). As no matches were found in the AntiMarin, SciFinder Scholar, Biosis and Web of Science databases, this is a new vulpinic acid derivative. The compound was given the trivial name of methyl-3',5'-dichloro-4,4'-di-*O*-methyl-atromentate, which was in keeping with the naming of other similar vulpinic acid derivatives. A full set of experimental NMR data is presented in Table 4.4.

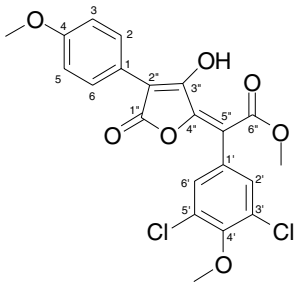

4.14

Table 4.4: *Experimental NMR data for* ***4.14****.*

Position	δ^{13}C ppm	δ^{1}H ppm, multiplicity, (J_{HH} Hz)	COSY	CIGAR
1	121.2 (C)			
2	129.5 (CH)	8.12 d (8.8)	H-3	C-4, C-6, C-3, C-2"
3	114.0 (CH)	6.97 d (8.8)	H-2	C-4, C-1, C-5
4	159.7 (C)			
5	114.0 (CH)	6.97 d (8.8)	H-6	C-4, C-1, C-3
6	129.5 (CH)	8.12 d (8.8)	H-5	C-4, C-2, C-5, C-2"
4-OCH_3	55.3 (CH_3)	3.85 s		C-4
1'	129.1 (C)			
2'	130.4 (CH)	7.19 s		C-4', C-2', C-3', C-5"
3'	129.4 (C)			
4'	152.4 (C)			
5'	129.4 (C)			
6'	130.4 (CH)	7.19 s		C-4', C-2', C-3', C-5"
4'-OCH_3	60.8 (CH_3)	3.96 s		C-4'
1"	165.6 (C)			
2"	105.8 (C)			
3"	158.0 (C)	13.42 (OH)		C-3", C-4", C-2"
4"	155.8 (C)			
5"	112.1 (C)			
6"	170.7 (C)			
CO_2CH_3	54.6 (CH_3)	3.89 s		C-6", C-5"

^{1}H and 2D experiments carried out at 500 MHz in $CDCl_3$.
^{13}C carried out at 75 MHz in $CDCl_3$.

The proposed structure was supported and confirmed, respectively, by EIMS and X-ray crystallography. In EIMS a fragment peak representing a mass of 418/420/422 was seen. This was presumed to be a dilactone peracetate derivative (**4.15**) formed by the loss of MeOH from the parent compound.

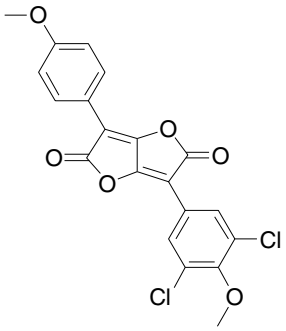

4.15

This phenomenon had been seen in the EI spectra of pulvinic derivatives previously.[110] X-ray crystallography confirmed the structure of **4.14** (Figure 4.16). The tables of structural coordinates are presented in Appendix 1.

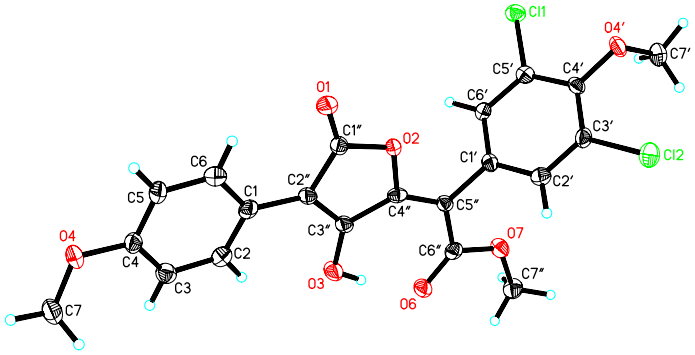

Figure 4.16: *Crystal structure drawing of* ***4.14****.*

4.14 was only weakly cytotoxic (IC_{50} 20.6 μM), but showed moderate activity against *B. subtilis* (4 mm zone of inhibition). The larger zone of inhibition that was initially seen in the crude extract (11 mm) was attributed to the two known compounds, 4,4'-dimethoxyvulpinic acid, and methyl-3'-chloro-4,4'-di-O-methylatromentate, which showed inhibition zones of 8 and 7 mm respectively.

4.6 Discussion

Purification of an extract from a *Scleroderma* sp. resulted in the isolation of four pulvinic acid derivatives. Interpretation of spectral data as well as AntiMarin and literature searches identified the first three compounds as the previously reported, 4,4'-dimethoxyvulpinic acid,[94,102] methyl 3'-chloro-4,4'-di-*O*-methylatromentate[102] and methyl 4,4'-dimethoxyvulpinate.[94,109] The fourth compound had no matches in the literature and was identified as a new dichlorinated pulvinic acid derivative and was named methyl-3',5'-dichloro-4,4'-di-*O*-methylatromentate. Dichlorinated pulvinic acids, as natural products, have been previously reported. These include methyl-2',5'-dichloro-4,4'-di-*O*-methyl-atromentate (**4.16)**,[109] where ring C is substituted, or where both rings, A and C are mono-substituted ortho to the methoxyl, as in dichloro-tri-*O*-methylxerocomicacid-methylester (**4.17**).[102]

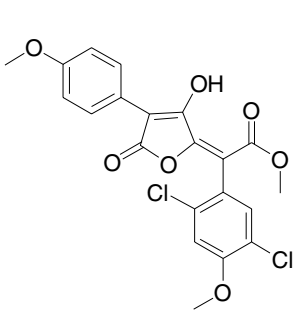

4.16

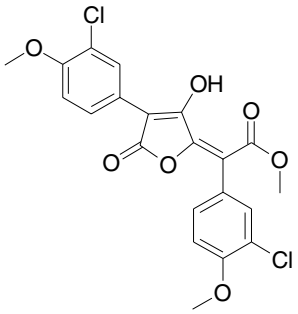

4.17

Chapter 5

An unidentified fungal endophyte (E57)

5.1 General introduction

5.1.1 Acylresorcinols

The acylresorcinols are a sizable class of polyketide compounds, with examples of this type of compound having been found in both the marine and terrestrial environment. Isolated from the marine environment is secocurvularin (**5.1**), originating from an unidentified fungus found inside the encrusting sponge, *Spirastrella vagabunda*.[111] Examples from the terrestrial environment are somewhat more plentiful. These include curvulinic acid (**5.2**), isolated from *Curvularia siddiqui*,[112] and *Oidiodendron rhodogenum*,[113] and its various analogues. Plants have also been found to be prolific producers of acylresorcinols. These differ from those of fungal origin by reason of their

long aliphatic side chains. This is clearly shown in suranone (**5.3**), isolated from the herb, *Peperomia sui*,[114] and also in **5.4**, a metabolite isolated from the stem bark of *Knema austrosiamensis*.[115]

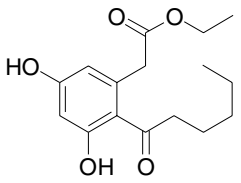

5.1

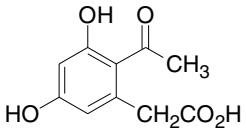

5.2

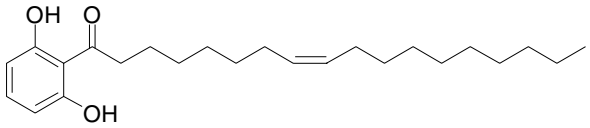

5.3

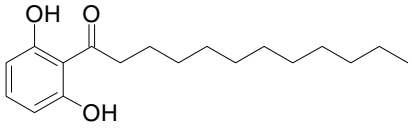

5.4

5.1.2 Monocyclic Acetogenins

In an interesting biosynthetic variation of the polyacetate pathway leading to the acylresorcinols, such as **5.2**, the introduction of an additional hydroxyl function, which is subsequently methylated, has given rise to a related group of monocyclic acetogenins. Curvulic acid (**5.5**) and curvin (**5.6**), also isolated from *Curvularia siddiqu*[116,117] and in the case of **5.5**, also from *Penicillium janthinellum*,[118] are just two examples of this type of compound. The basic skeleton of these compounds is derived from the head-tail condensation of one acetate, and four malonate units, whereas the source of the *O*-methyl is from the C-1 unit derived from formic acid or methionine.[119]

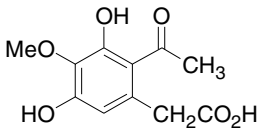

5.5

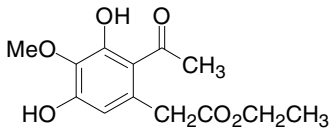

5.6

Curvulic acid (**5.5**) displayed antimicrobial activity against *Bacillus subtilis*, by the inhibition of cell wall synthesis.

5.2 Introduction

The non-sporolating endophytic fungus, E57, was isolated from the New Zealand native tree, *Coprosma* sp., located in a bush-pocket near Gebbies Pass on the Port Hills, Christchurch, New Zealand. The purified fungal material was grown on an agar slope (10 mL MYE) for small-scale biological and chemical screening.

5.3 Preliminary Investigations

The initial small-scale agar slope culture of E57 was extracted with EtOAc, and concentrated to give 1.8 mg of crude extract. The quick screen P388 assay showed excellent activity for this extract (3.6% which equates to 96.4 % inhibition of cell growth). An aliquot of the extract was chromatographed on reverse phase C18 HPLC (Figure 5.1) using the standard elution gradient (Section 7.1.4).

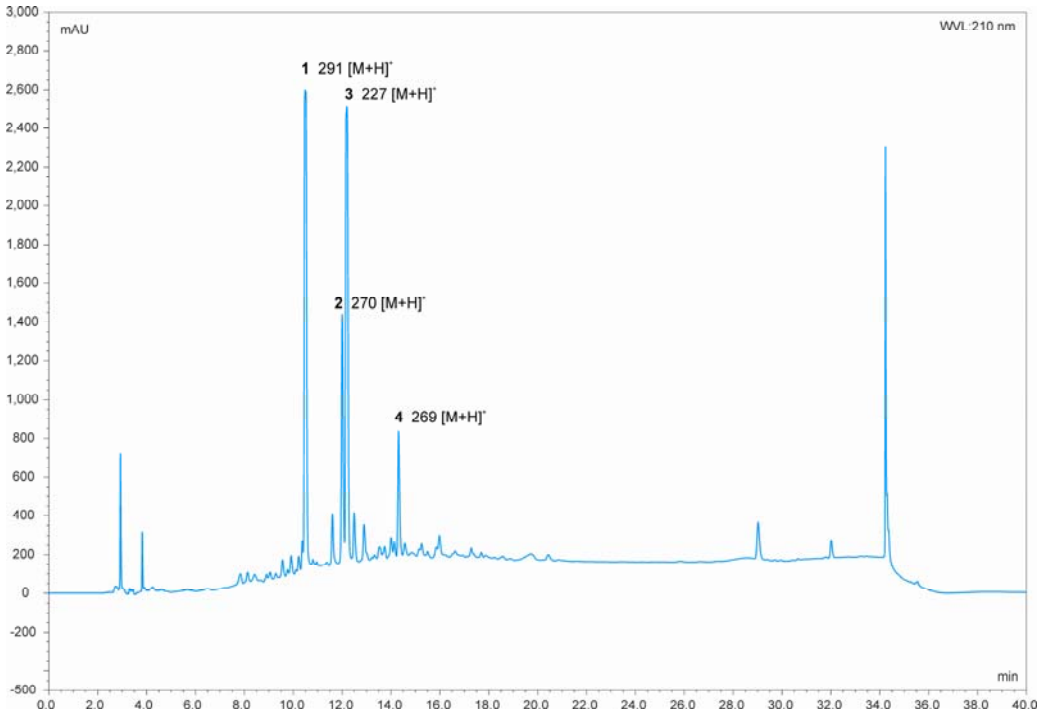

Figure 5.1: *HPLC chromatogram of the agar slope extract of E57. Numbered in bold are the four main metabolites and their molecular weights as determined by ESIMS.*

The UV profile of each peak (Figure 5.2) suggested that while peak 1 and 2 were similar to each other they were probably not related to peaks 3 and 4, which did have very similar profiles and thus were probably related compounds.

For the dereplication process, a 250 μg injection of the crude extract was made on to the analytical HPLC column. For each of the four peaks, the eluent was collected and submitted for ESIMS. This allowed a definitive mass profile to be obtained for each of the four major peaks (Figure 5.1). Although this information was useful, AntiMarin was unable to significantly narrow down the search field. It was clear at this stage that NMR spectra were required for identification of these compounds. Because there was very little of the initial extract left, a large-scale culture was grown.

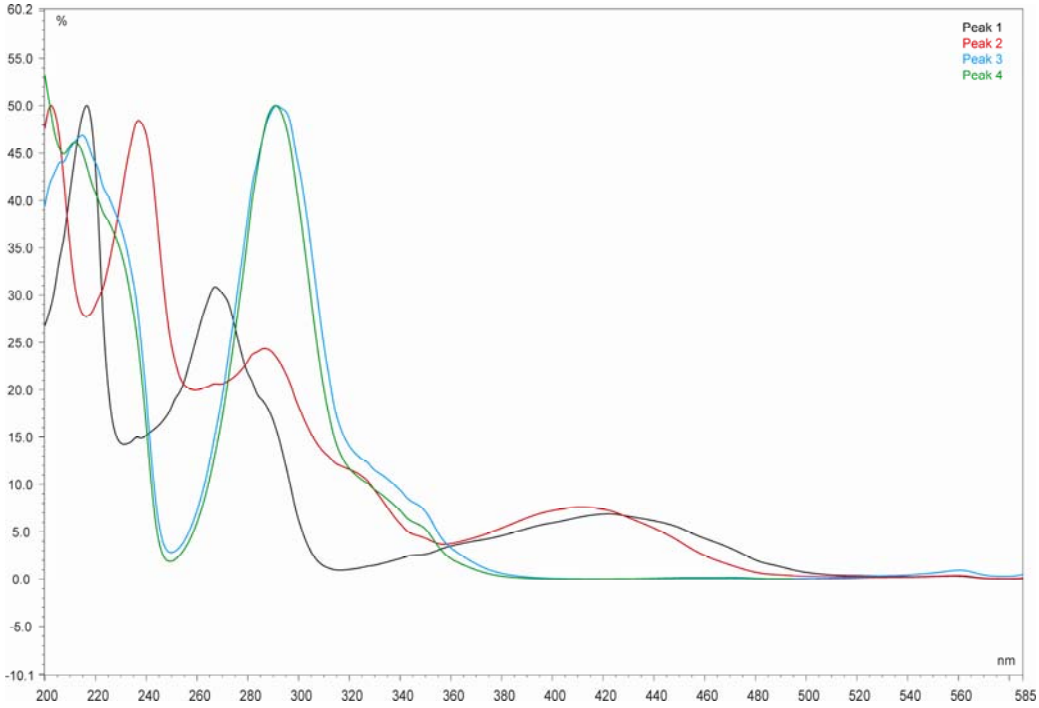

Figure 5.2: *Overlay of the UV chromophores of each of the four major peaks in the HPLC chromatogram shown in Figure 5.1.*

The 24 agar plates from the large-scale culture were extracted with EtOAc. Upon concentration, this fungus yielded just 23.5 mg. Although the fungus was cultured in an identical manner (see Experimental) to that of the small-scale culture, the metabolites produced in the large scale differed from those produced in the small-scale culture (See Figure 5.3). The large-scale extract showed one major peak, both in terms of PDA and ELSD detection. This was not one of the peaks seen previously from the agar slope extract, but it did show a UV chromophore which was almost identical to those of peaks 3 and 4 in the HPLC trace shown in Figure 5.1. To avoid wasting the extract it was decided to purify this major component. Although the minor compounds at 13.0, 14.0 and 14.5 minutes (see chromatogram 1 in Figure 5.3) showed identical UV chromophores to that of the main peak, 23 mg of a crude extract was proven too small an amount for isolation of the minor compounds.

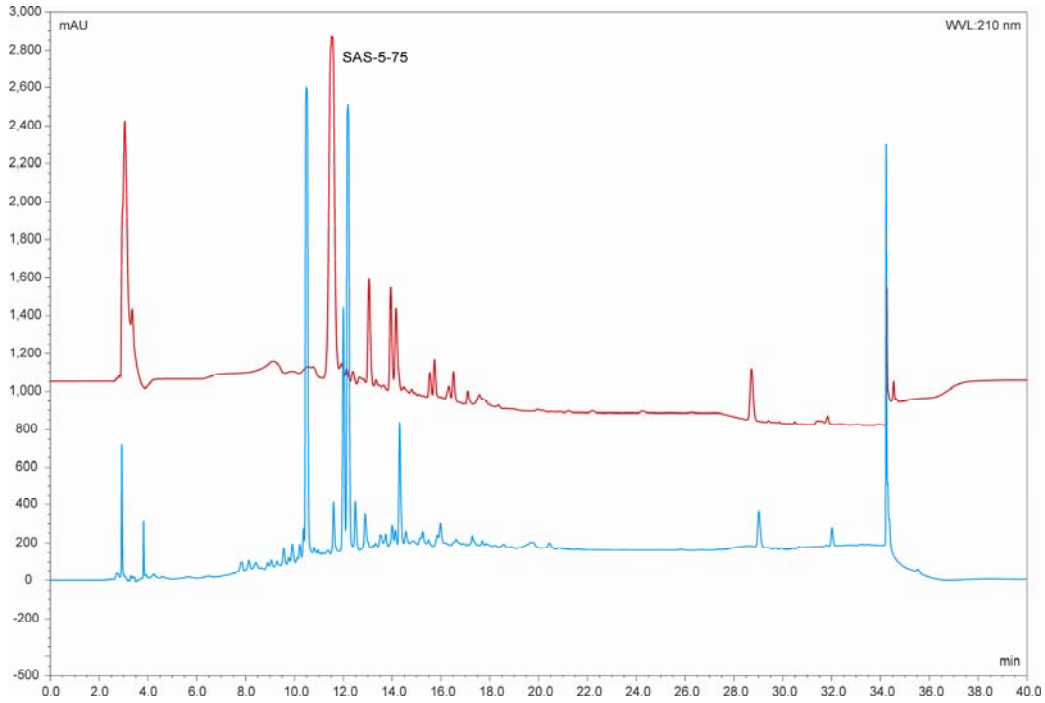

Figure 5.3: *HPLC chromatogram showing comparison of the small-scale agar slope extract (blue) with that of the large-scale extract (red).*

5.4 Chromatography of E57

As in the previous chapter, the simple nature of the crude extract allowed semi-preparative HPLC to be the only form of chromatography necessary to obtain the compound in a very pure form (Section 7.5.1, Experimental).

5.5 Structure Elucidation of SAS-5-75 (**5.7**)

SAS-5-75 (**5.7**) was isolated as a cream coloured powder. ESIMS determined the mass to be 227 ($[M+H]^+$). As well as the [M+H] ion peak, a peak at 209 ($[M-H_2O]^+$) was also seen. This is indicative of the presence of a hydroxyl functionality in the molecule. EIMS gave a molecular formula of $C_{11}H_{14}O_5$.

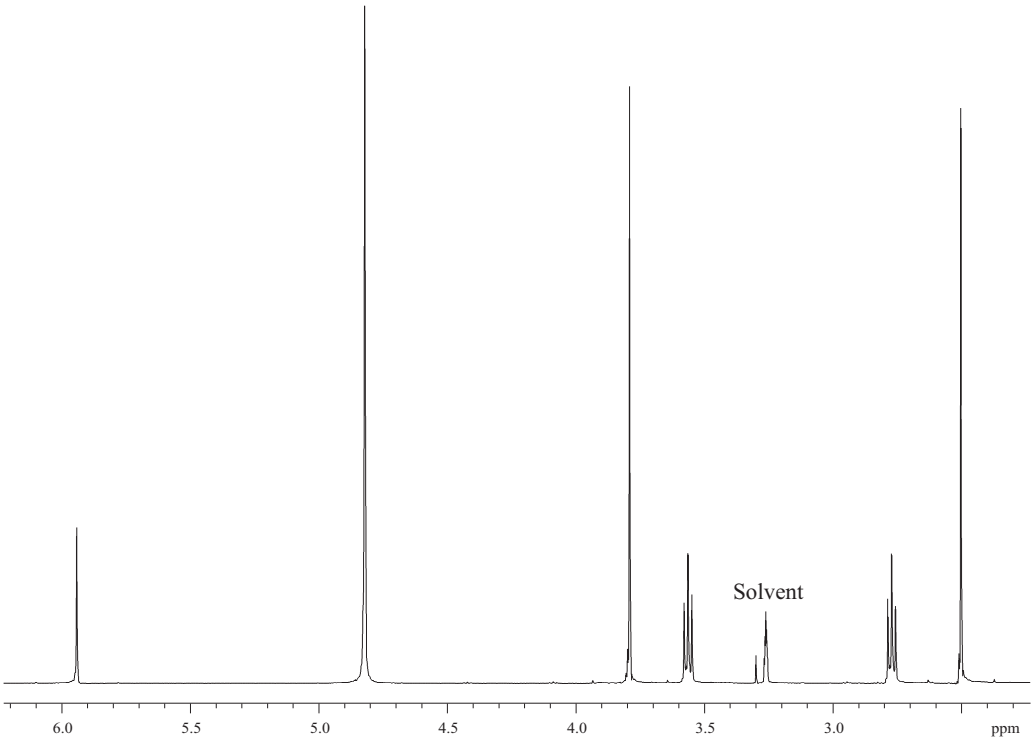

Figure 5.4: *^{1}H NMR spectrum of* ***5.7*** *in CD_3OD.*

The ^{1}H NMR (Figure 5.4) and COSY spectra indicated a pair of triplet methylenes at δ_H 2.77 (H-7) and δ_H 3.57 (H-8) coupled to each other, with the downfield nature of the protons at H-8 suggesting its close proximity to oxygen. This is partially confirmed at least by the multiplicity, a triplet, indicating only the one set of protons at H-7 were adjacent to this centre. The triplet nature of the methylene signal at H-7 when considered with a chemical shift of 2.77 ppm suggested that the other adjacent centre was most likely a quaternary carbon. Also from the ^{1}H NMR it was clear that the molecule contained one singlet methoxyl at δ_H 3.78 (H-11) and probably an acetyl, which is seen as a singlet at δ_H 2.50 (H-10). In addition, the ^{13}C NMR spectrum (Figure 5.5) showed one carbonyl at δ_C 205.4 (C-9), a $^{2}J_{CH}$ CIGAR correlation from H-10 to C-9 confirmed the acetyl nature of this carbon. Also clearly visible in the ^{13}C spectrum were three quaternary carbons at δ_C 167.3 (C-1), 165.8 (C-5), and 164.5 (C-3). In consideration of the molecular formula these carbons were proposed to be somewhat deshielded aromatic carbons rather than ester or acid carbonyl carbons.

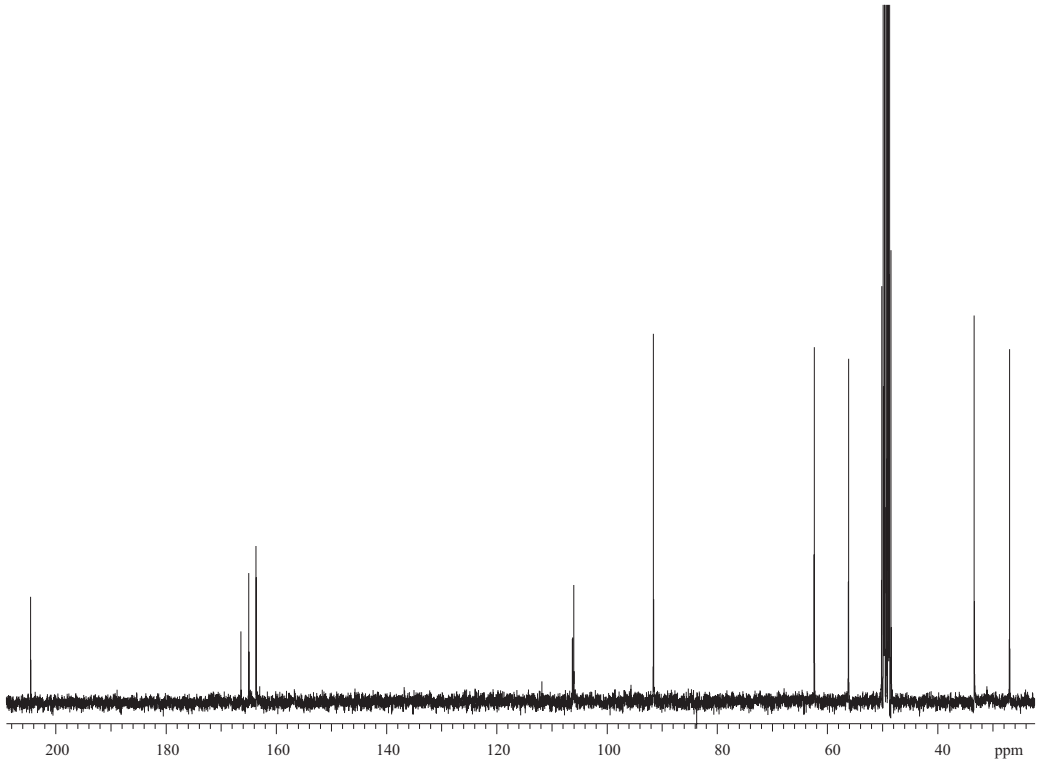

Figure 5.5: *^{13}C NMR spectrum of* ***5.7*** *in CD_3OD.*

HSQC and CIGAR NMR spectra confirmed the presence of a 2-hydroxyethyl group. This was seen by $^{1}J_{CH}$ correlation from the proton at H-8 to a carbon at δ_C 63.2 (C-8) confirming the hydroxyl substitution. It was postulated that the 2-hydroxyethyl moiety was directly attached to an aromatic ring (Figure 5.6). This was confirmed by CIGAR correlations from the H-7 protons to the quaternary carbons at δ_C 167.3, 165.8 and 106.9 (C-6).

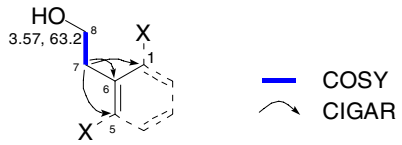

Figure 5.6: *Partial structure of* ***5.7*** *assumed from COSY and CIGAR correlations.*

At this point a search of the AntiMarin database was carried out using mass and the ^{1}H NMR data. A match was found with 2,4-dihydroxy-6-(2-hydroxyethyl)-3-

methoxyacetophenone (**5.8**), an acetogenin previously isolated from *Ophiosphaerella herpotricha*, a cause of spring dead spot (SDS) of bermudagrass.[120]

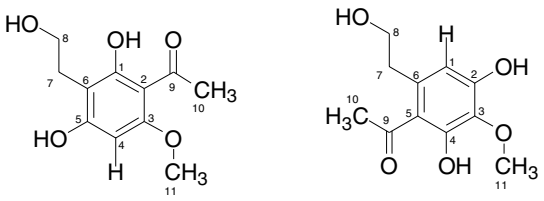

5.7 **5.8**

Although **5.8** had exactly the same molecular formula and seemed to contain all the necessary substituents, the pattern of the substitution on the aromatic ring did not fit the NMR data for the isolated compound. The prime reason was the lack of observable CIGAR correlations from the singlet proton at δ_H 5.94 (H-4) to C-7 or in the reverse direction. Nor were correlations observed to C-6 from H-4. Further evidence for an alternative substitution pattern was the upfield nature of the quaternary carbon at C-6. This suggested the carbon was shielded by the substituent effects of *ortho* or *para* oxygens. For this reason the two hydroxyl substituents were allocated to either side of the 2-hydroxyethyl group. This was a preferred arrangement over the methoxyl substituent being in one of these flanking positions. The shielded nature of the carbon at δ_C 92.4 (C-4) as well as that of the quaternary carbon at δ_C 107.1 (C-2) meant that these two carbons were also flanked on both sides by oxygen bearing carbons. A number of alternative structures fit this pattern, however only the structure shown in Figure **5.7**, fits all the CIGAR NMR correlations.

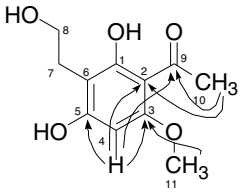

Figure 5.7: *Important CIGAR correlations for* ***5.7****.*

In order to confirm the pattern of substitution around the aromatic ring a 1D NOE experiment was carried out. In this experiment the methoxyl protons at δ_H 3.78 (H-11) were irradiated. If the substitution pattern is as in **5.7** not **5.8**, then NOE correlations should clearly be seen from the methoxyl protons to both the aromatic proton and the acetyl protons. If the arrangement of the substituents on the ring were the same as for **5.8**, NOE enhancements would be expected for at least the H-7 protons when the methoxyl protons were irradiated. The NOE spectrum (Figure 5.8) confirms the structure as **5.7**, as upon irradiation, both the acetyl and aromatic protons, but not the H-7 protons were enhanced.

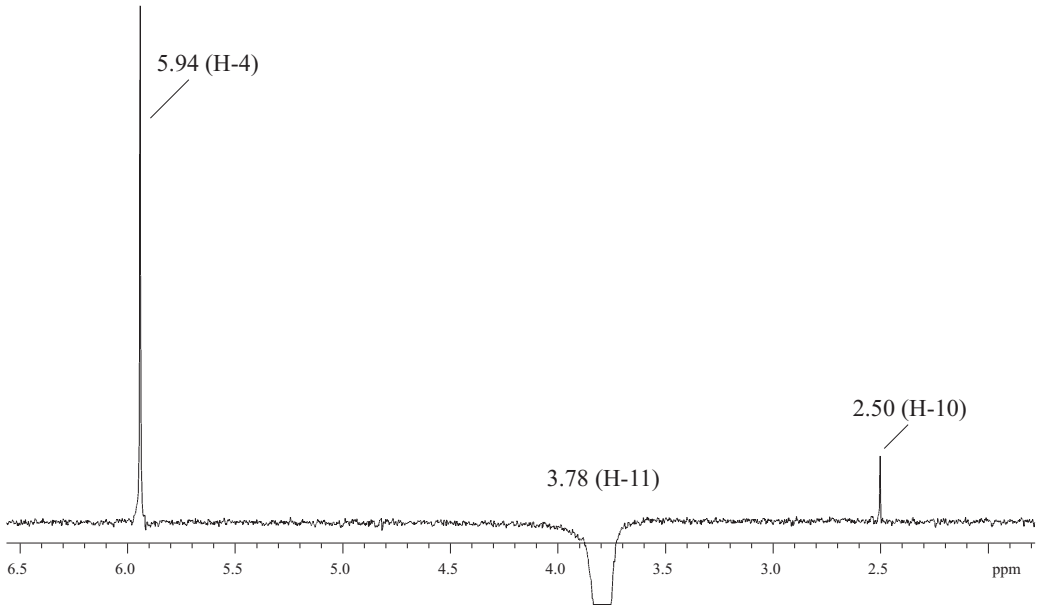

Figure 5.8: *1D NOE spectrum of* ***5.7*** *in CD_3OD, run with a mixing time of 0.5 s. Irradiation at H-11 shows enhancement of H-10 and H-4 resonances.*

Extensive literature searches showed no matches, hence this compound was a new structural isomer of the known compound, 2,4-dihydroxy-6-(2-hydroxyethyl)-3-methoxyacetophenone (**5.8**). This was subsequently confirmed by X-ray crystallographic analysis (X-ray data tables can be found in Appendix 1) of a small crystal (Figure 5.9). Although the numbering of the known compound was unusual, to avoid confusion, the same numbering system was used for the new isomer. The new compound was named

1,5-Dihydroxy-6-(2-hydroxyethyl)-3-methoxyacetophenone (**5.7**). The complete set of NMR data is presented in Table 5.1.

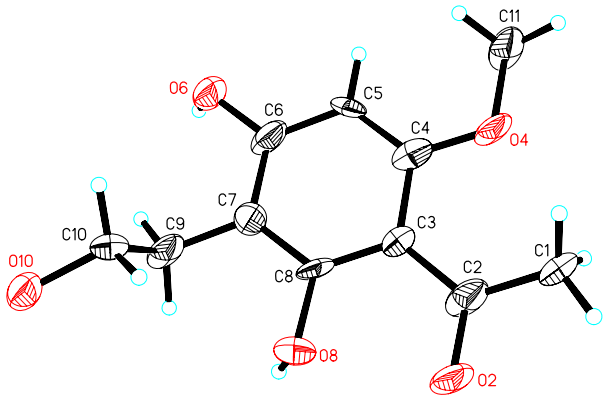

Figure 5.9: *Crystal structure drawing of* ***5.7****.*

Table 5.1: *Experimental NMR data for* ***5.7***

Position	δ^{13}C ppm	δ^{1}H ppm, multiplicity, (J_{HH} Hz)	NOE	COSY	CIGAR
1	167.3 (C)				
2	107.1 (C)				
3	164.5 (C)				
4	92.4 (CH)	5.94 s			C-9, C-5, C-3, C-2
5	165.8 (C)				
6	106.9 (C)				
7	27.8 (CH_2)	2.77 t (7.6, 7.6)		H-8	C-1, C-5, C-6, C-8
8	63.2 (CH_2)	3.57 t (7.6, 7.6)		H-7	C-6, C-7
9	205.4 (C)				
10	34.3 (CH_3)	2.50 s			C-9, C-2
11	57.0 (CH_3)	3.78 s	H-4, H-10		C-3, C-4

^{1}H and 2D experiments carried out at 500 Mhz in CD_3OD. ^{13}C carried out at 75 Mhz in CD_3OD.

1,5-dihydroxy-6-(2-hydroxyethyl)-3-methoxyacetophenone (**5.7**) was found to show only weak antimicrobial activity against *Bacillus subtilis* (2 mm zone of inhibition). It was noted earlier (Section 6.1.2) that the related compound, **5.5**, showed antimicrobial activity against *B. subtilis*. Structural studies showed that the methoxyl substituent played an important role in this antimicrobial activity.[118] It stands to reason therefore, that the

methoxyl group in **5.7** is perhaps the reason for the observed antimicrobial activity. Despite the initial small-scale culture showing very good activity in the P388 quick screen assay, no P388 activity was detected from the purified compound. This is not at all surprising given the change in composition of the extract following the scale-up (Section 5.3).

5.6 Discussion

The purification of an extract from a New Zealand endophytic fungus has resulted in the isolation of a new monocyclic acetogenin. This new compound, 1,5-dihydroxy-6-(2-hydroxyethyl)-3-methoxyacetophenone (**5.7**), closely resembles the known compound, 2,4-dihydroxy-6-(2-hydroxyethyl)-3-methoxyacetophenone (**5.8**). The substituents on the aromatic ring are identical, but the substitution pattern differs between the two compounds.

Due to the similarity of the new acetogenin, **5.7** to that of the known compound curvulic acid (**5.5**), the structure activity data for **5.5** was applied to that of **5.7**. Therefore it was proposed that the activity that **5.7** displayed against *B. subtilis* is possibly a consequence of disruption of cell membrane synthesis in the bacterium, suggesting that the methoxy group plays an important part in this inhibition.

Chapter 6

Dereplication Methods

6.1 General Introduction

The rapid identification of already known natural products, a process known as dereplication, is strategically important for scientists involved in screening crude extracts for novel bioactive compounds from natural sources.[121] The continued demand to get new drugs to the market more quickly and more cheaply, requires that the analytical technologies that support this work keep pace with, for example, the rate at which new chemical entities (NCEs) are synthesised for high-throughput screening programmes.[122] Relatively new techniques such as hyphenated LC systems and NMR cryoprobes are now used routinely by many operating high-throughput screening programmes.

The most common hyphenated techniques are those of LC-MS, LC-MS-MS and LC-NMR. These techniques all suffer, one way or another, from problems. For example any technique involving mass spectrometry will always potentially suffer from problems associated with ionisation (or lack thereof), of the compounds being studied. Adducts in

ESIMS can be an especially big problem, e.g $[M+NH_3]^+$, $[M+CH_3CN]^+$ appear rather than the usual $[M+H]^+$ and $[M+Na]^+$. Despite this, in the pharmaceutical industry these are very powerful techniques for the monitoring, characterisation and identification of impurities.[123] In the case of LC-NMR, there are three main coupling technologies, onflow, stopped flow and loop-storage, all of which have their disadvantages. Onflow results in poor S/N ratio for the NMR spectra unless a reduced flow rate is used, however reduced flow can then reduce the chromatographic separation. This method is really only suitable for the more intense signals of the major constituents. Stopped flow has the advantage that a number of chromatographic peaks can be studied, but the frequent stops then necessary for data acqusition can disturb the quality of separation, and concentrated compounds can contaminate the NMR detection cell. As a consequence this approach is most suitable for mixtures having only a small number of constituents. In the loop storage mode, the chromatographic run is not interrupted, instead each analyte is stored in a separate capillary loop in order for NMR acquisition to be carried out at a later stage. A prerequisite for this technique however, is that analyte must be stable during the long NMR analysis time.[124]

Another recent advancement in LC-NMR is the use of a cryoprobe. In NMR cryoprobes, the electronic components are cryogenically cooled to ~20 K while the sample remains at ambient temperature.[125] This has the effect of reducing the electronic noise.[125] Cryoprobes have been found to provide quite significant sensitivity gains, however there is sensitivity loss for experiments such as HMBC that contain a long delay as part of their pulse sequences.[126]

6.2 *Introduction*

The natural products chemistry group at the University of Canterbury is focussed on natural products of fungal origin. In working with fungal natural products one has to cope with the large number of already known metabolites from this source. Thus, effective dereplication techniques are essential. During the course of my PhD studies I have been involved in assisting with the development of the groups strategies towards

dereplication. Throughout it has been an integral, but not a focussed part of my research effort. This chapter represents an overview of dereplication undertaken within the group as well as contributions that I have made to the overall effort.

The group's approach to dereplication utilises a combination of HPLC-UV and the establishment of UV libraries using HPLC software, MS analysis, screening for bioactivity using the in-house assay system and capillary probe NMR. This is all used in conjunction with the combined MarinLit/Antibase database known as AntiMarin.[77]

During the first few months of my own research, the combination of AntiMarin, HPLC-UV and MS analysis was the standard dereplication protocol. This method worked but in order for it to be efficient, there was a heavy reliance on having a good memory for UV profiles, when the same compound was seen again in another extract. Of course sharing the knowledge of UV profiles with other group members was next to impossible.

The purchase of the Dionex HPLC system gave the group the opportunity to construct a UV library where anyone could get access to stored UV data for comparison with those present in other extracts. Involvement in this project was a joint one with Dr. Gerhard Lang and Dr. Maya Mitova. This involved setting up the different libraries and running standards and other compounds previously identified, through the HPLC in order to store the UV data.

Prior to purchase of a capNMR probe, it was necessary for this method to be assessed in terms of its usefulness to the work carried out in our research group. The crude extracts obtained from the *Scleroderma* sp. of fungus and the New Zealand endophyte, F5584, were very useful for this work. As the crude extract had a simple profile with well defined and separated peaks on the HPLC. F5584 was useful for the oppposite reason; it contained many compounds, most of which eluted very close to one another. This extract would test the capabilites of the fraction collector to separate these compounds while still retaining reasonable purity so that identification of the compounds through capNMR was feasible.

6.3 Dereplication Using an HPLC-UV Library Database

Normally, UV-libraries are generated from known compounds,[127] our approach however, has been to generate libraries of both known and unknown compounds. Using the Chromeleon software on the Dionex analytical HPLC system, this has enabled us, in conjunction with independently collected bioactivity data, to answer three key questions about every significant peak in the crude extract from a fungus or fungal culture.

1. Is the bioactive peak a new compound
2. Has the bioactive peak been observed in an extract previously
3. If it has been observed before, is it a known compound

The process begins with extracts that have already successfully passed the in-house requirements for bioactivity; that is, the extract must have an IC_{50} value <10,000 ng/mL for it to be considered bioactive enough for further work.

In the creation of the UV library, each crude extract was analysed by HPLC on a Phenomenex RP C18 column using a standard gradient, with simultaneous collection of fractions into a microtitre plate (see Experimental, Section 7.1.4). All significant peaks in the chromatogram (> 10% of the base UV peak) were entered into the UV library, logging both the retention times and UV spectra (Figure 6.1).

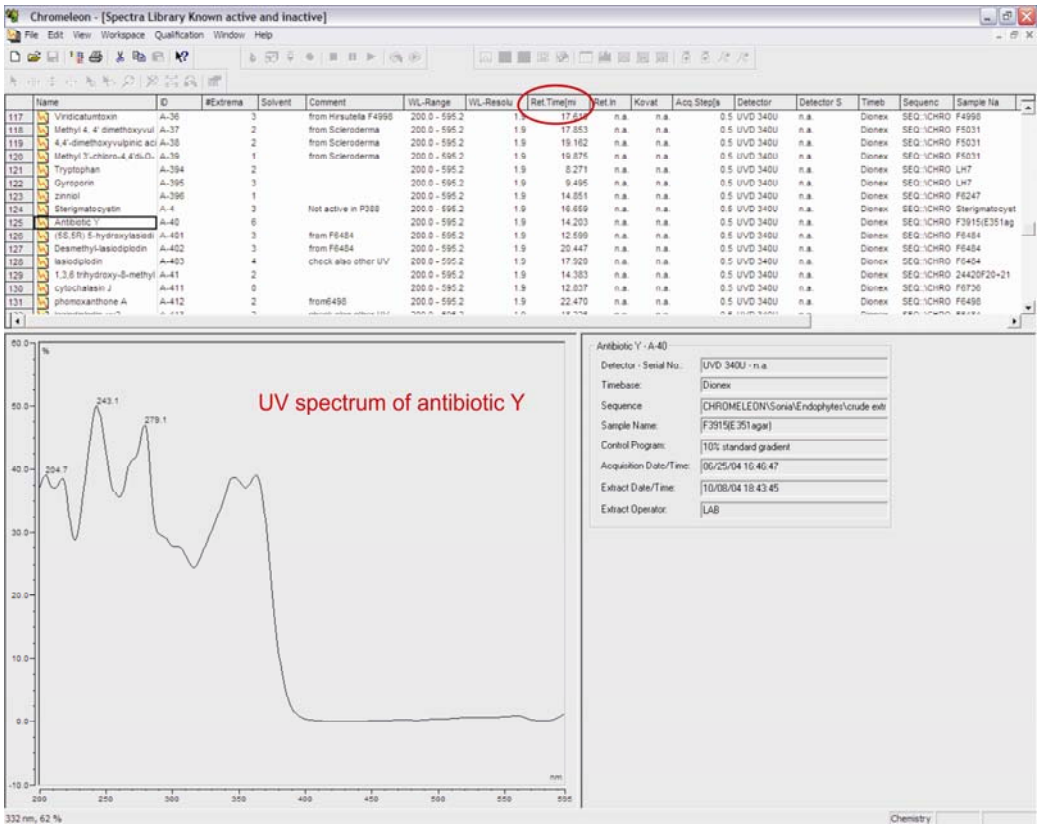

Figure 6.1: *Screenshot of UV library contained within the Dionex analytical HPLC system. Highlighted in red are the two key descriptors that are logged into the UV library*

Two libraries were constructed; "*all compounds, unknown and known*"; and "*known compounds*". Naturally, at first, all peaks were entered into the former. As standards were obtained and compounds identified, these spectra were copied over to the "*known compounds*" library.

When the numbers in the libraries started to reach significant proportions (>20), the microtitre step in the process was delayed until the extract had first been chromatographed. This meant that an extract was first checked to establish if any of the significant peaks were a match with any known compounds already contained within the database. If all such peaks resulted in "known hits" in the library further work on that extract was discontinued, bypassing the need for the P388 microtitre analysis thus saving time and money. Of course, if a significant peak in an extract was not matched in the database, then further dereplicative steps are carried out.

Even if a match to a known compound were found in the in-house UV library, MS analysis was usually carried out as confirmation. There are two ways that this can be carried out. The wells of the "master" microtitre plate that correspond to the peak(s) of interest are analysed directly by ESIMS. This creates an effective 3-D profile of mass versus well. Alternatively a small amount of the crude extract is submitted for LCMS. The problem with this approach is correlating the total-ion current (TIC) trace with the ELSD or UV profile of the HPLC trace as the LCMS is carried out on a different HPLC column.

An example of the dereplication process is presented below using the crude extract from the fungus *Tricoderma harzianum* as an example (Figure 6.2).

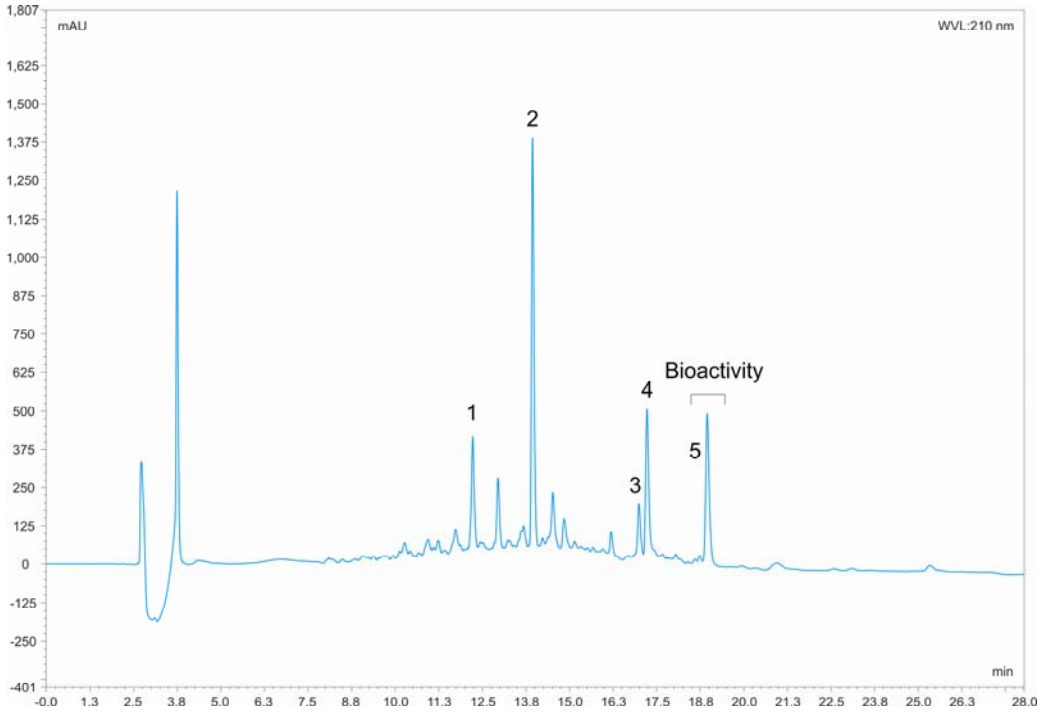

Figure 6.2: *HPLC chromatogram of the crude extract from the fungus Tricoderma harzianum.*

A search of the UV database on peaks 3 and 5 (Figure 6.2) showed matches in both UV chromophore and retention time to compounds already present in the database. Peaks 3 and 5 were thus identified has demethylharzianic acid (Figure 6.3)[128] and harzianic acid (Figure 6.4, bottom)[129] respectively.

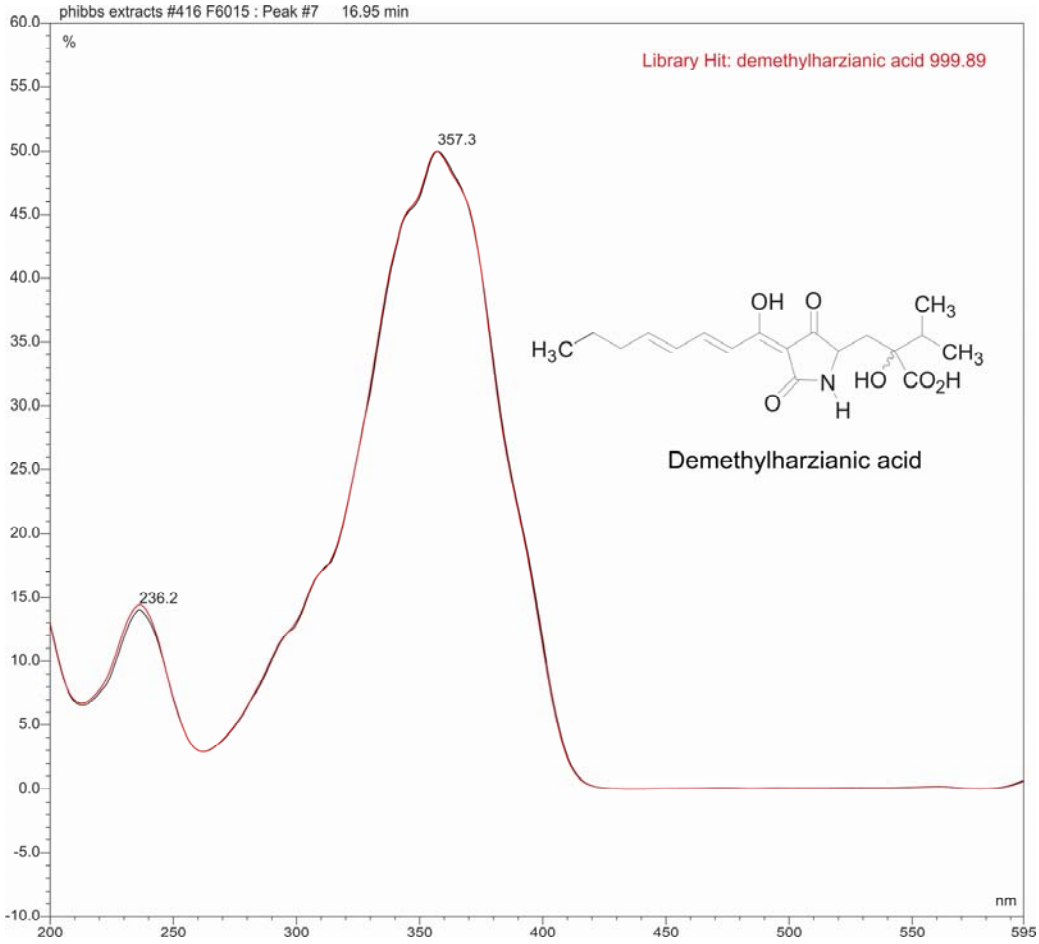

Figure 6.3: *UV library hit (red) of peak 3(black) with that of the known compound demethylharzianic acid already present in the database.*

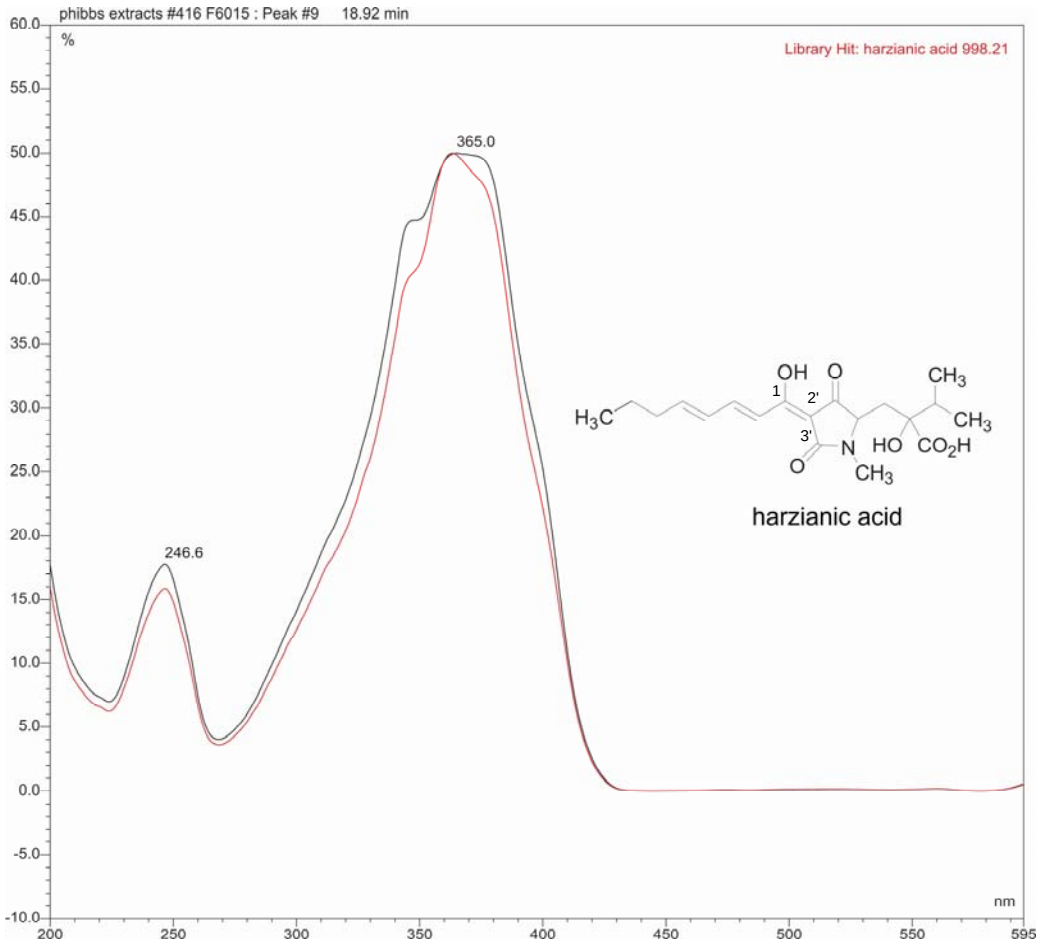

Figure 6.4: *Library hit of peak 5 with that of the known compound harzianic acid already present in the database.*

The input of UV data and retention time of peaks 1 and 2 displayed no hits to any compounds contained within the database. Although peak 4 also dispalyed a UV match with the known compound harzianic acid, the retention time differed significantly. For this reason it was considered to be most likely an isomer of harzianic acid. In light of this, peaks 1, 2 and 4 were purified using semi-preparative HPLC (Experimental, Section 6.7.1). Following purification, peak 2 was found to be the known compound, harzianolide A (**6.1**).[130,131] The NMR and mass data for peak 4 were found to be in agreement with this compound being an isomer of harzianic acid. For this reason it was given the name isoharzianic acid (see Figure 6.4 for structure). The stereochemistry of isoharzianic acid was not determined. This was primarily because of the unsuitability of

the molecule for Mosher's esterfication and the complication of keto-enol tautomerism between C-1 and C-2'/C-3'.

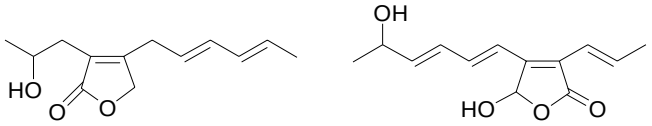

6.1 **6.2**

Peak 1, was found to be a new compound and was given the name, trichobutenolide (**6.2**).[132]

This approach to dereplication is simple and intuitive. An advantage of this system is that no file transfers are needed and large libraries can be constructed as the overhead is very low.

6.4 Dereplication from an Impure Fungal Extract

Without having to put effort in to the total purification of an extract, partially purified extracts can be effectively dereplicated using the power of the AntiMarin database. LCMS and a ^{1}H NMR spectrum of the impure compound is often all that is necessary in order to work with the database.

AntiMarin includes NMR-based functional group recognition. Many types of functional groups present in a molecule, such as the various types of methyl groups, olefin and aromatic spin systems can usually be recognised in the ^{1}H NMR of partially purified compounds. By entering recognised functionalites in the search profile, the number of candidate structures to be considered can be rapidly reduced. Furthermore, by including other descriptors, such as UV maxima or MS data, the search profile can be made even more discriminating.

The power of this database to rapidly dereplicate a compound from an impure terrestrial extract is demonstrated using the example of massarinolin C. This work was carried out by a visiting student from the University of Hanover, Mr. Stephan Busche.

From the ^{1}H NMR spectrum (Figure 6.5) of a partially purified sample a singlet methyl was identified as most likely belonging to the major compound. By searching AntiMarin on one singlet methyl, the number of possible compounds was reduced from a total of 44,000 to just 1245.

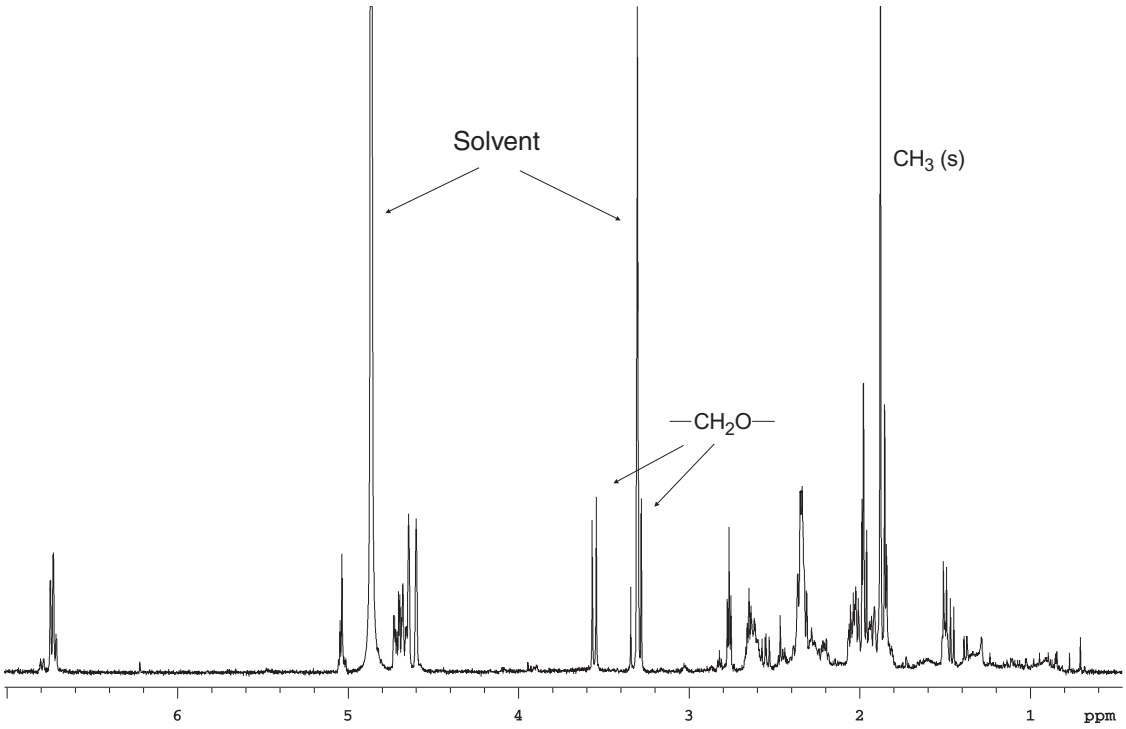

Figure 6.5: *The ^{1}H NMR spectrum of a partially purified extract from a terrestrial fungus.*

By use of both ^{1}H NMR and COSY spectra, a -CH_2O- was identified as being present in the major compound. By searching on both these structural features, the field was narrowed even further, so that the total number of possible structures was reduced to 270. LCMS on the impure extract resulted in a TIC trace showing that the major component had a retention time of 12.43 minutes, and a molecular formula of 266 Da (Figure 6.6). Addition of the mass data to the AntiMarin search reduced the number of possibilities from 270 to 3.

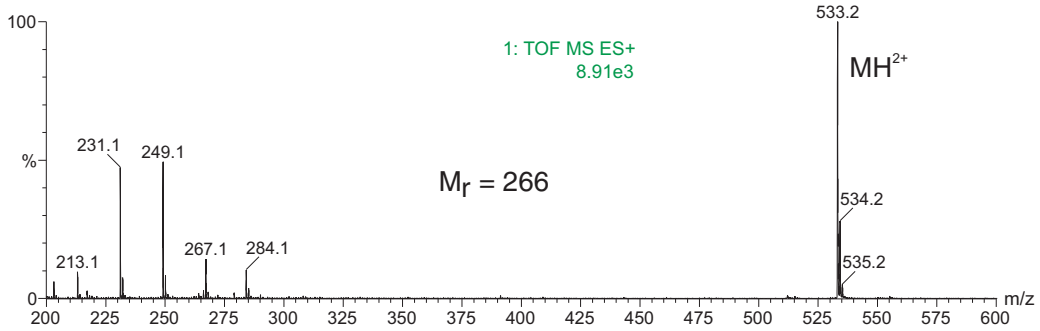

Figure 6.6: *TIC trace from LCMS showing $[M+H]^{2+}$ ion of the compound at 12.43 minutes.*

The original NMR data was then compared to the three different structures found in AntiMarin (Figure 6.7) as well as the calculated ^{1}H NMR spectra (using ACD software). From this data it was concluded that the extract contained the compound massarinolin C (**6.3**), that was originally isolated from the aquatic fungus, *Massarina tunicata*.[133]

Luisol B (**6.4**)[134] was excluded due to the presence of three aromatic protons, none of which were evident in the ^{1}H NMR spectrum presented in Figure 6.5. The nucleoside, 6-methyl-9-β-D-ribofuranosylpurine (**6.5**)[135] was also easily excluded due to the absence of any heteroaromatic protons. These would usually be present in the chemical shift range of 8-9 ppm.

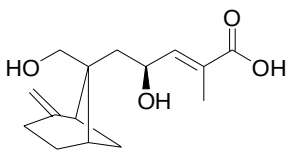

6.3

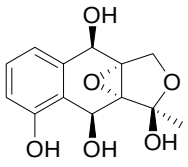

6.4

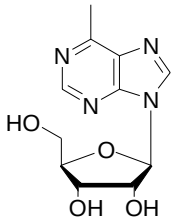

6.5

This is an extremely simple, yet effective method for the rapid dereplication of known compounds from impure extracts. The important thing to note with this method is that there had been absolutely no attempt to solve the structure of massarinolin C.

The efficiency of these dereplication methods at the University of Canterbury has recently been taken a step further by the acquisition of a capillary probe for the existing 500 MHz NMR.

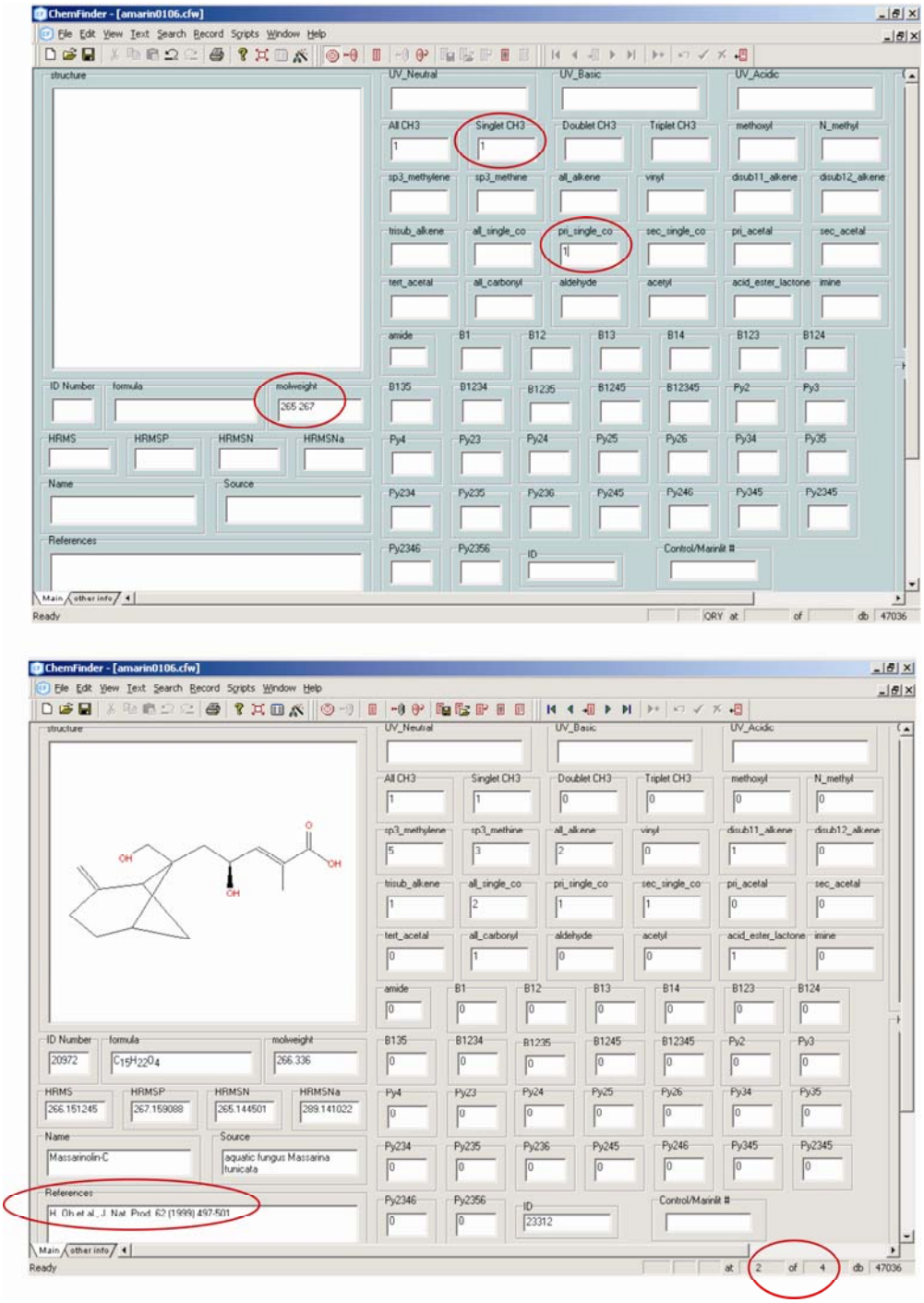

Figure 6.7: *Screenshots of the AntiMarin database showing the entry of functional groups and molecular weight range (top) and the results of this data input (bottom).*

6.5 Enhanced Dereplication Utilising a capNMR Probe

Many of the natural products with intense biological activity are only produced in extremely small quantities; a reflection of perhaps their natural potency.[126] The amounts able to be isolated of such compounds inevitably falls well below that needed to carry out complete structural elucidation using an inverse-detection probe and low-volume tubes (shigemi). This has led the Marine Chemistry group at the University of Canterbury, and others around the world[126] to investigate capNMR, not only as a method for obtaining data on the new, highly potent compounds, but also as a tool for the dereplication of natural product extracts.

6.5.1 An Introduction to Capillary Probe NMR (capNMR)

A capillary probe uses a flow cell that typically has a flow rate through the NMR probe of 1-50 μL/min and a sample volume in the range of 1-10 μL.[136] This is the reason why the capillary probe is sometimes known as a capillary microflow probe, although a capillary probe can also have a much larger volume capacity.

Capillary NMR probes were designed to acquire NMR spectra on mass-limited samples. It makes it possible to obtain high quality spectra from sample amounts that previously wouldn't have allowed such data acquisition. Alternatively, a larger amount of material can be used to get the same signal-to-noise (S/N) ratio in a shorter period of time.[122] Normal data acquisition typically requires at least 0.5 mg of material, give-or-take, depending on the molecular weight of the compound for an adequate S/N ratio to be achieved. Small volume NMR flow probes were first constructed in the laboratories of Sweedler and Albert in the 1990s.[137-139] These were developed especially for coupling to capillary electrophoresis (CE) and capillary HPLC (CapLC) for the detection of the small volumes associated with these techniques.

A diagrammatic view and photo of the Protasis capillary probe NMR system purchased by the Department of Chemistry is presented in Figure 6.8.

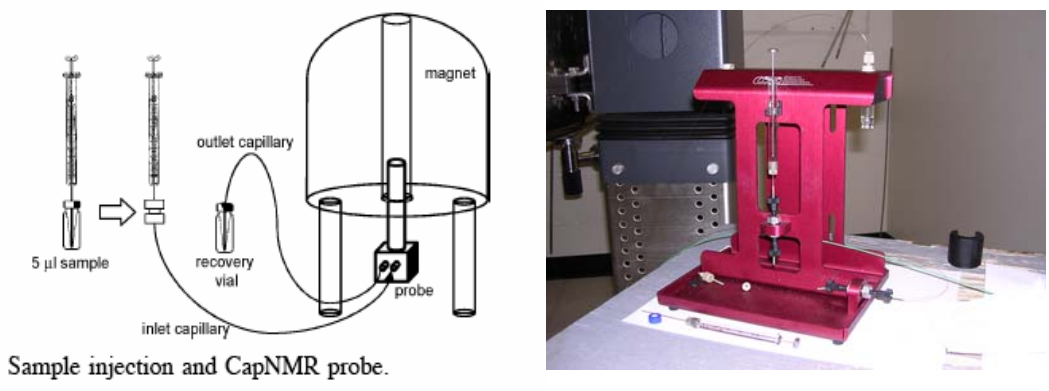

Figure 6.8: *Diagram showing the capillary probe set-up*[126] *and photo of the protasis capillary probe.*

The CapNMR probe has a small flow cell that is connected to two Teflon capillaries, called the inlet and outlet capillaries. For loading of the cell, the sample is dissolved in 6 μL of deuterated solvent and injected into the inlet capillary via a syringe. This is then followed by injection of 11 μL of deuterated "push" solvent to position the sample in the probe (see Figure 6.8). The sample for injection into the probe is sourced from individual or two combined wells from the microtitre plate collection of a crude extract, separated into 88 fractions by analytical HPLC.

6.5.2 Dereplication Utilising capNMR

Before the department obtained its own probe, work was conducted using the identical capillary probe installed at the Molecular Targets Development Program, NCI (National Cancer Institute), Frederick, USA. From this work, and work carried out since the department obtained its own capNMR, there are now many examples that demonstrate the power of this technique in the dereplication process. A selection of these are presented below.

6.5.2.1 A Malaysian Scleroderma *sp.*

Identification and dereplication of this extract was initially carried out using the conventional NMR system (this work is presented in Chapter 4). This extract however, was one of two that were used to establish the relative usefulness of the capNMR technique in the dereplication of fungal natural products. Figure 6.9, below shows three ^{1}H NMR spectra of the known compound, 4,4'-dimethoxyvulpinate (**4.13**), Figure 6.9 (top) shows the proton spectrum of **4.13** when carried out at 500 MHz on 1.2 mg of material in a shegemi tube using the standard inverse-detection probe. The ^{1}H NMR spectra represented in Figure 6.9 (centre and bottom) were obtained from individual wells of a microtitre plate following collection from the HPLC. Calculation of relative amount of material present (8.0 μg) was calculated based on published extinction coefficients (ε).[94] The power of this technique is clearly shown upon comparison of these two NMR spectra. In the centre, is the ^{1}H NMR spectrum of the material taken from a microtitre well and subsequently run at 500 MHz using the inverse probe with shigemi tube, and the bottom spectrum is the same material analysed with the capillary probe. The S/N ratio shows a marked increase so that the signals are clearly distinguishable, this is especially so, in the aromatic region.

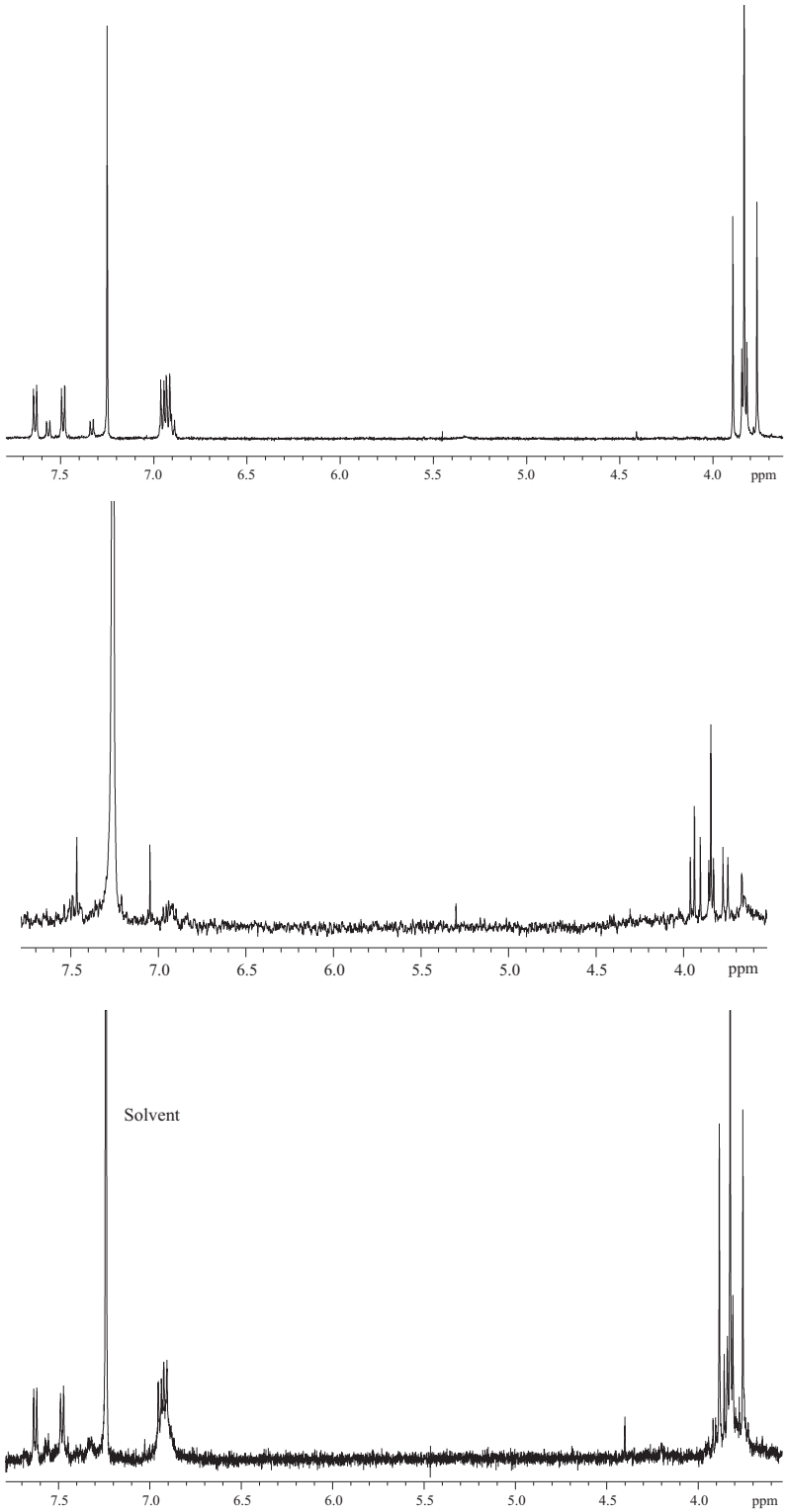

Figure 6.9: *^{1}H NMR spectra obtained in $CDCl_3$ at 500 MHz on 1.2 mg (top), 8.0 µg from a microtitre well (centre), and 8.0 µg using a capillary probe NMR (bottom).*

This work was carried out subsequent to the actual structure elucidation. Although the spectrum shows that the sample is slightly impure, the signals of the major compound are easily distinguished, so that a database search using the key NMR features (as described in Section 6.4) could have been carried out. This would have resulted in a positive identification.

6.5.2.2 Spirobisnaphthalenes from an Unidentified Endophytic Fungal Extract (F5584)

The fungal extract, F5584, was the other extract that was used for assessment of the capabilities of the capillary probe. This work was also carried out subsequent to structural elucidation of the active compounds (This work was originally presented in Chapter 3).

From the crude extract of F5584, the NMR spectra of spiro-mamakones A and C are presented below. The ability of the capillary probe to generate a full set of NMR spectra including ^{1}H, COSY, HSQC, and HMBC on just μg amounts of material is demonstrated very well with this extract.

Elution of the extract into a 96 well microtitre plate provided the way to generate pure compounds from the extract. These samples are then eminently suitable for NMR analysis without the requirement of further purification.

According to the ELSD trace (red) in Figure 6.10, the two main compounds present in the extract were spiro-mamakones A and C. Presented in Figures 6.11-14 are the ^{1}H and 2D NMR spectra for the combined wells E2-E3 which correspond to spiro-mamkone A. An estimation of the amount of material present in these combined wells was calculated based on the extinction coefficient of purified spiro-mamakone A. This revealed that these exceptionally good NMR spectra were obtained from just 20 μg of material. The HMBC spectrum was obtained via routine overnight experiments, the same as that for the regular inverse probe utilising shigemi tubes. COSY and HSQC-DEPT were also obtained in the same time frame of a sample containing mg of material utilising the regular inverse probe (30 minutes and 2 hours respectively).

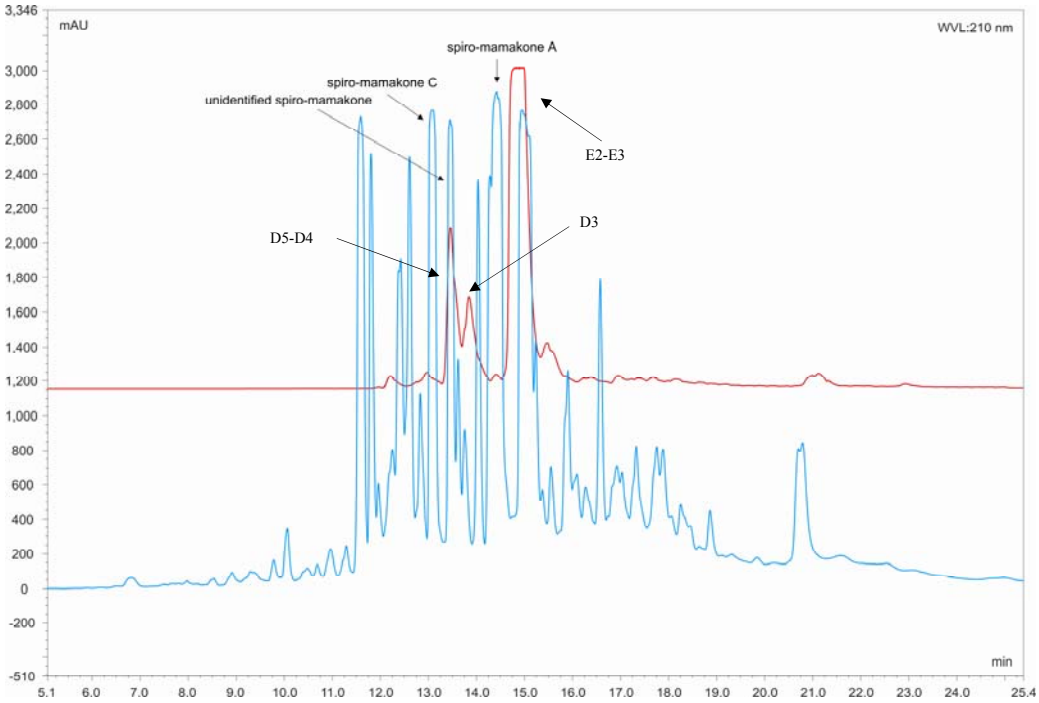

Figure 6.10: *HPLC chromatogram of the F5584 extract used to generate the microtitre plate for capNMR analysis. The ELSD trace is shown in red.*

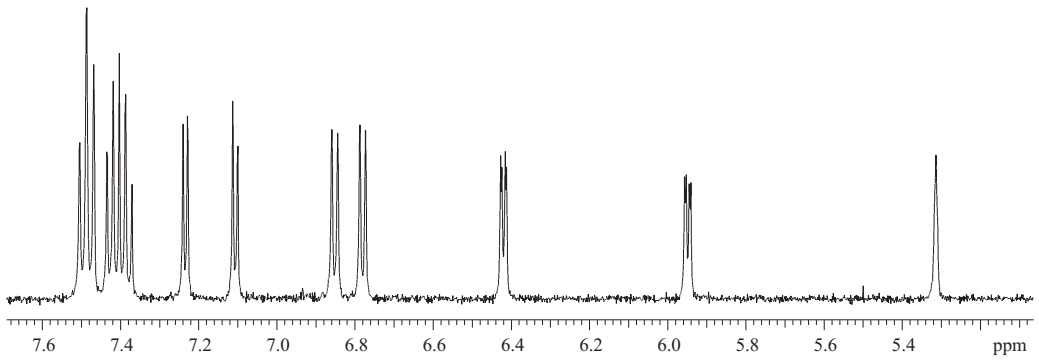

Figure 6.11*: ^{1}H NMR spectrum of spiro-mamakone A obtained in CD_3OD using the capNMR probe.*

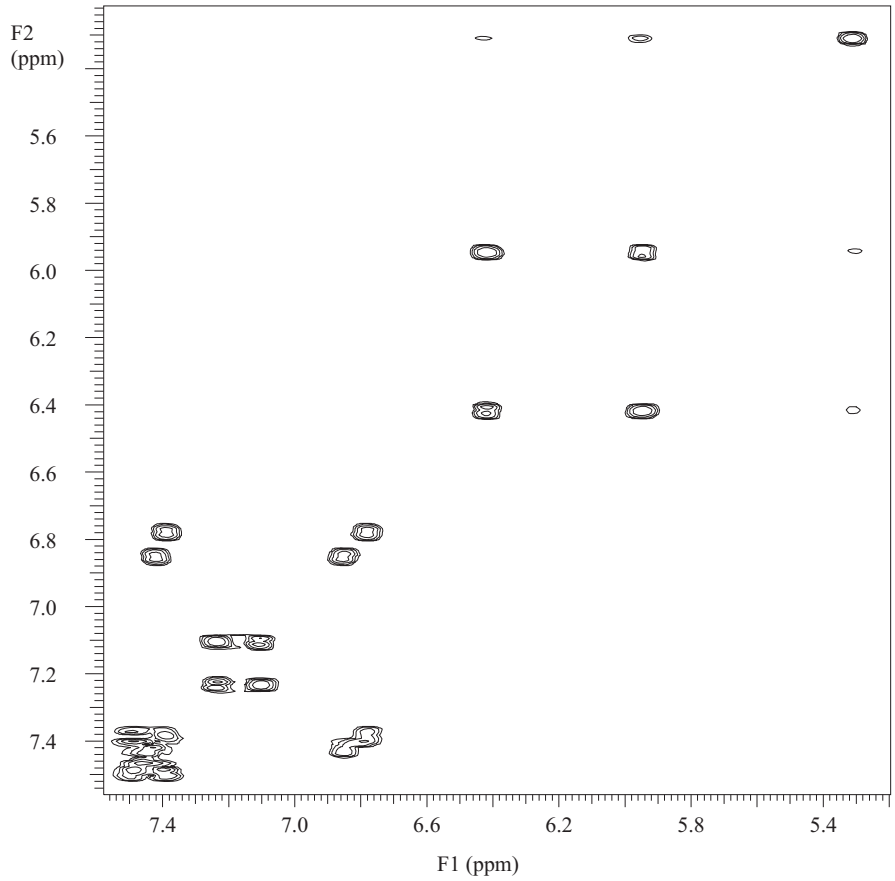

Figure 6.12: *COSY NMR spectrum of spiro-mamakone A obtained in CD_3OD using the capNMR probe.*

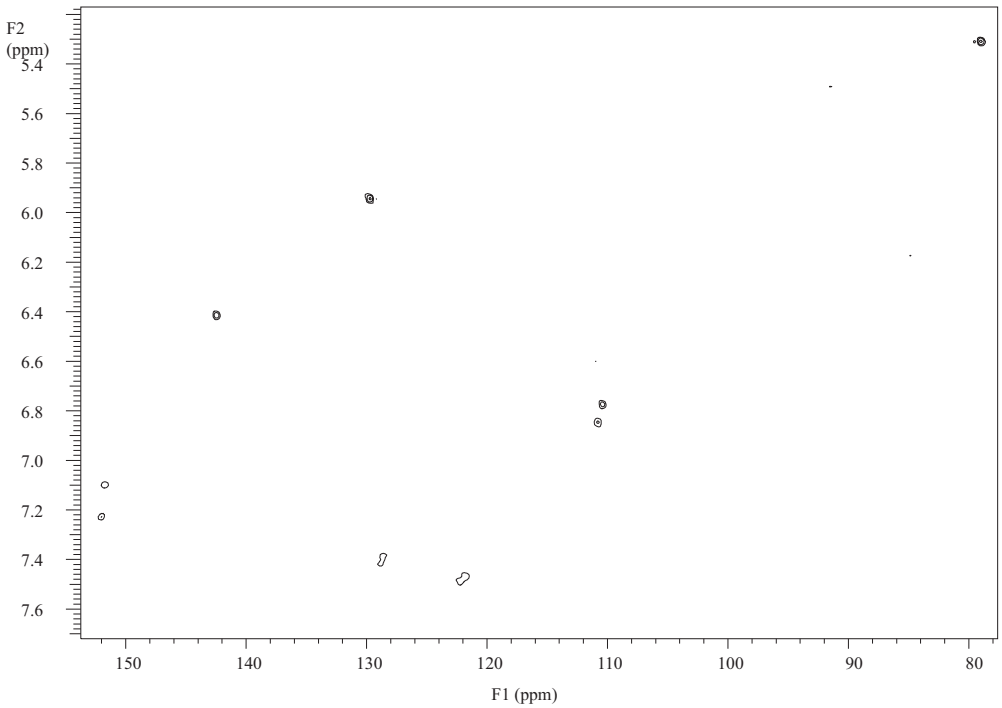

Figure 6.13: *HSQC-DEPT NMR spectrum of spiro-mamakone A obtained in CD_3OD using the capNMR probe.*

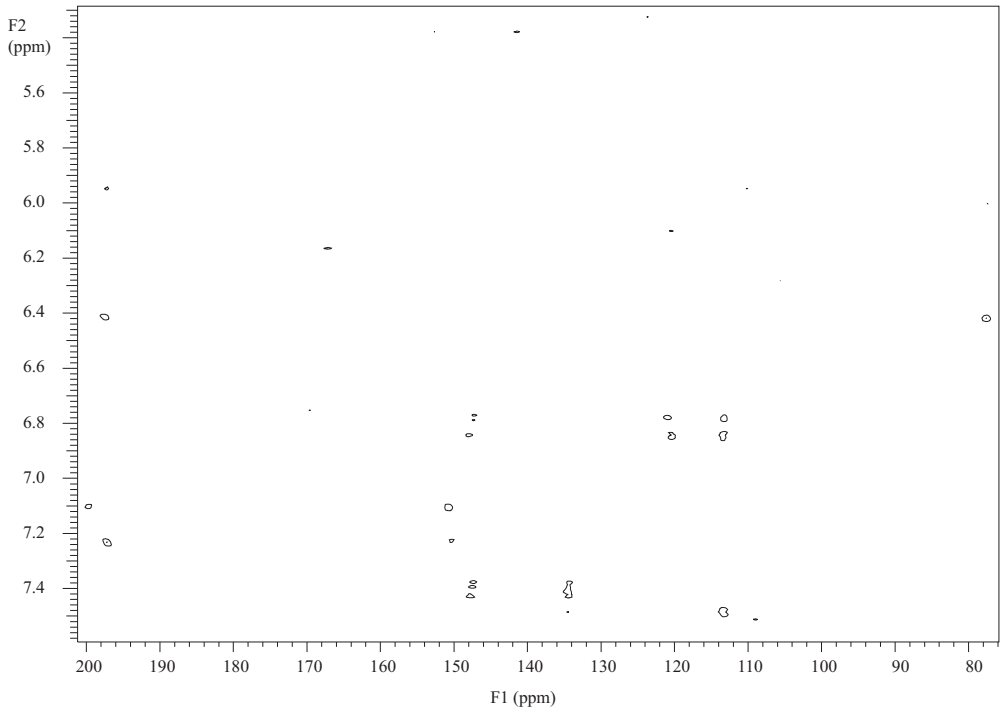

Figure 6.14: *HMBC NMR spectrum of spiro-mamakone A obtained in CD_3OD using the capNMR probe*

Equally good results were obtained for spiro-mamakone C from just one well (D5). Using the same methodology as for spiro-mamakone A, it was estimated that well D5 contained approximately 5 μg of material. The ^{1}H NMR spectrum for this is presented below (Figure 6.15).

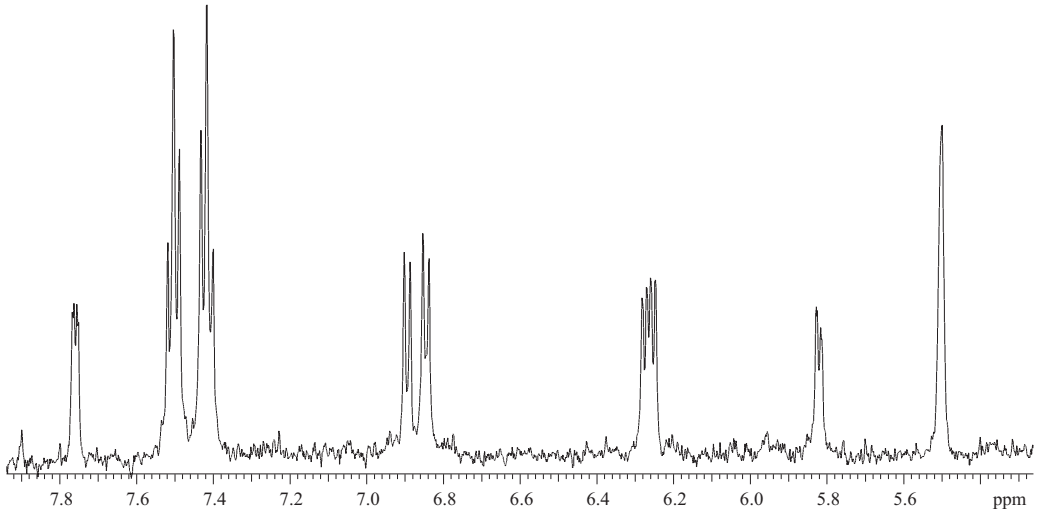

Figure 6.15: *^{1}H NMR spectrum of spiro-mamakone C obtained in CD_3OD from capNMR.*

It was assumed that when selecting microtitre wells containing peaks (compounds) of interest, that the UV detection would coincide well with that of the elution into the microtitre plate from the fraction collector. This however, was an incorrect assumption. For example wells D3 and D4 of the F5584 microtitre plate, containing the spiro-mamakones were combined. The resulting ^{1}H NMR spectrum (Figure 6.16) revealed a mixture of two compounds. The major compound, the signals of which are indicated by an asterix (*), was identified as spiro-mamakone C. It was at this point that the ELSD trace (Figure 6.10) was compared to the microtitre wells; it matched exactly.

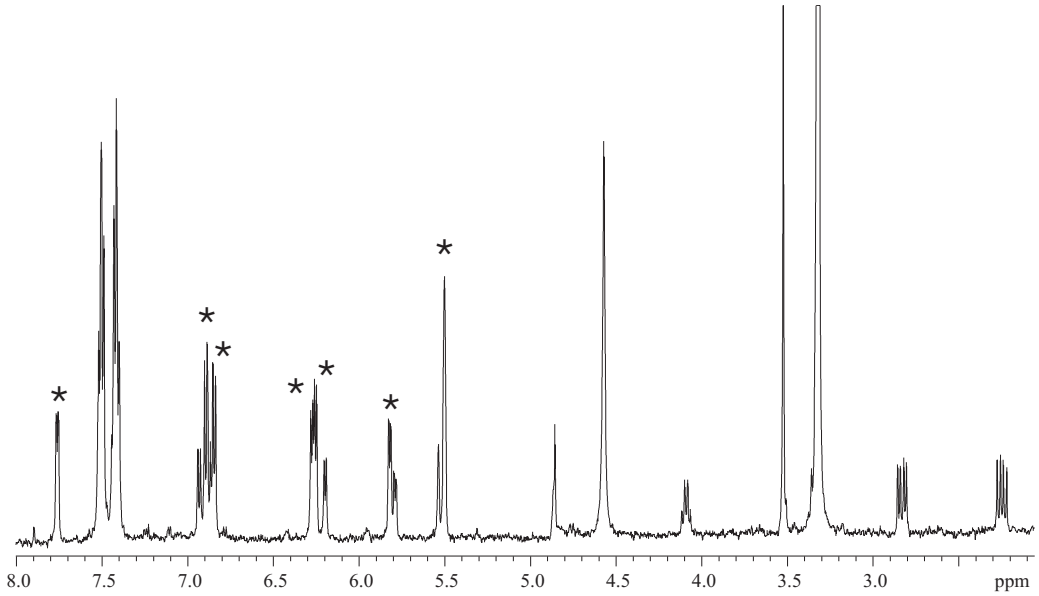

Figure 6.16: *^{1}H NMR spectrum of a new unidentified triol spiro-mamakone with contamination of spiro-mamakone C (*).*

The remaining signals in the ^{1}H NMR spectrum (Figure 6.16) were compared to those of the other spiro-mamakones. They most closely resembled those of the triols, spiro-mamakones D and E. However, the protons at positions 4 and 9 of the molecule were ambiguous. As can be seen in the spectrum, two broad singlets are present at approximately the correct chemical shift (δ_H 5.55 and 4.85). These, however, showed no coupling in the COSY NMR spectrum, hence the identity remains unconfirmed. Due to the low resolution and therefore lack of observed coupling between the methine proton at δ_H 4.09 (proposed as H-8) and the H-9 proton (proposed as the broad singlet at δ_H 4.86), even the *cis* or *trans* nature of the diol could not be proposed. Unfortunately, only ^{1}H and COSY NMR data were collected for this compound, so further work on the elucidation of this further member of the spiro-mamakones family can not be advanced until more compound is obtained through routine large scale extraction of a re-culture of the fungus.

6.6 Discussion

Effective methods for the rapid dereplication of natural products extracts should be regarded as of utmost importance to natural products groups. Here in the Marine Chemistry Group at the University of Canterbury, very effective procedures for dereplication have been introduced and gradually refined over the last couple of decades. The recent combination of the UV library database, P388 microtitre plate analysis, MS, AntiMarin and capNMR has enabled the dereplication process to proceed so rapidly so as to have in some cases an identification of the biologically active compound in question within minutes; either by comparison within the UV library or a combination of capNMR/MS/AntiMarin. Since installation of the Protasis capNMR in the department, and the UV database, the amount of extracts that individual group members are able to process has increased by at least two-fold.

Chapter 7

Experimental

7.1 General Methods

7.1.1 Sample Extraction-Solid Culture

Fungal cultures on solid agar plates (85 mm diameter) were macerated with EtOAc using a stainless steel potato masher. This extraction process was carried out twice. The ground agar was left sitting in a third aliquot of EtOAc overnight. The EtOAc was filtered off from the macerated agar using a glass funnel plugged with glass wool. All three quantities of EtOAc were combined and taken to dryness on a rotary evaporator. The extract was transferred to a pre-weighed vial, the weight determined and assayed for antitumour activity.

7.1.2 Sample Extraction-Liquid Culture

Cultures were homogenised with a Waring commercial blender for ~30 sec or until the mycelial mat was sufficiently macerated, then filtered through celite under vacuum. The

filtered broth was extracted three times with EtOAc. The solid mycelial residue was suspended in EtOAc and extracted three times. The first two EtOAc extractions were for one hour and the third overnight. All organic phases were combined and taken to dryness on a rotary evaporator. A small volume (20 mL) of the aqueous phase was also taken to dryness on a rotary evaporator. Both the aqueous and organic phases were then transferred to seperate vials, the weight determined and assayed for antitumour activity.

7.1.3 P388 Assay

Before further investigation, crude extracts were assayed for biological activity against the murine leukaemia cell line P388 (ATCC CCL 46, P388D1). This assay consists of a serial dilution of the sample of interest followed by incubation for 72 hours with P388 cells. Cell viability is determined colorimetrically by the addition of a yellow dye, MTT tetrazolium. Unhealthy or dead cells cannot metabolise this dye, thereby leaving a yellow colour. Healthy cells however are able to reduce the dye to MTT formazan resulting in an intense purple colour (Figure 7.1).

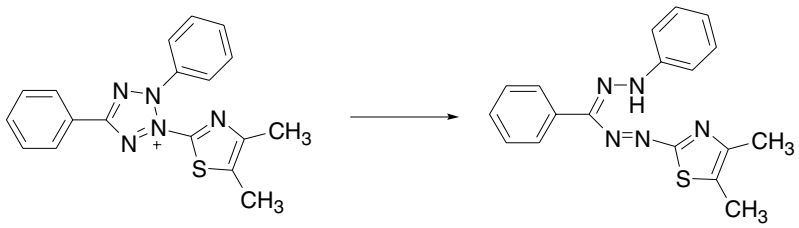

Figure 7.1: *Reduction of the yellow MTT tetrazolium salt to the purple MTT formazan by healthy P388 cells.*

The concentration of the sample required to reduce cell growth by 50%, when compared to a set of controls, is expressed as an IC_{50} in ng/mL. For pure compounds this was converted to a value in μM. All samples were dissolved in double distilled MeOH prior to assay submission.

7.1.4 HPLC Microtitre Plate Screening

As part of the dereplication process all small scale extracts were initially examined in the HPLC microtitre plate screen. An aliquot of the crude extract (250 μg) was analysed by reverse phase C18 HPLC using the following standard gradient solvent system: 2 minutes of 10% ACN/H_2O; a linear gradient to 75% ACN/H_2O for 12 minutes; isocratic at 75% for another 10 minutes; a linear gradient for 2 minutes to 100% ACN followed by isocratic at 100% ACN for 4 minutes then returned to 10% ACN/H_2O in 2 minutes and re-equilibriated for 8 minutes; with a flow rate of 1 mL/min. The eluant was collected into 96 well polystyrene microtitre plates, from which 50 and 5 μL "daughter plates" were made, which were then assayed for cytotoxicity against the P388 cell line.

7.1.5 Antimicrobial Assay

Antimicrobial activity was detected using a zone of inhibition assay. The bacteria tested against were *Bacillus subtilis* (ATCC 19659), *Escherichia coli* (ATCC 25922) and *Pseudomonas aeruginosa* (ATCC 27853). The fungi tested against were *Candida albicans* (ATCC 14053), *Trichophyton mentagrophytes* (ATCC 28185) and *Cladosporium resinae* (Department of Biological Sciences, University of Canterbury). Each bacterium or fungus (at a known concentration) was mixed with Mueller Hinton or potato dextrose agar and poured in Petri dishes to produce a 'lawn' of bacterium/fungus. Samples of interest were then pipetted onto 6 mm diameter filter paper disks. After evaporation of solvent, the disks were placed onto the above prepared seeded agar.

Antibiotic controls were run for each batch: gentamycin (10 μg/disk) was used for *E. coli* and *P. aeruginosa*; chloramphenicol (30 μg/disk) was used for *B. subtilis*; nystatin (100 units/disk) was used for *C. albicans*, *C. resinae* and *T. mentagrophytes*. Antimicrobial activity was measured in millimetres as the radius of inhibition (mass/disk).

Suitable solvent controls were used in every assay run.

7.1.6 Antiviral Assay

Two viruses, *Herpes simplex* virus type 1 (Strain F ATCC VR 733) and *Polio* virus type 1 (Pfizer vaccine strain) were used to detect antiviral activity. *Herpes simplex* virus type 1 is a non enveloped virus with a single stranded RNA genome and a site of replication in the host cell cytoplasm. *Polio* virus type 1 is an enveloped virus with a double stranded DNA genome and a site of replication in the host cell nucleus. BSC-1 cells (African Green Monkey kidney cell line, ATCC CCL 26) were used as the host cells for the above mentioned viruses. Samples of interest were pipetted onto 6 mm diameter filter paper disks, followed by evaporation of solvent. The disks were then placed directly onto infected BSC-1 cells and incubated for 24 hours at 37°C in an atmosphere containing 1.5% CO_2. The host cells were then examined, using an inverted microscope, for the size of antiviral (viral inhibition) and/or cytotoxic zones as well as the type of cytotoxicity.

7.1.7 Chromatography

7.1.7.1 Flash Column Chromatography

Column chromatography was performed with glass columns of stated dimensions or in pre-prepared cartridges as indicated. All solvents used for chromatography were of commercial grade and distilled once, except for MeOH, which was double distilled. Reversed phase C18 columns were run under pressure (0.5 kPa) with oxygen-free N_2 gas. Reversed phase chromatography (RP) used Bakerbond (40μm) octadecyl (C18) packing. Samples were either dissolved in a minimal volume of solvent and loaded directly on to the column, or absorbed to fresh C18 at a ratio of 1:50 using a minimum volume of solvent which was removed under vacuum prior to loading onto the column.

A standard elution profile was used for reversed phase C18 column chromatography (10g, 1.5 x 24 cm). Columns were equilibrated to 10% MeOH/H_2O prior to sample loading and then eluted with increasing concentrations of MeOH in steps of 10% per fraction, until 100% MeOH then 10% DCM/MeOH, 50% DCM/MeOH, and 100% DCM.

Any material remaining on the column was washed off using combinations of DCM and MeOH (with 0.05% TFA).

7.1.7.2 High Pressure Liquid Chromatography (HPLC)

In most projects the milli-Q H_2O was acidified with 0.05% TFA. All samples were filtered through 0.45 μm PTFE membrane filters immediately prior to injection.

Analytical High Pressure Liquid Chromatography (HPLC) was carried out on a Dionex liquid chromatograph equipped with a UVD 340U diode array detector, and connected to an Alltech ELSD 800. For reversed phase HPLC, a Phenomenex Prodigy C18 5 μ ODS3 column (5 μ, 250 x 4.6 mm) was used. A standard flow rate of 1 mL/min was used with variable concentrations of ACN (HPLC grade) in H_2O (milli-Q). The standard gradient given in Section 7.1.4 was used unless otherwise stated.

Preparative HPLC was performed on a Shimadzu LC-4A instrument equipped with a UV Spectrophotometric Detector SPD-2AS (wavelength λ=210 nm) and a Hewlett Packard 3390A integrator. Reversed phase HPLC was performed on a Phenomenex Luna C18, 10 x 250 mm, 5 μ column run at 5 mL/min. Variable concentrations of ACN (HPLC grade) in H_2O (milli-Q) were used for the mobile phase.
For all chapters, except chapter 2, when TFA was used in the mobile phase, the eluent was evaporated until only H_2O remained. The H_2O was then partitioned between EtOAc to extract the compound(s) of interest.

7.1.8 Mass Spectrometry

7.1.8.1 Electron Impact Mass Spectrometry

High Resolution Electron Impact Mass Spectra (HREIMS) were obtained on a Kratos MS80RFA spectrometer, operating with a 4kV accelerating potential, 70eV and a source temperature of 250°C.

7.1.8.2 Electrospray Ionisation Mass Spectrometry

High Resolution Electrospray Ionisation Mass Spectra (HRESIMS) were recorded on a Micromass LCT spectrometer using a probe voltage of 3200V, an operating temperature of 150°C and a source temperature of 80°C. The carrier solvent was 50:50 ACN/H_2O at 20 μL/minute (for direct inject mode). A 10 μL injection of sample was made from a 10 μg/mL sample.

When obtaining positive ESI mass spectra some samples were protonated with 10 μL/mL formic acid prior to injection. When recording negative ESI mass spectra samples were deprotonated, as required, with 10 μL/mL DEA prior to injection.

7.1.8.3 Liquid Chromatography Mass Spectrometry

Liquid Chromatography Mass Spectrometry (LCMS) samples were analysed on a Waters 2790 HPLC system equipped with a Waters photodiode array detector (PDA) coupled to a Micromass LCT spectrometer.

7.1.9 Nuclear Magnetic Resonance (NMR)

^{1}H, COSY, 1D NOE, HSQC, CIGAR, *J*2-resolved CIGAR described in Chapter 2, and modified ^{13}C NMR carried out in Chapter 3 were all recorded on a Varian INOVA 500 spectrometer at 23°C, operating at 500 MHz. The INOVA was equipped with a variable

temperature and inverse-detection 5 mm probe. The INADEQUATE NMR carried out in Chapter 3 was obtained on the Varian INOVA 500 spectrometer at 23°C, operating at 500 MHz but using a broadband 5mm probe. The ^{13}C NMR spectra were recorded on a Varian UNITY 300 NMR spectrometer, at 23°C, operating at 75 MHz. The UNITY was equipped with a variable temperature direct broadband 5 mm probe. Chemical shifts are expressed in parts per million (ppm) on the δ scale, and were referenced to the appropriate solvent peaks: $CDCl_3$ referenced to C**H**Cl_3 at δ_H 7.25 (^1H) and **C**HCl_3 at δ_C 77.0 (^{13}C), CD_3OD referenced to C**H**$_3OD$ at δ_H 3.3 (^1H) and **C**H_3OD at δ_C 49.3 (^{13}C) and DMSO-d_6 referenced to CD_3(C**H**D_2)SO at δ_H 2.6 (^1H) and (**C**D_3)$_2$SO at 39.6 (^{13}C).

7.1.10 X-ray Crystallography

For Chapters 2, 4, and 5, X-ray crystallographic data was collected on a Siemens P4 four circle diffractometer using graphite monochromised Mo Kα (λ=0.71073 Å) radiation at temperature indicated in appropriate tables in the Appendix.

For Chapter 3, X-ray crystallographic data was collected on a Bruker-Nonius APEX II area detector system equipped with a nitrogen low-temperature gas-flow device, which was used to collect a full sphere of data with Mo Kα radiation. For crystal processing the data processing program, SAINT[140] was used.

For all crystals, the structure, refinement, and resulting tables and diagrams were all produced using the SHELXTL suite of programs.[141,142]

7.1.11 UV-Vis Spectroscopy

Purified samples were dissolved in MeOH at a concentration dependent on the strength of the UV chromophore of the particular sample. The UV-vis spectra of these samples were recorded on a Varian Cary 50 Probe UV-Visible spectrophotometer.

7.1.12 Infrared Spectroscopy

Purified samples were dissolved in $CHCl_3$ or acetone and applied to a KBr disc, the solvent was evaporated on the disc by exposure to the air. IR spectra of these samples were recorded on a Shimadzu FTIR-8201 PC spectrometer.

7.1.13 Circular Dichroism Spectroscopy

CD spectra were measured in 0.8 mg/mL MeOH using a 10 mm quartz cell on a Jasco J 20-C spectropolarimeter.

7.1.14 Optical Rotation

Optical Rotation values were obtained on a Perkin Elmer 341 polarimeter at 20°C with a wavelength of 589 nm. The optical rotation was then calculated using the following equation:

$$[\alpha]_D = \alpha/LC$$

Where L is the pathlength (dm) and C is the concentration (g/L).

7.2 Experimental for Chapter 2

7.2.1 Chromatography of F2028

The crude extract (60 mg) was obtained from a fungal collection that had been stored at –80 °C for several years in the School of Biological Sciences. The simple nature of the extract allowed for minimal purification. Purification was carried out with semi-preparative HPLC using a linear gradient of 30-50% ACN/H_2O with TFA over 20 minutes to give three compounds. 1D and 2D NMR techniques and mass spectrometry determined these compounds to be a known compound, pseurotin A (**2.7**, 1.9 mg), and two previously undescribed diastereomers of pseurotin A, pseurotin A_2 (**2.8**, 0.6 mg) and A_3 (**2.9**, 0.8 mg).

7.2.2 X-ray Crystallography of Pseurotin A_2 (**2.8**)

The structure of **2.8** was confirmed by X-ray crystallography. Compound **2.8** was crystallised from MeOH at 4 °C. A plate crystal with dimensions $0.44 \times 0.24 \times 0.23$ mm^3 was used for data collection. The data processing yielded 32305 Bragg reflections, of which 29% were unique. The final *R* factor was 11.3 %. See Appendix 1 for tables of data.

7.2.3 $NaIO_4$ Oxidative Cleavage

Oxidative cleavage was carried out on all three pseurotins. Pseurotin A (**2.7**, 100 μg, 0.23 μmol) was dissolved in MeOH (100 μL) and mixed with 1.28 molar equivalents of $NaIO_4$ (63.5 μg, 0.30 μmol) dissolved in MeOH (63.5 μL), and acidified to pH 2 with H_2SO_4. After 4 h at 8 °C, the reaction mixture was diluted with H_2O and then extracted with EtOAc. LCMS was used to confirm the presence of the aldehyde product. This process was repeated for pseurotins A_2 and A_3.

7.2.4 Physical Data for the Pseurotins

Pseurotin A (2.7): colourless amorphous solid; $[\alpha]^{20}_{D}$ -10° (*c* 0.1, MeOH); ^{1}H and 2D-NMR data see Table 4.1; ESIMS *m/z* 454 $[M+Na]^{+}$.

Pseurotin A_2 (2.8): colourless plate crystal; UV (MeOH) λ_{max} (log ε) 210 (3.72), 252 (3.71), 280 (3.54) nm; IR (KBr disk) ν_{max} 3425, 1697, 1636, 1450, 1373, 1188, 1080 cm^{-1}; ^{1}H- and ^{13}C-NMR data, see Table 2.2; HRESIMS *m/z* 454.1492 $[M+Na]^{+}$ (calcd for $C_{22}H_{26}NO_8Na$, 454.1479).

Pseurotin A_3 (2.9): colourless amorphous solid; UV (MeOH) λ_{max} (log ε) 210 (3.72), 252 (3.68), 280 (3.54) nm; IR (KBr disk) ν_{max} 3402, 1736, 1690, 1636, 1458, 1370, cm^{-1}; ^{1}H- and ^{13}C-NMR data, see Table 2.3; HRESIMS *m/z* 454.1469 $[M+Na]^{+}$ (calcd for $C_{22}H_{26}NO_8Na$, 454.1479).

7.3 Experimental for Chapter 3

7.3.1 Culturing and Extraction of F5062 and F5584

The culture and extractions for both fungal cultures was identical. The fungus was grown on 24 plates (of dimensions stated in Section 7.1.1) of MYE (Malt Yeast Extract) agar for 24 days at 26°C. The resulting culture was extracted with EtOAc as given in the protocol in Section 7.1.1 to give the crude extract of 207.7 mg (F5062) and 248.7 mg (F5584).

7.3.2 Chromatography of F5062

The crude extract was first partitioned between Pet. ether and MeOH. The MeOH-soluble material was concentrated and partitioned between EtOAc and H_2O. The resulting EtOAc-souble material (161.0 mg) was absorbed to C18 (100 mg) and fractionated on a reverse phase (C18) column (13 g, 1.5 x 25 cm), using the standard

stepped gradient (Section 7.1.7.2). Fifteen fractions were collected. These were analysed by reverse phase HPLC and assayed for cytotoxicity against the P388 cell line. Fractions 10 and 11, both eluting with 100 % MeOH, showed excellent cytotoxicity (231 and 166 ng/mL respectively. UV visible detection on the HPLC showed that the compounds contained within the two fractions were closely related to each other. Fraction 11 was very pure, showing only two major peaks on the HPLC chromatogram, with only one of those associated with any relative mass, as shown by ELSD.

For final purification of fraction 11, semi-preparative HPLC was carried out using a linear gradient of 45-60% ACN/H_2O over 20 minutes. The single compound isolated, was determined, by a combination of mass spectrometry and 1D and 2D NMR to contain a structurally unprecedented type of spirobisnaphthalene (**3.11**) (2.3 mg).

Fraction 10, was found to contain, as well as **3.11**, three other compounds with similar UV chromophores. Semi-preparative HPLC using the same linear gradient as was used for fraction 11, was used to purify these compounds.

1D and 2D NMR as well as mass spectrometry determined these to be members of a new acidic class of spirobisnaphthalenes (**3.7**, **3.8**, and **3.10**) (1.9, 4.8, 1.1 mg respectively) and **3.11** (5.7 mg).

7.3.3 Physical Data for the Spirobisnaphthalenes

Mamakunoic acid B (3.7): cream amorphous solid; $[\alpha]^{20}_{D}$ 0.0° (*c* 0.066, MeOH); UV (MeOH) λ_{max} (log ε) 212 (sh), 230 (3.99), 288 (3.57), 314 (3.42), 328 (3.32) nm; IR (KBr disk) ν_{max} 1610, 1587, 1464, 1412, 1381, 1273, 1194, 1144, 822, 760 cm^{-1}; ^{1}H- and ^{13}C-NMR data, see Table 3.1; EIMS *m/z* (%): 350.1 $[M]^+$ (22), 279.1 (100), 160.1 (12), 115.1 (14); HREIMS *m/z* 350.0780 $[M]^+$ (calc for $C_{20}H_{14}O_6$ 350.0790).

Mamakunoic acid A (3.8): cream amorphous solid; UV (MeOH) λ_{max} 206, 224, 288, 298, 313, 328 nm; ^{1}H- and ^{13}C-NMR data, see Table 3.2; ESIMS *m/z*: 369 $[M+H]^+$

Mamakunoic acid A-deuterated methyl ester (3.9): cream amorphous solid; $[\alpha]^{20}_{D}$ +15 ° (*c* 0.026, MeOH); UV (MeOH) λ_{max} (log ε) 234 (3.98), 296 (4.00), 314 (3.88), 328 (3.74) nm; IR (KBr disk) ν_{max} 1732, 1609, 1589, 1474, 1412, 1381, 1273, 1072, 818, 756 cm^{-1}; ^{1}H NMR (DMSO-d_6, 500 MHz), δ 7.52 (2H, m, H14/H16), 7.51 (2H, m, H13/H17), 7.10 (2H, m, H12/H18), 6.78 (1H, dd, 1.0, 7.9, H3), 6.66 (1H, dd, 1.0, 7.8, H5), 6.43 (1H, t, 7.9, 7.9, H4), 4.83 (1H, dd, 2.7, 10.0, H8), 2.81 (1H, dd, 2.7, 15.0, H9b), 2.64 (1H, dd, 10.0, 15.0, H9a); ^{13}C shifts determined from HSQC-DEPT and CIGAR NMR experiments (DMSO-d_6, 500 MHz), δ 172.0 (C10), 148.0 (C11/C19), 146.3 (C6), 145.0 (C7), 134.0 (C15), 127.9 (C13/C17), 122.6 (C2), 120.5 (C3), 120.4 (C14/C16), 118.1 (C4), 115.9 (C5), 114.1 (C20), 109.4 (C12/C18), 104.2 (C1), 71.4 (C8), 37.4 (C9); EIMS *m/z* (%) 485.1 $[M]^+$ (6), 383.1 (3), 367.1 (13), 365.1 (2), 304.1 (7), 279.1 (100), 115.1 (9); HREIMS *m/z* 385.1241 $[M]^+$ (calc for $C_{21}H_{15}O_7D_3$ 385.1241).

Mamakunoic acid C (3.10): orange/red amorphous solid; UV (MeOH) λ_{max} 206 (sh), 228, 297, 314 (sh), 328 nm; ^{1}H- and ^{13}C-NMR data, see Table 3.3; EIMS *m/z* (%) 380.1 $[M]^+$ (64), 334.1 (32), 304.1 (10), 160.1 (100); HREIMS *m/z* 380.0881 $[M]^+$ (calc for $C_{21}H_{16}O_7$ 380.0896).

spiro-Mamakone A (3.11): yellow amorphous solid; $[\alpha]^{20}_{D}$ 0.0 ° (*c* 0.1, MeOH); UV (MeOH) λ_{max} (log ε) 230 (3.89), 300 (3.88), 315 (3.73), 330 (3.43) nm; IR (KBr disk) ν_{max} 1707, 1609, 1414, 1379, 1275, 1204, 1107, 1082 cm^{-1}; ^{1}H- and ^{13}C-NMR data, see Table 3.4; EIMS *m/z* (%): 320.1 $[M]^+$ (100), 291.1 (52), 265.1 (23), 197.1 (27), 170.0 (26), 160.1 (27), 133.0 (27), 114.0 (24); HREIMS *m/z* 320.0677 $[M]^+$ (calc for $C_{19}H_{12}O_5$ 320.0685).

*7.3.4 Oxidation of spiro-Mamakone A (**3.11**)*

spiro-Mamakone A (**3.11**, 2.0 mg, 6.2 μmol) and freshly precipitated MnO_2 (20 mg, 0.23 mmol), prepared following the procedure of Attenburrow *et al*.,[143] and $CHCl_3$ (0.5 mL)

were stirred together at room temperature for 2 h. The reaction mixture was filtered through a (0.45 μm) syringe filter to yield pure 4-oxo-spiro-mamakone A (**3.12**, 1.6 mg, 80.5%).

4-oxo-spiro-Mamakone A (3.12): pale yellow amorphous solid; UV (MeOH) λ_{max} (log ε) 232 (3.89), 295 (4.04), 314 sh, 330 (3.66) nm; IR (KBr disk) ν_{max} 1763, 1701, 1612, 1413, 1377, 1275, 1257, 1126, 1047 cm^{-1}; ^1H NMR ($CDCl_3$, 500 MHz) δ 7.77 (1H, d, 5.8, H3), 7.49 (2H, d, 8.3, H15/H13), 7.41 (2H, t, 8.3, 8.3, H16/H12), 7.00 (2H, s, H7/H8), 6.90 (2H, d, 8.3, H17/H11), 6.69 (1H, d, 5.8, H2); ^{13}C shifts determined from HSQC-DEPT and CIGAR experiments ($CDCl_3$, 500 MHz), δ196.0 (C4), 194.2 (C9/C6), 157.0 (C3), 150.8 (C8/C7), 146.2 (C10/C18), 137.7 (C2), 134.0 (C14), 127.6 (C16/C12), 121.6 (C15/C13), 113.4 (C19), 110.7 (C17/C11), 105.8 (C1), 70.5 (C5); EIMS *m/z* (%): 318.1 $[M]^+$ (100), 290.1 (7), 262.1 (19), 234.1 (13), 208.1 (14), 168.1 (9), 114.0 (25); HREIMS *m/z* 318.0533 $[M]^+$ (calc for $C_{19}H_{10}O_5$ 318.0528).

*7.3.5 Spiroketal Deprotection of spiro-Mamakone A (**3.11**)*

To a stirred solution of spiro-mamakone A (**3.11**, 2.0 mg, 6.2 μmol) in ACN (200 μL) at 70 °C was added in one portion a solution of cerium ammonium nitrate (CAN, 8.6 mg, 15.6 μmol) in H_2O (400 μL) following the procedure of Ates *et al.*[144,145] After 5 minutes, the crude extract was poured in H_2O and extracted with EtOAc twice. The oragnic layer was dried over $MgSO_4$ and then taken to dryness under a flow of N_2, to yield 9-hydroxy-spiro[4.4]nona-2,7-diene-1,4,6-trione (**3.13**, 0.4 mg)

9-hydroxy-spiro[4.4]nona-2,7-diene-1,4,6-trione (3.13): ^1H NMR (CD_3OD, 500 MHz) δ 8.10 (1H, dd, 2.0, 5.4, H3), 7.99 (1H, d, 5.8, H7), 7.94 (1H, d, 5.8, H8), 6.50 (1H, dd, 1.5, 5.4, H2), 5.15 (1H, br s, H4); ^{13}C shifts determined from HSQC-DEPT and CIGAR experiments (CD_3OD, 500 MHz) δ 201.4 (C6/C9), 199.2 (C1), 196.4 (C9/C6), 168.9 (C3), 154.0 (C8/C7), 153.2 (C7/C8), 133.4 (C2), 75.0 (C4), 72.3 (C5).

7.3.6 *Derivatisation of spiro-Mamakone A (**3.11**) with Mosher Acids*

To spiro-mamakone A (**3.11**, 2.5 mg, 7.8 μmol), a solution of (*S*)-MTPA chloride (5.8 μL, 33.5 μmol) in pyridine (50 μL) and a small crystal of DMAP were added. After 2 h the solvent was evaporated, the residue dissolved in MeOH (0.5 mL), and the solution analysed by HPLC (Phenomenex Luna C18, 250 x 4.6, 5μm; solvents: A water + 0.05% TFA, B ACN; linear gradient: min 10% B, 2 min 10% B, 14 min 75% B, 24 min 75% B; 40 °C; 1 mL min^{-1}). To give the (*R*)-MPTA ester the same experimental procedure for the production of the (*S*)-MPTA ester was followed.

7.3.7 *Chromatography of F5584*

The large-scale extract (248.7 mg) was absorbed on to C18 (100 mg) and fractionated on a reverse phase (C18) column (13 g, 1.5 x 25 cm), using a stepped gradient from MeOH/H_2O (1:3) over pure MeOH to pure DCM. Fourteen fractions were collected and analysed by reverse phase HPLC and assayed for cytotoxicity against the P388 cell line. Three sequential fractions (fractions SAS-5-103.9–11), eluting with 90-100% MeOH, showed the highest cytotoxicity. Analysis of the HPLC chromatograms of these fractions revealed a group of related compounds (as seen by the similarity of the UV spectra) eluting between 11.5-14.5 minutes. On comparison of SAS-5-103.10 and SAS-5-103.11 with that of SAS-5-64.10 from the first extract (F5062) it was revealed that these two fractions contained spiro-mamakone A. Fraction B also contained other related compounds apart from spiro-mamakone A. Based on this, fractions SAS-5-103.9 and SAS-5-103.10 were subjected to final purification by semi-preparative HPLC.

For the purification of SAS-5-103.9, a linear gradient of 30-45% ACN/H_2O was used. The two compounds purified were identified using mass spectrometry, 1D and 2D NMR as two novel compounds closely related to spiro-mamakone A, to which the names spiro-mamakone D (**3.17**) and B (**3.16**) were given.

In the separation of SAS-5-103.10, the gradient was changed to 42-55% ACN/H_2O over 20 minutes. Under these conditions more of spiro-mamakone A as well as two diastereoisomers of **3.16** and **3.17** were isolated (**3.15** and **3.18**). Both were identified, as before, on the basis of mass spectrometry as well as 1D and 2D NMR, and in keeping with the other compounds were given the names spiro-mamakone C and E respectively.

*7.3.8 X-ray Crystallography of **3.15***

The structure of **3.15** was confirmed by X-ray crystallography. **3.15** was crystallised from MeOH at 4 °C. A block crystal with dimensions 0.45 × 0.20 × 0.15 mm^3 was used for data collection. The data processing 1652 Bragg reflections, of which 83% were unique. The final *R* factor was 7.5 %. See Appendix 1 for tables of data.

7.3.9 Molecular Modelling

The eight possible combinations of the two diastereomers, spiro-mamakone D (**3.17**) and E (**3.18**) were constructed in silico using the Maestro build function of the 2005 Schrodinger molecular modeling suite. A Monte Carlo multiple minimum (MCMM) conformational search of each structure was carried out with MacroModel 9.0 using the OPLS2001 force field with the GB/SA water solvent model. The criteria for convergence of each conformational search was the generation of 3000 starting conformations and a maximum of 5000 iterations in the energy miminisation routine for each conformer, collecting the ensemble of conformers within 12 kJ of the global minima. A Boltzmann weighting for the conformers in each of the three ensembles was established using the following expression:

$$P_\alpha = \frac{\exp[-(E_\alpha / k_B T]}{\sum_{\alpha}^{N_A} \exp[-(E_\alpha / k_B T]}$$

Relevant H/H distances for all conformers within each ensemble was measured. The Boltzmann weighting of each conformer, where a H/H distance was within 2.5Å (Boltzmann-weighted percentage of H/H distances < 2.5 Å), was established. The same was calculated for H-H distances < 3Å. The Boltzmann average distance was also calculated. The Boltzmann weighted r^{-6} was calculated for each H/H distance within each ensemble which gave virtual NOE values. This data was used to compare the modelled data with the experimental data in order to determine the correct isomer.

7.3.10 Physical Data for spiro-Mamakones B-E

spiro-Mamakone C (3.15): pale yellow block crystals, (MeOH): m.p. 110-111°C; $[\alpha]^{20}_{D}$ +309° (c 0.1, MeOH); IR (KBr disk) ν_{max} 3364, 1717, 1609, 1585, 1410, 1379, 1339, 1275 cm^{-1}; UV (MeOH) λ_{max} (log ε) 232 (3.88), 300 (3.80), 314 (3.67), 328 (3.50) nm; ^{1}H- and ^{13}C-NMR, see Table 3.5; EIMS *m/z* (%): 322.1 $[M]^{+}$ (100), 304.1 (66), 293.1 (25), 221.1 (16), 197.1 (34), 160.1 (49). HREIMS *m/z* 322.0830 $[M]^{+}$ (calc for $C_{19}H_{14}O_5$ 322.0841).

spiro-Mamakone B (3.16): pale yellow amorphous solid; $[\alpha]^{20}_{D}$ -215° (*c* 0.1, MeOH); IR (KBr disk) ν_{max} 3385, 1717, 1609, 1585, 1411, 1381, 1339, 1273, 1111 cm^{-1}; UV (MeOH) λ_{max} (log ε) 232 (3.88), 300 (3.65), 314 (3.55), 328 (3.40) nm; ^{1}H- and ^{13}C-NMR, see Table 3.6; EIMS *m/z* (%): 322.1 $[M]^{+}$ (60), 304.1 (27), 267.0 (22), 197.1 (31), 160.1 (100); HREIMS *m/z* 322.0840 $[M]^{+}$ (calc for $C_{19}H_{14}O_5$ 322.0841).

spiro-Mamakone D (3.17): pale yellow amorphous solid; $[\alpha]^{20}_{D}$ +162° (*c* 0.033, MeOH); IR (KBr disk) ν_{max} 3364, 1749, 1609, 1585, 1412, 1381, 1340, 1273, 1067 cm^{-1}; UV (MeOH) λ_{max} (log ε) 232 (3.91), 300 (3.78), 314 (3.68), 328 (3.51) nm; ^{1}H- and ^{13}C-NMR, see Table 3.7; EIMS *m/z* (%): 340.1 $[M]^{+}$ (6), 322.1 (18), 304.1 (9), 252.1 (5), 197.1 (15), 160.1 (21); HREIMS *m/z* 340.0947 $[M]^{+}$ (calc for $C_{19}H_{16}O_6$ 340.0947).

spiro-Mamakone E (3.18): pale yellow amorphous solid; UV (MeOH) λ_{max} 232, 300, 314, 328 nm; ^{1}H- and ^{13}C-NMR, see Table 3.8; EIMS *m/z* (%): 340.1 $[M]^+$ (4), 322.1 (80), 304.1 (100), 252.1 (5); HREIMS *m/z* 340.0960 $[M]^+$ (calc for $C_{19}H_{16}O_6$ 340.0947).

7.3.11 Time-Course Experiments

Two quantities of sterile MYE broth (250 mL) were inoculated with a growing agar culture of the spiro-mamakone producing fungus, E484. Both cultures were inoculated with four plugs from the same agar plate. One inoculated broth was placed in static conditions, the other under shake conditions, at 26 °C.

The difference in the morphology of the fungus under these conditions was extensive. For example after four days incubation, the static culture showed a clear broth with formation of some plaques. The shake culture at the same time period showed a darkened broth heavily laden with mycelia, including balls of mycelia.

Monitoring of the cultures for production of spiro-mamakone A (**3.11**) began four days after inoculation. At days 4, 6, 7, 8, and 12, a 10 mL aliquot of the shake culture was removed and extracted with EtOAc according to the protocol outlined in Section 7.1.2. The resulting extract was chromatographed using the standard gradient (Section 7.1.4) on the analytical HPLC in conjunction with the ELSD (Section 7.1.7.2). This same process was repeated for the static culture, except that an aliquot of culture was not taken on day 7. These results lead to the use of shake conditions for the growth of isotopically-labelled cultures.

7.3.12 Biosynthetic ^{13}C labelling

Feeding experiments were performed using [1-^{13}C]-CH_3COONa, [2-^{13}C]-CH_3COONa, and [1,2-$^{13}C_2$]-CH_3COONa (99% ^{13}C). The precursors were added to the E484 cultures (200 mL) 24 hours after inoculation of broth. Each of the labelled acetates (200 mg) were added to sterile H_2O (10 mL). A half concentration of [1,2-$^{13}C_2$]-CH_3COONa was made up using the labelled precursor (100mg) and unlabelled sodium acetate (100mg).

The final concentration of the labelled acetates was 1 mg/mL except in the case of the half strength doubly labelled precursor, whereby the final concentration was 0.5 mg/mL. Under sterile conditions, the precursor solutions were filtered through 0.2 μm filters into the growing cultures. The labelled cultures were put under shake conditions for a further five days. Extraction of the cultures was carried out as before using the protocol given in Section 7.1.2. Analytical HPLC using the standard gradient without TFA ascertained that spiro-mamakone A (**3.11**) was present and in good quantity, in all labelled cultures. Also present was mamakunoic acid B (**3.7**), but in significantly smaller quantities. Purification of labelled spiro-mamakone A, and mamakunoic acid B was carried out with semi-preparative HPLC using a linear gradient of 45-60% ACN/H_2O without TFA. This resulted in the isolation of labelled spiro-mamakone A (**3.11**) from [1-^{13}C]-CH_3COONa (23.5 mg), [2-^{13}C]-CH_3COONa (19.9 mg), and [1,2-$^{13}C_2$]-CH_3COONa (18.8 mg). Isolation of labelled mamakunoic acid B (**3.7**) from [1-^{13}C]-CH_3COONa (7.2 mg), [2-^{13}C]-CH_3COONa (6.6 mg), and [1,2-$^{13}C_2$]-CH_3COONa (6.5 mg) material was also achieved. The half strength doubly labelled material was not purified as analysis of the full strength indicated this was not necessary due to very low incorporation.

*7.3.13 Acetylation of Isotopically Labelled spiro-Mamakone A (**3.11**)*

The acetylation of unlabelled spiro-mamakone A is used as an example. Spiro-mamakone A (**3.11**, 3.0 mg, 9.38 $\times 10^{-3}$ mmol), was dissolved in dry pyridine (200 μL), to which was added acetic anhydride (200 μL, 2.12 mmol). After 15 h the reaction mixture was diluted with dH_2O to 10% and then eluted through a C18 cartridge (Bakerbond spe, 1g) conditioned to 100% H_2O. Using the Vac-elute system the column was run to dryness, a further column volume of H_2O was used in the same way, followed by 100 % MeOH to elute the product, *O*-acetyl-spiro-mamakone A (**3.21**, 2.7 mg, 79.5%).

To give acetylated labelled material, the same experimental procedure was used whereby for every 1.5 mg of starting material (11.8 and 9.9 mg of [1-^{13}C]- and [2-^{13}C]-acetate labelled material respectively) 100 μL each of pyridine and acetic anhydride were used.

***O*-acetyl-spiro-mamakone A (3.21):** pale yellow amorphous solid; $[\alpha]^{20}_{D}$ +0.0° (*c* 0.05, MeOH); UV (MeOH) λ_{max} (log ε) 230 (3.95), 298 (3.72), 314 (3.58), 328 (3.43) nm; IR (KBr disk) ν_{max} 1736, 1713, 1605, 1412, 1373, 1258, 1227, 1204, 1134,1057 cm^{-1}; ^{1}H NMR (CD_3OD, 500 MHz) δ 7.51 (1H, d, 8.3, H15/H13), 7.50 (1H, d, 8.3, H13/H15), 7.41 (2H, t, 7.4, 7.4, H12/H16), 7.18 (1H, d, 6.3, H8), 7.12 (1H, d, 6.3, H7),6.85 (1H, d, 7.3, H11/H17), 6.83 (1H, d, 7.3, H17/H11), 6.45 (1H, dd, 2.0, 5.6, H3), 6.12 (1H, dd, 1.7, 5.8, H2), 5.81 (1H, brs, H4), 1.97 (3H, s, H21); ^{13}C NMR (CD_3OD, 125 MHz) δ 199.4 (C9), 197.1 (C6), 172.9 (C20), 151.4 (C8), 150.9 (C7), 148.8 (C10/C18), 148.5 (C18/C10), 138.2 (C3), 136.0 (C14), 133.2 (C2), 129.0 (C12/C16), 128.9 (C16/C12), 122.6 (C15/C13), 122.5 (C13/C15), 114.8 (C19), 112.3 (C1), 111.14 (C11/C17), 111.1 (C17/C11), 80.2 (C4), 65.7 (C5), 20.7 (C21); EIMS *m/z* (%): 362.1 $[M]^+$ (100), 320.1 (37), 291.1 (17), 266.1 (15), 237.1 (8), 197.1 (20), 161.0 (24), 133.0 (17), 114.0 (11); HREIMS *m/z* 362.0784 $[M]^+$ (calc for $C_{21}H_{14}O_6$ 362.0790).

7.3.14 Quantitative ^{13}C NMR

The ester carbonyl of the acetylated and labelled spiro-mamakone A was used as the standard to determine the incorporation of the singly labelled precursors into **3.11**.

The ^{13}C NMR was carried out as usual but with the following changes to the operating parameters:

dm = ‘nny’
at = 0.8 s
d1 = 12 s

Rather than the standard run time of 2 hours, due to the long delay, these spectra were obtained in 12 hours, for the small amount of unlabelled material, this run time was increased to 40 hours.

7.4 Experimental for Chapter 4

7.4.1 Identification, and Extraction of F5031

Identification of the fungal material was carried out by Professor A. L. J. Cole. The sample was identified by the characteristic tuberous earth ball fruiting body, differing from many other known *Scleroderma* sp. by the yellow colour and thick rooting stalk.

Fresh fungal material, consisting of three fruiting bodies (12.53 g) were dried and then extracted repeatedly with MeOH (100 mL). The extract was dried under vacuum to yield an intense orange solid crude extract (1.479 g). This was then transported to the University of Canterbury, where it was assayed for cytotoxicity, antimicrobial and antiviral activity.

7.4.2 Chromatography of F5031

The extract showed only weak cytotoxicity but very strong activity against *B. subtilis* (Sm 11) in the antimicrobial assay. Based on these results the extract was further analysed by analytical HPLC using the standard 10% gradient (Section 7.1.7.2). The HPLC profile revealed the extract to be very simple, seemingly containing a single family of four compounds that eluted between 18 and 22 minutes. The ELSD confirmed these to be the major sources of mass in the extract.

Due to the simplicity of the extract and the clear separation of the four metabolites, flash chromatography was deemed unnecessary. The extract (1.48 g) was first partitioned between MeOH and Pet ether. The resulting MeOH-soluble material (474 mg) was analysed by HPLC using the standard 10% gradient and was found to contain the metabolites in question. A portion (50 mg) of the MeOH-soluble fraction was purified using semi-preparative HPLC (Section 7.1.7.2) using a linear gradient (ACN/H_2O; 60:40-80:20% with 0.05% TFA over 20 minutes). This gave four metabolites (SAS-6-6.1–3 and SAS-6-14). On the basis of 1D and 2D NMR spectroscopy and mass spectrometry, SAS-6-6.1-3 were identified as three known vulpinic acid derivatives (**4.12**, **4.13**, **4.11**)

(3.1, 1.6, and 1.2 mg respectively), while SAS-6-14 was found to be a novel dichloro-vulpinic acid derivative (**4.14**) (2.1 mg).

*7.4.3 X-ray Crystallography of **4.14***

The structure of **4.14** was confirmed by X-ray crystallography. **4.14** was crystallised from MeOH. A plate crystal with dimensions 0.70 × 0.35 × 0.02 mm^3 was used for data collection. The data processing yielded 5260 Bragg reflections, of which 53% were unique. The final *R* factor was 3.8 %. See Appendix 1 for tables of data.

7.4.4 Physical Data for the Vulpinic Acid Derivatives

4,4'-dimethoxyvulpinic acid (4.11): orange/yellow powder; ^{1}H and ^{13}C-NMR data see Table 4.1; LCMS *m/z* 383 $[M+H]^+$.

methyl-3'-chloro-4,4'-di-O-methylatromentate (4.12): yellow/green amorphous solid; ^{1}H and ^{13}C-NMR data see Table 4.2; ESIMS *m/z* 417/419 $[M+H]^+$.

methyl 4,4'-dimethoxyvulpinate (4.13): yellow amorphous solid; ^{1}H and ^{13}C-NMR data, see Table 4.3; LCMS *m/z* 397 $[M+H]^+$.

Methyl-3',5'-dichloro-4,4'-di-*O*-methylatromentate (4.14): yellow needles (MeOH): m.p. 170-171°C; UV (MeOH) λ_{max} (log ε) 277 (3.84), 399 (3.60) nm; IR (KBr disk) ν_{max} 1733, 1710, 1600, 1225, 1255, 1188, 1072, 1311 cm^{-1}; ^{1}H- and ^{13}C-NMR data, see Table 4.4; EIMS *m/z* (%) 450/452/454 $[M]^+$ (7/5/1), 418/420/422 (100/67/13), 362/364/366 (35/20/5), 306/308/310 (28/18/4), 175 (19), 147 (57), 119 (41); HREIMS *m/z* 450.0266 $[M]^+$ (calc for $C_{21}H_{16}{}^{35}Cl_2O_7$ 450.0273).

7.5 Experimental for Chapter 5

7.5.1 Extraction and Chromatography of F5202

The second re-grow of F5202 was cultured on 24 MYE agar plates of dimensions stated in Section 7.1.1, at 26°C. After four weeks the plates were extracted with EtOAc according to the protocol also given in Section 7.1.1. This yielded the crude extract (23.5 mg). The extract was analysed by analytical HPLC using the standard 10% gradient (Section 7.1.7.2) and ELSD. The resulting chromatogram was not complex, and showed just one major compound. Semi-preparative HPLC using a linear gradient (35-60% ACN/H_2O with 0.05% TFA over 20 minutes) was used to purify the major compound. 1D and 2D NMR in conjunction with mass spectrometry confirmed the compound as a new acetophenone derivative (**5.7**) (3.9 mg).

7.5.2 X-ray Crystallography of **5.7**

The structure of **5.7** was confirmed by X-ray crystallography. **5.7** was crystallised from MeOH by slow evaporation at 4 °C. A plate crystal with dimensions 0.67 × 0.40 × 0.28 mm^3 was used for data collection. The data processing yielded 4327 Bragg reflections, of which 43% were unique. The final *R* factor was 14.1 %. See Appendix 1 for tables of data.

7.5.3 Physical Data for **5.7**

2,4 dihydroxy-3-(2-hydroxyethyl)-6-methoxyacetophenone (5.7): cream amorphous solid; UV (MeOH) λ_{max} (log ε) 226 (sh), 290 (3.99) nm; IR (KBr disk) ν_{max} 1618, 1294, 1151, 1111, 1011, 806 cm^{-1}; ^{1}H- and ^{13}C-NMR data, see Table 5.1; EIMS *m/z* (%) 226 $[M]^+$ (33), 208 (54), 195 (100); HREIMS *m/z* 226.0836 $[M]^+$ (calc for $C_{11}H_{14}O_5$ 226.0841).

7.6 Experimental for Chapter 6

7.6.1 Semi-Preparative HPLC Purification of the Trichoderma harzianum extract

A linear gradient of 10-70% ACN/H_2O with 0.05% TFA was used for purification this yielded the pure compounds, trichobutenolide, harzianolide A, and isoharzinaic acid.

7.6.2 Capillary Probe NMR

All NMR spectra, including the extracts from *Scleroderma* and the endophyte F5584 that were carried out at the Molecular Targets Development Program, National Cancer Institute, Fort Detrick, Frederick, Maryland. These data were recorded on a Varian INOVA 500 spectrometer at 23°C, operating at 500 MHz. The INOVA was equipped with with a variable temperature and capillary probe. Microtitre plates used in the analysis were obtained from the analytical HPLC using the standard method given in Section 7.1.4. Rather than making daughter plates however, the plates were dried using a centrifugal evaporator.

References and Notes

(1) Mann, J. *Chemical aspects of biosynthesis*; 1st ed.; Oxford University Press Inc.: New York, 1999.

(2) Bisset, N. G. *J. Ethnopharmacol.* **1992**, *36*, 1-26.

(3) Buss, A. D.; Waigh, R. D. In *Burger's Medicinal Chemistry and Drug Discovery*; 5th ed.; Wolff, M. E., Ed.; John Wiley & Sons, Inc.: 1995; Vol. 1, p 983-1033.

(4) Cragg, G. M.; Newman, D. J. *Pure Appl. Chem.* **2005**, *77*, 7-24.

(5) Butler, M. S. *J. Nat. Prod.* **2004**, *67*, 2141-2153.

(6) Aldrich, J. V. In *Burger's Medicinal Chemistry and Drug Discovery*; 5th ed.; Wolff, M. E., Ed.; John Wiley & Sons, Inc.: 1996; Vol. 3, p 321-441.

(7) Wainwright, M. *Miracle Cure: The Story of Penicillin and the Golden Age of Antibiotics*; Blackwell: Oxford, UK, 1990.

(8) Newman, D. J.; Cragg, G. M.; Snader, K. M. *Nat. Prod. Rep.* **2000**, *17*, 215-234.

(9) Koehn, F. E.; Carter, G. T. *Nat. Rev. Drug Discov.* **2005**, *4*, 206-220.

(10) Newman, D. J.; Cragg, G. M.; Snader, K. M. *J. Nat. Prod.* **2003**, *66*, 1022-1037.

(11) Paterson, I.; Anderson E. A. *Science* **2005**, *310*, 451-3.

(12) Clardy, J.; Walsh, C. *Nature (London, United Kingdom)* **2004**, *432*, 829-837.

(13) Martin, Y. C. *J. Comb. Chem.* **2001**, *3*, 231-250.

(14) Borman, S. *Chem. Eng. News* **2002**, *80*, 47-50.

(15) Tulp, M.; Bohlin, L. *Drug Discov. Today* **2004**, *9*, 450-458.

(16) Piel, J.; Hui, D.; Wen, G.; Butzke, D.; Platzer, M.; Fusetani, N. *Proc. Natl. Acad. Sci. U. S. A.* **2004**, *101*, 16222-16227.

(17) Wenzel, S. C.; Mueller, R. *Curr. Opin. Biotechnol.* **2005**, *16*, 594-606.

(18) Alberts, A. W.; Chen, J.; Kuron, G.; Hunt, V.; Huff, J.; Hoffman, C.; Rothrock, J.; Lopez, M.; Joshua, H.; Harris, E.; Patchett, A.; Monaghan, R.; Currie, S.; Stapley, E.; Albers-Schonberg, G.; Hensens, O.; Hirshfield, J.; Hoogsteen, K.; Liesch, J.; Springer, J. *Proc. Natl. Acad. Sci. U. S. A.* **1980**, *77*, 3957-3961.

(19) Liesch, J. M.; Hensens, O. D.; Springer, J. P.; Chang, R. S.; Lotti, V. J. *J. Antibiot.* **1985**, *38*, 1638-41.

(20) Herranz, R. *Med. Res. Rev.* **2003**, *23*, 559-605.

(21) Stierle, A. A.; Stierle, D. B. *Stud. Nat. Prod. Chem.* **2000**, *24*, 933-977.

(22) Strobel, G.; Daisy, B.; Castillo, U.; Harper, J. *J. Nat. Prod.* **2004**, *67*, 257-268.

(23) Bacon, C. W.; White, J. F *Microbial Endophytes*; Marcel Dekker, Inc.: New York, 2000.

(24) Gusman, J.; Vanhaelen, M. *Recent Res. Devel. Phytochem.* **2000**, *4*, 187-206.

(25) Strobel, G. A. *Crit. Rev. Biotechnol.* **2002**, *22*, 315-333.

(26) Taylor, T. N.; Taylor, E. L. In *Microbial Endophytes*; Bacon, C. W., White, J. F., Eds.; Marcel Dekker, Inc.: New York, 2000.

(27) Metz, A. M.; Haddad, A.; Worapong, J.; Long, D. M.; Ford, E. J.; Hess, W. M.; Strobel, G. A. *Microbiology (Reading, United Kingdom)* **2000**, *146*, 2079-2089.

(28) Schiff, P. B.; Horwitz, S. B. *Proc. Natl. Acad. Sci. U. S. A.* **1980**, *77*, 1561-5.

(29) Stierle, A.; Strobel, G.; Stierle, D. *Science (Washington, DC, United States)* **1993**, *260*, 214-17.

(30) Li, J. Y.; Strobel, G.; Sidhu, R.; Hess, W. M.; Ford, E. J. *Microbiology (Reading, England)* **1996**, *142 (Pt 8)*, 2223-6.

(31) Strobel, G. A.; Hess, W. M.; Li, J.-Y.; Ford, E.; Sears, J.; Sidhu, R. S.; Summerell, B. *Aust. J. Bot.* **1997**, *45*, 1073-1082.

(32) Strobel, G. A.; Ford, E.; Li, J. Y.; Sears, J.; Sidhu, R. S.; Hess, W. M. *System. Appl. Microbiol.* **1999**, *22*, 426-433.

(33) Guo, B.; Dai, J.-R.; Ng, S.; Huang, Y.; Leong, C.; Ong, W.; Carte, B. K. *J. Nat. Prod.* **2000**, *63*, 602-604.

(34) Strobel, G. A.; Miller, R. V.; Martinez-Miller, C.; Condron, M. M.; Teplow, D. B.; Hess, W. M. *Microbiology (Reading, England)* **1999**, *145*, 1919-1926.

(35) Brady, S. F.; Singh, M. P.; Janso, J. E.; Clardy, J. *J. Am. Chem. Soc.* **2000**, *122*, 2116-2117.

(36) Singh, M. P.; Janso, J. E.; Luckman, S. W.; Brady, S. F.; Clardy, J.; Greenstein, M.; Maiese, W. M. *J. Antibiot.* **2000**, *53*, 256-261.

(37) Stierle, A. A.; Stierle, D. B.; Bugni, T. *J. Org. Chem.* **1999**, *64*, 5479-5484.

(38) Lee, J. C.; Lobkovsky, E.; Pliam, N. B.; Strobel, G.; Clardy, J. *J. Org. Chem.* **1995**, *60*, 7076-7077.

(39) Peberdy, J. F. *Penicillium and Acremonium*; 1st ed.; Plenum Press, New York, 1987; Vol. 1.

(40) Miedes, E.; Lorences, E. P. *J. Agric. Food Chem.* **2004**, *52*, 7957-7963.

(41) Brian, P. W.; Elson, G. W.; Lowe, D. *Nature* **1956**, *178*, 263-4.

(42) Arora, R.; Pandey, G. N. *Int. J. Food Sci. Technol.* **1979**, *16*, 102-5.

(43) Sirisanthana, T. *Ann. Acad. Med., Singapore* **1997**, *26*, 701-4.

(44) Cooper, C. R., Jr.; Haycocks, N. G. *J. Eukaryot. Microbiol.* **2000**, *47*, 24-8.

(45) Marques, S. A.; Robles, A. M.; Tortorano, A. M.; Tuculet, M. A.; Negroni, R.; Mendes, R. P. *Med. Mycol.* **2000**, *38 Suppl 1*, 269-79.

(46) Fleming, A. *Br. J. Exp. Pathol.* **1929**, *10*, 226-36.

(47) www.elmhurst.edu/~chm/vchembook/652penicillin.html.

(48) Endo, A. *Int. Congr. Ser.* **2004**, *1262*, 3-8.

(49) Oxford, A. E.; Raistrick, H.; Simonart, P. *Biochem. J.* **1939**, *33*, 240-8.

(50) www.nlm.nih.gov/medlineplus/druginfo/medmaster/a682295.html.

(51) Gull, K.; Trinci, A. P. J. *Nature (London, United Kingdom)* **1973**, *244*, 292-4.

(52) Bloch, P.; Tamm, C.; Bollinger, P.; Petcher, T. J.; Weber, H. P. *Helv. Chim. Acta* **1976**, *59*, 133-7.

(53) Ando, O.; Satake, H.; Nakajima, M.; Sato, A.; Nakamura, T.; Kinoshita, T.; Furuya, K.; Haneishi, T. *J. Antibiot.* **1991**, *44*, 382-9.

(54) Breitenstein, W.; Chexal, K. K.; Mohr, P.; Tamm, C. *Helv. Chim. Acta* **1981**, *64*, 379-88.

(55) Bloch, P.; Tamm, C. *Helv. Chim. Acta* **1981**, *64*, 304-15.

(56) Weber, H. P.; Petcher, T. J.; Bloch, P.; Tamm, C. *Helv. Chim. Acta* **1976**, *59*, 137-40.

(57) Wenke, J.; Anke, H.; Sterner, O. *Biosci., Biotechnol., Biochem.* **1993**, *57*, 961-4.

(58) Hellwig, V.; Mayer-Bartschmid, A.; Mueller, H.; Greif, G.; Kleymann, G.; Zitzmann, W.; Tichy, H.-V.; Stadler, M. *J. Nat. Prod.* **2003**, *66*, 829-837.

(59) Komagata, D.; Fujita, S.; Yamashita, N.; Saito, S.; Morino, T. *J. Antibiot.* **1996**, *49*, 958-959.

(60) Maebayashi, Y.; Horie, Y.; Satoh, Y.; Yamazaki, M. *Mycotoxins* **1985**, *22*, 33-4.

(61) MacLean, W. J. A thesis submitted in partial fulfilment of the requirements for the degree of Doctor of Philosophy in Chemistry, University of Canterbury, 2005.

(62) Krohn, K.; Michel, A.; Floerke, U.; Aust, H.-J.; Draeger, S.; Schulz, B. *Liebigs Ann. Chem.* **1994**, 1093-7.

(63) Weber, H. A.; Baenziger, N. C.; Gloer, J. B. *J. Am. Chem. Soc.* **1990**, *112*, 6718-19.

(64) McDonald, L. A.; Abbanat, D. R.; Barbieri, L. R.; Bernan, V. S.; Discafani, C. M.; Greenstein, M.; Janota, K.; Korshalla, J. D.; Lassota, P.; Tischler, M.; Carter, G. T. *Tetrahedron Lett.* **1999**, *40*, 2489-2492.

(65) Bode, H. B.; Wegner, B.; Zeeck, A. *J. Antibiot.* **2000**, *53*, 153-157.

(66) Kouam; Mpondo, T. N.; Lavaud, C.; Massiot, G.; Nuzillard, J.-M.; Connolly, J. D.; Rycroft, D. S. *Nat. Prod. Lett.* **1993**, *3*, 299-303.

(67) Ravindranath, N.; Ravinder Reddy, M.; Mahender, G.; Ramu, R.; Ravi Kumar, K.; Das, B. *Phytochemistry* **2004**, *65*, 2387-2390.

(68) Prajoubklang, A.; Sirithunyalug, B.; Charoenchai, P.; Suvannakad, R.; Sriubolmas, N.; Piyamongkol, S.; Kongsaeree, P.; Kittakoop, P. *Chem. Biodiversity* **2005**, *2*, 1358-1367.

(69) King, I.; Blood, C.; Chu, M.; Patel, M.; Liu, M.; Li, Z.; Robertson, N.; Maxwell, E.; Catino, J. J. *Oncol. Res.* **1995**, *7*, 1-5.

(70) Chu, M.; Truumees, I.; Patel, M. G.; Gullo, V. P.; Pai, J. K.; Das, P. R.; Puar, M. S. *Bioorg. Med. Chem. Lett.* **1994**, *4*, 1539-42.

(71) Chu, M.; Patel, M. G.; Pai, J.-K.; Das, P. R.; Puar, M. S. *Bioorg. Med. Chem. Lett.* **1996**, *6*, 579-84.

(72) Pai, J.-K.; Frank, E. A.; Blood, C.; Chu, M. *Anti-cancer Drug Des.* **1994**, *9*, 363-72.

(73) Sakemi, S.; Inagaka, T.; Kaneda, K.; Hirai, H.; Iwata, E.; Sakakibara, T.; Yamauchi, Y.; Norcia, M.; Wondrack, L. M.; et al. *J. Antibiot.* **1995**, *48*, 134-42.

(74) Singh, S. B.; Zink, D. L.; Liesch, J. M.; Ball, R. G.; Goetz, M. A.; Bolessa, E. A.; Giacobbe, R. A.; Silverman, K. C.; Bills, G. F.; et al. *J. Org. Chem.* **1994**, *59*, 6296-302.

(75) Wipf, P.; Hopkins, T. D.; Jung, J. K.; Rodriguez, S.; Birmingham, A.; Southwick, E. C.; Lazo, J. S.; Powis, G. *Bioorg. Med. Chem. Lett.* **2001**, *11*, 2637-2641.

(76) An HPLC-based UV database constructed using chromeleon software, operated by J. W. Blunt and M. H. G. Munro, University of Canterbury. UV chromatograms and retention times of all natural products run through the system are stored in libraries.

(77) A new database compiled from the MarinLit and AntiBase databases, owned and operated by Blunt and Munro, University of Canterbury and Laatsch, University of Goettingen.

(78) Weber, H. A.; Gloer, J. B. *J. Org. Chem.* **1991**, *56*, 4355-60.

(79) Ward, D. E.; Rhee, C. K. *Tetrahedron Lett.* **1991**, *32*, 7165-6.

(80) Krohn, K.; Michel, A.; Floerke, U.; Aust, H.-J.; Draeger, S.; Schulz, B. *Liebigs Ann. Chem.* **1994**, 1099-108.

(81) Misra, R.; Pandey, R. C.; Silverton, J. V. *J. Am. Chem. Soc.* **1982**, *104*, 4478-9.

(82) Seco, J. M.; Quiñoá, E.; Riguera, R. *Tetrahedron: Asymmetry* **2000**, *11*, 2781-2791.

(83) Freire, F.; Seco, J. M.; Quiñoá, E.; Riguera, R. *J. Org. Chem.* **2005**, *70*, 3778-3790.

(84) Fabro, S.; Smith, R. L.; Williams, R. T. *Nature (London, United Kingdom)* **1967**, *215*, 296.

(85) Bode, H. B.; Zeeck, A. *Phytochemistry* **2000**, *55*, 311-316.

(86) Byrne, K. M.; Hilton, B. D.; White, R. J.; Misra, R.; Pandey, R. C. *Biochemistry* **1985**, *24*, 478-86.

(87) Thomas, R. *ChemBioChem* **2001**, *2*, 612-627.

(88) Abraham, R. J.; Loftus, P. *Proton and Carbon-13 NMR Spectroscopy: An integrated approach*; Heyden & Son Ltd., 1980.

(89) Abell, C.; Garson, M. J.; Leeper, F. J.; Staunton, J. *J. Chem. Soc., Chem. Commun.* **1982**, 1011-13.

(90) Abell, C.; Doddrell, D. M.; Garson, M. J.; Laue, E. D.; Staunton, J. *J. Chem. Soc., Chem. Commun.* **1983**, 694-6.

(91) Hall, I. R.; Stephenson, S. L.; Buchanan, P. K.; Yun, W.; Cole, A. L. J. *Edible and poisonous mushrooms of the world*; New Zealand Institute for Crop & Food Research Limited: Christchurch, New Zealand, 2003.

(92) Sims, K. P.; Watling, R.; Jeffries, P. *Mycotaxon* **1995**, *LVI*, 403-420.

(93) Bresinsky, A.; Besl, H. *A colour atlas of Poisonous fungi: A handbook for Phamacists, Doctors and Biologists*; Wolfe Publishing Ltd., 1990.

(94) Kanokmedhakul, S.; Kanokmedhakul, K.; Prajuabsuk, T.; Soytong, K.; Kongsaeree, P.; Suksamrarn, A. *Planta Med.* **2003**, *69*, 568-571.

(95) Entwistle, N.; Pratt, A. D. *Tetrahedron* **1968**, *24*, 3949-53.

(96) Gill, M.; Steglich, W. *Prog. Chem. Org. Nat. Prod.* **1987**, *51*, 286 pp.

(97) Mueller, K. *Appl. Microbiol. Biotechnol.* **2001**, *56*, 9-16.

(98) Foden, F. R.; McCormick, J.; O'Mant, D. M. *J. Med. Chem.* **1975**, *18*, 199-203.

(99) Soderberg, U. *Acta Physiol. Scand.* **1952**, *27*, 97-8.

(100) Binder, M.; Bresinsky, A. *Mycologia* **2002**, *94*, 85-98.

(101) Steglich, W.; Furtner, W.; Prox, A. *Z. Naturforsch., B: Chem. Sci.* **1968**, *23*, 1044-50.

(102) Marumoto, R.; Kilpert, C.; Steglich, W. *Z. Naturforsch., C: Biosci.* **1986**, *41*, 363-5.

(103) Singh, P.; Anchel, M. *Phytochemistry* **1971**, *10*, 3259-62.

(104) Winner, M.; Gimenez, A.; Schmidt, H.; Sontag, B.; Steffan, B.; Steglich, W. *Angew. Chem.* **2004**, *43*, 1883-1886.

(105) Beaumont, P. C.; Edwards, R. L.; Elsworthy, G. C. *J. Chem. Soc. C* **1968**, 2968-74.

(106) Steffan, B.; Steglich, W. *Angew. Chem.* **1984**, *23*, 445-7.

(107) Aumann, D. C.; Clooth, G.; Steffan, B.; Steglich, W. *Angew. Chem.* **1989**, *28*, 453-454.

(108) Gill, M. *Nat. Prod. Rep.* **2003**, *20*, 615-639.

(109) Arnold, N.; Steglich, W.; Besl, H. *Z. Mykol.* **1996**, *62*, 69-73.

(110) Letcher, R. M.; Eggers, S. H. *Tetrahedron Lett.* **1967**, 3541-6.

(111) Abrell, L. M.; Borgeson, B.; Crews, P. *Tetrahedron Lett.* **1996**, *37*, 8983-8984.

(112) Kamal, A.; Ahmad, N.; Khan, M. A.; Qureshi, I. H. *Tetrahedron* **1962**, *18*, 433-6.

(113) Crawley, G. C. *J. Chem. Soc., Perkin Trans. 1* **1981**, 221-3.

(114) Cheng, M.-J.; Lee, S.-J.; Chang, Y.-Y.; Wu, S.-H.; Tsai, I.-L.; Jayaprakasam, B.; Chen, I.-S. *Phytochemistry* **2003**, *63*, 603-608.

(115) Gonzalez, M. J. T. G.; DeOliveira, C. J. C.; Fernandes, J. O.; Kijjoa, A.; Herz, W. *Phytochemistry* **1996**, *43*, 1333-1337.

(116) Kamal, A.; Qureshi, A. A.; Khan, M. A.; Khan, F. M. *Tetrahedron* **1963**, *19*, 117-22.

(117) Kamal, A.; Qureshi, A. A.; Ahmad, A.; Rickards, R. W. *Tetrahedron* **1965**, *21*, 1411-15.

(118) Nakakita, Y.; Shima, S.; Sakai, H. *Agri. Biol. Chem.* **1984**, *48*, 1899-900.

(119) Kamal, A.; Begum, T.; Qureshi, A. A. *Pak. J. Sci. Ind. Res.* **1971**, *14*, 86-9.

(120) Venkatasubbaiah, P.; Tisserat, N. A.; Chilton, W. S. *Mycopathologia* **1994**, *128*, 155-9.

(121) Bradshaw, J.; Butina, D.; Dunn, A. J.; Green, R. H.; Hajek, M.; Jones, M. M.; Lindon, J. C.; Sidebottom, P. J. *J. Nat. Prod.* **2001**, *64*, 1541-1544.

(122) Bailey, N. J. C.; Marshall, I. R. *Anal. Chem.* **2005**, *77*, 3947-3953.

(123) Ermer, J.; Vogel, M. *Biomed. Chromatogr.* **2000**, *14*, 373-383.

(124) Exarchou, V.; Krucker, M.; van Beek, T. A.; Vervoort, J.; Gerothanassis, I. P.; Albert, K. *Magn. Reson. Chem.* **2005**, *43*, 681-687.

(125) Spraul, M.; Freund, A. S.; Nast, R. E.; Withers, R. S.; Maas, W. E.; Corcoran, O. *Anal. Chem.* **2003**, *75*, 1536-1541.

(126) Gronquist, M.; Meinwald, J.; Eisner, T.; Schroeder, F. C. *J. Am. Chem. Soc.* **2005**, *127*, 10810-10811.

(127) Nielsen, K. F.; Smedsgaard, J. *J. Chromatogr. A.* **2003**, *1002*, 111-136.

(128) Kawada, M.; Yoshimoto, Y.; Kumagai, H.; Someno, T.; Momose, I.; Kawamura, N.; Isshiki, K.; Ikeda, D. *J. Antibiot.* **2004**, *57*, 235-237.

(129) Sawa, R.; Mori, Y.; Iinuma, H.; Naganawa, H.; Hamada, M.; Yoshida, S.; Furutani, H.; Kajimura, Y.; Fuwa, T.; Takeuchi, T. *J. Antibiot.* **1994**, *47*, 731-2.

(130) Claydon, N.; Hanson, J. R.; Truneh, A.; Avent, A. G. *Phytochemistry* **1991**, *30*, 3802-3.

(131) Avent, A. G.; Hanson, J. R.; Truneh, A. *Phytochemistry* **1992**, *31*, 791-3.

(132) Mitova, M. I. Unpublished data.

(133) Oh, H.; Gloer, J. B.; Shearer, C. A. *J. Nat. Prod.* **1999**, *62*, 497-501.

(134) Cheng, X. C.; Jensen, P. R.; Fenical, W. *J. Nat. Prod.* **1999**, *62*, 608-10.

(135) Thines, E.; Daussmann, T.; Semar, M.; Sterner, O.; Anke, H. *Z. Naturforsch., C: Biosci.* **1995**, *50*, 813-19.

(136) Olson, D. L.; Norcross, J. A.; O'Neil-Johnson, M.; Molitor, P. F.; Detlefsen, D. J.; Wilson, A. G.; Peck, T. L. *Anal. Chem.* **2004**, *76*, 2966-2974.

(137) Wu, N.; Peck, T. L.; Webb, A. G.; Magin, R. L.; Sweedler, J. V. *J. Am. Chem. Soc.* **1994**, *116*, 7929-7930.

(138) Wu, N.; Peck, T. L.; Webb, A. G.; Magin, R. L.; Sweedler, J. V. *Anal. Chem.* **1994**, *66*, 3849-3857.

(139) Behnke, B.; Schlotterbeck, G.; Tallarek, U.; Strohschein, S.; Tseng, L.-H.; Keller, T.; Albert, K.; Bayer, E. *Anal. Chem.* **1996**, *68*, 1110-1115.

(140) *APEX II. User Manual*; Bruker AXS, Inc. Karlsruhe, Germany 2005.

(141) Sheldrick, G. M. *Acta Crystallogr., Sect. A: Found. Crystallogr.* **1990**, *46*, 467-473.

(142) Sheldrick, G. M. *SHELXTL Reference Manual*; Siemens Energy and Automation Inc. Madison, W1, 1997; Vol. version 5.

(143) Attenburrow, J.; Cameron, A. F. B.; Chapman, J. H.; Evans, R. M.; Hems, B. A.; Jansen, A. B. A.; Walker, T. *J. Chem. Soc., Abst.* **1952**, 1094-111.

(144) Ates, A.; Gautier, A.; Leroy, B.; Plancher, J.-M.; Quesnel, Y.; Mark, I. E. *Tetrahedron Lett.* **1999**, *40*, 1799-1802.

(145) Marko, I. E.; Ates, A.; Gautier, A.; Leroy, B.; Plancher, J.-M.; Quesnel, Y.; Vanherck, J.-C. *Angew. Chem.* **1999**, *38*, 3207-3209.

Appendix 1

X-ray crystallographic data for:

*pseurotin A_2 (**2.8**)*

*spiro-mamakone C (**3.15**)*

*methyl-3',5'-dichloro-4,4'-di-O-methylatromentate (**4.14**)*

*1,5-dihydroxy-6-(2-hydroxyethyl)-3-methoxyacetophenone (**5.7**)*

Table 1.1: *Crystal data and structure refinement for* ***2.8***

Empirical formula	C44 H50 N2 O16
Formula weight	862.86
Temperature	113(2) K
Wavelength	0.71073 A
Crystal system, space group	Tetragonal, P4(1)
Unit cell dimensions	a = 10.538(10) A alpha = 90 deg.
	b = 10.538(19) A beta = 90 deg.
	c = 41.99(7) A gamma = 90 deg.
Volume	4663(10) A^3
Z, Calculated density	4, 1.229 Mg/m^3
Absorption coefficient	0.094 mm^-1
F(000)	1824
Crystal size	0.44 x 0.24 x 0.23 mm
Theta range for data collection	1.94 to 26.43 deg.
Reflections collected / unique	32305 / 9312 [R(int) = 0.1175]
Completeness to theta = 26.43	97.9%
Absorption correction	none
Max. and min. transmission	0.9847 and 0.9551
Refinement method	Full-matrix least-squares on F^2
Data / restraints / parameters	9312 / 217 / 572
Goodness-of-fit on F^2	1.531
Final R indices [I>2sigma(I)]	R1 = 0.1575, wR2 = 0.3806
R indices (all data)	R1 = 0.195, wR2 = 0.4038
Largest diff. peak and hole	3.228 and -0.693 e.A^-3

Table 1.2: *Atomic coordinates (x 10^4) and equivalent isotropic displacement Parameters (A^2 x 10^3) for pseurotin* A_2 *(***2.8***). U(eq) is defined as one third of the trace of the orthogonalised Uij tensor.*

	x	**y**	**z**	**U(eq)**
O(1)	1800(14)	8648(13)	1493(3)	19(3)
C(2)	1810(20)	9895(19)	1598(5)	17(4)
C(3)	2220(20)	10090(20)	1905(6)	26(5)
C(4)	2430(20)	8770(20)	2020(5)	24(5)
C(5)	2100(20)	7850(20)	1783(5)	20(4)
C(6)	3186(19)	6966(18)	1700(5)	12(4)
N(7)	2843(17)	5771(17)	1790(4)	19(4)
C(8)	1586(19)	5702(17)	1937(5)	15(4)
C(9)	890(30)	6920(20)	1827(7)	37(6)
C(10)	1549(17)	10833(18)	1321(4)	13(4)
C(11)	2662(18)	10933(19)	1111(5)	15(4)
C(12)	2420(20)	11860(20)	844(6)	29(5)

C(13)	2140(20)	11650(20)	531(6)	30(5)
C(14)	2200(30)	10370(30)	376(5)	34(6)
C(15)	800(30)	9760(30)	378(8)	54(8)
C(16)	2420(20)	11270(20)	2069(6)	30(5)
C(17)	848(18)	4509(18)	1826(4)	13(4)
C(18)	-480(20)	4220(20)	1939(5)	22(4)
C(19)	-1090(20)	4940(20)	2168(6)	31(5)
C(20)	-2400(20)	4710(30)	2244(6)	30(6)
C(21)	-2970(50)	3630(40)	2092(9)	71(12)
C(22)	-2460(20)	3090(20)	1861(6)	33(6)
C(23)	-1110(20)	3250(20)	1767(6)	25(5)
C(24)	2240(20)	4550(20)	2404(5)	26(5)
O(4)	2718(17)	8508(16)	2321(4)	28(4)
O(7)	4184(15)	7319(14)	1589(4)	26(4)
O(8)	1670(14)	5647(13)	2274(4)	23(3)
O(9)	316(15)	6673(15)	1555(4)	25(3)
O(10)	417(15)	10488(13)	1186(4)	21(3)
O(11)	3767(16)	11338(15)	1270(4)	30(4)
O(17)	1460(20)	3838(16)	1628(4)	39(5)
O(1')	6699(17)	1198(13)	1055(4)	27(4)
C(2')	6843(18)	-104(19)	961(5)	14(4)
C(3')	7153(18)	-196(18)	651(5)	13(4)
C(4')	7296(19)	1015(19)	504(5)	15(4)
C(5')	7010(20)	1965(19)	791(5)	18(4)
C(6')	8130(30)	2840(20)	847(7)	40(7)
N(7')	7739(17)	4026(17)	758(4)	18(4)
C(8')	6528(19)	4158(18)	612(5)	13(4)
C(9')	5884(17)	2904(16)	703(4)	8(3)
C(10')	6621(19)	-1030(19)	1206(5)	15(4)
C(11')	7660(20)	-1050(20)	1460(5)	22(4)
C(12')	7440(20)	-2040(20)	1731(5)	25(5)
C(13')	7570(30)	-1690(30)	2037(10)	56(10)
C(14')	7890(40)	-340(40)	2150(11)	76(11)
C(15')	6160(80)	30(50)	2166(17)	173(13)
C(16')	7380(20)	-1480(20)	465(5)	23(5)
C(17')	5830(20)	5300(20)	768(5)	22(4)
C(18')	4432(19)	5571(18)	656(5)	15(4)
C(19')	3870(20)	4990(20)	387(5)	22(5)
C(20')	2770(30)	5440(30)	308(6)	48(8)
C(21')	1970(20)	6200(20)	487(5)	17(4)
C(22')	2640(30)	6790(20)	762(5)	32(6)
C(23')	3770(20)	6510(20)	816(5)	22(5)
C(24')	7205(18)	5202(18)	130(5)	14(4)
O(4')	7541(17)	1308(16)	230(4)	35(4)
O(6')	9133(18)	2576(15)	980(4)	32(4)

O(8')	6564(14)	4145(14)	282(4)	21(3)
O(9')	5168(16)	3244(16)	1013(3)	25(3)
O(10')	5441(13)	-609(15)	1383(4)	26(4)
O(11')	8785(14)	-1542(14)	1269(4)	21(3)
O(17')	6341(13)	6055(12)	919(3)	17(3)

Table 1.3: *Bond lengths [A] and angles [deg] for pseurotin A_2 (**2.8**)*

O(1)-C(2)	1.39(3)	C(2)-O(1)-C(5)	105.4(15)
O(1)-C(5)	1.51(3)	O(1)-C(2)-C(3)	116.3(18)
C(2)-C(3)	1.37(3)	O(1)-C(2)-C(10)	111.3(16)
C(2)-C(10)	1.55(3)	C(3)-C(2)-C(10)	131.8(19)
C(3)-C(16)	1.45(3)	C(2)-C(3)-C(16)	128(2)
C(3)-C(4)	1.48(3)	C(2)-C(3)-C(4)	103(2)
C(4)-O(4)	1.33(3)	C(16)-C(3)-C(4)	129(2)
C(4)-C(5)	1.43(3)	O(4)-C(4)-C(5)	125(2)
C(5)-C(6)	1.52(3)	O(4)-C(4)-C(3)	123(2)
C(5)-C(9)	1.62(3)	C(5)-C(4)-C(3)	111.5(19)
C(6)-O(7)	1.21(3)	C(4)-C(5)-O(1)	103.6(17)
C(6)-N(7)	1.36(3)	C(4)-C(5)-C(6)	112.9(18)
N(7)-C(8)	1.46(3)	O(1)-C(5)-C(6)	108.1(16)
C(8)-O(8)	1.42(2)	C(4)-C(5)-C(9)	122(2)
C(8)-C(9)	1.55(3)	O(1)-C(5)-C(9)	105.5(17)
C(8)-C(17)	1.55(3)	C(6)-C(5)-C(9)	104.2(17)
C(9)-O(9)	1.32(3)	O(7)-C(6)-N(7)	128.4(18)
C(10)-O(10)	1.37(2)	O(7)-C(6)-C(5)	123.8(18)
C(10)-C(11)	1.47(3)	N(7)-C(6)-C(5)	107.6(17)
C(11)-O(11)	1.41(3)	C(6)-N(7)-C(8)	113.8(16)
C(11)-C(12)	1.51(3)	O(8)-C(8)-N(7)	111.5(16)
C(12)-C(13)	1.36(3)	O(8)-C(8)-C(9)	111.2(16)
C(13)-C(14)	1.51(4)	N(7)-C(8)-C(9)	105.3(16)
C(14)-C(15)	1.61(4)	O(8)-C(8)-C(17)	107.4(15)
C(17)-O(17)	1.27(3)	N(7)-C(8)-C(17)	111.6(15)
C(17)-C(18)	1.51(3)	C(9)-C(8)-C(17)	110.0(17)
C(18)-C(23)	1.41(3)	O(9)-C(9)-C(8)	108.5(18)
C(18)-C(19)	1.39(3)	O(9)-C(9)-C(5)	112(2)
C(19)-C(20)	1.43(3)	C(8)-C(9)-C(5)	99.5(19)
C(20)-C(21)	1.43(5)	O(10)-C(10)-C(11)	117.5(16)
C(21)-C(22)	1.24(5)	O(10)-C(10)-C(2)	107.4(16)
C(22)-C(23)	1.49(3)	C(11)-C(10)-C(2)	110.6(16)
C(24)-O(8)	1.41(3)	O(11)-C(11)-C(10)	113.2(16)
O(1')-C(5')	1.41(3)	O(11)-C(11)-C(12)	107.2(18)
O(1')-C(2')	1.44(2)	C(10)-C(11)-C(12)	111.0(17)
C(2')-C(3')	1.34(3)	C(13)-C(12)-C(11)	130(2)
C(2')-C(10')	1.44(3)	C(12)-C(13)-C(14)	123(2)

C(3')-C(4')	1.43(3)	C(13)-C(14)-C(15)	109(2)
C(3')-C(16')	1.58(3)	O(17)-C(17)-C(18)	124.5(19)
C(4')-O(4')	1.22(3)	O(17)-C(17)-C(8)	113.1(17)
C(4')-C(5')	1.59(3)	C(18)-C(17)-C(8)	122.4(16)
C(5')-C(6')	1.52(3)	C(23)-C(18)-C(19)	122(2)
C(5')-C(9')	1.59(3)	C(23)-C(18)-C(17)	114.8(19)
C(6')-O(6')	1.22(4)	C(19)-C(18)-C(17)	123(2)
C(6')-N(7')	1.37(3)	C(18)-C(19)-C(20)	120(2)
N(7')-C(8')	1.42(3)	C(21)-C(20)-C(19)	116(3)
C(8')-O(8')	1.39(2)	C(22)-C(21)-C(20)	122(3)
C(8')-C(17')	1.56(3)	C(21)-C(22)-C(23)	125(3)
C(8')-C(9')	1.53(3)	C(18)-C(23)-C(22)	113(2)
C(9')-O(9')	1.55(2)	C(24)-O(8)-C(8)	116.5(16)
C(10')-O(10')	1.51(3)	C(5')-O(1')-C(2')	107.8(15)
C(10')-C(11')	1.53(3)	C(3')-C(2')-O(1')	111.2(16)
C(11')-O(11')	1.52(3)	C(3')-C(2')-C(10')	133.1(19)
C(11')-C(12')	1.56(3)	O(1')-C(2')-C(10')	115.7(17)
C(12')-C(13')	1.34(5)	C(2')-C(3')-C(4')	112.3(17)
C(13')-C(14')	1.53(5)	C(2')-C(3')-C(16')	125.3(18)
C(14')-C(15')	1.87(9)	C(4')-C(3')-C(16')	122.4(17)
C(17')-O(17')	1.15(3)	O(4')-C(4')-C(3')	131.1(19)
C(17')-C(18')	1.57(3)	O(4')-C(4')-C(5')	126.5(19)
C(18')-C(23')	1.39(3)	C(3')-C(4')-C(5')	102.4(16)
C(18')-C(19')	1.42(3)	O(1')-C(5')-C(6')	114.3(19)
C(19')-C(20')	1.30(4)	O(1')-C(5')-C(9')	111.2(16)
C(20')-C(21')	1.39(3)	C(6')-C(5')-C(9')	103.9(18)
C(21')-C(22')	1.49(3)	O(1')-C(5')-C(4')	106.1(16)
C(22')-C(23')	1.25(4)	C(6')-C(5')-C(4')	110.7(17)
C(24')-O(8')	1.45(2)	C(9')-C(5')-C(4')	110.7(15)

Table 1.4: *Anisotropic displacement parameters (A^2 x 10^3) for pseurotin A_2 (**2.8**). The anisotropic displacement factor takes the form: -2pi^2 [h^2 a*^2 U11 + ... +2hka*b* U12].*

	U11	**U22**	**U33**	**U23**	**U13**	**U12**
O(1)	16(7)	19(7)	24(8)	9(6)	9(6)	8(6)
C(2)	17(4)	17(4)	17(4)	0(2)	0(2)	0(2)
C(3)	26(5)	26(5)	26(5)	0(2)	0(2)	0(2)
C(4)	24(5)	24(5)	24(5)	1(2)	0(2)	0(2)
C(5)	20(5)	20(5)	20(5)	0(2)	0(2)	0(2)
C(6)	13(4)	12(4)	12(4)	0(2)	0(2)	0(2)
N(7)	19(4)	19(4)	19(4)	0(2)	0(2)	0(2)
C(8)	19(10)	7(8)	18(9)	-2(7)	9(8)	7(7)
C(9)	46(16)	15(11)	49(16)	-7(10)	22(13)	-7(10)
C(10)	13(4)	13(4)	12(4)	1(2)	0(2)	0(2)

C(11)	15(4)	15(4)	16(4)	1(2)	0(2)	0(2)
C(12)	25(12)	33(13)	29(12)	11(10)	9(10)	19(10)
C(13)	30(5)	30(5)	30(5)	0(2)	0(2)	0(2)
C(14)	54(16)	40(14)	9(9)	-6(10)	-7(10)	18(12)
C(15)	54(8)	53(8)	54(8)	0(3)	-2(3)	0(3)
C(16)	31(6)	29(6)	30(6)	2(3)	1(3)	1(3)
C(17)	13(4)	12(4)	13(4)	0(2)	0(2)	0(2)
C(18)	22(5)	22(5)	23(5)	0(2)	-1(2)	1(2)
C(19)	31(6)	31(6)	30(6)	0(2)	1(2)	0(2)
C(20)	13(10)	49(15)	28(12)	-10(12)	14(9)	16(10)
C(21)	100(30)	60(20)	60(20)	4(18)	20(20)	-30(20)
C(22)	33(6)	33(6)	33(6)	0(2)	1(2)	-1(2)
C(23)	19(11)	13(9)	42(13)	-16(10)	-6(10)	9(8)
C(24)	26(6)	27(6)	27(6)	1(3)	1(3)	2(3)
O(4)	37(9)	30(9)	18(7)	-13(7)	4(7)	-8(7)
O(7)	20(8)	11(7)	48(10)	4(7)	9(7)	11(6)
O(8)	22(7)	11(7)	35(8)	-1(6)	-4(7)	5(6)
O(9)	23(8)	18(7)	35(9)	6(7)	-16(7)	-6(6)
O(10)	30(9)	9(7)	23(8)	9(6)	-7(7)	2(6)
O(11)	33(9)	25(8)	32(8)	-12(7)	8(8)	-13(7)
O(17)	71(14)	24(8)	21(8)	-11(7)	-3(9)	6(9)
O(1')	49(10)	4(6)	28(8)	5(6)	13(8)	4(7)
C(2')	8(8)	19(10)	16(9)	10(8)	2(7)	9(7)
C(3')	13(4)	13(4)	13(4)	0(2)	0(2)	0(2)
C(4')	15(4)	15(4)	15(4)	-1(2)	1(2)	0(2)
C(5')	18(4)	18(4)	18(4)	0(2)	1(2)	0(2)
C(6')	48(16)	33(13)	38(14)	-7(11)	25(13)	-5(12)
N(7')	18(4)	18(4)	19(4)	0(2)	0(2)	0(2)
C(8')	13(4)	14(4)	13(4)	-1(2)	0(2)	-1(2)
C(9')	8(4)	8(4)	8(4)	-1(2)	1(2)	0(2)
C(10')	16(4)	15(4)	15(4)	0(2)	0(2)	0(2)
C(11')	22(5)	22(5)	22(5)	1(2)	0(2)	0(2)
C(12')	25(5)	25(5)	25(5)	0(2)	0(2)	1(2)
C(13')	22(14)	36(15)	110(30)	21(17)	2(15)	23(12)
C(14')	76(11)	76(11)	76(11)	0(2)	0(2)	0(2)
C(15')	261(14)	83(14)	174(14)	0(3)	194(3)	0(3)
C(16')	24(5)	22(5)	24(5)	1(3)	1(3)	-1(3)
C(17')	22(5)	22(5)	22(5)	0(2)	1(2)	0(2)
C(18')	14(4)	15(4)	15(4)	0(2)	-1(2)	0(2)
C(19')	21(5)	22(5)	22(5)	0(2)	0(2)	0(2)
C(20')	65(19)	70(20)	13(11)	1(13)	3(12)	27(16)
C(21')	17(4)	17(4)	17(4)	0(2)	0(2)	-1(2)
C(22')	56(16)	23(11)	18(10)	-18(10)	2(11)	-8(11)
C(23')	23(5)	22(5)	22(5)	0(2)	1(2)	0(2)
C(24')	15(5)	12(5)	14(5)	1(3)	1(3)	1(3)

O(4')	41(10)	18(8)	46(10)	10(8)	18(8)	1(7)
O(6')	41(10)	23(8)	33(9)	5(7)	-20(8)	17(8)
O(8')	21(3)	20(3)	21(3)	0(2)	0(2)	-1(2)
O(9')	31(8)	30(8)	14(7)	-1(6)	6(6)	-14(7)
O(10')	5(6)	33(9)	39(9)	32(7)	-2(6)	-8(6)
O(11')	21(4)	19(4)	24(4)	0(3)	0(3)	-2(3)
O(17')	14(7)	4(6)	32(8)	-4(6)	-5(6)	-1(5)

Table1.5: *Hydrogen coordinates (x10^4) and isotropic displacement parameters (A^2x10^3) for pseurotin A_2 (**2.8**).*

	x	**y**	**z**	**U(eq)**
H(7)	3333	5103	1762	23
H(9)	284	7235	1992	44
H(10)	1420	11688	1419	15
H(11)	2830	10079	1015	18
H(12)	2471	12728	904	35
H(13)	1899	12361	404	36
H(14A)	2798	9814	494	41
H(14B)	2512	10452	154	41
H(15A)	547	9570	597	80
H(15B)	801	8970	253	80
H(15C)	197	10358	284	80
H(16A)	3100	11748	1961	45
H(16B)	2671	11106	2290	45
H(16C)	1640	11776	2066	45
H(19)	-644	5593	2276	37
H(20)	-2856	5235	2386	36
H(21)	-3753	3314	2171	86
H(22)	-2976	2550	1735	40
H(23)	-705	2748	1608	30
H(24A)	1595	3901	2442	40
H(24B)	2657	4767	2606	40
H(24C)	2880	4222	2255	40
H(9A)	-438	6928	1565	38
H(10A)	-163	10962	1254	31
H(11A)	4187	11819	1150	45
H(7')	8224	4693	790	22
H(9')	5315	2565	532	10
H(10')	6500	-1894	1112	18
H(11')	7830	-180	1548	26
H(12')	7218	-2888	1680	30
H(13')	7452	-2321	2195	67
H(14C)	8360	164	1991	91

H(14D)	8312	-317	2360	91
H(15D)	5865	299	1955	259
H(15E)	6009	715	2320	259
H(15F)	5685	-727	2232	259
H(16D)	8265	-1741	490	35
H(16E)	7195	-1350	239	35
H(16F)	6819	-2137	551	35
H(19')	4268	4314	273	26
H(20')	2478	5229	101	58
H(21')	1096	6335	440	21
H(22')	2216	7381	896	39
H(23')	4208	6975	977	27
H(24D)	6880	6001	217	20
H(24E)	7050	5175	-100	20
H(24F)	8119	5143	171	20
H(9'1)	4523	2780	1030	37
H(10B)	5197	-1194	1504	38
H(11B)	9295	-1911	1392	32

Table 1.6: *Crystal data and structure refinement for* ***3.15***

Empirical formula	C19 H14 O5
Formula weight	322.3
Temperature	93(2) K
Wavelength	0.71073 A
Crystal system, space group	Monoclinic, P2(1)/c
Unit cell dimensions	a = 7.0404(19) A alpha = 90 deg.
	b = 8.6194(19) A beta = 91.611(13) deg.
	c = 24.924(6) A gamma = 90 deg.
Volume	1511.9(7) A^3
Z, Calculated density	4, 1.416 Mg/m^3
Absorption coefficient	0.103 mm^-1
F(000)	672
Crystal size	0.45 x 0.20 x 0.15 mm
Theta range for data collection	1.63 to 24.99 deg.
Limiting indices	-7<=h<=7, -8<=k<=9, -29<=l<=20
Reflections collected / unique	1652 / 1369 [R(int) = 0.0758]
Completeness to theta = 24.99	51.40%
Absorption correction	Semi-empirical from equivalents
Max. and min. transmission	0.9847 and 0.9551
Refinement method	Full-matrix least-squares on F^2
Data / restraints / parameters	1369 / 24 / 219
Goodness-of-fit on F^2	1.056
Final R indices [I>2sigma(I)]	R1 = 0.0745, wR2 = 0.2008
R indices (all data)	R1 = 0.0872, wR2 = 0.2151
Largest diff. peak and hole	0.512 and -0.361 e.A^-3

Table 1.7: *Atomic coordinates (x 10^4) and equivalent isotropic displacement parameters (A^2 x 10^3) for* ***3.15****. U(eq) is defined as one third of the trace of the orthogonalized Uij tensor.*

	x	y	z	U(eq)
C(1)	3085(8)	6051(5)	3982(2)	14(1)
C(2)	2343(8)	4878(6)	4382(2)	17(1)
C(3)	2422(8)	5477(5)	4874(2)	18(1)
C(4)	3211(8)	7110(5)	4884(2)	16(1)
C(5)	2957(9)	7612(5)	4279(2)	17(1)
C(6)	983(8)	8400(6)	4218(2)	17(1)
C(7)	1310(9)	10061(6)	4153(2)	22(1)
C(8)	3154(9)	10353(6)	4085(2)	21(1)
C(9)	4344(8)	8900(5)	4089(2)	16(1)
C(10)	2262(8)	4821(5)	3160(2)	14(1)
C(11)	877(8)	4468(6)	2773(2)	18(1)
C(12)	1255(8)	3207(6)	2415(2)	23(1)
C(13)	2879(9)	2353(6)	2467(2)	21(1)
C(14)	4305(9)	2687(5)	2870(2)	20(1)
C(15)	5997(8)	1856(6)	2942(2)	22(1)
C(16)	7376(8)	2346(6)	3306(2)	23(1)
C(17)	7070(8)	3692(6)	3633(2)	20(1)
C(18)	5405(7)	4449(5)	3586(2)	14(1)
C(19)	3938(8)	3974(5)	3216(2)	16(1)
O(4)	2189(6)	8088(4)	5239(1)	20(1)
O(6)	-552(6)	7709(4)	4230(1)	22(1)
O(9)	5985(6)	9133(4)	4430(1)	21(1)
O(10)	2002(5)	6118(4)	3486(1)	15(1)
O(18)	5052(5)	5793(4)	3881(1)	16(1)

Table 1.8: *Bond lengths [A] and angles [deg] for* ***3.15****.*

C(1)-O(18)	1.432(7)	O(18)-C(1)-O(10)	110.3(3)	C(10)-C(11)-C(12)	117.4(5)
C(1)-O(10)	1.435(5)	O(18)-C(1)-C(2)	111.3(4)	C(10)-C(11)-H(11)	121.3
C(1)-C(2)	1.523(6)	O(10)-C(1)-C(2)	114.0(4)	C(12)-C(11)-H(11)	121.3
C(1)-C(5)	1.539(6)	O(18)-C(1)-C(5)	106.9(4)	C(13)-C(12)-C(11)	121.3(4)
C(2)-C(3)	1.329(6)	O(10)-C(1)-C(5)	110.0(4)	C(13)-C(12)-H(12)	119.4
C(2)-H(2)	0.93	C(2)-C(1)-C(5)	103.8(3)	C(11)-C(12)-H(12)	119.4
C(3)-C(4)	1.513(7)	C(3)-C(2)-C(1)	109.9(4)	C(12)-C(13)-C(14)	121.9(4)
C(3)-H(3)	0.93	C(3)-C(2)-H(2)	125.1	C(12)-C(13)-H(13)	119
C(4)-O(4)	1.430(5)	C(1)-C(2)-H(2)	125.1	C(14)-C(13)-H(13)	119
C(4)-C(5)	1.575(5)	C(2)-C(3)-C(4)	112.5(4)	C(15)-C(14)-C(13)	124.6(4)
C(4)-H(4)	0.98	C(2)-C(3)-H(3)	123.8	C(15)-C(14)-C(19)	119.1(5)
C(5)-C(6)	1.551(8)	C(4)-C(3)-H(3)	123.8	C(13)-C(14)-C(19)	116.3(5)
C(5)-C(9)	1.561(7)	O(4)-C(4)-C(3)	111.6(4)	C(16)-C(15)-C(14)	120.7(5)
C(6)-O(6)	1.235(7)	O(4)-C(4)-C(5)	112.6(4)	C(16)-C(15)-H(15)	119.6
C(6)-C(7)	1.460(7)	C(3)-C(4)-C(5)	102.0(3)	C(14)-C(15)-H(15)	119.6
C(7)-C(8)	1.338(8)	O(4)-C(4)-H(4)	110.1	C(15)-C(16)-C(17)	120.5(5)
C(7)-H(7)	0.93	C(3)-C(4)-H(4)	110.1	C(15)-C(16)-H(16)	119.7
C(8)-C(9)	1.507(7)	C(5)-C(4)-H(4)	110.1	C(17)-C(16)-H(16)	119.7
C(8)-H(8)	0.93	C(1)-C(5)-C(6)	113.6(4)	C(18)-C(17)-C(16)	119.0(4)
C(9)-O(9)	1.429(6)	C(1)-C(5)-C(9)	115.5(4)	C(18)-C(17)-H(17)	120.5
C(9)-H(9)	0.98	C(6)-C(5)-C(9)	103.0(4)	C(16)-C(17)-H(17)	120.5
C(10)-C(11)	1.386(7)	C(1)-C(5)-C(4)	102.4(3)	C(17)-C(18)-O(18)	121.6(4)
C(10)-C(19)	1.391(8)	C(6)-C(5)-C(4)	107.0(4)	C(17)-C(18)-C(19)	122.1(4)
C(10)-O(10)	1.397(5)	C(9)-C(5)-C(4)	115.5(4)	O(18)-C(18)-C(19)	116.2(4)
C(11)-C(12)	1.437(6)	O(6)-C(6)-C(7)	128.1(5)	C(10)-C(19)-C(18)	120.7(4)
C(11)-H(11)	0.93	O(6)-C(6)-C(5)	124.6(5)	C(10)-C(19)-C(14)	120.9(4)
C(12)-C(13)	1.362(8)	C(7)-C(6)-C(5)	107.3(5)	C(18)-C(19)-C(14)	118.2(5)
C(12)-H(12)	0.93	C(8)-C(7)-C(6)	110.8(5)	C(4)-O(4)-H(4A)	109.5
C(13)-C(14)	1.430(8)	C(8)-C(7)-H(7)	124.6	C(9)-O(9)-H(9A)	109.5
C(13)-H(13)	0.93	C(6)-C(7)-H(7)	124.6	C(10)-O(10)-C(1)	113.2(3)
C(14)-C(15)	1.397(8)	C(7)-C(8)-C(9)	112.6(5)		
C(14)-C(19)	1.433(6)	C(7)-C(8)-H(8)	123.7		
C(15)-C(16)	1.375(8)	C(9)-C(8)-H(8)	123.7		
C(15)-H(15)	0.93	O(9)-C(9)-C(8)	109.1(4)		
C(16)-C(17)	1.438(6)	O(9)-C(9)-C(5)	114.9(3)		
C(16)-H(16)	0.93	C(8)-C(9)-C(5)	104.0(5)		
C(17)-C(18)	1.344(8)	O(9)-C(9)-H(9)	109.5		
C(17)-H(17)	0.93	C(8)-C(9)-H(9)	109.5		
C(18)-O(18)	1.398(5)	C(5)-C(9)-H(9)	109.5		
C(18)-C(19)	1.425(7)	C(11)-C(10)-C(19)	122.2(4)		
O(4)-H(4A)	0.82	C(11)-C(10)-O(10)	118.6(4)		
O(9)-H(9A)	0.82	C(19)-C(10)-O(10)	119.1(4)		

Table 1.9: *Anisotropic displacement parameters (A^2 x 10^3) for* ***3.15****. The anisotropic displacement factor exponent takes the form:-2 pi^2 [h^2 a*^2 U11 + 2 h k a* b* U12]*

	U11	U22	U33	U23	U13	U12
C(1)	15(4)	13(3)	15(2)	-2(2)	11(2)	2(2)
C(2)	23(4)	12(3)	17(2)	0(2)	5(2)	-1(2)
C(3)	23(4)	15(3)	17(2)	1(2)	17(2)	5(2)
C(4)	19(4)	16(3)	11(2)	-1(2)	10(2)	-2(2)
C(5)	26(4)	12(3)	13(2)	-1(2)	13(2)	1(2)
C(6)	22(4)	21(3)	10(2)	-4(2)	8(2)	3(2)
C(7)	27(4)	19(3)	20(2)	1(2)	12(3)	9(2)
C(8)	30(4)	16(3)	17(2)	2(2)	9(2)	0(2)
C(9)	20(4)	17(3)	13(2)	0(2)	12(2)	-4(2)
C(10)	15(1)	13(1)	14(1)	1(1)	4(1)	-1(1)
C(11)	19(4)	18(3)	18(2)	4(2)	13(2)	0(2)
C(12)	25(4)	25(3)	19(2)	-3(2)	7(2)	-9(2)
C(13)	28(4)	16(3)	21(2)	-6(2)	11(2)	-3(2)
C(14)	31(4)	15(3)	16(2)	1(2)	15(2)	-1(2)
C(15)	23(2)	21(1)	21(1)	-2(1)	5(1)	1(1)
C(16)	20(4)	30(3)	18(2)	2(2)	11(2)	11(2)
C(17)	19(4)	31(3)	9(2)	1(2)	7(2)	0(2)
C(18)	15(1)	14(1)	14(1)	1(1)	4(1)	0(1)
C(19)	16(2)	16(1)	15(1)	1(1)	4(1)	-2(1)
O(4)	26(3)	22(2)	13(1)	-6(1)	14(2)	-2(2)
O(6)	20(3)	23(2)	23(2)	-4(1)	11(2)	2(2)
O(9)	19(3)	20(2)	26(2)	-7(1)	11(2)	-1(2)
O(10)	14(2)	20(2)	13(1)	-2(1)	9(1)	2(1)
O(18)	13(3)	20(2)	15(1)	-3(1)	13(2)	-1(1)

Table 1.10: *Hydrogen coordinates (x 10^4) and isotropic displacement parameters (A^2 x 10^3) for* ***3.15****.*

	x	y	z	U(eq)
H(2)	1901	3890	4296	20
H(3)	2035	4950	5178	22
H(4)	4562	7093	4990	19
H(7)	365	10814	4157	26
H(8)	3647	11344	4040	25
H(9)	4740	8669	3724	19
H(11)	-253	5025	2747	21
H(12)	375	2968	2142	27
H(13)	3065	1530	2233	25
H(15)	6194	961	2743	26
H(16)	8514	1804	3340	27
H(17)	8012	4033	3875	24
H(4A)	2829	8857	5313	30
H(9A)	6838	8551	4338	32

Table 1.11: *Hydrogen bonds for* ***3.15*** *[A and deg.].*

D-H...A	d(D-H)	d(H...A)	d(D...A)	<(DHA)
O(4)-H(4A)...O(9)#1	0.82	2.02	2.831(5)	170.1
O(9)-H(9A)...O(6)#2	0.82	2	2.787(5)	160.4

Symmetry transformations used to generate equivalent atoms: #1 -x+1,-y+2,-z+1 #2 x+1,y,z

Table 1.12: *Torsion angles (deg]) for* ***3.15***

O(18)-C(1)-C(2)-C(3)	95.5(5)	C(6)-C(5)-C(9)-C(8)	14.4(4)
O(10)-C(1)-C(2)-C(3)	-138.9(4)	C(4)-C(5)-C(9)-C(8)	-101.8(5)
C(5)-C(1)-C(2)-C(3)	-19.2(6)	C(19)-C(10)-C(11)-C(12)	-1.9(7)
C(1)-C(2)-C(3)-C(4)	0.0(7)	O(10)-C(10)-C(11)-C(12)	174.9(4)
C(2)-C(3)-C(4)-O(4)	139.1(5)	C(10)-C(11)-C(12)-C(13)	2.5(7)
C(2)-C(3)-C(4)-C(5)	18.6(6)	C(11)-C(12)-C(13)-C(14)	-1.5(9)
O(18)-C(1)-C(5)-C(6)	156.3(3)	C(12)-C(13)-C(14)-C(15)	-179.9(5)
O(10)-C(1)-C(5)-C(6)	36.5(6)	C(12)-C(13)-C(14)-C(19)	-0.3(8)
C(2)-C(1)-C(5)-C(6)	-85.9(4)	C(13)-C(14)-C(15)-C(16)	173.6(5)
O(18)-C(1)-C(5)-C(9)	37.7(5)	C(19)-C(14)-C(15)-C(16)	-6.1(8)
O(10)-C(1)-C(5)-C(9)	-82.2(5)	C(14)-C(15)-C(16)-C(17)	2.4(8)
C(2)-C(1)-C(5)-C(9)	155.4(4)	C(15)-C(16)-C(17)-C(18)	1.1(8)
O(18)-C(1)-C(5)-C(4)	-88.7(4)	C(16)-C(17)-C(18)-O(18)	-177.9(4)
O(10)-C(1)-C(5)-C(4)	151.5(4)	C(16)-C(17)-C(18)-C(19)	-0.8(8)
C(2)-C(1)-C(5)-C(4)	29.0(5)	C(11)-C(10)-C(19)-C(18)	174.5(4)
O(4)-C(4)-C(5)-C(1)	-148.3(4)	O(10)-C(10)-C(19)-C(18)	-2.3(7)
C(3)-C(4)-C(5)-C(1)	-28.6(5)	C(11)-C(10)-C(19)-C(14)	0.2(8)
O(4)-C(4)-C(5)-C(6)	-28.6(6)	O(10)-C(10)-C(19)-C(14)	-176.6(4)
C(3)-C(4)-C(5)-C(6)	91.1(5)	C(17)-C(18)-C(19)-C(10)	-177.2(5)
O(4)-C(4)-C(5)-C(9)	85.3(6)	O(18)-C(18)-C(19)-C(10)	0.0(7)
C(3)-C(4)-C(5)-C(9)	-154.9(4)	C(17)-C(18)-C(19)-C(14)	-2.8(7)
C(1)-C(5)-C(6)-O(6)	40.4(6)	O(18)-C(18)-C(19)-C(14)	174.4(4)
C(9)-C(5)-C(6)-O(6)	166.0(4)	C(15)-C(14)-C(19)-C(10)	-179.4(5)
C(4)-C(5)-C(6)-O(6)	-71.8(5)	C(13)-C(14)-C(19)-C(10)	0.9(7)
C(1)-C(5)-C(6)-C(7)	-140.2(4)	C(15)-C(14)-C(19)-C(18)	6.2(7)
C(9)-C(5)-C(6)-C(7)	-14.6(4)	C(13)-C(14)-C(19)-C(18)	-173.5(4)
C(4)-C(5)-C(6)-C(7)	107.6(4)	C(11)-C(10)-O(10)-C(1)	158.0(4)
O(6)-C(6)-C(7)-C(8)	-171.4(4)	C(19)-C(10)-O(10)-C(1)	-25.1(6)
C(5)-C(6)-C(7)-C(8)	9.3(5)	O(18)-C(1)-O(10)-C(10)	54.0(5)
C(6)-C(7)-C(8)-C(9)	0.7(5)	C(2)-C(1)-O(10)-C(10)	-72.1(5)
C(7)-C(8)-C(9)-O(9)	-133.2(4)	C(5)-C(1)-O(10)-C(10)	171.7(4)
C(7)-C(8)-C(9)-C(5)	-10.1(4)	C(17)-C(18)-O(18)-C(1)	-152.8(4)
C(1)-C(5)-C(9)-O(9)	-102.0(5)	C(19)-C(18)-O(18)-C(1)	30.0(5)
C(6)-C(5)-C(9)-O(9)	133.6(4)	O(10)-C(1)-O(18)-C(18)	-57.2(4)
C(4)-C(5)-C(9)-O(9)	17.4(6)	C(2)-C(1)-O(18)-C(18)	70.5(4)
C(1)-C(5)-C(9)-C(8)	138.8(4)	C(5)-C(1)-O(18)-C(18)	-176.8(3)

Table 1.13: *Crystal data and structure refinement for SAS-6-14 (**4.14**)*

Empirical formula	C21 H16 Cl2 O7
Formula weight	451.24
Temperature	113(2) K
Wavelength	0.71073 A
Crystal system, space group	Monoclinic, P2(1)/c
Unit cell dimensions	a = 16.216(5) A alpha = 90
	b = 17.340(5) A beta = 92
	c = 7.0255(19) A gamma = 90
Volume	1974.2(10) A^3
Z, Calculated density	4, 1.518 Mg/m^3
Absorption coefficient	0.372 mm^-1
F(000)	928
Crystal size	0.70 x 0.35 x 0.02 mm
Theta range for data collection	3.41 to 25.00 deg.
Limiting indices	-17<=h<=16, -19<=k<=19, -3<=l<=8
Reflections collected / unique	5260 / 2781 [R(int) = 0.0429]
Completeness to theta = 25.00	79.70%
Absorption correction	None
Refinement method	Full-matrix least-squares on F^2
Data / restraints / parameters	2781 / 0 / 275
Goodness-of-fit on F^2	1.089
Final R indices [I>2sigma(I)]	R1 = 0.0416, wR2 = 0.0757
R indices (all data)	R1 = 0.0818, wR2 = 0.0860
Largest diff. peak and hole	0.230 and -0.210 e.A^-3

Table 1.14: *Atomic coordinates (x 10^4) and equivalent isotropic displacement parameters (A^2 x 10^3) for Compound* ***4.14****. U(eq) is defined as one third of the trace of the orthogonalized Uij tensor.*

	x	**y**	**z**	**U(eq)**
Cl(1)	1799(1)	1756(1)	541(1)	24(1)
Cl(2)	1081(1)	4784(1)	1166(1)	37(1)
C(1')	3145(2)	3660(2)	-31(4)	18(1)
C(2')	2569(2)	4241(2)	273(4)	21(1)
C(3')	1769(2)	4049(2)	666(4)	22(1)
C(4')	1507(2)	3279(2)	727(4)	19(1)
C(5')	2093(2)	2717(2)	437(4)	18(1)
C(6')	2901(2)	2896(2)	78(4)	18(1)
C(1'')	5114(2)	3215(2)	3639(4)	19(1)
C(2'')	5828(2)	3495(2)	2620(4)	18(1)
C(3'')	5519(2)	3784(2)	952(4)	19(1)
C(4'')	4626(2)	3690(2)	832(4)	18(1)
C(5'')	4012(2)	3867(2)	-447(4)	17(1)
C(6'')	4161(2)	4272(2)	-2242(4)	20(1)
C(1)	6676(2)	3471(2)	3410(4)	21(1)
C(2)	7332(2)	3731(2)	2340(4)	23(1)
C(3)	8129(2)	3770(2)	3115(4)	24(1)
C(4)	8293(2)	3548(2)	4965(4)	22(1)
C(5)	7657(2)	3260(2)	6036(4)	27(1)
C(6)	6867(2)	3225(2)	5275(4)	27(1)
O(4)	9054(1)	3579(1)	5889(3)	27(1)
C(7)	9689(2)	3956(2)	4894(5)	33(1)
O(4')	722(1)	3091(1)	1192(3)	25(1)
C(7')	113(2)	3149(2)	-343(4)	27(1)
O(7)	3474(1)	4352(1)	-3283(3)	24(1)
C(7'')	3511(2)	4721(2)	-5125(4)	27(1)
O(1)	5037(1)	2932(1)	5167(3)	26(1)
O(2)	4402(1)	3336(1)	2484(3)	18(1)
O(3)	5960(1)	4115(1)	-388(3)	27(1)
O(6)	4830(1)	4513(1)	-2759(3)	25(1)

Table 1.15: *Bond lengths [A] and angles [deg] for* ***4.14****.*

Cl(1)-C(5')	1.736(3)	C(7")-H(7"1)	0.98
Cl(2)-C(3')	1.738(3)	C(7")-H(7"2)	0.98
C(1')-C(6')	1.386(4)	C(7")-H(7"3)	0.98
C(1')-C(2')	1.395(4)	O(3)-H(3)	0.84
C(1')-C(5")	1.491(4)	C(6')-C(1')-C(2')	119.2(3)
C(2')-C(3')	1.376(4)	C(6')-C(1')-C(5")	121.0(3)
C(2')-H(2')	0.95	C(2')-C(1')-C(5")	119.9(3)
C(3')-C(4')	1.402(4)	C(3')-C(2')-C(1')	119.8(3)
C(4')-O(4')	1.365(3)	C(3')-C(2')-H(2')	120.1
C(4')-C(5')	1.381(4)	C(1')-C(2')-H(2')	120.1
C(5')-C(6')	1.378(4)	C(2')-C(3')-C(4')	121.7(3)
C(6')-H(6')	0.95	C(2')-C(3')-Cl(2)	118.6(2)
C(1")-O(1)	1.191(3)	C(4')-C(3')-Cl(2)	119.6(2)
C(1")-O(2)	1.402(3)	O(4')-C(4')-C(5')	121.3(3)
C(1")-C(2")	1.467(4)	O(4')-C(4')-C(3')	121.5(3)
C(2")-C(3")	1.354(4)	C(5')-C(4')-C(3')	117.1(3)
C(2")-C(1)	1.464(4)	C(6')-C(5')-C(4')	122.2(3)
C(3")-O(3)	1.333(3)	C(6')-C(5')-Cl(1)	119.2(2)
C(3")-C(4")	1.457(4)	C(4')-C(5')-Cl(1)	118.7(2)
C(4")-C(5")	1.351(4)	C(5')-C(6')-C(1')	120.0(3)
C(4")-O(2)	1.373(3)	C(5')-C(6')-H(6')	120
C(5")-C(6")	1.472(4)	C(1')-C(6')-H(6')	120
C(6")-O(6)	1.228(3)	O(1)-C(1")-O(2)	118.2(3)
C(6")-O(7)	1.318(4)	O(1)-C(1")-C(2")	133.4(3)
C(1)-C(2)	1.399(4)	O(2)-C(1")-C(2")	108.4(2)
C(1)-C(6)	1.403(4)	C(3")-C(2")-C(1")	105.7(3)
C(2)-C(3)	1.386(4)	C(3")-C(2")-C(1)	130.7(3)
C(2)-H(2)	0.95	C(1")-C(2")-C(1)	123.6(3)
C(3)-C(4)	1.373(4)	O(3)-C(3")-C(2")	125.4(3)
C(3)-H(3A)	0.95	O(3)-C(3")-C(4")	124.4(3)
C(4)-O(4)	1.374(4)	C(2")-C(3")-C(4")	110.2(3)
C(4)-C(5)	1.391(4)	C(5")-C(4")-O(2)	116.9(3)
C(5)-C(6)	1.371(4)	C(5")-C(4")-C(3")	136.0(3)
C(5)-H(5)	0.95	O(2)-C(4")-C(3")	107.1(2)
C(6)-H(6)	0.95	C(4")-C(5")-C(6")	122.6(3)
O(4)-C(7)	1.425(4)	C(4")-C(5")-C(1')	119.5(3)
C(7)-H(7A)	0.98	C(6")-C(5")-C(1')	117.9(3)
C(7)-H(7B)	0.98	O(6)-C(6")-O(7)	122.6(3)
C(7)-H(7C)	0.98	O(6)-C(6")-C(5")	126.1(3)
O(4')-C(7')	1.439(4)	O(7)-C(6")-C(5")	111.3(3)
C(7')-H(7'1)	0.98	C(2)-C(1)-C(6)	116.9(3)
C(7')-H(7'2)	0.98	C(2)-C(1)-C(2")	120.6(3)
C(7')-H(7'3)	0.98	C(6)-C(1)-C(2")	122.4(3)
O(7)-C(7")	1.447(3)	O(4)-C(4)-C(5)	115.4(3)

C(3)-C(2)-H(2)	119.3	C(6)-C(5)-C(4)	120.4(3)
C(1)-C(2)-H(2)	119.3	C(6)-C(5)-H(5)	119.8
C(4)-C(3)-C(2)	120.3(3)	C(4)-C(5)-H(5)	119.8
C(4)-C(3)-H(3A)	119.8	C(5)-C(6)-C(1)	121.5(3)
C(2)-C(3)-H(3A)	119.8	C(5)-C(6)-H(6)	119.2
C(3)-C(4)-O(4)	125.2(3)	C(1)-C(6)-H(6)	119.2
C(3)-C(4)-C(5)	119.4(3)	C(4)-O(4)-C(7)	116.1(3)
O(4)-C(4)-C(5)	115.4(3)	O(4)-C(7)-H(7A)	109.5
C(6)-C(5)-C(4)	120.4(3)	O(4)-C(7)-H(7B)	109.5
C(6)-C(5)-H(5)	119.8	H(7A)-C(7)-H(7B)	109.5
C(4)-C(5)-H(5)	119.8	O(4)-C(7)-H(7C)	109.5
C(5)-C(6)-C(1)	121.5(3)	H(7A)-C(7)-H(7C)	109.5
C(5)-C(6)-H(6)	119.2	H(7B)-C(7)-H(7C)	109.5
C(1)-C(6)-H(6)	119.2	C(4')-O(4')-C(7')	115.1(2)
C(4)-O(4)-C(7)	116.1(3)	O(4')-C(7')-H(7'1)	109.5
O(4)-C(7)-H(7A)	109.5	O(4')-C(7')-H(7'2)	109.5
O(4)-C(7)-H(7B)	109.5	H(7'1)-C(7')-H(7'2)	109.5
H(7A)-C(7)-H(7B)	109.5	O(4')-C(7')-H(7'3)	109.5
O(4)-C(7)-H(7C)	109.5	H(7'1)-C(7')-H(7'3)	109.5
H(7A)-C(7)-H(7C)	109.5	H(7'2)-C(7')-H(7'3)	109.5
H(7B)-C(7)-H(7C)	109.5	C(6")-O(7)-C(7")	118.8(2)
C(4')-O(4')-C(7')	115.1(2)	O(7)-C(7")-H(7"1)	109.5
O(4')-C(7')-H(7'1)	109.5	O(7)-C(7")-H(7"2)	109.5
O(4')-C(7')-H(7'2)	109.5	H(7"1)-C(7")-H(7"2)	109.5
H(7'1)-C(7')-H(7'2)	109.5	O(7)-C(7")-H(7"3)	109.5
O(4')-C(7')-H(7'3)	109.5	H(7"1)-C(7")-H(7"3)	109.5
H(7'1)-C(7')-H(7'3)	109.5	H(7"2)-C(7")-H(7"3)	109.5
H(7'2)-C(7')-H(7'3)	109.5	C(4")-O(2)-C(1")	108.6(2)
C(6")-O(7)-C(7")	118.8(2)	C(3")-O(3)-H(3)	109.5
O(7)-C(7")-H(7"1)	109.5		
O(7)-C(7")-H(7"2)	109.5		
H(7"1)-C(7")-H(7"2)	109.5		
O(7)-C(7")-H(7"3)	109.5		
H(7"1)-C(7")-H(7"3)	109.5		
H(7"2)-C(7")-H(7"3)	109.5		
C(4")-O(2)-C(1")	108.6(2)		
C(3")-O(3)-H(3)	109.5		
C(3)-C(2)-H(2)	119.3		
C(1)-C(2)-H(2)	119.3		
C(4)-C(3)-C(2)	120.3(3)		
C(4)-C(3)-H(3A)	119.8		
C(2)-C(3)-H(3A)	119.8		
C(3)-C(4)-O(4)	125.2(3)		
C(3)-C(4)-C(5)	119.4(3)		

Table 1.16: *Anisotropic displacement parameters (A^2 x 10^3) for* ***4.14****. The anisotropic displacement factor exponent takes the form:*
-2 pi^2 [h^2 a^2 U11 + ... + 2 h k a* b* U12]*

	U11	U22	U33	U23	U13	U12
Cl(1)	25(1)	22(1)	25(1)	1(1)	-1(1)	-5(1)
Cl(2)	32(1)	28(1)	52(1)	0(1)	14(1)	9(1)
C(1')	15(2)	22(2)	17(2)	0(1)	0(1)	0(2)
C(2')	25(2)	19(2)	20(2)	0(1)	0(1)	-2(2)
C(3')	19(2)	22(2)	24(2)	2(1)	4(1)	6(2)
C(4')	14(2)	27(2)	17(2)	5(1)	2(1)	-2(2)
C(5')	21(2)	23(2)	10(2)	0(1)	-1(1)	-2(2)
C(6')	18(2)	17(2)	18(2)	-1(1)	-2(1)	2(2)
C(1'')	18(2)	16(2)	23(2)	-2(1)	-2(1)	-1(2)
C(2'')	18(2)	14(2)	23(2)	-2(1)	0(1)	-2(1)
C(3'')	18(2)	14(2)	25(2)	-3(1)	1(1)	-2(1)
C(4'')	23(2)	12(2)	18(2)	-1(1)	4(1)	-2(1)
C(5'')	15(2)	15(2)	20(2)	-1(1)	2(1)	-1(1)
C(6'')	22(2)	14(2)	23(2)	-3(1)	2(1)	2(2)
C(1)	24(2)	13(2)	26(2)	-3(1)	-2(1)	2(1)
C(2)	27(2)	22(2)	21(2)	1(1)	0(1)	2(2)
C(3)	22(2)	23(2)	28(2)	-1(1)	3(1)	0(2)
C(4)	18(2)	18(2)	30(2)	-2(1)	-3(1)	2(2)
C(5)	20(2)	32(2)	28(2)	8(1)	-5(1)	1(2)
C(6)	26(2)	25(2)	29(2)	5(1)	2(1)	-3(2)
O(4)	16(2)	33(1)	33(1)	3(1)	-3(1)	-2(1)
C(7)	20(2)	40(2)	38(2)	2(2)	-2(2)	-2(2)
O(4')	14(1)	36(2)	24(1)	5(1)	2(1)	0(1)
C(7')	20(2)	32(2)	27(2)	-2(1)	-3(1)	2(2)
O(7)	20(2)	34(1)	18(1)	4(1)	-2(1)	-3(1)
C(7'')	29(2)	32(2)	20(2)	4(1)	1(1)	3(2)
O(1)	25(2)	28(1)	25(1)	9(1)	1(1)	-2(1)
O(2)	13(1)	21(1)	21(1)	4(1)	0(1)	1(1)
O(3)	20(2)	38(2)	23(1)	11(1)	0(1)	-4(1)
O(6)	19(2)	32(1)	26(1)	9(1)	2(1)	-2(1)

Table 1.17: *Hydrogen coordinates (x 10^4) and isotropic displacement parameters (A^2 x 10^3) for* ***4.14***

	x	y	z	U(eq)
H(2')	2728	4767	210	25
H(6')	3290	2495	-94	21
H(2)	7229	3884	1054	28
H(3A)	8563	3952	2363	29
H(5)	7770	3088	7302	32
H(6)	6440	3028	6029	32
H(7A)	9806	3664	3741	49
H(7B)	10189	3987	5716	49
H(7C)	9508	4478	4541	49
H(7'1)	42	3691	-707	40
H(7'2)	-413	2941	70	40
H(7'3)	297	2853	-1439	40
H(7"1)	3988	5067	-5131	40
H(7"2)	3005	5018	-5377	40
H(7"3)	3564	4327	-6113	40
H(3)	5645	4253	-1300	40

Table 1.18: *Torsion angles [deg] for* ***4.14***

C(6')-C(1')-C(2')-C(3')	-0.4(4)	C(6')-C(1')-C(5")-C(4")	-66.1(4)
C(5")-C(1')-C(2')-C(3')	-179.7(3)	C(2')-C(1')-C(5")-C(4")	113.2(3)
C(1')-C(2')-C(3')-C(4')	-1.5(4)	C(6')-C(1')-C(5")-C(6")	114.9(3)
C(1')-C(2')-C(3')-Cl(2)	176.6(2)	C(2')-C(1')-C(5")-C(6")	-65.8(3)
C(2')-C(3')-C(4')-O(4')	177.3(3)	C(4")-C(5")-C(6")-O(6)	-2.4(5)
Cl(2)-C(3')-C(4')-O(4')	-0.7(4)	C(1')-C(5")-C(6")-O(6)	176.6(3)
C(2')-C(3')-C(4')-C(5')	2.1(4)	C(4")-C(5")-C(6")-O(7)	177.4(3)
Cl(2)-C(3')-C(4')-C(5')	-176.0(2)	C(1')-C(5")-C(6")-O(7)	-3.6(4)
O(4')-C(4')-C(5')-C(6')	-176.0(2)	C(3")-C(2")-C(1)-C(2)	-4.6(5)
C(3')-C(4')-C(5')-C(6')	-0.8(4)	C(1")-C(2")-C(1)-C(2)	178.4(3)
O(4')-C(4')-C(5')-Cl(1)	3.6(4)	C(3")-C(2")-C(1)-C(6)	172.5(3)
C(3')-C(4')-C(5')-Cl(1)	178.9(2)	C(1")-C(2")-C(1)-C(6)	-4.6(4)
C(4')-C(5')-C(6')-C(1')	-1.0(4)	C(6)-C(1)-C(2)-C(3)	-2.4(4)
Cl(1)-C(5')-C(6')-C(1')	179.3(2)	C(2")-C(1)-C(2)-C(3)	174.8(3)
C(2')-C(1')-C(6')-C(5')	1.6(4)	C(1)-C(2)-C(3)-C(4)	0.4(5)
C(5")-C(1')-C(6')-C(5')	-179.1(3)	C(2)-C(3)-C(4)-O(4)	-178.4(3)
O(1)-C(1")-C(2")-C(3")	-177.6(3)	C(2)-C(3)-C(4)-C(5)	2.0(5)
O(2)-C(1")-C(2")-C(3")	1.4(3)	C(3)-C(4)-C(5)-C(6)	-2.3(5)
O(1)-C(1")-C(2")-C(1)	0.1(5)	O(4)-C(4)-C(5)-C(6)	178.1(3)
O(2)-C(1")-C(2")-C(1)	179.1(2)	C(4)-C(5)-C(6)-C(1)	0.2(5)
C(1")-C(2")-C(3")-O(3)	178.4(3)	C(2)-C(1)-C(6)-C(5)	2.1(4)
C(1)-C(2")-C(3")-O(3)	0.9(5)	C(2")-C(1)-C(6)-C(5)	-175.1(3)
C(1")-C(2")-C(3")-C(4")	-0.9(3)	C(3)-C(4)-O(4)-C(7)	7.6(4)
C(1)-C(2")-C(3")-C(4")	-178.4(3)	C(5)-C(4)-O(4)-C(7)	-172.7(3)
O(3)-C(3")-C(4")-C(5")	0.2(5)	C(5')-C(4')-O(4')-C(7')	-103.1(3)
C(2")-C(3")-C(4")-C(5")	179.5(3)	C(3')-C(4')-O(4')-C(7')	81.8(3)
O(3)-C(3")-C(4")-O(2)	-179.2(3)	O(6)-C(6")-O(7)-C(7")	1.5(4)
C(2")-C(3")-C(4")-O(2)	0.1(3)	C(5")-C(6")-O(7)-C(7")	-178.4(2)
O(2)-C(4")-C(5")-C(6")	177.7(2)	C(5")-C(4")-O(2)-C(1")	-178.7(3)
C(3")-C(4")-C(5")-C(6")	-1.6(5)	C(3")-C(4")-O(2)-C(1")	0.8(3)
O(2)-C(4")-C(5")-C(1')	-1.3(4)	O(1)-C(1")-O(2)-C(4")	177.8(3)
C(3")-C(4")-C(5")-C(1')	179.4(3)	C(2")-C(1")-O(2)-C(4")	-1.4(3)

Table 1.19: *Crystal and structure refinement for* ***5.7***

Empirical formula	C11 H14 O5
Formula weight	226.22
Temperature	93(2) K
Wavelength	0.71073 A
Crystal system, space group	Orthorhombic, P2(1)2(1)2(1)
Unit cell dimensions	a = 4.320(8) A alpha = 90 deg.
	b = 11.64(2) A beta = 90 deg.
	c = 21.33(4) A gamma = 90 deg
Volume	1072(4) A^3
Z, Calculated density	4, 1.402 Mg/m^3
Absorption coefficient	0.111 mm^-1
F(000)	480
Crystal size	0.67 x 0.40 x 0.28 mm
Theta range for data collection	1.99 to 26.26 deg.
Limiting indices	-4<=h<=4, -13<=k<=14, -2 6<=l<=21
Reflections collected / unique	4327 / 1879 [R(int) = 0. 2194]
Completeness to theta = 25.00	91.00%
Absorption correction	None
Max. and min. transmission	0.9696 and 0.9293
Refinement method	Full-matrix least-square s on F^2
Data / restraints / parameters	1879 / 0 / 150
Goodness-of-fit on F^2	1.281
Final R indices [I>2sigma(I)]	R1 = 0.1413, wR2 = 0.3437
R indices (all data)	R1 = 0.2273, wR2 = 0.4317
Absolute structure parameter	10(7)
Largest diff. peak and hole	0.629 and -0.556 e.A^-3

Table 1.20: *Atomic coordinates (x 10^4) and equivalent isotropic displacement parameters (A^2 x 10^3) for* ***5.7****. U(eq) is defined as one third of the trace of the orthogonalized Uij tensor.*

	x	y	z	U(eq)
O(10)	12190(20)	4515(5)	6651(4)	44(2)
O(8)	10920(20)	1700(6)	5364(4)	45(2)
O(4)	5590(20)	-1672(6)	6037(3)	49(3)
O(2)	8580(20)	359(6)	4577(3)	52(3)
O(6)	9860(20)	986(6)	7507(3)	42(2)
C(5)	7640(30)	-357(7)	6792(5)	26(3)
C(4)	7050(30)	-680(8)	6192(5)	34(3)
C(2)	7360(40)	-231(8)	5015(5)	52(4)
C(9)	12360(30)	2390(8)	6580(5)	42(3)
C(8)	9790(30)	1008(9)	5819(4)	39(3)
C(10)	10180(30)	3454(8)	6583(5)	42(3)
C(7)	10450(30)	1345(8)	6434(5)	33(3)
C(1)	5170(30)	-1130(10)	4819(5)	41(3)
C(3)	8200(30)	5(9)	5668(5)	35(3)
C(11)	4630(40)	-2402(9)	6550(5)	54(4)
C(6)	9300(40)	652(9)	6923(5)	42(3)

Table 1.21: *Bond lengths [A] and angles [deg] for* ***5.7***

O(10)-C(10)	1.518(13)	C(8)-O(8)-H(8)	109.5	C(2)-C(1)-H(1B)	109.5
O(10)-H(10)	0.84	C(4)-O(4)-C(11)	116.7(8)	H(1A)-C(1)-H(1B)	109.5
O(8)-C(8)	1.353(12)	C(6)-O(6)-H(6)	109.5	C(2)-C(1)-H(1C)	109.5
O(8)-H(8)	0.84	C(4)-C(5)-C(6)	121.0(9)	H(1A)-C(1)-H(1C)	109.5
O(4)-C(4)	1.355(14)	C(4)-C(5)-H(5)	119.5	H(1B)-C(1)-H(1C)	109.5
O(4)-C(11)	1.446(12)	C(6)-C(5)-H(5)	119.5	C(8)-C(3)-C(2)	120.0(9)
O(2)-C(2)	1.272(13)	C(5)-C(4)-O(4)	123.5(9)	C(8)-C(3)-C(4)	116.8(9)
O(6)-C(6)	1.328(13)	C(5)-C(4)-C(3)	120.3(10)	C(2)-C(3)-C(4)	122.6(10)
O(6)-H(6)	0.84	O(4)-C(4)-C(3)	116.0(9)	O(4)-C(11)-H(11A)	109.5
C(5)-C(4)	1.359(14)	O(2)-C(2)-C(3)	119.5(12)	O(4)-C(11)-H(11B)	109.5
C(5)-C(6)	1.403(16)	O(2)-C(2)-C(1)	116.2(10)	H(11A)-C(11)-H(11B)	109.5
C(5)-H(5)	0.95	C(3)-C(2)-C(1)	124.3(10)	O(4)-C(11)-H(11C)	109.5
C(4)-C(3)	1.460(15)	C(7)-C(9)-C(10)	108.2(10)	H(11A)-C(11)-H(11C)	109.5
C(2)-C(3)	1.467(15)	C(7)-C(9)-H(9A)	110.1	H(11B)-C(11)-H(11C)	109.5
C(2)-C(1)	1.471(18)	C(10)-C(9)-H(9A)	110.1	O(6)-C(6)-C(7)	117.5(10)
C(9)-C(7)	1.502(15)	C(7)-C(9)-H(9B)	110.1	O(6)-C(6)-C(5)	121.7(9)
C(9)-C(10)	1.556(16)	C(10)-C(9)-H(9B)	110.1	C(7)-C(6)-C(5)	120.8(9)
C(9)-H(9A)	0.99	H(9A)-C(9)-H(9B)	108.4		
C(9)-H(9B)	0.99	O(8)-C(8)-C(7)	115.6(10)		

C(8)-C(7)	1.398(14)	O(8)-C(8)-C(3)	120.7(9)
C(8)-C(3)	1.391(15)	C(7)-C(8)-C(3)	123.6(9)
C(10)-H(10A)	0.99	O(10)-C(10)-C(9)	107.5(9)
C(10)-H(10B)	0.99	O(10)-C(10)-H(10A)	110.2
C(7)-C(6)	1.409(15)	C(9)-C(10)-H(10A)	110.2
C(1)-H(1A)	0.98	O(10)-C(10)-H(10B)	110.2
C(1)-H(1B)	0.98	C(9)-C(10)-H(10B)	110.2
C(1)-H(1C)	0.98	H(10A)-C(10)-H(10B)	108.5
C(11)-H(11A)	0.98	C(8)-C(7)-C(6)	117.5(10)
C(11)-H(11B)	0.98	C(8)-C(7)-C(9)	122.3(9)
C(11)-H(11C)	0.98	C(6)-C(7)-C(9)	120.2(10)
C(10)-O(10)-H(10)	109.5	C(2)-C(1)-H(1A)	109.5

Symmetry transformations used to generate equivalent atoms

Table 1.22: *Anisotropic displacement parameters (A^2 x 10^3) for* ***5.7****. The anisotropic displacement factor exponent takes the form: -2 pi^2 [h^2 a*^2 U11 + 2 h k a* b* U12]*

	U11	U22	U33	U23	U13	U12
O(10)	73(7)	34(4)	26(4)	-3(3)	2(4)	2(4)
O(8)	64(7)	42(4)	27(4)	11(3)	7(4)	-12(4)
O(4)	104(9)	33(4)	12(3)	2(3)	11(4)	-10(4)
O(2)	99(8)	40(4)	16(4)	7(3)	7(4)	-5(4)
O(6)	65(7)	37(4)	23(4)	-2(3)	4(4)	-5(4)
C(5)	19(7)	29(4)	30(5)	8(4)	12(4)	-4(5)
C(4)	42(9)	37(5)	22(5)	3(4)	5(5)	14(5)
C(2)	111(13)	23(5)	21(5)	6(4)	5(7)	7(7)
C(9)	74(10)	38(5)	13(5)	3(4)	-3(6)	8(6)
C(8)	66(10)	42(5)	10(4)	4(4)	12(6)	-7(6)
C(10)	65(10)	39(5)	22(5)	4(4)	14(6)	-11(6)
C(7)	48(8)	25(5)	28(6)	3(4)	1(5)	0(5)
C(1)	56(10)	52(6)	16(5)	-6(4)	6(6)	-5(6)
C(3)	47(9)	40(5)	19(5)	-4(4)	3(5)	-8(5)
C(11)	112(14)	33(5)	18(5)	8(5)	-10(7)	-15(7)
C(6)	76(11)	33(5)	17(5)	-1(4)	7(6)	8(6)

Table 1.23: *Hydrogen coordinates (x 10^4) and isotropic displacement parameters (A^2 x 10^3) for* ***5.7****.*

	x	y	z	U(eq)
H(10)	13979	4319	6763	66
H(8)	12864	1696	5377	67
H(6)	11746	888	7589	63
H(5)	6913	-820	7129	31
H(9A)	13996	2489	6260	50
H(9B)	13361	2303	6995	50
H(10A)	8987	3490	6187	50
H(10B)	8699	3402	6936	50
H(1A)	3305	-1090	5080	62
H(1B)	6139	-1886	4867	62
H(1C)	4603	-1012	4378	62
H(11A)	4233	-1930	6922	82
H(11B)	6276	-2957	6643	82
H(11C)	2741	-2814	6433	82

Appendix 2

Molecular modelling data for the diastereomers, spiro-mamakones D (**3.17**) and E (**3.18**)

Tables are to be read across. Shaded areas indicate point of attachment to the table on the following page or below.

Column title meanings

A Potential energy of each conformer calculated by the OPLS2003 force field.

B, C, D, E Each of these columns calculates part of the Boltzmann weighting of each conformer (column A). The overall equation being

$$P_\alpha = \frac{\exp[-(E_\alpha / k_B T]}{\sum_{\alpha}^{N_A} \exp[-(E_\alpha / k_B T]}$$

B E/kT, E = negative potential energy (the negative of column A), k = Boltzmann constant (8.32441 $J \cdot K^{-1} \cdot mol^{-1}$), T = temperature (300K). Formula =(-A2*1000)/(8.31451*300).

C e-E/kT, e = natural log. Formula =IF(B2=0,0,EXP(B2)).

D Ne-E/kT, N = number of conformers (entries in column A). Formula =COUNT($A$2:$A$300)*(C2).

E Boltzmann. Final calculation performed to give the Boltzmann weighting of each conformer (entries in column A). Formula =(D2)/SUM($C$2:$C$300).

F %. Calculates the Boltzmann weighted % of each conformer. Formula =(E2)/SUM($E$2:$E$300)*100

G E*%. Potential energy (column A) x Boltzmann weighted % (column F). Formula =(A2*F2)

H Bolt.Ave.E. Calculates the Boltzmann average potential energy of the system within 12 kJ of the global minima. Formula =SUM(G2:G300)/100

J, K, L, M, N, O, P These columns are headed with the relevant H atom numbers and measures the distance between each of these H atoms in Angstroms for each conformer. At the bottom of these columns the smallest H-H distance in the ensemble is given for each measured H-H.

R, S, T, U, V, W, X These columns are headed with the relevant H atom numbers and gives the Boltzmann weighted % for each conformer if less than 3 Angstroms otherwise zero is displayed. At the bottom of these columns is the Boltzmann weighted % of conformers with a H-H distance less than 3 Angstroms. Formula example for column R =IF(J2>3,0,F2). Note J changes with each column eg K, L, M, N, O, P.

Z, AA, AB, AC, AD, AE, AF These columns are headed with the relevant H atom numbers and gives the Boltzmann weighted % for each conformer if less than 2.5 Angstroms otherwise zero is displayed. At the bottom of these columns is the Boltzmann weighted % of conformers with a H-H distance less than 2.5 Angstroms. Formula example for column Z =IF(J2>2.5,0,F2). Note J changes with each column eg K, L, M, N, O, P

AH, AI, AJ, AK, AL, AM, AN These columns are headed with the relevant H atom numbers and give the Boltzmann weighted % x the H-H distance for each conformer. At the bottom of these columns is the Boltzmann weighted average distance for each H-H. Formula example for

column AH =(J2*F2). Note J changes with each column eg K, L, M, N, O, P

AP, AQ, AR, AS, AT, AU, AV These columns are headed with the relevant H atom numbers and calculates 1/r^6 (r = H-H distance) for each H-H distance. At the bottom of these columns is the sum of each of the above columns and calculates a virtual NOE. Formula example for column AP =(1/(J2^6))*E2. Note J changes with each column eg K, L, M, N, O

AX, AY, AX Dihedral angles.

***Table 2.1**: Calculations for 4S, 5S, 8S, 9S.*

Potential Energy-OPLS-AA	E/kT	e-E/kT	Ne-E/kT	Boltzmann	%	E*%	Bolt.Ave.E
340.61	-136.55	4.97E-60	1.44E-58	12.66	43.67	14873.79	344.06
343.47	-137.70	1.58E-60	4.58E-59	4.02	13.86	4761.74	
344.51	-138.12	1.04E-60	3.01E-59	2.65	9.13	3145.89	
346.13	-138.77	5.43E-61	1.57E-59	1.38	4.77	1649.44	
346.84	-139.05	4.08E-61	1.18E-59	1.04	3.59	1243.56	
346.94	-139.09	3.93E-61	1.14E-59	1.00	3.45	1197.49	
348.14	-139.57	2.42E-61	7.02E-60	0.62	2.13	740.58	
348.26	-139.62	2.32E-61	6.71E-60	0.59	2.03	708.29	
348.99	-139.91	1.73E-61	5.01E-60	0.44	1.52	529.05	
349.09	-139.95	1.66E-61	4.82E-60	0.42	1.46	509.37	
349.22	-140.00	1.57E-61	4.56E-60	0.40	1.38	482.47	
349.26	-140.02	1.55E-61	4.48E-60	0.39	1.36	474.37	
349.74	-140.21	1.28E-61	3.71E-60	0.33	1.12	392.91	
349.79	-140.23	1.25E-61	3.63E-60	0.32	1.10	385.05	
350.07	-140.35	1.12E-61	3.25E-60	0.29	0.98	344.13	
350.26	-140.42	1.04E-61	3.00E-60	0.26	0.91	318.47	
350.70	-140.60	8.70E-62	2.52E-60	0.22	0.76	268.13	
350.73	-140.61	8.60E-62	2.50E-60	0.22	0.76	265.04	
350.73	-140.61	8.58E-62	2.49E-60	0.22	0.75	264.36	
350.74	-140.61	8.56E-62	2.48E-60	0.22	0.75	263.59	
351.16	-140.78	7.24E-62	2.10E-60	0.18	0.64	223.26	
351.39	-140.87	6.59E-62	1.91E-60	0.17	0.58	203.52	
351.67	-140.98	5.90E-62	1.71E-60	0.15	0.52	182.39	
351.70	-141.00	5.81E-62	1.69E-60	0.15	0.51	179.61	
351.74	-141.01	5.74E-62	1.66E-60	0.15	0.50	177.37	
351.76	-141.02	5.69E-62	1.65E-60	0.14	0.50	175.77	
352.14	-141.17	4.88E-62	1.42E-60	0.12	0.43	150.98	
352.15	-141.18	4.87E-62	1.41E-60	0.12	0.43	150.57	
352.24	-141.22	4.69E-62	1.36E-60	0.12	0.41	145.00	

	H4-H9	H4-H8	H8-H9	H9-H7a	H9-H7b	H8-H7a	H8-H7b
	2.94	4.86	2.71	3.98	4.17	2.37	2.76
	2.95	4.86	2.70	3.98	4.17	2.37	2.77
	2.94	4.90	2.70	3.98	4.18	2.36	2.77
	2.97	4.87	2.71	4.00	4.16	2.36	2.77
	3.03	4.84	2.71	3.98	4.15	2.37	2.76
	3.01	4.85	2.71	3.97	4.17	2.37	2.75
	3.63	3.56	3.05	3.88	2.89	2.37	3.04
	3.00	4.85	2.71	4.00	4.14	2.36	2.77
	2.97	4.87	2.70	4.00	4.16	2.36	2.78
	3.60	3.65	3.05	3.89	2.91	2.37	3.03
	2.95	4.89	2.71	4.00	4.16	2.35	2.78
	3.57	3.78	3.05	3.92	2.95	2.36	3.03
	2.97	4.91	2.70	4.00	4.16	2.35	2.78
	3.01	4.85	2.70	3.96	4.17	2.37	2.76
	3.60	3.69	3.05	3.91	2.95	2.36	3.03
	3.01	4.77	2.75	4.00	4.14	2.35	2.76
	2.99	4.90	2.70	3.97	4.18	2.36	2.76
	2.98	4.89	2.70	3.97	4.17	2.36	2.76
	3.03	4.84	2.70	3.97	4.16	2.38	2.76
	3.60	3.65	3.05	3.90	2.93	2.36	3.03
	2.96	4.87	2.71	3.99	4.16	2.37	2.77
	3.61	3.69	3.04	3.90	2.92	2.37	3.03
	3.56	3.81	3.04	3.92	2.95	2.36	3.03
	3.53	3.90	3.04	3.94	2.96	2.37	3.03
	3.61	3.64	3.04	3.88	2.88	2.38	3.04
	3.64	3.51	3.03	3.85	2.85	2.38	3.04
	3.54	3.89	3.04	3.95	3.01	2.35	3.02
	3.00	4.85	2.70	3.99	4.14	2.37	2.78
	3.57	3.75	3.04	3.90	2.91	2.38	3.04
Shortest	2.94	3.51	2.70	3.85	2.85	2.35	2.75

	H4-H9	H4-H8	H8-H9	H9-H7a	H9-H7b	H8-H7a	H8-H7b
	43.67	0.00	43.67	0.00	0.00	43.67	43.67
	13.86	0.00	13.86	0.00	0.00	13.86	13.86
	9.13	0.00	9.13	0.00	0.00	9.13	9.13
	4.77	0.00	4.77	0.00	0.00	4.77	4.77
	0.00	0.00	3.59	0.00	0.00	3.59	3.59
	0.00	0.00	3.45	0.00	0.00	3.45	3.45
	0.00	0.00	0.00	0.00	2.13	2.13	0.00
	0.00	0.00	2.03	0.00	0.00	2.03	2.03
	1.52	0.00	1.52	0.00	0.00	1.52	1.52
	0.00	0.00	0.00	0.00	1.46	1.46	0.00
	1.38	0.00	1.38	0.00	0.00	1.38	1.38
	0.00	0.00	0.00	0.00	1.36	1.36	0.00
	1.12	0.00	1.12	0.00	0.00	1.12	1.12
	0.00	0.00	1.10	0.00	0.00	1.10	1.10
	0.00	0.00	0.00	0.00	0.98	0.98	0.00
	0.00	0.00	0.91	0.00	0.00	0.91	0.91
	0.76	0.00	0.76	0.00	0.00	0.76	0.76
	0.76	0.00	0.76	0.00	0.00	0.76	0.76
	0.00	0.00	0.75	0.00	0.00	0.75	0.75
	0.00	0.00	0.00	0.00	0.75	0.75	0.00
	0.64	0.00	0.64	0.00	0.00	0.64	0.64
	0.00	0.00	0.00	0.00	0.58	0.58	0.00
	0.00	0.00	0.00	0.00	0.52	0.52	0.00
	0.00	0.00	0.00	0.00	0.51	0.51	0.00
	0.00	0.00	0.00	0.00	0.50	0.50	0.00
	0.00	0.00	0.00	0.00	0.50	0.50	0.00
	0.00	0.00	0.00	0.00	0.00	0.43	0.00
	0.00	0.00	0.43	0.00	0.00	0.43	0.43
	0.00	0.00	0.00	0.00	0.41	0.41	0.00
% < 3 Ang	77.61	0.00	89.87	0.00	9.70	100.00	89.87

	H4-H9	H4-H8	H8-H9	H9-H7a	H9-H7b	H8-H7a	H8-H7b
	128.52	212.31	118.32	173.73	182.24	103.28	120.54
	40.85	67.38	37.45	55.11	57.83	32.84	38.38
	26.85	44.71	24.64	36.33	38.16	21.52	25.25
	14.15	23.21	12.92	19.06	19.81	11.23	13.22
	10.86	17.35	9.72	14.26	14.89	8.50	9.88
	10.38	16.75	9.35	13.70	14.39	8.17	9.50
	7.73	7.58	6.48	8.24	6.15	5.05	6.46
	6.11	9.86	5.52	8.14	8.42	4.81	5.64
	4.51	7.38	4.10	6.06	6.30	3.58	4.22
	5.26	5.32	4.44	5.68	4.24	3.46	4.43
	4.07	6.76	3.74	5.53	5.75	3.25	3.84
	4.85	5.14	4.14	5.32	4.01	3.21	4.11
	3.34	5.52	3.04	4.49	4.68	2.64	3.12
	3.31	5.34	2.97	4.36	4.59	2.61	3.04
	3.53	3.63	3.00	3.84	2.90	2.32	2.98
	2.74	4.34	2.50	3.64	3.77	2.13	2.51
	2.29	3.74	2.06	3.03	3.19	1.80	2.11
	2.25	3.69	2.04	3.00	3.15	1.79	2.09
	2.28	3.65	2.04	2.99	3.13	1.79	2.08
	2.70	2.74	2.29	2.93	2.20	1.77	2.28
	1.88	3.10	1.72	2.54	2.64	1.51	1.76
	2.09	2.14	1.76	2.26	1.69	1.37	1.76
	1.85	1.97	1.58	2.03	1.53	1.23	1.57
	1.80	1.99	1.55	2.01	1.51	1.21	1.55
	1.82	1.84	1.53	1.96	1.45	1.20	1.53
	1.82	1.76	1.52	1.92	1.42	1.19	1.52
	1.52	1.67	1.30	1.69	1.29	1.01	1.29
	1.28	2.07	1.16	1.71	1.77	1.01	1.19
	1.47	1.54	1.25	1.61	1.20	0.98	1.25
bolt.Ave.dist	3.02	4.74	2.74	3.97	4.04	2.36	2.79

	H4-H9	H4-H8	H8-H9	H9-H7a	H9-H7b	H8-H7a	H8-H7b		H8-H9	H8-H7a	H8-H7b
	0.02	0.00	0.03	0.00	0.00	0.07	0.10		-83.86	-30.41	91.33
	0.01	0.00	0.01	0.00	0.00	0.02	0.03		-83.82	-30.31	91.51
	0.00	0.00	0.01	0.00	0.00	0.02	0.02		-83.38	-29.45	92.22
	0.00	0.00	0.00	0.00	0.00	0.01	0.01		-84.45	-28.20	93.55
	0.00	0.00	0.00	0.00	0.00	0.01	0.01		-86.31	-31.09	90.62
	0.00	0.00	0.00	0.00	0.00	0.01	0.01		-84.77	-31.66	90.12
	0.00	0.00	0.00	0.00	0.00	0.00	0.00		-163.06	32.57	155.54
	0.00	0.00	0.00	0.00	0.00	0.00	0.00		-86.42	-28.38	93.26
	0.00	0.00	0.00	0.00	0.00	0.00	0.00		-84.47	-28.15	93.69
	0.00	0.00	0.00	0.00	0.00	0.00	0.00		-161.43	32.82	155.89
	0.00	0.00	0.00	0.00	0.00	0.00	0.00		-84.04	-27.33	94.43
	0.00	0.00	0.00	0.00	0.00	0.00	0.00		-159.20	32.06	154.96
	0.00	0.00	0.00	0.00	0.00	0.00	0.00		-84.17	-27.36	94.33
	0.00	0.00	0.00	0.00	0.00	0.00	0.00		-84.72	-31.60	90.25
	0.00	0.00	0.00	0.00	0.00	0.00	0.00		-160.13	31.74	154.49
	0.00	0.00	0.00	0.00	0.00	0.00	0.00		-88.74	-28.64	92.94
	0.00	0.00	0.00	0.00	0.00	0.00	0.00		-83.97	-30.65	91.04
	0.00	0.00	0.00	0.00	0.00	0.00	0.00		-83.97	-30.56	91.20
	0.00	0.00	0.00	0.00	0.00	0.00	0.00		-85.80	-31.42	90.39
	0.00	0.00	0.00	0.00	0.00	0.00	0.00		-161.80	33.19	156.24
	0.00	0.00	0.00	0.00	0.00	0.00	0.00		-84.83	-29.64	91.95
	0.00	0.00	0.00	0.00	0.00	0.00	0.00		-160.75	32.40	155.31
	0.00	0.00	0.00	0.00	0.00	0.00	0.00		-158.14	32.40	155.42
	0.00	0.00	0.00	0.00	0.00	0.00	0.00		-156.67	33.05	156.09
	0.00	0.00	0.00	0.00	0.00	0.00	0.00		-161.96	33.98	157.06
	0.00	0.00	0.00	0.00	0.00	0.00	0.00		-163.23	33.47	156.60
	0.00	0.00	0.00	0.00	0.00	0.00	0.00		-155.58	30.90	153.57
	0.00	0.00	0.00	0.00	0.00	0.00	0.00		-85.91	-28.69	93.06
	0.00	0.00	0.00	0.00	0.00	0.00	0.00		-159.70	34.09	157.30
1/r^6	0.04	0.00	0.07	0.01	0.01	0.17	0.21				

Table 2.2: *Molecular modelling data for 4S, 5S, 8R, 9R*

Potential Energy-OPLS-AA	E/kT	e-E/kT	Ne-E/kT	Boltzmann	%	E*%	Bolt.Ave.E
356.68	-143.00	7.91E-63	2.37E-61	10.27	34.24	12214.16	359.43
357.05	-143.14	6.82E-63	2.05E-61	8.86	29.55	10549.10	
361.59	-144.96	1.10E-63	3.31E-62	1.44	4.79	1730.36	
362.56	-145.35	7.50E-64	2.25E-62	0.97	3.25	1177.79	
362.58	-145.36	7.44E-64	2.23E-62	0.97	3.22	1168.07	
362.58	-145.36	7.43E-64	2.23E-62	0.96	3.22	1166.22	
362.67	-145.40	7.17E-64	2.15E-62	0.93	3.11	1126.11	
363.53	-145.74	5.08E-64	1.52E-62	0.66	2.20	800.39	
364.08	-145.96	4.07E-64	1.22E-62	0.53	1.76	641.87	
364.26	-146.03	3.79E-64	1.14E-62	0.49	1.64	598.63	
364.44	-146.10	3.53E-64	1.06E-62	0.46	1.53	557.07	
364.51	-146.13	3.42E-64	1.03E-62	0.44	1.48	540.59	
364.74	-146.23	3.12E-64	9.36E-63	0.41	1.35	493.08	
365.62	-146.58	2.20E-64	6.60E-63	0.29	0.95	348.33	
365.68	-146.60	2.14E-64	6.43E-63	0.28	0.93	339.53	
366.72	-147.02	1.41E-64	4.24E-63	0.18	0.61	224.60	
366.73	-147.02	1.41E-64	4.22E-63	0.18	0.61	223.55	
366.84	-147.07	1.35E-64	4.04E-63	0.18	0.58	214.19	
366.86	-147.08	1.34E-64	4.01E-63	0.17	0.58	212.19	
367.01	-147.14	1.26E-64	3.77E-63	0.16	0.54	199.92	
367.05	-147.15	1.24E-64	3.71E-63	0.16	0.54	196.73	
367.26	-147.24	1.14E-64	3.41E-63	0.15	0.49	180.96	
367.85	-147.47	8.99E-65	2.70E-63	0.12	0.39	143.30	
367.86	-147.48	8.96E-65	2.69E-63	0.12	0.39	142.71	
367.86	-147.48	8.95E-65	2.69E-63	0.12	0.39	142.65	
367.94	-147.51	8.65E-65	2.59E-63	0.11	0.37	137.83	
367.97	-147.52	8.55E-65	2.57E-63	0.11	0.37	136.32	
368.38	-147.69	7.25E-65	2.18E-63	0.09	0.31	115.76	
368.48	-147.73	6.97E-65	2.09E-63	0.09	0.30	111.31	
368.53	-147.74	6.84E-65	2.05E-63	0.09	0.30	109.27	

	H4-H9	H4-H8	H8-H9	H9-H7a	H9-H7b	H8-H7a	H8-H7b
	2.94	4.86	2.71	3.98	4.17	2.37	2.76
	2.95	4.86	2.70	3.98	4.17	2.37	2.77
	2.94	4.90	2.70	3.98	4.18	2.36	2.77
	2.97	4.87	2.71	4.00	4.16	2.36	2.77
	3.03	4.84	2.71	3.98	4.15	2.37	2.76
	3.01	4.85	2.71	3.97	4.17	2.37	2.75
	3.63	3.56	3.05	3.88	2.89	2.37	3.04
	3.00	4.85	2.71	4.00	4.14	2.36	2.77
	2.97	4.87	2.70	4.00	4.16	2.36	2.78
	3.60	3.65	3.05	3.89	2.91	2.37	3.03
	2.95	4.89	2.71	4.00	4.16	2.35	2.78
	3.57	3.78	3.05	3.92	2.95	2.36	3.03
	2.97	4.91	2.70	4.00	4.16	2.35	2.78
	3.01	4.85	2.70	3.96	4.17	2.37	2.76
	3.60	3.69	3.05	3.91	2.95	2.36	3.03
	3.01	4.77	2.75	4.00	4.14	2.35	2.76
	2.99	4.90	2.70	3.97	4.18	2.36	2.76
	2.98	4.89	2.70	3.97	4.17	2.36	2.76
	3.03	4.84	2.70	3.97	4.16	2.38	2.76
	3.60	3.65	3.05	3.90	2.93	2.36	3.03
	2.96	4.87	2.71	3.99	4.16	2.37	2.77
	3.61	3.69	3.04	3.90	2.92	2.37	3.03
	3.56	3.81	3.04	3.92	2.95	2.36	3.03
	3.53	3.90	3.04	3.94	2.96	2.37	3.03
	3.61	3.64	3.04	3.88	2.88	2.38	3.04
	3.64	3.51	3.03	3.85	2.85	2.38	3.04
	3.54	3.89	3.04	3.95	3.01	2.35	3.02
	3.00	4.85	2.70	3.99	4.14	2.37	2.78
	3.57	3.75	3.04	3.90	2.91	2.38	3.04
	2.65	4.68	3.04	2.82	3.79	3.04	2.37
Shortest	2.65	3.51	2.70	2.82	2.85	2.35	2.37

	H4-H9	H4-H8	H8-H9	H9-H7a	H9-H7b	H8-H7a	H8-H7b
	34.24	0.00	34.24	0.00	0.00	34.24	34.24
	29.55	0.00	29.55	0.00	0.00	29.55	29.55
	4.79	0.00	4.79	0.00	0.00	4.79	4.79
	3.25	0.00	3.25	0.00	0.00	3.25	3.25
	0.00	0.00	3.22	0.00	0.00	3.22	3.22
	0.00	0.00	3.22	0.00	0.00	3.22	3.22
	0.00	0.00	0.00	0.00	3.11	3.11	0.00
	0.00	0.00	2.20	0.00	0.00	2.20	2.20
	1.76	0.00	1.76	0.00	0.00	1.76	1.76
	0.00	0.00	0.00	0.00	1.64	1.64	0.00
	1.53	0.00	1.53	0.00	0.00	1.53	1.53
	0.00	0.00	0.00	0.00	1.48	1.48	0.00
	1.35	0.00	1.35	0.00	0.00	1.35	1.35
	0.00	0.00	0.95	0.00	0.00	0.95	0.95
	0.00	0.00	0.00	0.00	0.93	0.93	0.00
	0.00	0.00	0.61	0.00	0.00	0.61	0.61
	0.61	0.00	0.61	0.00	0.00	0.61	0.61
	0.58	0.00	0.58	0.00	0.00	0.58	0.58
	0.00	0.00	0.58	0.00	0.00	0.58	0.58
	0.00	0.00	0.00	0.00	0.54	0.54	0.00
	0.54	0.00	0.54	0.00	0.00	0.54	0.54
	0.00	0.00	0.00	0.00	0.49	0.49	0.00
	0.00	0.00	0.00	0.00	0.39	0.39	0.00
	0.00	0.00	0.00	0.00	0.39	0.39	0.00
	0.00	0.00	0.00	0.00	0.39	0.39	0.00
	0.00	0.00	0.00	0.00	0.37	0.37	0.00
	0.00	0.00	0.00	0.00	0.00	0.37	0.00
	0.00	0.00	0.31	0.00	0.00	0.31	0.31
	0.00	0.00	0.00	0.00	0.30	0.30	0.00
	0.30	0.00	0.00	0.30	0.00	0.00	0.30
% < 3 Ang	78.49	0.00	89.29	0.30	10.04	99.70	89.59

	H4-H9	H4-H8	H8-H9	H9-H7a	H9-H7b	H8-H7a	H8-H7b
	0.00	0.00	0.00	0.00	0.00	34.24	0.00
	0.00	0.00	0.00	0.00	0.00	29.55	0.00
	0.00	0.00	0.00	0.00	0.00	4.79	0.00
	0.00	0.00	0.00	0.00	0.00	3.25	0.00
	0.00	0.00	0.00	0.00	0.00	3.22	0.00
	0.00	0.00	0.00	0.00	0.00	3.22	0.00
	0.00	0.00	0.00	0.00	0.00	3.11	0.00
	0.00	0.00	0.00	0.00	0.00	2.20	0.00
	0.00	0.00	0.00	0.00	0.00	1.76	0.00
	0.00	0.00	0.00	0.00	0.00	1.64	0.00
	0.00	0.00	0.00	0.00	0.00	1.53	0.00
	0.00	0.00	0.00	0.00	0.00	1.48	0.00
	0.00	0.00	0.00	0.00	0.00	1.35	0.00
	0.00	0.00	0.00	0.00	0.00	0.95	0.00
	0.00	0.00	0.00	0.00	0.00	0.93	0.00
	0.00	0.00	0.00	0.00	0.00	0.61	0.00
	0.00	0.00	0.00	0.00	0.00	0.61	0.00
	0.00	0.00	0.00	0.00	0.00	0.58	0.00
	0.00	0.00	0.00	0.00	0.00	0.58	0.00
	0.00	0.00	0.00	0.00	0.00	0.54	0.00
	0.00	0.00	0.00	0.00	0.00	0.54	0.00
	0.00	0.00	0.00	0.00	0.00	0.49	0.00
	0.00	0.00	0.00	0.00	0.00	0.39	0.00
	0.00	0.00	0.00	0.00	0.00	0.39	0.00
	0.00	0.00	0.00	0.00	0.00	0.39	0.00
	0.00	0.00	0.00	0.00	0.00	0.37	0.00
	0.00	0.00	0.00	0.00	0.00	0.37	0.00
	0.00	0.00	0.00	0.00	0.00	0.31	0.00
	0.00	0.00	0.00	0.00	0.00	0.30	0.00
	0.00	0.00	0.00	0.00	0.00	0.00	0.30
% < 2.5 Ang	0.00	0.00	0.00	0.00	0.00	99.70	0.30

	H4-H9	H4-H8	H8-H9	H9-H7a	H9-H7b	H8-H7a	H8-H7b
	100.78	166.49	92.79	136.24	142.91	80.99	94.53
	87.06	143.59	79.82	117.45	123.24	69.98	81.79
	14.07	23.43	12.91	19.04	20.00	11.28	13.23
	9.65	15.82	8.81	12.99	13.51	7.66	9.01
	9.76	15.59	8.73	12.81	13.38	7.64	8.88
	9.67	15.61	8.72	12.76	13.41	7.62	8.85
	11.28	11.06	9.46	12.03	8.98	7.37	9.42
	6.62	10.67	5.97	8.81	9.11	5.20	6.11
	5.24	8.58	4.77	7.04	7.33	4.16	4.90
	5.92	5.99	5.00	6.39	4.78	3.89	4.98
	4.50	7.48	4.14	6.12	6.36	3.60	4.25
	5.29	5.61	4.52	5.81	4.37	3.50	4.49
	4.02	6.64	3.65	5.41	5.63	3.18	3.76
	2.87	4.62	2.57	3.78	3.97	2.26	2.63
	3.34	3.43	2.83	3.63	2.74	2.19	2.81
	1.85	2.92	1.68	2.45	2.54	1.44	1.69
	1.82	2.98	1.64	2.42	2.55	1.44	1.68
	1.74	2.85	1.58	2.32	2.44	1.38	1.61
	1.75	2.80	1.56	2.30	2.40	1.38	1.60
	1.96	1.99	1.66	2.12	1.59	1.28	1.65
	1.59	2.61	1.45	2.14	2.23	1.27	1.48
	1.78	1.82	1.50	1.92	1.44	1.17	1.49
	1.39	1.48	1.18	1.53	1.15	0.92	1.18
	1.37	1.51	1.18	1.53	1.15	0.92	1.18
	1.40	1.41	1.18	1.50	1.12	0.92	1.18
	1.36	1.32	1.14	1.44	1.07	0.89	1.14
	1.31	1.44	1.13	1.46	1.12	0.87	1.12
	0.94	1.52	0.85	1.25	1.30	0.74	0.87
	1.08	1.13	0.92	1.18	0.88	0.72	0.92
	0.79	1.39	0.90	0.84	1.12	0.90	0.70
bolt.Ave.dist	3.02	4.74	2.74	3.97	4.04	2.37	2.79

	H4-H9	H4-H8	H8-H9	H9-H7a	H9-H7b	H8-H7a	H8-H7b		H8-H9	H8-H7a	H8-H7b
	0.02	0.00	0.03	0.00	0.00	0.06	0.08		169.08	-152.29	-29.47
	0.01	0.00	0.02	0.00	0.00	0.05	0.07		169.45	-154.51	-31.67
	0.00	0.00	0.00	0.00	0.00	0.01	0.01		169.39	-154.10	-31.31
	0.00	0.00	0.00	0.00	0.00	0.01	0.01		168.47	-155.70	-32.74
	0.00	0.00	0.00	0.00	0.00	0.01	0.01		169.22	-153.09	-30.14
	0.00	0.00	0.00	0.00	0.00	0.01	0.01		168.47	-153.24	-30.33
	0.00	0.00	0.00	0.00	0.00	0.01	0.00		169.48	-155.42	-32.44
	0.00	0.00	0.00	0.00	0.00	0.00	0.00		82.72	-90.18	31.65
	0.00	0.00	0.00	0.00	0.00	0.00	0.00		169.32	-152.29	-29.57
	0.00	0.00	0.00	0.00	0.00	0.00	0.00		169.63	-154.71	-31.97
	0.00	0.00	0.00	0.00	0.00	0.00	0.00		169.56	-155.50	-32.55
	0.00	0.00	0.00	0.00	0.00	0.00	0.00		169.43	-153.27	-30.36
	0.00	0.00	0.00	0.00	0.00	0.00	0.00		82.91	-89.81	32.04
	0.00	0.00	0.00	0.00	0.00	0.00	0.00		166.24	-148.88	-26.36
	0.00	0.00	0.00	0.00	0.00	0.00	0.00		167.22	-151.45	-28.89
	0.00	0.00	0.00	0.00	0.00	0.00	0.00		167.47	-152.66	-29.91
	0.00	0.00	0.00	0.00	0.00	0.00	0.00		170.62	-153.01	-30.22
	0.00	0.00	0.00	0.00	0.00	0.00	0.00		166.57	-149.99	-27.28
	0.00	0.00	0.00	0.00	0.00	0.00	0.00		82.42	-90.34	31.47
	0.00	0.00	0.00	0.00	0.00	0.00	0.00		170.96	-155.09	-32.29
	0.00	0.00	0.00	0.00	0.00	0.00	0.00		82.75	-90.09	31.73
	0.00	0.00	0.00	0.00	0.00	0.00	0.00		169.43	-154.98	-32.05
	0.00	0.00	0.00	0.00	0.00	0.00	0.00		167.49	-151.87	-29.36
	0.00	0.00	0.00	0.00	0.00	0.00	0.00		168.31	-155.48	-32.56
	0.00	0.00	0.00	0.00	0.00	0.00	0.00		166.47	-149.10	-26.64
	0.00	0.00	0.00	0.00	0.00	0.00	0.00		167.26	-152.88	-30.15
	0.00	0.00	0.00	0.00	0.00	0.00	0.00		166.39	-150.18	-27.50
	0.00	0.00	0.00	0.00	0.00	0.00	0.00		168.22	-151.05	-28.23
	0.00	0.00	0.00	0.00	0.00	0.00	0.00		81.85	-89.68	32.27
	0.00	0.00	0.00	0.00	0.00	0.00	0.00		167.76	-152.83	-30.12
1/r^6	0.04	0.00	0.07	0.01	0.01	0.17	0.22				

Table 2.3: *Molecular modelling data for 4R, 5S, 8S, 9S.*

Potential Energy-OPLS-AA	E/kT	e-E/kT	Ne-E/kT	Boltzmann	%	E*%	Bolt.Ave.E
324.99	-130.29	2.60E-57	5.20E-56	5.13	25.66	8340.13	326.79
325.01	-130.30	2.58E-57	5.16E-56	5.09	25.46	8276.28	
326.08	-130.73	1.68E-57	3.36E-56	3.32	16.59	5408.98	
327.88	-131.45	8.18E-58	1.64E-56	1.61	8.07	2647.11	
328.87	-131.84	5.51E-58	1.10E-56	1.09	5.44	1788.07	
329.16	-131.96	4.89E-58	9.77E-57	0.96	4.82	1588.19	
329.82	-132.23	3.75E-58	7.51E-57	0.74	3.71	1222.48	
330.21	-132.38	3.21E-58	6.43E-57	0.63	3.17	1048.11	
331.17	-132.77	2.18E-58	4.37E-57	0.43	2.16	713.90	
333.26	-133.61	9.45E-59	1.89E-57	0.19	0.93	310.93	
334.09	-133.94	6.79E-59	1.36E-57	0.13	0.67	223.87	
334.26	-134.01	6.32E-59	1.26E-57	0.12	0.62	208.66	
334.56	-134.12	5.63E-59	1.13E-57	0.11	0.56	185.89	
335.27	-134.41	4.22E-59	8.44E-58	0.08	0.42	139.66	
335.61	-134.55	3.68E-59	7.36E-58	0.07	0.36	121.97	
335.65	-134.56	3.63E-59	7.25E-58	0.07	0.36	120.17	
336.25	-134.81	2.85E-59	5.70E-58	0.06	0.28	94.60	
336.48	-134.90	2.60E-59	5.21E-58	0.05	0.26	86.54	
336.65	-134.96	2.43E-59	4.86E-58	0.05	0.24	80.82	
336.93	-135.08	2.17E-59	4.34E-58	0.04	0.21	72.21	

	H4-H9	H4-H8	H8-H9	H9-H7a	H9-H7b	H8-H7a	H8-H7b
	3.95	4.85	2.71	3.99	4.16	2.36	2.77
	3.95	4.84	2.71	3.99	4.16	2.36	2.78
	3.93	4.82	2.71	3.99	4.16	2.36	2.78
	3.95	4.85	2.70	3.98	4.16	2.36	2.78
	3.96	4.85	2.70	3.98	4.16	2.36	2.78
	3.94	4.87	2.70	3.99	4.17	2.35	2.77
	3.93	4.83	2.70	3.98	4.16	2.36	2.78
	3.95	4.87	2.69	3.99	4.17	2.35	2.78
	3.92	4.86	2.69	3.99	4.17	2.35	2.78
	3.94	4.84	2.71	4.00	4.14	2.37	2.78
	3.98	4.68	2.75	4.02	4.12	2.33	2.79
	4.19	3.18	3.05	3.88	2.88	2.38	3.04
	3.99	4.68	2.75	4.02	4.12	2.34	2.78
	3.89	4.88	2.71	4.00	4.16	2.35	2.78
	4.18	3.32	3.04	3.91	2.92	2.37	3.03
	3.96	4.67	2.75	4.02	4.12	2.34	2.79
	3.89	4.89	2.71	4.00	4.16	2.35	2.78
	4.18	3.40	3.04	3.93	2.97	2.36	3.03
	4.18	3.02	3.04	3.83	2.82	2.39	3.04
	3.99	4.69	2.74	4.01	4.12	2.34	2.78
Shortest	3.89	3.02	2.69	3.83	2.82	2.33	2.77

	H4-H9	H4-H8	H8-H9	H9-H7a	H9-H7b	H8-H7a	H8-H7b
	0.00	0.00	25.66	0.00	0.00	25.66	25.66
	0.00	0.00	25.46	0.00	0.00	25.46	25.46
	0.00	0.00	16.59	0.00	0.00	16.59	16.59
	0.00	0.00	8.07	0.00	0.00	8.07	8.07
	0.00	0.00	5.44	0.00	0.00	5.44	5.44
	0.00	0.00	4.82	0.00	0.00	4.82	4.82
	0.00	0.00	3.71	0.00	0.00	3.71	3.71
	0.00	0.00	3.17	0.00	0.00	3.17	3.17
	0.00	0.00	2.16	0.00	0.00	2.16	2.16
	0.00	0.00	0.93	0.00	0.00	0.93	0.93
	0.00	0.00	0.67	0.00	0.00	0.67	0.67
	0.00	0.00	0.00	0.00	0.62	0.62	0.00
	0.00	0.00	0.56	0.00	0.00	0.56	0.56
	0.00	0.00	0.42	0.00	0.00	0.42	0.42
	0.00	0.00	0.00	0.00	0.36	0.36	0.00
	0.00	0.00	0.36	0.00	0.00	0.36	0.36
	0.00	0.00	0.28	0.00	0.00	0.28	0.28
	0.00	0.00	0.00	0.00	0.26	0.26	0.00
	0.00	0.00	0.00	0.00	0.24	0.24	0.00
	0.00	0.00	0.21	0.00	0.00	0.21	0.21
% < 3 Ang	0.00	0.00	98.52	0.00	1.48	100.00	98.52

	H4-H9	H4-H8	H8-H9	H9-H7a	H9-H7b	H8-H7a	H8-H7b
	0.00	0.00	0.00	0.00	0.00	25.66	0.00
	0.00	0.00	0.00	0.00	0.00	25.46	0.00
	0.00	0.00	0.00	0.00	0.00	16.59	0.00
	0.00	0.00	0.00	0.00	0.00	8.07	0.00
	0.00	0.00	0.00	0.00	0.00	5.44	0.00
	0.00	0.00	0.00	0.00	0.00	4.82	0.00
	0.00	0.00	0.00	0.00	0.00	3.71	0.00
	0.00	0.00	0.00	0.00	0.00	3.17	0.00
	0.00	0.00	0.00	0.00	0.00	2.16	0.00
	0.00	0.00	0.00	0.00	0.00	0.93	0.00
	0.00	0.00	0.00	0.00	0.00	0.67	0.00
	0.00	0.00	0.00	0.00	0.00	0.62	0.00
	0.00	0.00	0.00	0.00	0.00	0.56	0.00
	0.00	0.00	0.00	0.00	0.00	0.42	0.00
	0.00	0.00	0.00	0.00	0.00	0.36	0.00
	0.00	0.00	0.00	0.00	0.00	0.36	0.00
	0.00	0.00	0.00	0.00	0.00	0.28	0.00
	0.00	0.00	0.00	0.00	0.00	0.26	0.00
	0.00	0.00	0.00	0.00	0.00	0.24	0.00
	0.00	0.00	0.00	0.00	0.00	0.21	0.00
% < 2.5 Ang	0.00	0.00	0.00	0.00	0.00	100.00	0.00

	H4-H9	H4-H8	H8-H9	H9-H7a	H9-H7b	H8-H7a	H8-H7b
	101.36	124.42	69.45	102.30	106.76	60.55	71.07
	100.70	123.37	68.89	101.62	105.90	60.07	70.70
	65.20	80.03	44.87	66.22	68.97	39.12	46.07
	31.90	39.13	21.79	32.16	33.57	19.08	22.42
	21.50	26.36	14.66	21.66	22.62	12.85	15.13
	19.03	23.50	13.01	19.23	20.10	11.35	13.38
	14.57	17.89	9.99	14.77	15.42	8.76	10.32
	12.53	15.46	8.55	12.65	13.23	7.47	8.82
	8.46	10.47	5.81	8.60	8.98	5.07	5.99
	3.68	4.52	2.53	3.73	3.87	2.21	2.59
	2.67	3.14	1.84	2.70	2.76	1.56	1.87
	2.62	1.99	1.90	2.42	1.80	1.48	1.90
	2.21	2.60	1.53	2.23	2.29	1.30	1.54
	1.62	2.03	1.13	1.67	1.73	0.98	1.16
	1.52	1.21	1.10	1.42	1.06	0.86	1.10
	1.42	1.67	0.98	1.44	1.48	0.84	1.00
	1.09	1.38	0.76	1.13	1.17	0.66	0.78
	1.07	0.87	0.78	1.01	0.76	0.61	0.78
	1.00	0.72	0.73	0.92	0.68	0.57	0.73
	0.85	1.00	0.59	0.86	0.88	0.50	0.60
bolt.Ave.dist	3.95	4.82	2.71	3.99	4.14	2.36	2.78

	H4-H9	H4-H8	H8-H9	H9-H7a	H9-H7b	H8-H7a	H8-H7b		H8-H9	H8-H7a	H8-H7b
	0.00	0.00	0.01	0.00	0.00	0.03	0.06		-83.84	-28.89	92.90
	0.00	0.00	0.01	0.00	0.00	0.03	0.06		-84.11	-28.16	93.61
	0.00	0.00	0.01	0.00	0.00	0.02	0.04		-84.09	-27.99	93.78
	0.00	0.00	0.00	0.00	0.00	0.01	0.02		-83.85	-28.76	93.12
	0.00	0.00	0.00	0.00	0.00	0.01	0.01		-83.77	-28.39	93.48
	0.00	0.00	0.00	0.00	0.00	0.01	0.01		-83.57	-28.00	93.72
	0.00	0.00	0.00	0.00	0.00	0.00	0.01		-83.73	-28.28	93.58
	0.00	0.00	0.00	0.00	0.00	0.00	0.01		-83.59	-27.65	94.07
	0.00	0.00	0.00	0.00	0.00	0.00	0.00		-83.56	-27.46	94.25
	0.00	0.00	0.00	0.00	0.00	0.00	0.00		-84.83	-27.69	93.92
	0.00	0.00	0.00	0.00	0.00	0.00	0.00		-89.88	-24.83	96.72
	0.00	0.00	0.00	0.00	0.00	0.00	0.00		-161.79	33.83	156.89
	0.00	0.00	0.00	0.00	0.00	0.00	0.00		-89.80	-26.10	95.47
	0.00	0.00	0.00	0.00	0.00	0.00	0.00		-83.23	-27.01	94.76
	0.00	0.00	0.00	0.00	0.00	0.00	0.00		-158.30	33.92	157.10
	0.00	0.00	0.00	0.00	0.00	0.00	0.00		-89.36	-25.00	96.55
	0.00	0.00	0.00	0.00	0.00	0.00	0.00		-82.90	-26.89	94.91
	0.00	0.00	0.00	0.00	0.00	0.00	0.00		-156.31	32.68	155.53
	0.00	0.00	0.00	0.00	0.00	0.00	0.00		-164.08	34.30	157.39
	0.00	0.00	0.00	0.00	0.00	0.00	0.00		-89.65	-26.15	95.54
1/r^6	0.01	0.00	0.05	0.00	0.00	0.12	0.22				

Table 2.4: *Molecular modelling data for 4R, 5S, 8R, 9R*

Potential Energy-OPLS-AA	E/kT	e-E/kT	Ne-E/kT	Boltzmann	%	E*%	Bolt.Ave.E
343.34	-137.65	1.66E-60	2.16E-59	5.18	39.82	######	345.50
345.09	-138.35	8.25E-61	1.07E-59	2.57	19.76	6820.61	
346.28	-138.83	5.11E-61	6.64E-60	1.59	12.24	4239.23	
346.80	-139.04	4.15E-61	5.39E-60	1.29	9.93	3445.36	
347.15	-139.17	3.61E-61	4.69E-60	1.12	8.64	2999.39	
349.90	-140.28	1.20E-61	1.56E-60	0.37	2.87	1004.88	
350.89	-140.67	8.06E-62	1.05E-60	0.25	1.93	677.78	
351.36	-140.86	6.67E-62	8.68E-61	0.21	1.60	561.71	
351.94	-141.09	5.29E-62	6.88E-61	0.16	1.27	446.03	
353.79	-141.84	2.52E-62	3.27E-61	0.08	0.60	213.15	
353.99	-141.92	2.33E-62	3.02E-61	0.07	0.56	197.16	
354.90	-142.28	1.62E-62	2.10E-61	0.05	0.39	137.46	
354.94	-142.30	1.59E-62	2.07E-61	0.05	0.38	135.28	

	H4-H9	H4-H8	H8-H9	H9-H7a	H9-H7b	H8-H7a	H8-H7b
	2.87	4.88	3.05	2.82	3.79	3.04	2.38
	2.92	4.89	3.05	2.82	3.79	3.04	2.38
	2.85	4.87	3.05	2.82	3.79	3.04	2.38
	2.93	4.89	3.05	2.82	3.80	3.04	2.38
	2.83	4.90	3.04	2.85	3.79	3.03	2.37
	2.89	4.88	3.05	2.81	3.79	3.04	2.38
	2.81	4.89	3.04	2.85	3.79	3.03	2.37
	2.89	4.89	3.06	2.83	3.80	3.04	2.37
	2.89	4.88	3.05	2.83	3.80	3.04	2.37
	2.89	4.92	3.05	2.85	3.80	3.03	2.37
	2.86	4.91	3.04	2.84	3.79	3.03	2.37
	2.91	4.88	3.05	2.81	3.79	3.04	2.38
	2.86	4.92	3.05	2.86	3.80	3.03	2.36
Shortest	2.81	4.87	3.04	2.81	3.79	3.03	2.36

	H4-H9	H4-H8	H8-H9	H9-H7a	H9-H7b	H8-H7a	H8-H7b
	39.82	0.00	0.00	39.82	0.00	0.00	39.82
	19.76	0.00	0.00	19.76	0.00	0.00	19.76
	12.24	0.00	0.00	12.24	0.00	0.00	12.24
	9.93	0.00	0.00	9.93	0.00	0.00	9.93
	8.64	0.00	0.00	8.64	0.00	0.00	8.64
	2.87	0.00	0.00	2.87	0.00	0.00	2.87
	1.93	0.00	0.00	1.93	0.00	0.00	1.93
	1.60	0.00	0.00	1.60	0.00	0.00	1.60
	1.27	0.00	0.00	1.27	0.00	0.00	1.27
	0.60	0.00	0.00	0.60	0.00	0.00	0.60
	0.56	0.00	0.00	0.56	0.00	0.00	0.56
	0.39	0.00	0.00	0.39	0.00	0.00	0.39
	0.38	0.00	0.00	0.38	0.00	0.00	0.38
% < 3 Ang	100.00	0.00	0.00	100.00	0.00	0.00	100.00

	H4-H9	H4-H8	H8-H9	H9-H7a	H9-H7b	H8-H7a	H8-H7b
	0.00	0.00	0.00	0.00	0.00	0.00	39.82
	0.00	0.00	0.00	0.00	0.00	0.00	19.76
	0.00	0.00	0.00	0.00	0.00	0.00	12.24
	0.00	0.00	0.00	0.00	0.00	0.00	9.93
	0.00	0.00	0.00	0.00	0.00	0.00	8.64
	0.00	0.00	0.00	0.00	0.00	0.00	2.87
	0.00	0.00	0.00	0.00	0.00	0.00	1.93
	0.00	0.00	0.00	0.00	0.00	0.00	1.60
	0.00	0.00	0.00	0.00	0.00	0.00	1.27
	0.00	0.00	0.00	0.00	0.00	0.00	0.60
	0.00	0.00	0.00	0.00	0.00	0.00	0.56
	0.00	0.00	0.00	0.00	0.00	0.00	0.39
	0.00	0.00	0.00	0.00	0.00	0.00	0.38
% < 2.5 Ang	0.00	0.00	0.00	0.00	0.00	0.00	100.00

	H4-H9	H4-H8	H8-H9	H9-H7a	H9-H7b	H8-H7a	H8-H7b
	114.17	194.27	121.57	112.25	150.83	121.13	94.73
	57.70	96.68	60.37	55.75	74.98	60.09	46.98
	34.95	59.64	37.37	34.52	46.42	37.23	29.11
	29.14	48.58	30.35	28.03	37.73	30.21	23.62
	24.44	42.38	26.30	24.63	32.74	26.20	20.48
	8.30	14.03	8.76	8.06	10.87	8.73	6.83
	5.43	9.45	5.88	5.50	7.32	5.86	4.58
	4.61	7.81	4.89	4.52	6.07	4.85	3.79
	3.66	6.18	3.87	3.59	4.81	3.85	3.00
	1.74	2.97	1.83	1.72	2.29	1.83	1.43
	1.60	2.74	1.70	1.58	2.11	1.69	1.32
	1.13	1.89	1.18	1.09	1.47	1.18	0.92
	1.09	1.87	1.16	1.09	1.45	1.15	0.90
bolt.Ave.dist	2.88	4.88	3.05	2.82	3.79	3.04	2.38

	H4-H9	H4-H8	H8-H9	H9-H7a	H9-H7b	H8-H7a	H8-H7b		H8-H9	H8-H7a	H8-H7b
	0.01	0.00	0.01	0.01	0.00	0.01	0.22		169.38	-152.63	-29.75
	0.00	0.00	0.00	0.01	0.00	0.00	0.11		168.82	-152.67	-29.80
	0.00	0.00	0.00	0.00	0.00	0.00	0.07		169.15	-152.91	-30.00
	0.00	0.00	0.00	0.00	0.00	0.00	0.06		168.72	-153.04	-30.13
	0.00	0.00	0.00	0.00	0.00	0.00	0.05		166.71	-149.30	-26.70
	0.00	0.00	0.00	0.00	0.00	0.00	0.02		169.08	-153.34	-30.37
	0.00	0.00	0.00	0.00	0.00	0.00	0.01		166.74	-149.58	-26.94
	0.00	0.00	0.00	0.00	0.00	0.00	0.01		169.18	-152.49	-29.76
	0.00	0.00	0.00	0.00	0.00	0.00	0.01		169.34	-153.49	-30.55
	0.00	0.00	0.00	0.00	0.00	0.00	0.00		166.18	-149.20	-26.66
	0.00	0.00	0.00	0.00	0.00	0.00	0.00		166.55	-150.04	-27.33
	0.00	0.00	0.00	0.00	0.00	0.00	0.00		168.79	-153.92	-30.88
	0.00	0.00	0.00	0.00	0.00	0.00	0.00		166.49	-149.22	-26.75
1/r^6	0.02	0.00	0.02	0.03	0.00	0.02	0.55				

Figure 2.5: *Molecular modelling data for 4R, 5S, 8S, 9R*

Potential Energy-OPLS-AA	E/kT	e-E/kT	Ne-E/kT	Boltzmann	%	E*%	Bolt.Ave.E
342.68	-137.38	2.16E-60	3.46E-59	4.75	29.67	######	345.13
344.57	-138.14	1.02E-60	1.62E-59	2.23	13.93	4799.35	
345.05	-138.33	8.38E-61	1.34E-59	1.84	11.49	3966.31	
345.40	-138.47	7.27E-61	1.16E-59	1.60	9.98	3445.51	
345.97	-138.70	5.80E-61	9.28E-60	1.27	7.96	2752.40	
346.34	-138.85	4.99E-61	7.98E-60	1.10	6.85	2371.52	
346.79	-139.03	4.17E-61	6.67E-60	0.91	5.72	1982.50	
347.04	-139.13	3.78E-61	6.04E-60	0.83	5.18	1798.74	
348.23	-139.61	2.34E-61	3.74E-60	0.51	3.21	1117.60	
349.14	-139.97	1.62E-61	2.60E-60	0.36	2.23	777.71	
350.15	-140.38	1.08E-61	1.74E-60	0.24	1.49	520.99	
352.24	-141.22	4.69E-62	7.50E-61	0.10	0.64	226.62	
352.69	-141.40	3.92E-62	6.27E-61	0.09	0.54	189.49	
353.48	-141.71	2.85E-62	4.56E-61	0.06	0.39	138.25	
353.58	-141.75	2.74E-62	4.38E-61	0.06	0.38	132.69	
353.72	-141.81	2.60E-62	4.15E-61	0.06	0.36	125.98	

	H4-H9	H4-H8	H8-H9	H9-H7a	H9-H7b	H8-H7a	H8-H7b
	2.84	4.78	2.35	3.12	3.89	2.35	2.84
	3.32	3.10	2.40	4.19	3.94	2.39	3.05
	3.29	3.08	2.40	4.19	3.94	2.39	3.05
	2.83	4.76	2.35	3.13	3.90	2.35	2.84
	3.32	3.03	2.39	4.19	3.95	2.39	3.04
	3.35	3.03	2.40	4.19	3.95	2.39	3.04
	3.34	2.98	2.42	4.20	3.94	2.38	3.04
	3.37	2.98	2.42	4.21	3.94	2.39	3.04
	2.87	4.81	2.37	3.09	3.89	2.34	2.83
	2.85	4.80	2.37	3.08	3.88	2.36	2.83
	2.89	4.82	2.34	3.05	3.87	2.34	2.82
	2.80	4.62	2.29	3.28	3.91	2.33	2.88
	2.89	4.80	2.37	3.09	3.90	2.34	2.82
	2.86	4.83	2.34	3.03	3.84	2.34	2.83
	2.89	4.85	2.37	3.04	3.88	2.34	2.82
	2.87	4.79	2.37	3.09	3.89	2.35	2.82
Shortest	2.80	2.98	2.29	3.03	3.84	2.33	2.82

	H4-H9	H4-H8	H8-H9	H9-H7a	H9-H7b	H8-H7a	H8-H7b
	29.67	0.00	29.67	0.00	0.00	29.67	29.67
	0.00	0.00	13.93	0.00	0.00	13.93	0.00
	0.00	0.00	11.49	0.00	0.00	11.49	0.00
	9.98	0.00	9.98	0.00	0.00	9.98	9.98
	0.00	0.00	7.96	0.00	0.00	7.96	0.00
	0.00	0.00	6.85	0.00	0.00	6.85	0.00
	0.00	5.72	5.72	0.00	0.00	5.72	0.00
	0.00	5.18	5.18	0.00	0.00	5.18	0.00
	3.21	0.00	3.21	0.00	0.00	3.21	3.21
	2.23	0.00	2.23	0.00	0.00	2.23	2.23
	1.49	0.00	1.49	0.00	0.00	1.49	1.49
	0.64	0.00	0.64	0.00	0.00	0.64	0.64
	0.54	0.00	0.54	0.00	0.00	0.54	0.54
	0.39	0.00	0.39	0.00	0.00	0.39	0.39
	0.38	0.00	0.38	0.00	0.00	0.38	0.38
	0.36	0.00	0.36	0.00	0.00	0.36	0.36
% < 3 Ang	48.87	10.90	100.00	0.00	0.00	100.00	48.87

	H4-H9	H4-H8	H8-H9	H9-H7a	H9-H7b	H8-H7a	H8-H7b
	0.00	0.00	29.67	0.00	0.00	29.67	0.00
	0.00	0.00	13.93	0.00	0.00	13.93	0.00
	0.00	0.00	11.49	0.00	0.00	11.49	0.00
	0.00	0.00	9.98	0.00	0.00	9.98	0.00
	0.00	0.00	7.96	0.00	0.00	7.96	0.00
	0.00	0.00	6.85	0.00	0.00	6.85	0.00
	0.00	0.00	5.72	0.00	0.00	5.72	0.00
	0.00	0.00	5.18	0.00	0.00	5.18	0.00
	0.00	0.00	3.21	0.00	0.00	3.21	0.00
	0.00	0.00	2.23	0.00	0.00	2.23	0.00
	0.00	0.00	1.49	0.00	0.00	1.49	0.00
	0.00	0.00	0.64	0.00	0.00	0.64	0.00
	0.00	0.00	0.54	0.00	0.00	0.54	0.00
	0.00	0.00	0.39	0.00	0.00	0.39	0.00
	0.00	0.00	0.38	0.00	0.00	0.38	0.00
	0.00	0.00	0.36	0.00	0.00	0.36	0.00
% < 2.5 Ang	0.00	0.00	100.00	0.00	0.00	100.00	0.00

	H4-H9	H4-H8	H8-H9	H9-H7a	H9-H7b	H8-H7a	H8-H7b
	84.30	141.82	69.74	92.68	115.37	69.81	84.36
	46.25	43.15	33.43	58.36	54.81	33.32	42.43
	37.85	35.44	27.55	48.13	45.24	27.49	35.01
	28.22	47.45	23.43	31.25	38.86	23.45	28.35
	26.40	24.11	19.05	33.33	31.41	19.00	24.21
	22.96	20.76	16.43	28.71	27.04	16.36	20.85
	19.07	17.04	13.81	24.02	22.52	13.63	17.39
	17.46	15.47	12.55	21.80	20.42	12.36	15.77
	9.21	15.44	7.60	9.92	12.49	7.52	9.08
	6.36	10.70	5.27	6.86	8.64	5.25	6.30
	4.30	7.17	3.49	4.54	5.75	3.48	4.20
	1.80	2.97	1.47	2.11	2.52	1.50	1.86
	1.55	2.58	1.27	1.66	2.10	1.26	1.52
	1.12	1.89	0.92	1.19	1.50	0.92	1.11
	1.08	1.82	0.89	1.14	1.45	0.88	1.06
	1.02	1.71	0.84	1.10	1.39	0.84	1.01
bolt.Ave.dist	3.09	3.90	2.38	3.67	3.92	2.37	2.94

	H4-H9	H4-H8	H8-H9	H9-H7a	H9-H7b	H8-H7a	H8-H7b		H8-H9	H8-H7a	H8-H7b
	0.01	0.00	0.03	0.01	0.00	0.03	0.06		36.66	-18.12	103.69
	0.00	0.00	0.01	0.00	0.00	0.01	0.02		-37.75	32.75	155.83
	0.00	0.00	0.01	0.00	0.00	0.01	0.01		-37.49	32.66	155.73
	0.00	0.00	0.01	0.00	0.00	0.01	0.02		36.17	-18.18	103.62
	0.00	0.00	0.01	0.00	0.00	0.01	0.01		-39.80	32.63	155.61
	0.00	0.00	0.01	0.00	0.00	0.01	0.01		-40.24	32.63	155.62
	0.00	0.00	0.00	0.00	0.00	0.00	0.01		-41.62	33.50	156.40
	0.00	0.00	0.00	0.00	0.00	0.00	0.01		-42.02	33.53	156.44
	0.00	0.00	0.00	0.00	0.00	0.00	0.01		36.29	-19.81	102.04
	0.00	0.00	0.00	0.00	0.00	0.00	0.00		38.17	-20.63	101.13
	0.00	0.00	0.00	0.00	0.00	0.00	0.00		37.50	-20.25	101.49
	0.00	0.00	0.00	0.00	0.00	0.00	0.00		29.32	-9.71	112.08
	0.00	0.00	0.00	0.00	0.00	0.00	0.00		36.15	-20.62	101.24
	0.00	0.00	0.00	0.00	0.00	0.00	0.00		38.47	-19.31	102.44
	0.00	0.00	0.00	0.00	0.00	0.00	0.00		38.05	-20.93	100.76
	0.00	0.00	0.00	0.00	0.00	0.00	0.00		37.60	-21.21	100.56
1/r^6	0.02	0.01	0.09	0.01	0.00	0.09	0.16				

Table 2.6: *Molecular modelling data for 4S, 5S, 8S, 9R*

Potential Energy-OPLS-AA	E/kT	e-E/kT	Ne-E/kT	Boltzmann	%	E*%	Bolt.Ave.E
354.66	-142.19	1.77E-62	3.37E-61	5.65	29.75	######	356.87
355.22	-142.41	1.42E-62	2.69E-61	4.52	23.76	8441.79	
356.22	-142.81	9.49E-63	1.80E-61	3.02	15.92	5669.91	
358.45	-143.70	3.90E-63	7.40E-62	1.24	6.53	2340.85	
359.26	-144.03	2.81E-63	5.35E-62	0.90	4.72	1695.42	
360.33	-144.46	1.83E-63	3.47E-62	0.58	3.07	1104.43	
360.70	-144.61	1.58E-63	3.00E-62	0.50	2.64	953.70	
361.05	-144.75	1.37E-63	2.60E-62	0.44	2.29	828.62	
361.48	-144.92	1.15E-63	2.19E-62	0.37	1.93	698.78	
361.49	-144.92	1.15E-63	2.18E-62	0.37	1.93	696.10	
361.51	-144.93	1.14E-63	2.17E-62	0.36	1.91	691.42	
362.13	-145.18	8.91E-64	1.69E-62	0.28	1.49	540.95	
362.38	-145.28	8.04E-64	1.53E-62	0.26	1.35	488.19	
362.73	-145.42	6.99E-64	1.33E-62	0.22	1.17	425.14	
365.72	-146.62	2.11E-64	4.01E-63	0.07	0.35	129.34	
365.74	-146.63	2.09E-64	3.98E-63	0.07	0.35	128.38	
366.22	-146.82	1.73E-64	3.28E-63	0.06	0.29	106.07	
366.34	-146.87	1.65E-64	3.13E-63	0.05	0.28	101.13	
366.44	-146.91	1.58E-64	3.00E-63	0.05	0.26	96.91	

	H4-H9	H4-H8	H8-H9	H9-H7a	H9-H7b	H8-H7a	H8-H7b
	2.32	3.55	2.39	4.18	3.96	2.38	3.04
	2.34	3.52	2.39	4.18	3.97	2.38	3.04
	2.35	3.49	2.41	4.20	3.96	2.38	3.04
	2.31	3.60	2.39	4.19	3.94	2.39	3.05
	2.34	3.56	2.39	4.19	3.95	2.39	3.04
	2.34	3.52	2.41	4.20	3.94	2.38	3.04
	2.71	4.87	2.37	3.09	3.89	2.35	2.83
	2.69	4.86	2.35	3.15	3.91	2.35	2.84
	2.66	4.84	2.35	3.10	3.92	2.36	2.81
	2.70	4.86	2.37	3.04	3.89	2.35	2.81
	2.70	4.84	2.34	3.04	3.86	2.34	2.82
	2.70	4.86	2.37	3.08	3.88	2.36	2.83
	2.69	4.84	2.34	2.99	3.85	2.35	2.81
	2.69	4.86	2.37	3.03	3.88	2.36	2.81
	2.33	3.38	2.41	4.20	3.96	2.39	3.04
	2.34	3.52	2.39	4.18	3.96	2.38	3.04
	2.77	4.91	2.37	3.04	3.87	2.34	2.82
	2.73	4.88	2.37	3.04	3.89	2.35	2.81
	2.34	3.37	2.43	4.21	3.95	2.38	3.04
Shortest	2.31	3.37	2.34	2.99	3.85	2.34	2.81

	H4-H9	H4-H8	H8-H9	H9-H7a	H9-H7b	H8-H7a	H8-H7b
	29.75	0.00	29.75	0.00	0.00	29.75	0.00
	23.76	0.00	23.76	0.00	0.00	23.76	0.00
	15.92	0.00	15.92	0.00	0.00	15.92	0.00
	6.53	0.00	6.53	0.00	0.00	6.53	0.00
	4.72	0.00	4.72	0.00	0.00	4.72	0.00
	3.07	0.00	3.07	0.00	0.00	3.07	0.00
	2.64	0.00	2.64	0.00	0.00	2.64	2.64
	2.29	0.00	2.29	0.00	0.00	2.29	2.29
	1.93	0.00	1.93	0.00	0.00	1.93	1.93
	1.93	0.00	1.93	0.00	0.00	1.93	1.93
	1.91	0.00	1.91	0.00	0.00	1.91	1.91
	1.49	0.00	1.49	0.00	0.00	1.49	1.49
	1.35	0.00	1.35	1.35	0.00	1.35	1.35
	1.17	0.00	1.17	0.00	0.00	1.17	1.17
	0.35	0.00	0.35	0.00	0.00	0.35	0.00
	0.35	0.00	0.35	0.00	0.00	0.35	0.00
	0.29	0.00	0.29	0.00	0.00	0.29	0.29
	0.28	0.00	0.28	0.00	0.00	0.28	0.28
	0.26	0.00	0.26	0.00	0.00	0.26	0.00
% < 3 Ang	100.00	0.00	100.00	1.35	0.00	100.00	15.29

	H4-H9	H4-H8	H8-H9	H9-H7a	H9-H7b	H8-H7a	H8-H7b
	29.75	0.00	29.75	0.00	0.00	29.75	0.00
	23.76	0.00	23.76	0.00	0.00	23.76	0.00
	15.92	0.00	15.92	0.00	0.00	15.92	0.00
	6.53	0.00	6.53	0.00	0.00	6.53	0.00
	4.72	0.00	4.72	0.00	0.00	4.72	0.00
	3.07	0.00	3.07	0.00	0.00	3.07	0.00
	0.00	0.00	2.64	0.00	0.00	2.64	0.00
	0.00	0.00	2.29	0.00	0.00	2.29	0.00
	0.00	0.00	1.93	0.00	0.00	1.93	0.00
	0.00	0.00	1.93	0.00	0.00	1.93	0.00
	0.00	0.00	1.91	0.00	0.00	1.91	0.00
	0.00	0.00	1.49	0.00	0.00	1.49	0.00
	0.00	0.00	1.35	0.00	0.00	1.35	0.00
	0.00	0.00	1.17	0.00	0.00	1.17	0.00
	0.35	0.00	0.35	0.00	0.00	0.35	0.00
	0.35	0.00	0.35	0.00	0.00	0.35	0.00
	0.00	0.00	0.29	0.00	0.00	0.29	0.00
	0.00	0.00	0.28	0.00	0.00	0.28	0.00
	0.26	0.00	0.26	0.00	0.00	0.26	0.00
% < 2.5 Ang	84.71	0.00	100.00	0.00	0.00	100.00	0.00

	H4-H9	H4-H8	H8-H9	H9-H7a	H9-H7b	H8-H7a	H8-H7b
	68.98	105.68	71.22	124.40	117.66	70.90	90.49
	55.73	83.58	56.82	99.43	94.26	56.58	72.25
	37.41	55.56	38.38	66.81	62.97	37.83	48.36
	15.10	23.54	15.62	27.34	25.74	15.62	19.89
	11.03	16.78	11.28	19.77	18.66	11.27	14.37
	7.18	10.80	7.39	12.88	12.09	7.31	9.33
	7.17	12.86	6.26	8.16	10.29	6.20	7.48
	6.18	11.15	5.39	7.23	8.98	5.39	6.51
	5.15	9.36	4.54	5.98	7.57	4.55	5.44
	5.19	9.36	4.56	5.85	7.49	4.52	5.41
	5.17	9.26	4.48	5.82	7.38	4.48	5.40
	4.04	7.27	3.53	4.60	5.80	3.52	4.23
	3.63	6.52	3.16	4.03	5.19	3.17	3.78
	3.15	5.69	2.77	3.55	4.55	2.77	3.29
	0.82	1.20	0.85	1.48	1.40	0.84	1.08
	0.82	1.24	0.84	1.47	1.39	0.84	1.07
	0.80	1.42	0.69	0.88	1.12	0.68	0.82
	0.75	1.35	0.65	0.84	1.07	0.65	0.78
	0.62	0.89	0.64	1.11	1.04	0.63	0.80
bolt.Ave.dist	2.39	3.73	2.39	4.02	3.95	2.38	3.01

	H4-H9	H4-H8	H8-H9	H9-H7a	H9-H7b	H8-H7a	H8-H7b		H8-H9	H8-H7a	H8-H7b
	0.04	0.00	0.03	0.00	0.00	0.03	0.04		-36.18	31.41	154.40
	0.03	0.00	0.02	0.00	0.00	0.02	0.03		-38.42	31.54	154.46
	0.02	0.00	0.02	0.00	0.00	0.02	0.02		-40.10	32.51	155.36
	0.01	0.00	0.01	0.00	0.00	0.01	0.01		-35.80	32.88	156.00
	0.01	0.00	0.00	0.00	0.00	0.00	0.01		-38.29	32.96	155.99
	0.00	0.00	0.00	0.00	0.00	0.00	0.00		-40.08	33.84	156.80
	0.00	0.00	0.00	0.00	0.00	0.00	0.01		36.75	-19.96	101.88
	0.00	0.00	0.00	0.00	0.00	0.00	0.00		35.43	-18.71	103.06
	0.00	0.00	0.00	0.00	0.00	0.00	0.00		35.69	-22.57	99.07
	0.00	0.00	0.00	0.00	0.00	0.00	0.00		37.13	-22.89	98.82
	0.00	0.00	0.00	0.00	0.00	0.00	0.00		38.02	-20.09	101.63
	0.00	0.00	0.00	0.00	0.00	0.00	0.00		38.35	-20.57	101.17
	0.00	0.00	0.00	0.00	0.00	0.00	0.00		38.63	-23.00	98.61
	0.00	0.00	0.00	0.00	0.00	0.00	0.00		38.77	-23.61	98.02
	0.00	0.00	0.00	0.00	0.00	0.00	0.00		-40.58	31.87	154.84
	0.00	0.00	0.00	0.00	0.00	0.00	0.00		-37.23	32.21	155.11
	0.00	0.00	0.00	0.00	0.00	0.00	0.00		38.38	-20.99	100.70
	0.00	0.00	0.00	0.00	0.00	0.00	0.00		37.16	-22.41	99.28
	0.00	0.00	0.00	0.00	0.00	0.00	0.00		-41.93	32.54	155.41
1/r^6	0.11	0.01	0.10	0.01	0.01	0.11	0.14				

Figure 2.7*: Molecular modelling data for 4S, 5S, 8R, 9S*

Potential Energy-OPLS-AA	E/kT	e-E/kT	Ne-E/kT	Boltzmann	%	E*%	Bolt.Ave.E
327.78	-131.41	8.51E-58	1.79E-56	6.74	32.08	######	330.41
328.80	-131.82	5.66E-58	1.19E-56	4.48	21.36	7021.69	
330.10	-132.34	3.36E-58	7.05E-57	2.66	12.66	4180.29	
331.56	-132.93	1.87E-58	3.92E-57	1.48	7.04	2334.90	
332.87	-133.45	1.11E-58	2.32E-57	0.88	4.17	1389.14	
333.00	-133.50	1.05E-58	2.21E-57	0.83	3.96	1319.12	
333.97	-133.89	7.10E-59	1.49E-57	0.56	2.68	894.54	
333.98	-133.89	7.08E-59	1.49E-57	0.56	2.67	892.13	
334.76	-134.21	5.18E-59	1.09E-57	0.41	1.95	654.33	
335.20	-134.38	4.35E-59	9.14E-58	0.34	1.64	550.20	
335.31	-134.43	4.16E-59	8.74E-58	0.33	1.57	526.19	
335.31	-134.43	4.15E-59	8.72E-58	0.33	1.57	525.18	
335.62	-134.55	3.67E-59	7.71E-58	0.29	1.39	464.96	
335.76	-134.61	3.47E-59	7.28E-58	0.27	1.31	439.15	
336.81	-135.03	2.28E-59	4.79E-58	0.18	0.86	289.59	
337.06	-135.13	2.06E-59	4.33E-58	0.16	0.78	261.82	
337.30	-135.22	1.88E-59	3.94E-58	0.15	0.71	238.51	
337.82	-135.43	1.52E-59	3.20E-58	0.12	0.57	193.82	
338.75	-135.81	1.05E-59	2.20E-58	0.08	0.40	133.81	
339.11	-135.95	9.07E-60	1.91E-58	0.07	0.34	116.02	
339.50	-136.11	7.74E-60	1.62E-58	0.06	0.29	99.06	

	H4-H9	H4-H8	H8-H9	H9-H7a	H9-H7b	H8-H7a	H8-H7b
	2.98	4.76	2.39	3.95	4.18	3.04	2.38
	2.97	4.75	2.41	3.94	4.19	3.04	2.38
	2.95	4.76	2.41	3.97	4.18	3.04	2.38
	2.94	4.76	2.43	3.95	4.19	3.03	2.37
	3.04	4.78	2.37	3.94	4.18	3.04	2.39
	3.00	4.77	2.38	3.97	4.17	3.04	2.38
	3.02	4.77	2.40	3.94	4.19	3.04	2.38
	2.98	4.76	2.40	3.96	4.18	3.04	2.37
	2.95	4.75	2.41	3.96	4.18	3.04	2.38
	3.00	4.77	2.39	3.95	4.18	3.04	2.39
	2.99	4.78	2.40	3.96	4.18	3.04	2.38
	3.02	4.79	2.39	3.94	4.18	3.04	2.39
	2.99	4.77	2.41	3.94	4.19	3.05	2.39
	2.97	4.78	2.40	3.98	4.17	3.03	2.37
	2.98	4.77	2.42	3.95	4.19	3.04	2.38
	2.97	4.74	2.39	3.95	4.19	3.04	2.38
	2.96	4.77	2.42	3.97	4.18	3.03	2.36
	2.96	4.77	2.41	3.96	4.18	3.04	2.38
	2.99	4.79	2.41	3.95	4.18	3.04	2.38
	2.94	4.78	2.42	3.98	4.18	3.03	2.37
	2.97	4.79	2.42	3.95	4.19	3.04	2.38
Shortest	2.94	4.74	2.37	3.94	4.17	3.03	2.36

	H4-H9	H4-H8	H8-H9	H9-H7a	H9-H7b	H8-H7a	H8-H7b
	32.08	0.00	32.08	0.00	0.00	0.00	32.08
	21.36	0.00	21.36	0.00	0.00	0.00	21.36
	12.66	0.00	12.66	0.00	0.00	0.00	12.66
	7.04	0.00	7.04	0.00	0.00	0.00	7.04
	0.00	0.00	4.17	0.00	0.00	0.00	4.17
	3.96	0.00	3.96	0.00	0.00	0.00	3.96
	0.00	0.00	2.68	0.00	0.00	0.00	2.68
	2.67	0.00	2.67	0.00	0.00	0.00	2.67
	1.95	0.00	1.95	0.00	0.00	0.00	1.95
	1.64	0.00	1.64	0.00	0.00	0.00	1.64
	1.57	0.00	1.57	0.00	0.00	0.00	1.57
	0.00	0.00	1.57	0.00	0.00	0.00	1.57
	1.39	0.00	1.39	0.00	0.00	0.00	1.39
	1.31	0.00	1.31	0.00	0.00	0.00	1.31
	0.86	0.00	0.86	0.00	0.00	0.00	0.86
	0.78	0.00	0.78	0.00	0.00	0.00	0.78
	0.71	0.00	0.71	0.00	0.00	0.00	0.71
	0.57	0.00	0.57	0.00	0.00	0.00	0.57
	0.40	0.00	0.40	0.00	0.00	0.00	0.40
	0.34	0.00	0.34	0.00	0.00	0.00	0.34
	0.29	0.00	0.29	0.00	0.00	0.00	0.29
% < 3 Ang	91.58	0.00	100.00	0.00	0.00	0.00	100.00

	H4-H9	H4-H8	H8-H9	H9-H7a	H9-H7b	H8-H7a	H8-H7b
	95.67	152.69	76.54	126.88	134.10	97.59	76.50
	63.35	101.42	51.40	84.25	89.55	64.93	50.84
	37.35	60.31	30.47	50.22	52.94	38.45	30.11
	20.69	33.50	17.09	27.85	29.53	21.37	16.71
	12.69	19.97	9.90	16.46	17.42	12.70	9.96
	11.87	18.88	9.44	15.73	16.52	12.03	9.41
	8.09	12.78	6.42	10.54	11.22	8.15	6.38
	7.97	12.71	6.42	10.58	11.18	8.11	6.34
	5.77	9.29	4.71	7.75	8.18	5.94	4.65
	4.92	7.83	3.92	6.48	6.86	5.00	3.92
	4.70	7.50	3.76	6.21	6.56	4.77	3.74
	4.74	7.50	3.74	6.17	6.55	4.77	3.74
	4.14	6.60	3.33	5.45	5.81	4.22	3.31
	3.89	6.25	3.14	5.21	5.45	3.96	3.10
	2.57	4.10	2.08	3.39	3.60	2.61	2.04
	2.30	3.68	1.86	3.07	3.25	2.36	1.85
	2.09	3.37	1.71	2.81	2.96	2.14	1.67
	1.70	2.74	1.38	2.27	2.40	1.74	1.37
	1.18	1.89	0.95	1.56	1.65	1.20	0.94
	1.01	1.63	0.83	1.36	1.43	1.04	0.81
	0.87	1.40	0.71	1.15	1.22	0.89	0.70
bolt.Ave.dist	2.98	4.76	2.40	3.95	4.18	3.04	2.38

	H4-H9	H4-H8	H8-H9	H9-H7a	H9-H7b	H8-H7a	H8-H7b		H8-H9	H8-H7a	H8-H7b
	0.01	0.00	0.04	0.00	0.00	0.01	0.17		39.47	-154.35	-31.49
	0.01	0.00	0.02	0.00	0.00	0.01	0.12		41.23	-155.24	-32.47
	0.00	0.00	0.01	0.00	0.00	0.00	0.07		39.05	-152.44	-29.75
	0.00	0.00	0.01	0.00	0.00	0.00	0.04		40.65	-153.38	-30.79
	0.00	0.00	0.00	0.00	0.00	0.00	0.02		38.72	-155.51	-32.56
	0.00	0.00	0.00	0.00	0.00	0.00	0.02		39.49	-152.52	-29.69
	0.00	0.00	0.00	0.00	0.00	0.00	0.01		40.61	-156.35	-33.48
	0.00	0.00	0.00	0.00	0.00	0.00	0.01		41.19	-153.48	-30.75
	0.00	0.00	0.00	0.00	0.00	0.00	0.01		39.59	-152.02	-29.14
	0.00	0.00	0.00	0.00	0.00	0.00	0.01		38.02	-154.60	-31.64
	0.00	0.00	0.00	0.00	0.00	0.00	0.01		38.54	-153.68	-30.89
	0.00	0.00	0.00	0.00	0.00	0.00	0.01		38.07	-154.80	-31.81
	0.00	0.00	0.00	0.00	0.00	0.00	0.01		39.59	-154.87	-31.88
	0.00	0.00	0.00	0.00	0.00	0.00	0.01		37.92	-150.36	-27.71
	0.00	0.00	0.00	0.00	0.00	0.00	0.00		40.09	-154.57	-31.88
	0.00	0.00	0.00	0.00	0.00	0.00	0.00		39.77	-155.53	-32.56
	0.00	0.00	0.00	0.00	0.00	0.00	0.00		39.54	-151.49	-28.92
	0.00	0.00	0.00	0.00	0.00	0.00	0.00		37.90	-152.71	-29.92
	0.00	0.00	0.00	0.00	0.00	0.00	0.00		37.64	-152.95	-30.14
	0.00	0.00	0.00	0.00	0.00	0.00	0.00		37.39	-149.63	-26.95
	0.00	0.00	0.00	0.00	0.00	0.00	0.00		38.10	-152.97	-30.15
1/r^6	0.03	0.00	0.11	0.01	0.00	0.03	0.55				

Figure 2.8: *Molecular modelling data for 4R, 5S, 8R, 9S*

Potential Energy-OPLS-AA	E/kT	e-E/kT	Ne-E/kT	Boltzmann	%	E*%	Bolt.Ave.E
311.87	-125.03	5.02E-55	6.52E-54	2.35	18.06	5632.93	312.81
311.92	-125.05	4.92E-55	6.40E-54	2.30	17.72	5527.95	
312.57	-125.31	3.79E-55	4.92E-54	1.77	13.64	4262.24	
312.83	-125.41	3.42E-55	4.44E-54	1.60	12.30	3848.56	
312.90	-125.44	3.32E-55	4.31E-54	1.55	11.95	3739.93	
312.95	-125.46	3.25E-55	4.22E-54	1.52	11.70	3662.53	
314.04	-125.90	2.10E-55	2.73E-54	0.98	7.58	2379.07	
314.75	-126.19	1.58E-55	2.05E-54	0.74	5.69	1790.37	
321.48	-128.88	1.06E-56	1.38E-55	0.05	0.38	123.11	
322.31	-129.22	7.63E-57	9.92E-56	0.04	0.27	88.54	
322.50	-129.29	7.07E-57	9.19E-56	0.03	0.25	82.13	
322.52	-129.30	7.00E-57	9.10E-56	0.03	0.25	81.34	
323.20	-129.57	5.34E-57	6.95E-56	0.03	0.19	62.18	

	H4-H9	H4-H8	H8-H9	H9-H7a	H9-H7b	H8-H7a	H8-H7b
	3.98	4.90	2.38	3.96	4.17	3.04	2.38
	3.97	4.92	2.40	3.96	4.17	3.04	2.38
	3.97	4.92	2.40	3.98	4.16	3.03	2.37
	3.97	4.90	2.40	3.95	4.18	3.04	2.37
	3.96	4.94	2.42	3.98	4.17	3.03	2.37
	3.95	4.92	2.40	3.96	4.17	3.04	2.38
	3.96	4.91	2.42	3.96	4.18	3.03	2.36
	3.94	4.93	2.42	3.97	4.17	3.03	2.37
	3.92	4.92	2.40	3.97	4.18	3.04	2.38
	3.91	4.91	2.42	3.96	4.19	3.04	2.37
	3.96	4.89	2.38	3.96	4.17	3.04	2.37
	3.92	4.92	2.41	3.97	4.18	3.04	2.38
	3.91	4.91	2.42	3.96	4.19	3.04	2.37
Shortest	3.91	4.89	2.38	3.95	4.16	3.03	2.36

	H4-H9	H4-H8	H8-H9	H9-H7a	H9-H7b	H8-H7a	H8-H7b
	0.00	0.00	18.06	0.00	0.00	0.00	18.06
	0.00	0.00	17.72	0.00	0.00	0.00	17.72
	0.00	0.00	13.64	0.00	0.00	0.00	13.64
	0.00	0.00	12.30	0.00	0.00	0.00	12.30
	0.00	0.00	11.95	0.00	0.00	0.00	11.95
	0.00	0.00	11.70	0.00	0.00	0.00	11.70
	0.00	0.00	7.58	0.00	0.00	0.00	7.58
	0.00	0.00	5.69	0.00	0.00	0.00	5.69
	0.00	0.00	0.38	0.00	0.00	0.00	0.38
	0.00	0.00	0.27	0.00	0.00	0.00	0.27
	0.00	0.00	0.25	0.00	0.00	0.00	0.25
	0.00	0.00	0.25	0.00	0.00	0.00	0.25
	0.00	0.00	0.19	0.00	0.00	0.00	0.19
% < 3 Ang	0.00	0.00	100.00	0.00	0.00	0.00	100.00

	H4-H9	H4-H8	H8-H9	H9-H7a	H9-H7b	H8-H7a	H8-H7b
	0.00	0.00	18.06	0.00	0.00	0.00	18.06
	0.00	0.00	17.72	0.00	0.00	0.00	17.72
	0.00	0.00	13.64	0.00	0.00	0.00	13.64
	0.00	0.00	12.30	0.00	0.00	0.00	12.30
	0.00	0.00	11.95	0.00	0.00	0.00	11.95
	0.00	0.00	11.70	0.00	0.00	0.00	11.70
	0.00	0.00	7.58	0.00	0.00	0.00	7.58
	0.00	0.00	5.69	0.00	0.00	0.00	5.69
	0.00	0.00	0.38	0.00	0.00	0.00	0.38
	0.00	0.00	0.27	0.00	0.00	0.00	0.27
	0.00	0.00	0.25	0.00	0.00	0.00	0.25
	0.00	0.00	0.25	0.00	0.00	0.00	0.25
	0.00	0.00	0.19	0.00	0.00	0.00	0.19
% < 2.5 Ang	0.00	0.00	100.00	0.00	0.00	0.00	100.00

	H4-H9	H4-H8	H8-H9	H9-H7a	H9-H7b	H8-H7a	H8-H7b
	71.81	88.58	42.98	71.58	75.25	54.85	42.93
	70.33	87.28	42.53	70.17	73.94	53.86	42.16
	54.09	67.04	32.71	54.24	56.77	41.32	32.30
	48.80	60.23	29.54	48.63	51.43	37.35	29.20
	47.33	59.03	28.90	47.51	49.82	36.23	28.33
	46.17	57.52	28.09	46.34	48.84	35.57	27.84
	30.01	37.18	18.33	30.04	31.65	22.94	17.91
	22.39	28.02	13.76	22.61	23.71	17.25	13.49
	1.50	1.88	0.92	1.52	1.60	1.16	0.91
	1.08	1.35	0.66	1.09	1.15	0.83	0.65
	1.01	1.24	0.61	1.01	1.06	0.77	0.60
	0.99	1.24	0.61	1.00	1.05	0.77	0.60
	0.75	0.95	0.47	0.76	0.81	0.58	0.46
bolt.Ave.dist	3.96	4.92	2.40	3.96	4.17	3.03	2.37

	H4-H9	H4-H8	H8-H9	H9-H7a	H9-H7b	H8-H7a	H8-H7b		H8-H9	H8-H7a	H8-H7b
	0.00	0.00	0.01	0.00	0.00	0.00	0.10		39.13	-152.82	-29.99
	0.00	0.00	0.01	0.00	0.00	0.00	0.10		38.11	-151.96	-29.11
	0.00	0.00	0.01	0.00	0.00	0.00	0.08		38.21	-150.61	-27.96
	0.00	0.00	0.01	0.00	0.00	0.00	0.07		40.97	-153.80	-31.05
	0.00	0.00	0.01	0.00	0.00	0.00	0.07		36.82	-149.56	-26.91
	0.00	0.00	0.01	0.00	0.00	0.00	0.06		38.28	-151.97	-29.12
	0.00	0.00	0.00	0.00	0.00	0.00	0.04		39.90	-151.75	-29.20
	0.00	0.00	0.00	0.00	0.00	0.00	0.03		37.06	-149.60	-26.94
	0.00	0.00	0.00	0.00	0.00	0.00	0.00		41.23	-152.31	-29.45
	0.00	0.00	0.00	0.00	0.00	0.00	0.00		42.72	-153.21	-30.44
	0.00	0.00	0.00	0.00	0.00	0.00	0.00		39.97	-154.53	-31.55
	0.00	0.00	0.00	0.00	0.00	0.00	0.00		41.65	-152.31	-29.42
	0.00	0.00	0.00	0.00	0.00	0.00	0.00		43.07	-153.10	-30.31
1/r^6	0.00	0.00	0.07	0.00	0.00	0.02	0.56				

Appendix 3

Publications (to date) arising from this thesis

spiro-Mamakone A: A Unique Relative of the Spirobisnaphthalene Class of Compounds

Bioactivity Profiling Using HPLC/Microtitrer-Plate Analysis: Application to a New Zealand Marine Alga-Derived Fungus, Gliocladium sp.

Dichlorinated Pulvinic Acid Derivative from a Malaysian Scleroderma sp.

ORGANIC LETTERS

2006
Vol. 8, No. 10
2059−2061

spiro-Mamakone A: A Unique Relative of the Spirobisnaphthalene Class of Compounds

Sonia A. van der Sar, John W. Blunt, and Murray H. G. Munro*

Department of Chemistry, University of Canterbury, Private Bag 4800, Christchurch, New Zealand

murray.munro@canterbury.ac.nz

Received February 19, 2006

ABSTRACT

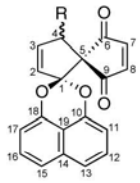

1 R = H, OH
2 R = O

A spirobisnaphthalene derivative with a new spiro-nonadiene skeleton, spiro-mamakone A (1), has been isolated from the extract of a cultured nonsporulating fungal endophyte derived from the New Zealand native tree *Knightia excelsa* (rewarewa). The carbon skeleton of spiro-mamakone A represents a new structural entity and an intriguing addition to the structurally diverse spirobisnaphthalene group of compounds. spiro-Mamakone A is potently cytotoxic and is also antimicrobial.

The spirobisnaphthalenes are a relatively new class of compounds that were first isolated 15 years ago[1] and which contain two naphthalene-derived C_{10} units bridged through a spiroketal linkage. This class of compounds is generally divided into three subclasses: those with two oxygen bridges, for example, palmarumycin CP_1,[2] those with three oxygen bridges, as in preussomerin A,[1] and those with two oxygen bridges and one C−C bridge, such as spiroxin A.[3] These compounds are normally isolated from fungi, although spirobisnaphthalenes have also been isolated on two occasions from plant sources. The most recent report is that from the fruit of *Diospyros ehretioides*.[4] However, as the authors have suggested, the source is probably an endophytic fungus, as is most likely for all spirobisnaphthalenes reported from plants.

In our continued investigation into novel bioactive compounds from New Zealand endophytic fungi, we report the isolation and structure elucidation of a new relative of the spirobisnaphthalenes, spiro-mamakone A (**1**),[5] from a nonsporulating endophytic fungus isolated from the New Zealand native tree rewarewa. The carbon skeleton of the spiro-

(1) Weber, H. A.; Baenziger, N. C.; Gloer, J. B. *J. Am. Chem. Soc.* **1990**, *112*, 6718−6719.
(2) Krohn, K.; Michel, A.; Floerke, U.; Aust, H.-J.; Draeger, S.; Schulz, B. *Liebigs Ann. Chem.* **1994**, 1093−1097.
(3) McDonald, L. A.; Abbanat, D. R.; Barbieri, L. R.; Bernan, V. S.; Discafani, C. M.; Greenstein, M.; Janota, K.; Korshalla, J. D.; Lassota, P.; Tischler, M.; Carter, G. T. *Tetrahedron Lett.* **1999**, *40*, 2489−2492.
(4) Prajoubklang, A.; Sirithunyalug, B.; Charoenchai, P.; Suvannakad, R.; Sriubolmas, N.; Piyamongkol, S.; Kongsaeree, P.; Kittakoop, P. *Chem. Biodiversity* **2005**, *2*, 1358−1367.

(5) Compound **1**: amorphous yellow solid; $[\alpha]^{20}_D$ 0.0 (*c* 0.1, MeOH); UV λ_{max} (MeOH) (log ϵ) 230.0 (3.89), 300.0 (3.88), 314.8 (3.73), 330.0 (3.43) nm; IR (KBr disk) ν_{max} 3477, 1707, 1609, 1414, 1379, 1275, 1204, 1107, 1082 cm^{-1}; $C_{19}H_{12}O_5$ by HREIMS [M]$^+$ *m/z* 320.0677 (calcd 320.0685); ^{1}H NMR (CD_3OD, 500 MHz) δ 7.47 (1H, d, 8.8, H15/H13), 7.45 (1H, d, 8.8, H13/H15), 7.40 (1H, t, 7.8, 7.8, H12/H16), 7.36 (1H, t, 7.8, 7.8, H16/H12), 7.22 (1H, d, 5.7, H8/H7), 7.09 (1H, d, 5.7, H7/H8), 6.83 (1H, d, 7.3, H11/H17), 6.76 (1H, d, 7.3, H17), 6.40 (1H, dd, 5.8, 1.9, H3), 5.93 (1H, dd, 5.8, 2.0, H2), 5.30 (1H, br s, H4); ^{13}C NMR (CD_3OD, 75 MHz) δ 201.1 (C9/C6), 198.6 (C6/C9), 152.2 (C8/C7), 151.9 (C7/C8), 149.4 (C10/C18), 148.8 (C18/C10), 142.7 (C3), 136.1 (C14), 129.9 (C2), 129.0 (C12/C16), 128.7 (C16/C12), 122.5 (C15/C13), 122.0 (C13/C15), 114.8 (C19), 111.7 (C1), 111.0 (C11/C17), 110.6 (C17/C11), 79.1 (C4), 68.9 (C5).

10.1021/ol060434k CCC: $33.50
Published on Web 04/14/2006

nonadiene portion of the molecule is unprecedented in any naturally occurring compounds.

The endophytic fungus was isolated from surface-sterilized leaves of rewarewa, commonly known as New Zealand honeysuckle (*Knightia excelsa*), which were collected from a mixed broadleaf-podocarp forest in the Kamai-Mamaku Forest Park, Bay of Plenty, New Zealand.[6] The fungus was cultivated on 24 plates (85 mm diameter) of MYE (malt yeast extract) agar. After 24 days at 26 °C, the plates were extracted exhaustively with EtOAc. The resulting crude extract (208 mg) showed potent cytotoxicity (IC_{50} 0.12 μg/mL) against the P388 cell line. The extract was subjected to reversed-phase (C18) flash chromatography,[7] eluting with a steep, stepped gradient from MeOH/H_2O (1:3) through MeOH to DCM. Final purification was achieved by semi-preparative HPLC (Phenomenex Luna C18, 10 × 250 mm, 5 μm; 30−45% MeCN/H_2O; 5 mL/min) to yield the major compound, spiro-mamakone A (**1**) (10.7 mg), as an amorphous yellow solid.[5]

HREIMS analysis of the molecular ion (*m/z* 320.0677 $[M]^+$) suggested a molecular formula of $C_{19}H_{12}O_5$, which was supported by the ^{13}C NMR spectrum (19 resonances) and was indicative of 14 degrees of unsaturation. The ^1H NMR spectrum showed just one oxymethine and 10 olefinic/aromatic signals. Using ^{13}C and HSQC/DEPT experiments, the carbon resonances were assigned as one oxymethine (C-4), two carbonyls (C-6 and C-9), 14 sp^2 carbons, four of them nonprotonated (C-2, C-3, C-7, C-8, C-10-C-19), and two quaternary sp^3 carbons (C-1 and C-5).

COSY and HSQC experiments were used to define spin systems a−d (Figure 1 in blue). The remaining signals were

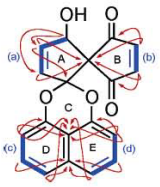

Figure 1. Important COSY and CIGAR correlations for spiro-mamakone A in CD_3OD.

assigned based on a detailed analysis of CIGAR experimental data. Protons H-11 to H-13 (spin system d) and H-15 to H-17 (spin system c) showed correlations to the two nonprotonated carbons, C-14 and/or C-19, indicating a common ring junction between the two spin systems. H-11 and H-12 were also found to correlate to C-10, whereas H-16 and H-17 correlated to C-18. The chemical shifts of C-10 and C-18, δ_C 149.4 and 148.8, respectively, suggested oxygenation. These correlations closed the ring system and defined a 1,8-dioxygenated naphthalene (rings D and E, Figure 1).

The chemical shift of the quaternary carbon at C-1 (δ_C 111.7) was ketal-like, which, when combined with the lack of CIGAR correlations linking spin systems c and d to those of a and b, suggested that C-1 formed a spiroketal bridge (ring C) between the two isolated parts of the molecule. Support for this assignment came from a substructure search in the AntiMarin database,[8] which confirmed that the spiroketal bridge-containing spirobisnaphthalenes all showed comparable ^{13}C chemical shift data for the spiroketal center. The only correlation to C-1 was from H-3 of ring A, establishing the attachment of the spiroketal bridge to ring A. Ring B was found to be a cyclopentene-dione unit by means of the correlations from H-7 and H-8 to the carbonyls at C-6 and C-9 and the quaternary carbon at C-5. Correlations to C-5 were also seen from the H-2 and H-3 olefinic protons, confirming C-5 as a spirocenter joining the two cyclopentene rings, A and B. The oxymethine proton at H-4 also showed correlations to C-6 and C-9, confirming the proximity of ring A to ring B. This analysis of the NMR spectral features accounted for all degrees of unsaturation and all but one proton. Therefore, the oxygenation at C-4 was assigned as an hydroxyl in keeping with the observed OH stretch in the IR spectrum (3477 cm^{-1}), leading to the structural assignment of spiro-mamakone A as **1**. As a result of the near-symmetry of rings B, D, and E, the NMR assignments in these regions are interchangeable.

To confirm the spiro-nonadiene portion of spiro-mamakone A (**1**), the allylic alcohol was oxidized (MnO_2, $CHCl_3$, rt). This cleanly afforded the tri-keto analog, 4-oxo-spiro-mamakone A (**2**).[9] The nonequivalence of the ring B chemical shifts observed in the ^1H and ^{13}C NMR spectra of **1** are a consequence of the stereocenter at C-4; hence, oxidation at this stereocenter should render ring B symmetric. The NMR data for **2** confirmed that this indeed was the case. The H-7 and H-8 olefinic protons appeared as one singlet integrating for two protons at δ_H 7.00. Likewise, both the olefinic and carbonyl carbons showed identical chemical shifts of δ_C 150.8 and 194.2, respectively. Furthermore, oxidation also results in symmetrization of the intact naphthalene subunit. This is a consequence of the newly introduced mirror plane, which passes through both spiro centers, making rings D and E symmetrically equivalent. This change from C_1 to C_s symmetry is also reflected in the simplified NMR spectra of **2** and provides further support for the proposed structure of **1**.

(6) A voucher specimen (UOC-E484) has been deposited in the collection at the School of Biological Sciences, University of Canterbury, New Zealand.

(7) Blunt, J. W.; Calder, V. L.; Fenwick, G. D.; Lake, R. J.; McCombs, J. D.; Munro, M. H. G.; Perry, N. B. *J. Nat. Prod.* **1987**, *50*, 290−292.

(8) A new database compiled from the MarinLit and AntiBase databases (J. W. Blunt and M. H. G. Munro, University of Canterbury, and H. Laatsch, University of Goettingen).

(9) Compound **2**: amorphous yellow solid; UV λ_{max} ($CHCl_3$) (log ϵ) 232.0 (3.89), 295.0 (4.04), 313.9 (3.85), 330.5 (3.66) nm; IR (KBr disk) ν_{max} 1763, 1701, 1612, 1414, 1377, 1270, 1256, 1126, 1047 cm^{-1}; $C_{19}H_{10}O_5$ by HREIMS $[M]^+$ *m/z* 318.0533 (calcd 318.0528), ^1H NMR ($CDCl_3$, 500 MHz) δ 7.77 (1H, d, 5.8, H3), 7.49 (2H, d, 8.3, H15/H13), 7.41 (2H, t, 8.3, 8.3, H16/H12), 7.00 (2H, s, H7/H8), 6.90 (2H, d, 8.3, H17/H11), 6.69 (1H, d, 5.8, H2), ^{13}C shifts determined from HSQC-DEPT and CIGAR experiments, δ 196.0 (C4), 194.2 (C9/C6), 157.0 (C3), 150.8 (C8/C7), 146.2 (C10/C18), 137.7 (C2), 134.0 (C14), 127.6 (C16/C12), 121.6 (C15/C13), 113.4 (C19), 110.7 (C17/C11), 105.8 (C1), 70.5 (C5).

spiro-Mamakone A (**1**) showed no optical activity and was therefore proposed to be racemic. To confirm this, (*R*)- and (*S*)-Mosher esters of the alcohol at C-4 were prepared.[10] HPLC analysis of the Mosher esters established the racemic nature of **1**. This was concluded from the identical nature of the two peaks, for each ester, which were the two diastereomeric esters formed from each of the starting (*R*)- and (*S*)-acid chlorides. ESIMS confirmed that the two diastereomeric peaks observed for each experiment were those of the Mosher's ester (*m*/*z* 559 $[M + Na]^+$).

spiro-Mamakone A (**1**) was found to show potent *in vitro* cytotoxicity (0.33 μM) toward the P388 murine luekemia cell line and was also particularly effective against the following microorganisms: *Bacillus subtilis* (12 mm), *Trichophyton mentagrophytes* (10 mm), and *Cladosporium resinae* (6 mm) in the agar diffusion assay.[11,12] 4-Oxo-spiromamakone A (**2**) was also cytotoxic (1.13 μM) in the same range as that of **1**. Inhibition of growth of the same range of microorganisms however, was significantly lower (inhibition zones of 3 mm) than that of **1**.

It is most probable that the biosynthesis of spiro-mamakone A proceeds as for the regular spirobisnaphthalenes with both halves of the molecule being derived from dihydroxynaphthalene (DHN).[13] Our working biogenetic hypothesis (Scheme 1) suggests an epoxy derivative (or equivalent) as the key intermediate. Such epoxides have been found previously among the spirobisnaphthalene metabolites.[14−18] Several steps involving rearrangement, C−C bond cleavage, decarboxylation, and recyclization could then lead to the formation of the spiro-nonadiene system. The suggested final step in the scheme is a Knoevenagel-type addition. Although in principle the *re* and *si* faces of the formyl group are distinguishable, with this combination of functionalities the isolation of spiro-mamakone A (**1**) as a racemate is not unreasonable and lends some credence to this biogenetic hypothesis.

Scheme 1. Potential biogenesis of the spiro-mamakone A (**1**) skeleton

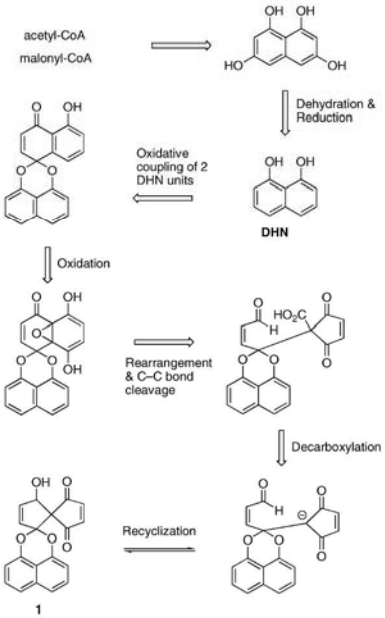

Future work will focus on the synthesis of spiro-mamakone A and analogs for structure/activity studies within this new group. Biosynthetic studies will also be included.

Acknowledgment. Assistance from Mr. Nicholas Cummings for isolation of the endophyte, Ms. Gill Ellis for biological assays, and Mr. Bruce Clark for MS operations is gratefully acknowledged.

Supporting Information Available: ^{1}H, ^{13}C, HSQC-DEPT, and CIGAR NMR spectra for **1**; ^{1}H, HSQC-DEPT, and CIGAR NMR data for **2**. This material is available free of charge via the Internet at http://pubs.acs.org.

OL060434K

(10) A solution of (*S*)-MTPA chloride (5.8 μL) in pyridine (50 μL) and a small crystal of DMAP were added to spiro-mamakone A (2.5 mg). After 2 h, the solvent was evaporated, the residue dissolved in MeOH (0.5 mL), and the solution analyzed by HPLC (Phenomenex Luna C18, 250 × 4.6, 5 μm; solvents: A water + 0.05% TFA, B MeCN; linear gradient: 0 min 10% B, 2 min 10% B, 14 min 75% B, 24 min 75% B; 40 °C; 1 mL min^{-1}). To generate the (*S*)-MPTA ester, the same experimental procedure for the production of the (*R*)-MPTA ester was followed, except that (*R*)-MTPA chloride was used.

(11) Perry, N. B.; Benn, M. H.; Brennan, N. J.; Burgess, E. J.; Ellis, G.; Galloway, D. J.; Lorimer, S. D.; Tangney, R. S. *Lichenologist* **1999**, *31*, 627−636.

(12) In each case, 40 μg of material was applied to each disk for antimicrobial assays.

(13) Bode, H. B.; Wegner, B.; Zeeck, A. *J. Antibiot.* **2000**, *53*, 153−157.

(14) Krohn, K.; Michel, A.; Floerke, U.; Aust, H.-J.; Draeger, S.; Schulz, B. *Liebigs Ann. Chem.* **1994**, 1099−1108.

(15) Chu, M.; Truumees, I.; Patel, M. G.; Gullo, V. P.; Blood, C.; King, I.; Pai, J. K.; Puar, M. S. *Tetrahedron Lett.* **1994**, *35*, 1343−1346.

(16) Schlingmann, G.; West, R. R.; Milne, L.; Pearce, C. J.; Carter, G. T. *Tetrahedron Lett.* **1993**, *34*, 7225−7228.

(17) Thiergardt, R.; Rihs, G.; Hug, P.; Peter, H. H. *Tetrahedron* **1995**, *51*, 733−742.

(18) Bode, H. B.; Zeeck, A. *Phytochemistry* **2000**, *55*, 311−316.

J. Nat. Prod. **2006**, *69*, 621−624 621

Bioactivity Profiling Using HPLC/Microtiter-Plate Analysis: Application to a New Zealand Marine Alga-Derived Fungus, *Gliocladium* sp.

Gerhard Lang,† Maya I. Mitova,† Gill Ellis,† Sonia van der Sar,† Richard K. Phipps,† John W. Blunt,† Nicholas J. Cummings,‡ Anthony L. J. Cole,‡ and Murray H. G. Munro*,†

Department of Chemistry and School of Biological Sciences, University of Canterbury, Private Bag 4800, Christchurch, New Zealand

Received November 27, 2005

Using HPLC/microtiter-plate-based generation of activity profiles the extract of a marine alga-derived fungus, identified as *Gliocladium* sp., was shown to contain the known strongly cytotoxic metabolite 4-keto-clonostachydiol (**1**) and also clonostachydiol (**2**) as well as gliotide (**3**), a new cyclodepsipeptide containing several D-amino acids. The absolute configuration of **1** was elucidated by reduction to **2**, and two further oxidized derivatives of clonostachydiol (**5**, **6**) were prepared and evaluated for biological activity.

Fungi from the marine environment are well-known producers of novel and pharmacologically active secondary metabolites.[1] Chemically productive strains have been isolated from a wide variety of marine substrates, e.g., sponges,[2] algae,[3] driftwood,[4] and sediment.[5] During the investigation of fungi derived from marine algae and driftwood collected around the South Island of New Zealand, the highly cytotoxic and antibacterial extract of a *Gliocladium* sp., cultured from a thallus sample of the macroalga *Durvillaea antarctica*, attracted our attention. Fungi of this genus have been described before as producers of structurally diverse metabolites, e.g., glycosylated polyketides,[6] cytotoxic diketopiperazines,[7] and cyclopeptides.[8]

Results and Discussion

To identify which of the components (HPLC analysis) of the *Gliocladium* extract was responsible for the biological activities observed, a "bioactivity chromatogram" was generated. To achieve this, the eluent of an analytical HPLC separation of the extract (100 μg) was collected over 22 min into a 96-well microtiter plate (88 × 0.25 mL fractions), and a daughter plate was then prepared (5 μL transferred from each well of the master plate; equivalent to a total of 2 μg of extract). This daughter microtiter plate, after drying, was inoculated with P388 cells and incubated for 3 days. The distribution of the bioactivity across the plate was revealed using the yellow MTT dye, which is reduced by living cells to the purple MTT formazan.[9] Correlating the plate-reader output against well position (each well is equivalent to a 15 s fragment of the HPLC) allows generation of a HPLC-bioactivity profile. Typically, under the HPLC conditions used, peak widths are around 30−60 s, which corresponds to two to four consecutive wells on the microtiter plate, allowing ready identification of the bioactive peak(s) in an HPLC chromatogram (Figure 1). In our experience it has been useful to compare the bioactivity profile to both the ELSD data and the UV-DAD output, as the ELSD output reflects the actual mass of compound in a peak and is not biased toward compounds with strong UV chromophores.

In the same way a microtiter plate using 500 μg of extract was prepared and tested against *Bacillus subtilis*. For an appropriate response from this organism it is necessary to use a considerably higher concentration of sample per well. Both the resulting "cytotoxicity chromatogram" and the "anti-*Bacillus* chromatogram" (Figure 1) showed the bioactivity to be located around a retention time of 12.5 min, correlating to one of the major HPLC peaks.

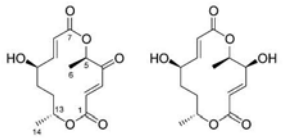

1 **2**

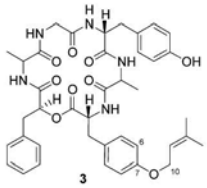

3

The cytotoxic compound (**1**) and the other two major compounds (**2** and **3**) were then isolated by semipreparative HPLC. Evaluation of NMR and MS data showed the active compound to be the macrodiolide 4-keto-clonostachydiol (**1**), a structure recently patented for its cytotoxic and antibacterial activities.[10] Compound **2** was, by analysis of the NMR and MS data, unequivocally identified as clonostachydiol,[11] a related fungal macrodiolide. Comparison of NMR data and the optical rotation of **2** with values published for the natural product and two diastereomers[12,13] confirmed the stereochemistry to be that of the previously described natural product. The relative and absolute configuration of **1** was established by reduction of the compound with $NaBH_4/CeCl_3$. This reaction resulted in two products, **4a** and **4b** (Scheme 1). Compound **4a** was, by HPLC retention time, ^1H NMR, and optical rotation, identical to clonostachydiol **2**, thus indicating for **1** a stereochemistry analogous to that of **2**, i.e., (5*R*,10*R*,13*R*). Compound **4b** was the previously undescribed 4-*epi*-clonostachydiol.

In comparison with 4-keto-clonostachydiol (**1**), which is strongly cytotoxic against P388 cells (IC_{50} 0.55 μM) and active against *Bacillus subtilis* and the fungi *Trichophyton mentagrophytes* and *Cladosporium resinae*, clonostachydiol (**2**) is significantly less cytotoxic and does not possess antimicrobial activity (Table 1). To explore the biological activity potential of related structures, **2** was oxidized with Dess−Martin periodinane (Scheme 2). Under these conditions the alcohol at C-10 was readily oxidized to the ketone, while oxidation at C-4 proceeded only slowly. This made it possible to isolate compound **5**, an isomer of 4-keto-clonostachydiol (**1**) with the oxidation states of C-4 and C-10 interchanged. Full oxidation

* To whom correspondence should be addressed. Tel: +64-3-3642434. Fax: +64-3-3642429. E-mail: murray.munro@canterbury.ac.nz.
† Department of Chemistry.
‡ School of Biological Sciences.

10.1021/np0504917 CCC: $33.50
Published on Web 03/17/2006

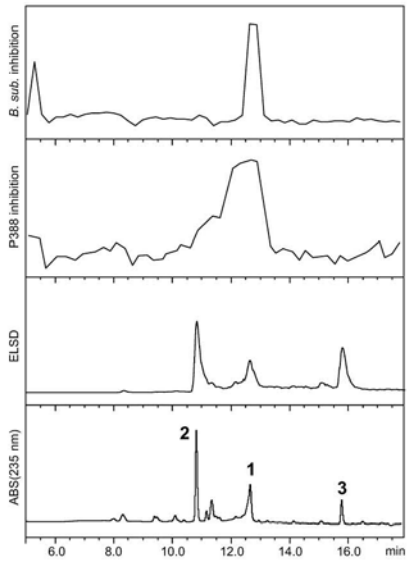

Figure 1. HPLC of the *Gliocladium* extract: UV absorption at 235 nm, ELSD signal, cytotoxicity against P388 cells, and anti-*B. subtilis* activity.

Scheme 1. Reduction of 4-Keto-clonostachydiol (**1**)

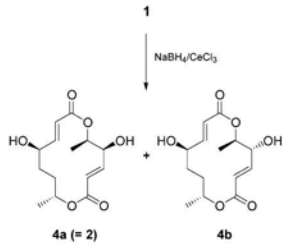

Table 1. Cytotoxic and Antimicrobial[a] Activities of Compounds **1**, **2**, **5**, and **6**

	IC_{50}(P388) [μM]	*B. subtilis*	*T. ment.*	*C. resinae*
1	0.55	6	2	1
2	25	not active	not active	not active
5	1.9	3	3	5
6	3.9	1	1	not active

[a] Widths of inhibition zones (in mm) around disks loaded with 40 μg of compound.

of **2** to the diketone **6** was achieved with MnO_2. Both oxidation products of clonostachydiol are antimicrobial and markedly cytotoxic (Table 1), but less so than the natural product **1**. This suggests that the presence of at least one α,β-unsaturated ketone moiety is essential for the biological activity. The reduced activity of **6**, in comparison to **1** and **5**, may be due to the nonpolar nature of this compound, which is barely soluble in water.

HRESIMS indicated a *m/z* of 742.3424, corresponding to a molecular formula of $C_{40}H_{48}N_5O_9$, for the $[M + H]^+$ ion of compound **3**, which was named gliotide after the producing

Scheme 2. Oxidation of Clonostachydiol (**2**): (i) Dess−Martin, (ii) MnO_2

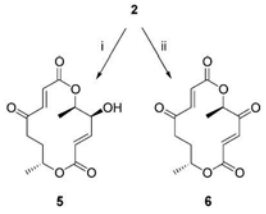

organism. The ^{1}H NMR spectrum was characteristic of a peptide, with six partially overlapping signals for the α-protons of the α-amino acid and the α-hydroxy acid residues between 3.8 and 5.2 ppm. A TOCSY experiment revealed the presence of five amino acid units, namely, glycine, two alanine, and two tyrosine residues and an α-hydroxy acid, 3-phenyllactic acid. Long-range H,C-correlations of the α-protons to the carbonyl carbons of the adjacent amino acid provided the information necessary for assembling the sequence of the amino acids and the 3-phenyllactic acid (Figure 2). The carbonyl resonances were narrowly spaced in the range of 171 to 175 ppm, so the IMPRESS technique[14] was applied, as this approach provides better resolution in the F1 dimension than a conventional HMBC experiment. This established that the peptide had the sequence phenyllactoyl-Ala-Gly-Tyr-Ala-Tyr with the ring-closing ester bond between the hydroxyl group of the phenyllactic acid and the second tyrosine residue. The ^{1}H NMR resonances of two singlet methyl groups, one double-bond proton, and an oxymethylene group were also identified and assigned to an *O*-prenyl residue. This *O*-prenyl group was attached to the *C*-terminal tyrosine unit, as the methylene protons (H-10) showed an HMBC correlation to C-7 as well as an ROE interaction with one of the aromatic proton signals (H-6/H-8) of this amino acid (Figure 2). A further IMPRESS experiment was required to establish that these aromatic protons did not belong to one of the two other aromatic groups.

Acid hydrolysis of **3** and Marfey's analysis[15] of the amino acid mixture showed that both tyrosine units were of D-configuration, while one of the alanines was D- and the other L-configured. The 3-phenyllactic acid was found to have an *S*-configuration by reacting the acid hydrolyzate of **3** with (*S*)-MTPA-Cl and HPLC comparison of the resulting (*R*)-MTPA-phenyllactic acid ester with standards. The only stereochemical detail remaining unclear was which alanine was of L- and which was of D-configuration. The conformational flexibility of the molecule limits the value of the observed ROE correlations when applied to potential molecular modeling studies of the two stereochemical options, while attempts to crystallize the compound have been as yet unsuccessful. Gliotide (**3**) was inactive in the cytotoxicity and antimicrobial assays.

The value of the microtiter-plate-based system lies in the simple generation of bioactivity profiles of the HPLC chromatogram of

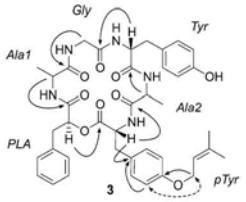

Figure 2. Long-range H,C-couplings (arrows) and one ROE interaction (dashed arrow) define the amino acid sequence of **3** and the position of the prenyl group.

Table 2. NMR Data of Gliotide (**3**; 500 MHz, MeOH-d_4)

position	δ_C		δ_H	position	δ_C		δ_H
Ala1				pTyr[a]			
1	174.7			1	173.8		
2	50.3		4.39 dd 7.0, 7.0	2	57.6		4.48 dd 9.1, 5.3
3	18.2		1.09 d 7.2	3	37.3	a	3.05 m
Gly						b	2.92 dd 13.5, 9.2
1	172.5			4	129.4		
2	43.9	a	3.88 d 16.2	5/9	131.8		7.00 d
		b	3.47 d 16.2	6/8	116.3		6.58 d 8.6
Tyr				7	159.9		
1	173.6			10	66.0		4.43 d 6.5
2	58.2		4.31 m	11	121.5		5.34 bt 6.1
3	37.2	a	3.01 m	12	138.9		
		b	2.82 dd 14.1, 9.7	13	18.4		1.64 s
4	129.1			14	26.1		1.67 s
5/9	131.5		7.00 d m	PLA[b]			
6/8	116.6		6.68 d 8.6	1	171.2		
7	157.7			2	76.1		5.19 dd 5.7, 4.2
Ala2				3	38.8	a	3.03 m
1	174.5					b	2.74 dd 14.3, 3.9
2	50.8		4.31 m	4	136.9		
3	18.9		1.35 d 7.2	5/9	131.5		6.88 bd 7.7
				6/8	129.5		7.19 m
				7	128.4		7.18 m

[a] *O*-Prenyltyrosine. [b] 3-Phenyllactic acid.

crude extracts. This then allows strategic decisions to be made for the subsequent purification steps. The bioactivity profile can also be used to assist in the dereplication of extracts containing known bioactive compounds.

Experimental Section

General Experimental Procedures. Optical rotations were measured with a Perkin-Elmer 341 polarimeter and UV spectra on a GBC UV/vis 920 spectrometer. NMR spectra were recorded on a Varian (UNITY INOVA) AS-500 spectrometer (500 and 125 MHz for ^{1}H and ^{13}C NMR, respectively), using the signals of the residual solvent protons (δ_H 3.30 and 2.60 for MeOH-d_4 and DMSO-d_6, respectively) and the solvent carbons (δ_C 49.3 and 39.6 for MeOH-d_4 and DMSO-d_6, respectively) as internal references. HRESIMS were acquired using a Micromass LCT TOF mass spectrometer, which was also used for LC-MS. HPLC was performed on a Dionex system equipped with an ISCO Foxy Jr. sample collector using a reversed-phase analytical column (Phenomenex Prodigy C18, 4.6 × 250 mm, 5 μm) with photodiode array (DAD) and evaporative light scattering detection (ELSD; Alltech). Solvents used for extraction and isolation were distilled prior to use.

Biological Assays. For the P388 cytotoxicity assays the following medium was used: MEM, fetal calf serum (10%), penicillin (266 u/mL), streptomycin (132 μg/mL), L-glutamine (2 mM), $NaHCO_3$ (2.2 g/L), HEPES (7.4 mM). For the *Bacillus subtilis* assay a RPMI-1640 medium was used, supplemented with L-glutamine (2 mM) and MOPS (34.53 g/L) and adjusted to pH 7 with NaOH (1 M). Cytotoxicity against P388 cells and antimicrobial activities were measured using standard protocols.[16]

Fungus. A small cube from the interior of the alga *Durvillaea antarctica*, collected at the coast of Tauranga Bay, New Zealand, was placed on filtered seawater agar (fresh filtered seawater, agar 15 g/L, chloramphenicol 100 μg/L, ampicillin 100 μg/L, and streptomycin sulfate 50 μg/L). After cultivation at 15 °C for 7 days, hyphae growing on the substrate were transferred onto seawater potato dextrose agar (fresh filtered seawater, Gibco PDA 39 g/L, chloramphenicol 100 μg/L, ampicillin 100 μg/L, and streptomycin sulfate 50 μg/L). One of the isolates was identified as a species of *Gliocladium* due to the densely penicillate conidiophores bearing one-celled, ellipsoidal, smooth-walled conidia in slimy heads.[17]

Extraction. For chemical investigation the *Gliocladium* sp. was grown at 26 °C in half-strength potato dextrose broth (PDB; 3 × 500 mL). The cultures were agitated on a shaker (first 14 days of growth) and then left growing under static conditions (16 more days). The cultures were filtered, and broth and cells were extracted exhaustively with ethyl acetate. The combined organic phases were concentrated, partitioned against water, and dried to give a crude extract, which was subsequently partitioned between petroleum ether and methanol/water (9:1). The resulting methanol/water phase was concentrated to dryness (184 mg).

Generation of Bioactivity Profiles. An aliquot of the extract (100 μg) was analyzed by HPLC (solvents: (A) H_2O + 0.05% TFA, (B) MeCN; gradient: 0 min 10% B, 2 min 10% B, 14 min 75% B, 24 min 75% B, 26 min 100% B; flow: 1 mL/min; 40 °C). The eluent from the DAD was split in a 1:10 ratio between the ELSD and the fraction collector configured to collect into a 96-well microtiter plate (15 s/well). A total of 88 wells were collected (2.5−24.5 min). A daughter plate was prepared by transferring an aliquot (5 μL) from each well of the master plate. After complete evaporation of the solvent the wells in the plate were analyzed for activity against P388 murine leukemia cells as follows: aliquots of P388 cell suspension (150 μL; 1.26×10^4 cells) were added to each well except wells H1 and H2, which as a positive control were loaded with medium (150 μL) only. After incubation (36 °C, 3 days) an MTT solution was added to each well (20 μL, 3.8 mg/mL in PBS) and incubated (4 h at 36 °C). To dissolve the formazan product, HCl in isopropanol (170 μL, 0.08 M) was added to each well.[9] Cell viability was assessed by measuring the absorption of each well at 540 nm, subtracting the absorption at 690 nm and using the negative control (wells H1 and H2) and the analyte free cell control (wells H3−H5) as 0% and 100% growth reference, respectively.

For the antibacterial profile a second microtiter plate was prepared using identical conditions, but injecting 500 μg of extract. After evaporation of the solvent this plate was tested directly for activity against *B. subtilis*: 200 μL of a *B. subtilis* suspension (OD(610 nm) = 0.04) was added to each well except the negative control wells H1 and H2, which were loaded with 200 μL of medium each. After incubation (24 h; 30 °C) a resazurin solution (0.2 mg/mL PBS; 30 μL) was added to all wells except H4 and the plate further incubated (15 min; 30 °C). Cell viability was assessed the same way as described above for the cytotoxicity profile, but measuring the absorption at 600 nm and subtracting the absorption at 690 nm.

Isolation. The extract was subjected to semipreparative HPLC (Phenomenex Luna C18, 10 × 250 mm, 5 μm; H_2O + 0.05% TFA (A), MeCN (B); 0 min 20% B, 13 min 75% B; 5 mL/min; 40 °C). Clonostachydiol (**2**; 13.2 mg), 4-keto-clonostachydiol (**1**; 8.2 mg), and gliotide (**3**; 7.1 mg) were eluted after 5.9, 8.4, and 12.5 min, respectively.

4-Keto-clonostachydiol (1): colorless oil; $[\alpha]^{20}_D$ +49 (*c* 0.33, MeOH); ^{1}H and ^{13}C NMR data were consistent with those reported in the literature;[10] for full 1D and 2D NMR data, see Supporting Information; ESIMS *m/z* 283.1 $[M + H]^+$.

Clonostachydiol (2): white solid; $[\alpha]^{20}_D$ +90 (*c* 1.0, MeOH) (lit.[10] +103, *c* 1.0 MeOH); ^{1}H and ^{13}C NMR data and results from CIGAR

and COSY were identical with, or consistent with, reported data;[11] ESIMS *m/z* 285.2 $[M + H]^+$.

Gliotide (3): white solid; $[\alpha]^{20}_D$ +6.6 (*c* 0.33, MeOH); for ^1H and ^{13}C NMR data (in MeOH-d_4), see Table 2; for additional NMR data (HMBC, COSY, ROESY data in MeOH-d_4; ^1H, ^{13}C, and ROESY in DMSO-d_6), see Supporting Information; HRESIMS *m/z* 742.3424 $[M + H]^+$ (calcd for $C_{40}H_{48}N_5O_9$, 742.3452).

Preparation and Analysis of Marfey Derivatives. Compound **3** (0.8 mg) was hydrolyzed by heating (110 °C for 24 h) in HCl (6 M; 1 mL). After cooling, the solution was evaporated to dryness and redissolved in H_2O (100 μL). A 1% (w/v) solution (100 μL) of FDAA (Marfey's reagent, N^{α}-(2,4-dinitro-5-fluorophenyl)-L-alaninamide)[15] in acetone was added to an aliquot (50 μL) of the acid hydrolysate solution (or to 50 μL of a 50 mM solution of the respective amino acid). After addition of $NaHCO_3$ solution (1 M; 20 μL) the mixture was incubated (1 h at 40 °C). The reaction was stopped by addition of HCl (2 M; 10 μL), the solvents were evaporated to dryness, and the residue was redissolved in MeOH−H_2O (1:1; 1 mL). An aliquot of this solution (10 μL) was analyzed by HPLC (Phenomenex Luna C18, 250 × 4.6, 5 μm; solvents: A H_2O + 0.05% TFA, B MeCN; linear gradient: 0 min 35% B, 30 min 45% B; 25 °C; 1 mL min^{-1}). Retention times (min) of the amino acid derivatives were as follows: L-Ala (6.4), D-Ala (7.6), L-Tyr (25.1), and D-Tyr (29.5).

Preparation and Analysis of (*R*)-MTPA Esters of 3-Phenyllactic Acid. To (*R*)- or (*S*)-3-phenyllactic acid (0.1 mg), synthesized from D- or L-phenylalanine, respectively,[18] or to dried acid hydrolysate of **3** (from 0.4 mg peptide) were added a solution of (*S*)-MTPA chloride (0.5 mg) in CH_2Cl_2 (0.5 mL), Et_3N (3 μL), and a small crystal of DMAP. After 3 h the solvent was evaporated, the residue dissolved in MeOH (0.5 mL), and the solution analyzed by HPLC (Phenomenex Luna C18, 250 × 4.6, 5 μm; solvents: A H_2O + 0.05% TFA, B MeCN; linear gradient: 0 min 10% B, 2 min 10% B, 14 min 75% B, 24 min 75% B; 40 °C; 1 mL min^{-1}). Retention times of the (*R*)- and (*S*)-3-phenyllactic acid esters were 17.86 and 18.00 min, respectively.

Reduction of 1. To a stirred solution of **1** (1.3 mg, 4.6 μmol) and $CeCl_3 \cdot 7H_2O$ (3 mg, 8.0 μmol) in MeOH (2.5 mL) was added $NaBH_4$ (2 mg, 53 μmol). After 5 min the solvent was evaporated in vacuo, dissolved in EtOAc (3 mL), and washed with HCl (0.5 M; 3 mL). Semipreparative HPLC on a C_{18} column yielded the two reduced products (0.3 mg of each). **4a**: $[\alpha]^{20}_D$ +100 (*c* 0.03, MeOH); ^1H NMR data and HPLC retention time identical to those of clonostachydiol (**2**). **4b** (4-*epi*-clonostachydiol): $[\alpha]^{20}_D$ +60 (*c* 0.03, MeOH); ^1H NMR (MeOH-d_4; 500 MHz) δ 6.84 (1H, dd, J = 15.8, 4.3 Hz, H-9), 6.77 (1H, dd, J = 15.7, 3.0 Hz, H-3), 6.14 (1H, dd, J = 15.7, 2.0 Hz, H-2), 5.85 (1H, dd, J = 15.8, 1.9 Hz, H-8), 5.25 (1H, qd, J = 6.5, 2.1 Hz, H-5), 5.12 (1H, m, H-13), 4.57 (1H, m, H-10), 4.40 (1H, m, H-4), 1.97 (1H, m, H_a-11), 1.70 (1H, m, H_b-11), 1.66 (1H, m, H_a-12), 1.50 (1H, m, H_b-12), 1.38 (3H, d, J = 6.5 Hz, H-6), 1.21 (3H, J = 6.5 Hz, H-14).

Preparation of 5. A solution of clonostachydiol (**2**; 3.7 mg; 0.013 mmol) and Dess−Martin periodinane (20 mg; 0.047 mmol) in CH_2Cl_2 (3 mL) was stirred at room temperature for 3 h. The mixture was washed twice with saturated $NaHCO_3$ solution and dried over Na_2SO_4. Purification by chromatography on a RP18 cartridge (MeOH/H_2O) yielded compound **5** (1.9 mg; 0.007 mmol; 54%) as a white solid: $[\alpha]^{20}_D$ +35 (*c* 0.1, MeOH); ^1H NMR ($CDCl_3$; 500 MHz) δ 6.87 (1H, d, J = 16.0 Hz, H-9), 6.63 (1H, d, J = 15.7 Hz, H-8), 6.60 (1H, dd, J = 15.9, 8.4 Hz, H-3), 5.74 (1H, d, J = 15.8 Hz, H-2), 5.02 (1H, m, H-5), 5.02 (1H, m, H-13), 3.99 (1H, t, J = 8.8 Hz, H-4), 2.64 (1H, m, H_a-11), 2.55 (1H, m, H_b-11), 2.10 (1H, m, H_a-12), 1.97 (1H, m, H_b-12), 1.49 (3H, d, J = 6.2 Hz, H-6), 1.23 (3H, d, J = 6.2 Hz, H-14); ^{13}C NMR ($CDCl_3$, 125 MHz) δ 201.0 (C, C-10), 167.5 (C, C-7), 166.2 (C, C-1), 147.2 (CH, C-3), 140.0 (CH, C-9), 132.6 (CH, C-8), 126.8 (CH, C-2), 77.7 (CH, C-4), 74.1 (CH, C-5), 72.6 (CH, C-13), 40.2 (CH_2, C-11), 33.4 (CH_2, C-12), 20.4 (CH_3, C-14), 18.3 (CH_3, C-6); HRESIMS *m/z* 283.1147 $[M + H]^+$ (calcd for $C_{14}H_{19}O_6$, 283.1182).

Preparation of 6. A solution of clonostachydiol (**2**; 2.8 mg; 0.010 mmol) in CH_2Cl_2 (3 mL) was stirred with freshly prepared MnO_2 (30 mg) at room temperature for 24 h. Filtering and drying the reaction mixture gave **6** (1.6 mg; 0.006 mmol; 60%) as a colorless oil: $[\alpha]^{20}_D$ +25 (*c* 0.1, MeOH); ^1H NMR ($CDCl_3$; 500 MHz) δ 7.06 (1H, d, J = 16.0 Hz, H-9), 6.97 (1H, d, J = 16.6 Hz, H-3), 6.75 (1H, d, J = 16.0 Hz, H-8), 6.45 (1H, d, J = 16.6 Hz, H-2), 5.32 (1H, q, J = 7.3 Hz, H-5), 5.10 (1H, m, H-13), 2.71 (1H, ddd, J = 13.5, 8.9, 3.3 Hz, H_a-11), 2.53 (1H, ddd, J = 13.5, 8.9, 3.3 Hz, H_b-11), 2.03 (2H, m, H-12), 1.57 (3H, d, J = 7.0 Hz, H-6), 1.30 (3H, d, J = 6.6 Hz, H-14); ^{13}C NMR ($CDCl_3$, 125 MHz) δ 198.5 (C, C-10), 197.8 (C, C-4), 165.0 (C, C-7), 163.4 (C, C-1), 138.3 (CH, C-9), 135.0 (CH, C-3), 129.6 (CH, C-8), 129.6 (CH, C-2), 75.7 (CH, C-5), 71.6 (CH, C-13), 37.4 (CH_2, C-11), 30.4 (CH_2, C-12), 17.9 (CH_3, C-14), 15.3 (CH_3, C-6); HRMS (APCI, pos.) *m/z* 281.1028 $[M + H]^+$ (calcd for $C_{14}H_{17}O_6$, 281.1025).

Acknowledgment. This work was supported by a fellowship within the Postdoc-Programme of the German Academic Exchange Service (DAAD). We thank Mr. B. Clark for mass spectrometric analyses.

Supporting Information Available: ^1H and ^{13}C NMR spectra as well as tabulated NMR data of compounds **1** and **3** and HPLC of the 3-phenyllactic-acid (*R*)-MTPA esters are available free of charge via the Internet at http://pubs.acs.org.

References and Notes

(1) Blunt, J. W.; Copp, B. R.; Munro, M. H. G.; Northcote, P. T.; Prinsep, M. R. *Nat. Prod. Rep.* **2005**, *22*, 15−61.
(2) Bringmann, G.; Lang, G.; Steffens, S.; Schaumann, K. *J. Nat. Prod.* **2004**, *67*, 311−315.
(3) Klemke, C.; Kehraus, S.; Wright, A. D.; König, G. M. *J. Nat. Prod.* **2004**, *67*, 1058−1063.
(4) Tsuda, M.; Mugishima, T.; Komatsu, K.; Sone, T.; Tanaka, M.; Mikami, Y.; Shiro, M.; Hirai, M.; Ohizumi, Y.; Kobayashi, J. *Tetrahedron* **2003**, *59*, 3227−3230.
(5) Liu, W.; Gu, Q.; Zhu, W.; Cui, C.; Fan, G.; Zhu, T.; Liu, H.; Fang, Y. *Tetrahedron Lett.* **2005**, *46*, 4993−4996.
(6) Kasai, Y.; Komatsu, K.; Shigemori, H.; Tsuda, M.; Mikami, Y.; Kobayashi, J. *J. Nat. Prod.* **2005**, *68*, 777−79.
(7) Usami, Y.; Yamaguchi, J.; Numata, A. *Heterocycles* **2004**, *63*, 1123−1129.
(8) Arai, N.; Shiomi, K. Iwai, Y.; Omura, S. *J. Antibiot.* **2000**, *53*, 609−614.
(9) Alley, M. C.; Scudiero, D. A.; Monks, A.; Hursey, M. L.; Czerwinski, M. J.; Fine, D. L.; Abbott, B. J.; Mayo, A.; Shoemaker, R. H.; Boyd, M. R. *Cancer Res.* **1988**, *48*, 589−601.
(10) Kano, C.; Adachi, K.; Shizusato, Y. Patent JP 5247737, 2005, 15 pp.
(11) Grabley, S.; Hammann, P.; Thiericke, R.; Wink, J.; Philipps, S.; Zeeck, A. *J. Antibiot.* **1993**, *46*, 343−345.
(12) Rao, A. V. R.; Murthy, V. S.; Sharma, G. V. M. *Tetrahedron Lett.* **1995**, *36*, 139−142.
(13) Rao, A. V. R.; Murthy V. S.; Sharma, G. V. M. *Tetrahedron Lett.* **1995**, *36*, 143−146.
(14) Crouch, R.; Boyer, R. D.; Johnson, R.; Krishnamurthy, K. *Magn. Reson. Chem.* **2004**, *42*, 301−307.
(15) Marfey, P. *Carlsberg Res. Commun.* **1984**, *49*, 591−596.
(16) Lang, G.; Blunt, J. W.; Cummings, N. J.; Cole, A. L. J.; Munro, M. H. G. *J. Nat. Prod.* **2005**, *68*, 1303−1305.
(17) Domsch, K. H.; Gams, W.; Anderson, T. H. *Compendium of Soil Fungi*; Academic Press: London, 1980; Vol. 1, pp 368−377.
(18) Bauer, T.; Gajewiak, J. *Tetrahedron* **2004**, *60*, 9163−9170.

NP0504917

J. Nat. Prod. **2005,** *68,* 1799−1801 **1799**

Dichlorinated Pulvinic Acid Derivative from a Malaysian *Scleroderma* sp.

Sonia A. van der Sar,† John W. Blunt,† Anthony L. J. Cole,‡ Laily B. Din,§ and Murray H. G. Munro*,†

Department of Chemistry and School of Biological Sciences, University of Canterbury, Private Bag 4800, Christchurch, New Zealand, and School of Chemical Sciences and Food Technology, Faculty of Science and Technology, Universiti Kebangsaan Malaysia, 43600 UKM, Selangar D.E., Malaysia

Received September 9, 2005

A new dichlorinated pulvinic acid derivative, methyl-3′,5′-dichloro-4,4′-di-*O*-methylatromentate (**1**), was isolated from the fruiting body of a *Scleroderma* sp. The structure of **1** was determined using spectroscopic methods, and an X-ray analysis was carried out for confirmation of the structure. Compound **1** was found to display moderate antimicrobial activity against *Bacillus subtilis*.

Scleroderma spp., otherwise known as "earthballs" or "poison puff balls", occur as ecto-mycorrhizal associates of a wide range of trees, including oak and eucalyptus,[1] or as saprotrophs in soil or rotting wood.[2] The fruiting bodies are formed at the surface of the soil, or just below, and are reminiscent of a potato in appearance.[1,3] They have a brown outer peridium and when the spores are mature a dark, blackish purple interior. About 25 species of *Scleroderma* have been described worldwide,[2] and at least four species are known to be poisonous: *S. albidum*, *S. areolatum*, *S. cepa*, and *S. citrinum*. Symptoms of poisoning can occur within an hour of eating and include loss of consciousness, nausea, severe abdominal pains, vomiting, perspiration, generalized tingling sensations, spasms, cramps, paralysis, and anaphylactic shock.[1,3] The chemistry of the "earthballs" has not, however, been well studied.[3] In our search for biologically active natural products from Malaysian fungi, we discovered that the methanol extract of a *Scleroderma* sp. showed antibacterial activity against *Bacillus subtilis* (11 mm inhibition zone). Purification of this extract resulted in the isolation of a new pulvinic acid derivative, methyl-3′,5′-dichloro-4,4′-di-*O*-methylatromentate (**1**), as well as three known pulvinic acid derivatives.Compound

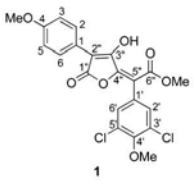

1

1 was isolated as a minor compound by semipreparative HPLC and was obtained as an intense yellow colored amorphous solid. EIMS on 1 revealed the molecular ion as a 9:6:1 triplet at *m/z* 450/452/454. This was followed by HREIMS on the ion at *m/z* 450, which established a molecular formula of $C_{21}H_{16}O_7{}^{35}Cl_2$, indicative of 13 degrees of unsaturation. The 1H NMR spectrum (Table 1) showed only seven signals, three of these being methoxyl (δ_H = 3.85, 4-OCH_3, 3.96, 4′-OCH_3, and 3.89, H7″). Also present

Table 1. 1D and 2D NMR Data for Compound **1** in $CDCl_3$

position	δ_C	δ ^{1}H, multiplicity (J_{HH} Hz)	CIGAR
1	121.2 (C)		
2	129.5 (CH)	8.12 d (8.8)	4, 6, 3, 2″
3	114.0 (CH)	6.97 d (8.8)	4, 1, 5
4	159.7 (C)		
5	114.0 (CH)	6.97 d (8.8)	4, 1, 3
6	129.5 (CH)	8.12 d (8.8)	4, 2, 5, 2″
4-OCH_3	55.3 (CH_3)	3.85 *s*	4
1′	129.1 (C)		
2′	130.4 (CH)	7.19 *s*	4′, 6′, 3′, 5″
3′	129.4 (C)		
4′	152.4 (C)		
5′	129.4 (C)		
6′	130.4 (CH)	7.19 *s*	4′, 2′, 5′, 5″
4′-OCH_3	60.8 (CH_3)	3.96 *s*	4′
1″	165.6 (C)		
2″	105.8 (C)		
3″	158.0 (C)	13.42 (OH)	3″, 4″, 2″
4″	155.8 (C)		
5″	112.1 (C)		
6″	170.7 (C)		
CO_2CH_3	54.6 (CH_3)	3.89 *s*	6″, 5″

were three sets of signals (δ_H = 8.12−6.97) in the aromatic region, which integrated in total for seven protons, with four of the protons originating from a 1,4-disubstituted aromatic system (δ_H = 8.12, H2,6; *J* = 8.8 Hz, 6.97, H3,5; *J* = 8.8 Hz). The other aromatic signal was a 2H singlet (δ_H 7.19) suggestive of a symmetric tetrasubstituted aromatic ring. An additional NMR singlet at δ_H = 13.42 indicated a hydrogen-bonded hydroxyl proton. The ^{13}C NMR spectrum (Table 1) showed 17 signals. The three methoxyls at δ_C = 55.3 (C-4), 60.8 (C-4′), and 54.6 (C-7″) and probably two ester carbonyls at δ_C 165.6 and 170.7 were immediately apparent.

The carbon skeleton of **1** was in part deduced from analysis of the CIGAR and ^{13}C NMR experiments. Analysis of the CIGAR spectrum confirmed the presence of two aromatic rings, one of them 1,2,4,6-tetrasubstituted and the other 1,4-disubstituted, as well as a methyl ester functionality. The remaining signals were quaternary carbons, and only two CIGAR correlations were observed to that part of the molecule that lay between the aromatic rings. Consultation with the AntiMarin database[4] yielded structures for related compounds.[5,6] The NMR data were compared with those reported in the literature, and this suggested that the system linking the two aromatic rings was a hydroxylated furanone and that the compound was a pulvinic acid derivative.

* To whom correspondence should be addressed. Tel: +64-3-3642434. Fax: +64-3-3642429. E-mail: murray.munro@canterbury.ac.nz.
† Department of Chemistry, University of Canterbury.
‡ School of Biological Sciences, University of Canterbury.
§ School of Chemical Sciences and Food Technology, Universiti Kebangsaan Malaysia.

10.1021/np0503395 CCC: $30.25
Published on Web 11/10/2005

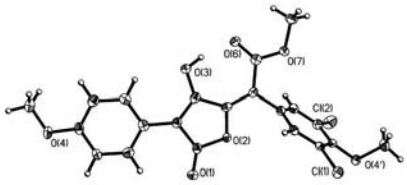

Figure 1. ORTEP diagram of methyl-3′,5′-dichloro-4,4′-di-*O*-methylatromentate (**1**).

With a working structure in hand, the NMR signals (Table 1) of compound **1** were assigned. Crystallization of **1** by slow evaporation of MeOH yielded needles of an intense yellow color suitable for X-ray analysis, which confirmed the structure of **1** (Figure 1). The new natural product was given the trivial name of methyl-3′,5′-dichloro-4,4′-di-*O*-methylatromentate. This is the first X-ray structure of an atromentate structure. The only other X-ray structure in this series is that of vulpinic acid.[7] Further confirmation of the structure came from the EIMS. The major fragment peak in the EIMS at 418/420/422 was indicative of formation of a dilactone peracetate derivative through loss of MeOH from the parent compound. This phenomenon had previously been seen in other vulpinic acid derivatives.[8]

In addition to the new dichlorinated pulvinic derivative, methyl-3′,5′-dichloro-4,4′-di-*O*-methylatromentate (**1**), three known compounds, 4,4′-dimethoxyvulpinic acid,[5] methyl-3′-chloro-4,4′-di-*O*-methylatromentate,[6] and methyl 4,4′-dimethoxyvulpinate,[5,9] were also isolated. The structures of these known compounds were identified by spectroscopic (^{1}H NMR, ^{13}C NMR, 2D NMR) and MS data measurement and by comparison with published values.

Dichlorinated pulvinic acids as natural products have been previously reported. These include methyl-2′,5′-dichloro-4,4′-di-*O*-methylatromentate,[5] in which the two chlorines are *para*-substituted, or dichloro-tri-*O*-methylxerocomic acid methyl ester,[6] where both aromatic rings are monosubstituted *ortho* to the methoxyl. Many halogenated pulvinic acid derivatives have also been synthesized for in vivo evaluation as potential anti-inflammatory agents.[10] Compound **1**, however, has not been reported as a synthetic product.

Compound **1** was found to be inactive (IC_{50} value 20.6 μM) against the P388 murine leukemia cell line, but when tested as an inhibitor of bacterial and fungal pathogens, was found to show moderate inhibition of *B. subtilis* (an inhibition zone of 4 mm was observed at a concentration of 40 μg). The larger zone of inhibition that had been initially seen in the crude extract (11 mm) was attributed to the two known compounds, 4,4′-dimethoxyvulpinic acid and methyl-3′-chloro-4,4′-di-*O*-methylatromentate, which showed inhibition zones of 8 and 7 mm, respectively, under identical assay conditions. No inhibition of *B. subtilis* has previously been reported for any chlorinated pulvinic acid derivatives.

Experimental Section

General Experimental Procedures. Melting points were obtained on a Reichert Hotstage melting-point apparatus. NMR experiments were recorded in $CDCl_3$ on a Varian INOVA 500 spectrometer at 23 °C, operating at 500 MHz using the signals of the residual solvent protons and the solvent carbons as internal references (δ_H 7.25 and δ_C 77.01 ppm for $CDCl_3$). IR spectra were recorded on a Shimadzu FTIR-8201 PC spectrometer. UV spectra were recorded on a Varian Cary 50 Probe UV−visible spectrophotometer. Electron impact mass spectra were obtained on a Kratos MS80RFA spectrometer, operating with a 4 kV accelerating potential, 70 eV, and a source temperature of 250 °C. Preparative HPLC was performed on a Shimadzu LC-4A instrument equipped with a UV spectrophotometric detector SPD-2AS (wavelength λ = 210 nm) and was carried out on a Phenomenex Luna C18, 10 × 250 mm, 5 μm column run at 5 mL/min. Solvents used for extraction and isolation were distilled prior to use. Cytotoxicity against P388 cells and antimicrobial activities were measured using a standard protocol.[11] X-ray crystallographic data were recorded on a Siemens P4 four-circle diffractometer using graphite-monochromated Mo Kα (λ = 0.71073 Å) radiation at the temperature indicated in Table S1 (see Supporting Information).

Fungal Material. Specimens were collected in the forest in Kuala Lompat, Pahang, in Malaysia in June 2004. A voucher specimen of this *Scleroderma* sp. has been deposited in the collection at the School of Chemical Sciences and Food Technology, Universiti Kebangsaan Malaysia (UKM-F5031). Identification of the fungal material was carried out by one of the authors (A.L.J.C.). The sample was identified by the characteristic tuberous earth ball fruiting body, differing from many other known *Scleroderma* sp. by the yellow color and thick rooting stalk.

Extraction and Isolation. Fresh fungal material, consisting of three fruiting bodies (12.53 g), was dried and then extracted repeatedly with MeOH (100 mL). The extract was dried under vacuum to yield an intense orange solid crude extract (1.479 g). The EtOAc-soluble extract was found to show good activity against *B. subtilis* in the antimicrobial assay. The crude extract was divided into MeOH-soluble (473 mg) and -insoluble fractions (1.006 g). The MeOH-soluble extract was found to show good activity against *B. subtilis* in an antimicrobial assay. A portion (50 mg) of the MeOH-soluble fraction was purified by HPLC using a C18 semipreparative column (Luna 5μm, 250 × 10.00 mm, ACN/H_2O, 60:40−80:20, with 0.05% TFA over 20 min, 5 mL/min, detection at 210 nm) and provided compound **1** (2.1 mg), 4,4′-dimethoxyvulpinic acid (3.1 mg), methyl-3′-chloro-4,4′-di-*O*-methylatromentate (1.6 mg), and methyl 4,4′-dimethoxyvulpinate (1.2 mg).

Methyl-3′,5′-dichloro-4,4′-di-*O*-methylatromentate (1): yellow needles (MeOH); mp 170−171 °C; UV (MeOH) λ_{max} (log ϵ) 277 (3.84), 399 (3.60) nm; IR (KBr disk) ν_{max} 1733, 1710, 1600, 1255, 1225, 1188, 1072, 1311 cm^{-1}; ^{1}H and ^{13}C NMR data, see Table 1; EIMS *m/z* (%) 450/452/454 [M]$^+$ (7/5/1), 418/420/422 (100/67/13), 362/364/366 (35/20/5), 306/308/310 (28/18/4), 175 (19), 147 (57), 119 (41); HREIMS *m/z* 450.0266 [M]$^+$ (calc for $C_{21}H_{16}{}^{35}Cl_2O_7$ 450.0273). Crystallographic data for compound **1** has been deposited with the Cambridge Crystallographic Data Centre.[12]

Acknowledgment. Assistance from Prof. W. Robinson for X-ray analysis, Ms. G. Ellis for biological assays, and Mr. B. Clark for MS operation and analyses is gratefully acknowledged.

Note Added after ASAP Publication. "Pyranone" was changed to "furanone" in the last sentence on the first page.

Supporting Information Available: ^{1}H NMR spectrum and X-ray data tables containing structure refinement, atomic coordinates, bond lengths and angles, anisotropic displacement parameters, hydrogen coordinates, torsion angles, and hydrogen bonds for compound **1** are available free of charge from the Internet at http://pubs.acs.org.

References and Notes

(1) Hall, I. R.; Stephenson, S. L.; Buchanan, P. K.; Yun, W.; Cole, A. L. J. *Edible and Poisonous Mushrooms of the World*; New Zealand Institute for Crop & Food Research Limited: Christchurch, New Zealand, 2003.
(2) Sims, K. P.; Watling, R.; Jeffries, P. *Mycotaxon* **1995**, *LVI*, 403−420.
(3) Bresinsky, A.; Besl, H. *A Colour Atlas of Poisonous Fungi: A Handbook for Pharmacists, Doctors and Biologists*; Wolfe Publishing Ltd., 1990.

(4) A new database compiled from the MarinLit and AntiBase databases, owned and operated by Blunt and Munro, University of Canterbury and Laatsch, University of Goettingen.
(5) Arnold, N.; Steglich, W.; Besl, H. Z. *Mykologie* **1996**, *62*, 69−73.
(6) Marumoto, R.; Kilpert, C.; Steglich, W. Z. *Naturforsch., C: J. Biosci.* **1986**, *41*, 363−5.
(7) Brassy, C.; Bachet, B.; Molho, L.; Molho, D. *Acta Crystallogr., Sect. C: Cryst. Struct. Commun.* **1985**, *C41*, 781−3.
(8) Letcher, R. M.; Eggers, S. H. *Tetrahedron Lett.* **1967**, 3541−6.
(9) Kanokmedhakul, S.; Kanokmedhakul, K.; Prajuabsuk, T.; Soytong, K.; Kongsaeree, P.; Suksamrarn, A. *Planta Med.* **2003**, *69*, 568−571.
(10) Foden, F. R.; McCormick, J.; O'Mant, D. M. *J. Med. Chem.* **1975**, *18*, 199−203.
(11) Perry, N. B.; Benn, M. H.; Brennan, N. J.; Burgess, E. J.; Ellis, G.; Galloway, D. J.; Lorimer, S. D.; Tangney, R. S. *Lichenologist* **1999**, *31*, 627−636.
(12) Copies of the data can be obtained free of charge, on application to the director, CCDC, 12 Union Road, Cambridge CB2 1EZ, UK (fax: +44-(0)1223-336033 or e-mail: deposit@code.cam.ac.uk).

NP0503395